Università degli Studi di Ferrara

DOTTORATO DI RICERCA IN

SCIENZE DELL'INGEGNERIA

Ciclo XXX

COORDINATORE Prof.S.Trillo

ON THE MODAL PARAMETER ESTIMATION METHODS:

CRITICAL REVIEW, IMPLEMENTATION IN MATLAB

ENVIRONMENT AND EFFECTIVENESS

Settore Scientifico Disciplinare ING/IND 13

Dottorando   **Tutore**

Dott. Zrayka Abdel Kader   Prof. Mucchi
Emiliano

Anni 2014/2017

1

Acknowledgment

I want to express my gratitude to many people who have been supporting me in some way or another during the past three years. To my adviser professor, Dr. Mucchi Emiliano, who has been a tremendous mentor for me, a special appreciation and thanks for giving me the opportunity to work with him, for encouraging my research and for allowing me to grow as a researcher.

A special thanks to my family. Words cannot express how grateful I am to my mother, father and my brothers, for all of the sacrifices that they made on my behalf. Their prayers for me were what sustained me thus far.

Also, I would also like to thank all of my friends who were big supported me and encouraged me to persuade my goals.

At the end I would like express appreciation to my beloved wife for her encouragement, dedication and support in the moments when there was no one to answer my queries.

Contents

Chapter 4

Chapter 5

Chapter 1

INTRODUCTION

1.1   Research aim

Nowadays, technologies play a great role in the human life, advancing their ways of living and working but engineers still have many issues to solve in the technological field. The vibration of mechanical structure still one of the most studied problems since it is hard to completely avoid vibration in many applications. In Airplanes, wings vibrate because of the air circulation effect, and many components present in the machines can cause vibrations.

In general, vibration cannot be avoided. Major displacement, visual effects and noises are related to vibration's resonance. This is why the work is still carried on avoiding a resonance for the least or decreases its outcomes as much as possible. In the goal of controlling vibrations it can be referred to updating the construction design, using special damping elements and controlling excitation effects…, however, in any which way, it is fundamental to begin with a deep understanding of vibrations and their descriptions, also to learn their methods of predicting and measurement. For this reason, a theory was built; it consists of using modal parameters in order to hold the subjects complex character. These parameters are composed of: natural frequency, damping factors and mode shape. This theoretical approach is followed by an experimental view concerning the modal analysis that collects information from previously made constructions.

It became very easy today to perform a theoretical modal analysis for any geometry using the finite element method (FEM). Although this method is considered very convenient, it presents some disadvantages, since the material properties and the loading history cannot be usually known. At this stage, a experimental approach is required in order to collect the modal properties by using Experimental Modal Analysis or Operation Modal Analysis on existing parts. The properties can be used lately to verify the numerical FEM mode or to other employments.

The aim of this thesis is to investigate how the accuracy of the natural frequency estimation, the damping ratio and the mode shapes extracted from the Frequency Response Function can be affected by the modal parameters extraction techniques, close mode, separated mode, truncation in the FRF or the free response function. This enquiry relies mainly on six modal parameter extraction techniques which are the Peak Amplitude, Circle Fit, Least square complex

exponential Method, Eigensystem Realization Algorithm, Rational Fraction Polynomial. The original contribution of this thesis is related to the implementation of these methods in Maltab to extract their modal parameters in order to then compare their results, discuss in details the limits of each method and its suitable domain of employment

To accomplish these goals, a simulated analytical and experimental (Experimental Modal Analysis and Operation Modal Analysis) data were analyzed by estimating the modal parameters. In the simulated analytical data the exact values are already defined and the characteristics of the FRF can be varied in order to observe how the modal parameters are affected. The experimental data was measured at various locations of a structure, and then analyzed in the same way as the simulated analytical data along with the addition of several other procedures to seek further precision. Noted in the experimental data the exact vales are undefined and the error cannot be calculated. The synthesis of the Frequency Response Function (FRF) is carried out using the modal parameters extracted. In order to test the similarity of the curve fit and the experimental data the Frequency Response Assurance Criterion (FRAC) was used.

1.2   Organization of the Text.

In this thesis, the focus will not be laid on modal testing but mainly on the estimation of the modal parameters that is considered the major part of the modal testing. In the first part of Chapter 1 the main purposes and aims of this thesis were summarized.

Chapter 2 contains a theoretical background, where at the beginning a classic modal theory was presented about single-degrees-of-freedom systems and multi-degrees-of-freedom systems and the estimation of FRF in the experimental case. This theory is very necessary in intend to understand the principles of modal parameters as the derivation FRFs.

After presenting the theory, the modal parameters were described and discussed. Then various methods are studied and arranged in groups in Chapter 3. Five of these methods were described in details, which are Peak Picking method, Circle Fit method, Least Square methods, Eigen system Realization Algorithm and

Rational Fraction Polynomial. In the end of the chapter, Least Square Error, Singular Value Decomposition and function of a stabilization diagram is briefly described along with some standard versions of it. Then an explanation was given on the Criterions Modal Assurance Criterion (MAC) and Frequency Response Assurance Criterion (FRAC) respectively used to compare the mode shapes and the FRF fitted with the Experimental FRF.

In Chapter 4 these methods were applied on three stages. The first involves the Analytical case considering a 3DOFs with modes close to each other and 3DOFs with well separated modes; in both cases a proportional damper was used. The second deals with the Experimental Model Analysis, for which two examples using experimental data, were considered; a plate and a gearbox for estimating the modal parameters and the Test-Lab Polymax Methods were applied using LMS Test-Lab software and the LSCE Matlab toolbox [2] to validate the modal parameters. The last stage handles the Operation Modal analysis where experimental vibration free response of an airplane on which we applied only the LSCE, LSCE Matlab toolbox, ERA, RFP and Test-Lab Polymax was considered.

Chapter 5 summarizes the conclusion of this thesis and points out some future research topic.

In the Appendix B the steps used in Matlab to extract the modal parameters are reported in details for the five methods.

Chapter 2

Mathematical background on SDOF and MDOF with General definition of EMA and OMA

Introduction.

This chapter gives a technical background about modal analysis. In the time when it is quite simple to used modal analysis to extract a modal database from a set of f FRFs without the need to a complete knowledge of the theoretical aspects of modal analysis taking the time to understand the full performance of the technique will always make it easier to get better results in less time using a several software.

Readers who have some comprehensive to complex variables, basic vibrations and matrix methods will be more familiar with the material of this section and will benefit more out of it. Even if these subjects are not required to gain intuitive aspect for the process. Each attempt was made in order to interpret the equations in a physical approach.

This section will not present entirely the detailed technology referred as modal analysis and cannot substitute a good look about vibrations. This bibliography that this manual provides in details also defines many sources furnishing detailed information on various topics.

This chapter is meant to help the users of modal analysis in making a better use of the software by a comprehensive of the analysis techniques basis. Particularly, it presents the theoretical aspects to get a complete and valid mathematical modal known as modal database from FRF's resulting of an artificial excitation test in the case of using a single point force input.

2.1.1 Single- degree-of-freedom system theory.

For single degree of freedom (SDOF) system shown in Fig 2.1, it was considered a mass m, a viscous damping c, and stiffness k. The equation of motion is:
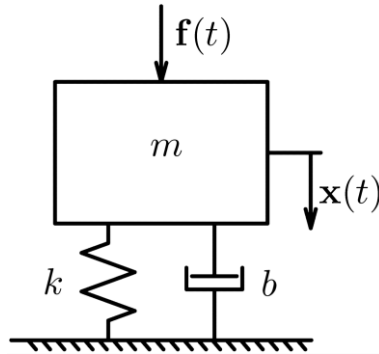

Figure 2.1: Single degree of freedom system

$$mx\ddot{}(t) + cx\dot{}(t) + kx(t) = f(t) \tag{2,1}$$

The solution of the equation (2, 1) takes on the following form involving the homogenous and the particular part as follow:

$$x(t) = x(t)_{homogenous} + x(t)_{particular} \tag{2,2}$$

$x(t)_{homogenous}$ depends on the system characteristic and initial conditions. And it is the transient portion of the solution [3] [4].

$x(t)_{particular}$, depends upon the system characteristic and harmonic forcing functions. And it is sometimes referred to as the steady state portion of the solution.

Frequently, one portion of the solution will be taken into consideration due to the application under study, if both portions are of interest; the initial conditions will be applied on the total solution (homogenous and particular portions).

 The solution of the homogenous equation (2, 1) is:

$$x(t) = Xe^{\lambda t} \tag{2,3}$$

λ is the complex number; substituting (2, 3) in (2,1) the equation becomes:

$$m\lambda^2 + c\lambda + k = 0 \tag{2,4}$$

The roots of the characteristic equation (2, 4) are:

$$\lambda_{1,2} = \frac{-c \mp \sqrt{c^2 - 4mk}}{2m} \tag{2,5}$$

When the discriminant of the equation (1, 4) is $\Delta = c^2 - 4mk$; Using the relationship of m, c, and k, the behavior of this system will be studied as follow:

$$\begin{cases} \Delta > 0 \;\to\; two\; distint\; real\; roots \\ \Delta = 0 \;\to\; two\; equal\; real\; roots \\ \Delta < 0 \;\to\; one\; pair\; of\; complex\; roots \end{cases}$$

The first case when $\Delta > 0$ then $c^2 > 4mk$; is called over-damped system. The second case for $\Delta = 0$, $c^2 = 4mk$; is called critically-damped system. And the third case when $\Delta < 0$, $c^2 < 4mk$; represent the over-damped system.

The first and the second case do not form subjects of interest because the system don't have any vibration, the interesting oscillatory behavior occurs in the third case, thus $c^2 < 4mk$; and we will define the system poles λ as follow:

$$\lambda_{1,2} = \frac{-c}{2m} \mp j\sqrt{\frac{k}{m} - \left(\frac{c}{2m}\right)^2} \tag{2,6}$$

Or,

$$\lambda = \sigma_d + j\omega_d$$

Where,

$\sigma_d = -\frac{c}{2m}$ is the damping for the one mode and $\omega_d = \sqrt{\frac{k}{m} - \left(\frac{c}{2m}\right)^2}$ is the damped natural for one mode.

Then the homogenous [5] solution for the under-damped system is:

$$x(t) = Xe^{\sigma_d t}\sin(\omega_d t + \alpha) \tag{2,7}$$

X is a constant that depends on the initial conditioning. The period of one oscillation is $T_d = \frac{2\pi}{\omega_d}$.

Considering $c=0$; the equation (2, 1) becomes:

$$Mx\ddot{}(t) + kx(t) = f(t) \tag{2,8}$$

The homogenous equation part of (2, 8) has the same solution of the homogenous part of equation (2, 1), thus substituting (2, 3) in (2, 8) contributes to the following expression:

$$m\lambda + k = 0 \tag{2,9}$$

The roots of this equation are:

$$\lambda_{1,2} = \mp j\sqrt{\frac{k}{m}} = \mp j\omega_n$$

This is called the undamped natural frequency, when ω_n is the frequency at which the system will oscillate if there is no damping in system:

The solution of the homogenous part of equation (1,8) in the time domain is a harmonic oscillation as follow:

$$x(t) = Xsin(\omega_n t + \alpha) \tag{2,10}$$

Now considering the damping ratios as:

$$\zeta = \frac{c}{c_c}$$

With, $c_c = 2\sqrt{km}$ representing the critically damping, the real and the imaginary part of the poles (λ) can be expressed as function of the ω_n and ζ, as follow:

$$\sigma_d = -\frac{c}{2m} = -\zeta\omega_n \tag{2,11}$$

$$\omega_d = \mp\sqrt{\left(\frac{k}{m}\right) - \left(\frac{c}{2m}\right)^2} = \mp\sqrt{1 - \zeta_d^2} \tag{2,12}$$

Then the ω_n and ζ, can be determined as follow:

$$\omega_n = \sqrt{\sigma_d{}^2 + \omega_n{}^2} \quad rad/s \tag{2,13}$$

$$\zeta = \frac{-\sigma_d}{\omega_n} \tag{2,14}$$

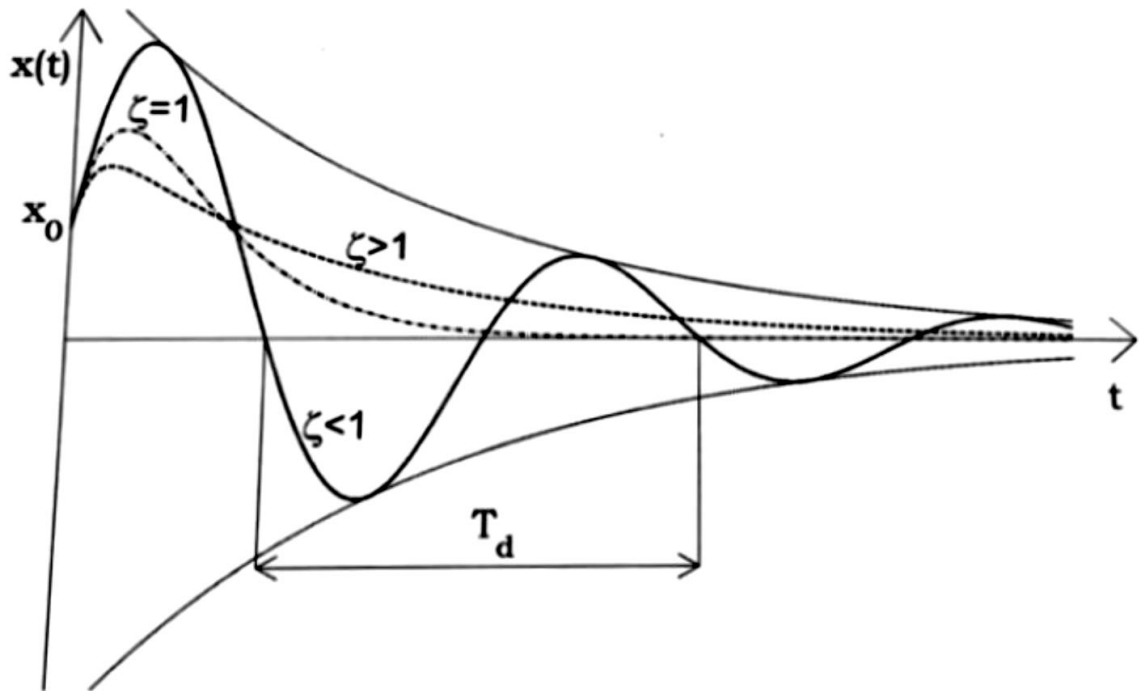The physical significance of these two parts is shown in a free response plot of SDOF in Fig 2.2:

Figure 2.2: Free vibration characteristic of damped SDOF system in three cases[5].

2.1.2 Response Model Derivation SDOF.

Assuming that the excitation $f(t) = Fe^{j\omega t}$ is sinusoidal, and the response is $x(t) = Xe^{j\omega t}$; after substituting (1,3) in (1,1) the following equation is obtained:

$$(k - j\omega c - \omega^2 m)Xe^{j\omega t} = Fe^{j\omega t} \tag{2,15}$$

From equation (2, 15) the Receptance (FRF) can be defined in the form below:

$$\alpha(\omega) = \frac{X(\omega)}{F(\omega)} = \frac{1}{(k - \omega^2 m) + j\omega c} \qquad (2,16)$$

Now an alternative forms of FRF will be established considering the velocity as a response of the system $v(t) = \dot{x}(t)$. Therefore [6] the Mobility can be defined as:

$$Y(\omega) = \frac{V(\omega)}{F(\omega)} = \frac{V e^{j\omega t}}{F e^{j\omega t}} \qquad (2,17)$$

Or,

$$Y(\omega) = j\omega \alpha(\omega) \qquad (2,18)$$

Using the acceleration as the Response the FRF can be determined in other ways like Inertance or Accelerance as:

$$A(\omega) = \frac{a(\omega)}{F(\omega)} = -\omega^2 \alpha(\omega) \qquad (2,19)$$

In the experimental case it's convenient to measure the acceleration of the system; therefor the Accelerance will be used as a date for estimation the modal parameter. To note here that the FRF is a complex, but it is still independent on the excitation.

2.1.3 Multi - Degree - of - Freedom – System.

Now for a more general condition, the multi degree of freedom (MDOF) will be discussed. The mathematical description of its dynamics behavior remains the same. Matrices and vectors are presented in the analysis instead of the scalar quantities.

If the equation of motion (2, 1) is considered for NDOF with viscous damping:

$$\underbrace{[M]}_{N \times N} \underbrace{[\ddot{x}]}_{N \times 1} + \underbrace{[c]}_{N \times N} \underbrace{[\dot{x}]}_{N \times 1} + \underbrace{[k]}_{N \times N} \underbrace{[x]}_{N \times 1} = \underbrace{[f]}_{N \times 1} \qquad (2,20)$$

[M]= mass matrix

[c]= viscous damping matrix

17

[k]= stiffness matrix

More types of the damping model exist, which are described in [1]. If [c] is proportional to [k] and [M], the damping is distributed through a structure in the same manner as mass and stiffness.

Eigenvalues analysis yields real normal modes:

$$[c] = \alpha[M] + \beta[k] \qquad (2,21)$$

Where α and β are real scalar; coefficient α models a structural damping, β represents a material damping.

If a general case consider that [c] is not proportional to [k] and [M], the solution can be found reformulating the second order system into a so-called state-space formulate on, this yields in fact into the reduction of the equation order. Thus the state vector *Z(t)* is defined as follow [4]:

$$\{Z(t)\} = \begin{Bmatrix} \dot{x}(t) \\ x(t) \end{Bmatrix} \qquad (2,22)$$

The derivative of (2, 22) is:

$$\{\dot{Z}(t)\} = \begin{Bmatrix} \ddot{x}(t) \\ \dot{x}(t) \end{Bmatrix} \qquad (2,23)$$

Now considering the following equations:

$$\begin{cases} [M]\ddot{x}(t) + [c]x(t) + [k]\dot{x}(t) = f(t) \\ \quad [M]\ddot{x}(t) + [M]\ddot{x}(t) = 0 \end{cases} \qquad (2,24)$$

Or,

$$\begin{cases} [c \ M] \begin{Bmatrix} \dot{x}(t) \\ \ddot{x}(t) \end{Bmatrix} + [k \ 0] \begin{Bmatrix} x(t) \\ \dot{x}(t) \end{Bmatrix} = f(t) \\ [M \ 0] \begin{Bmatrix} \dot{x}(t) \\ \ddot{x}(t) \end{Bmatrix} + [0 \ -M] \begin{Bmatrix} x(t) \\ \dot{x}(t) \end{Bmatrix} = 0 \end{cases} \qquad (2,25)$$

Substituting equation (2, 22) and (2, 23) in (2, 25), consequently:

$$\begin{bmatrix} c & M \\ M & 0 \end{bmatrix} Z(\dot{t}) + \begin{bmatrix} k & 0 \\ 0 & -M \end{bmatrix} Z(t) = \begin{Bmatrix} f(t) \\ 0 \end{Bmatrix} \qquad (2,26)$$

Or more compactly:

$$[A]Z(\dot{t}) + [B]Z(t) = F' \qquad (2,27)$$

In order to find the solution to equation (2, 27) for the case of harmonic input, the solution of the homogenous part taking *F'=0* becomes:

$$Z(t) = \{\phi\}e^{\lambda t} = \begin{Bmatrix} \{\psi\} \\ \lambda\{\psi\} \end{Bmatrix} e^{\lambda t} \qquad (2,28)$$

Hence, substituting (2, 28) in (2, 27) the following equation results:

$$([B] + \lambda[A])\{\phi\} = 0 \qquad (2,29)$$

The equation (2, 29) is solved using Eigenvalue – Eigenvector; which 2N Eigenvalues gives 2N corresponding eigenvectors of length 2N since the coefficient matrices [A] and [B] are real. The Eigenvalues must be a real or complex pairs, in that case the system will have N complex conjugate pairs of Eigenvalues, and N complex conjugate pairs of Eigenvector.

When the pole matrix of the system is defined as follow:

$$\Lambda = \begin{bmatrix} \lambda_1 & 0 & 0 & 0 \\ 0 & \lambda_1{}^* & 0 & 0 \\ 0 & 0 & \ddots & 0 \\ 0 & 0 & 0 & \lambda_{2N} \end{bmatrix} \qquad (2,30)$$

And the Eigenvector or Mode Shape as [7] [8]:

$$\{\phi\} = \begin{bmatrix} \{\psi_1\} & \{\psi_1{}^*\} & \cdots & \{\psi_{2N}\} & \{\psi_{2N}{}^*\} \\ \{\lambda\psi_1\} & \{\lambda\psi_1{}^*\} & \cdots & \{\lambda\psi_{2N}\} & \{\lambda\psi_{2N}{}^*\} \end{bmatrix} \qquad (2,31)$$

From equation (2, 31) the modes Shapes that are the upper halves of $\{\phi\}$ will be deduced.

The above Eigenvectors [9] have the orthogonally conditions. It can show that the rth and the pth Eigenvector $\{\psi^r\}$ and $\{\psi^p\}$ considered satisfy the Equation (2, 29). First consider the rth mode in equation (2, 29) and pre-multiply by the transposed $\{\psi^p\}^T$ thus.

$$\{\psi^r\}^T [B] \{\psi^p\} + \lambda_r \{\psi^r\}^T [A] \{\psi^p\} = 0 \qquad (2,32)$$

Taking into account now the same equation (2, 29) for p^{th} mode and pre-multiply by $\{\psi^r\}^T$ therefore.

$$\{\psi^r\}^T [B] \{\psi^p\} + \lambda_p \{\psi^r\}^T [A] \{\psi^p\} = 0 \qquad (2,33)$$

Subtracting equation (2, 32) from (2, 33) the following expression is derived:

$$(\lambda_r - \lambda_p)\left(\underbrace{\{\psi^r\}^T}_{1 \text{x} N} \underbrace{[A]}_{N \text{x} N} \underbrace{\{\psi^p\}}_{N \text{x} 1} \right) = 0 \qquad (2,34)$$

If $\lambda_r \neq \lambda_p$ then:

$$\{\psi^r\}^T [A] \{\psi^p\} = 0 \qquad (2,35)$$

$\{\psi^r\}$ and $\{\psi^p\}$ are orthogonal respect to the matrix [A] and also are orthogonal with respect to matrix [B] then:

$$\{\psi^r\}^T [B] \{\psi^p\} = 0 \qquad (2,36)$$

2.1.4   Response Model Derivation MDOF

In order to find the response [8] [9] [10] model, the excitation is counted as:

$$F' = [F]e^{j\omega t} \qquad (2,37)$$

And seek a solution in the form:

$$z(t) = [Z]e^{j\omega t} \qquad (2,38)$$

Substituting equation (2, 37) and (2, 38) in equation (2, 27) the following equation is obtained:

$$j\omega[A][Z] + [B][Z] = [F] \qquad (2,39)$$

The solution of equation (2, 38) can be written as a linear combination of 2N Vectors.

$$[Z] = \sum_{r=1}^{2N} \gamma_r [\psi^r] \qquad (2,40)$$

Substitute equation (2, 40) in (2, 39) and multiply both sides by $\{\psi^p\}^T$ to obtain:

$$j\omega\{\psi^p\}^T[A] \sum_{r=1}^{2N} \gamma_r [\psi^r] + \{\psi^p\}^T[B] \sum_{r=1}^{2N} \gamma_r [\psi^r] = \{\psi^p\}^T[Z] \qquad (2,41)$$

Then;

$$j\omega a_p(\gamma_p) + b_p(\gamma_p) = \{\psi^p\}^T[F] \qquad (2,42)$$

With;

$$a_p = \{\psi^p\}^T[A]\{\psi^p\}$$

$$b_p = \{\psi^p\}^T[B]\{\psi^p\}$$

Solving equation (2, 42), the following expression come by:

$$\gamma_p = \frac{\{\psi^p\}^T[F]}{j\omega a_p + b_p} \qquad (2,43)$$

Substituting equation (2, 43) in (2, 40), then:

$$[Z] = \sum_{r=1}^{2N} \frac{\{\psi^r\}^T[F]\{\psi^r\}}{a_r(j\omega - \lambda_r)} \qquad (2,44)$$

From equation (2, 29) λ_r can be determined as follow:

$$b_r + \lambda_r a_r = 0 \;\rightarrow\; \lambda_r = -\frac{b_r}{a_r}$$

Frequently the eigenvalues λ_r is obtained by the homogenous solution of the characteristic equation or:

$$\lambda_r = -\zeta_r \omega_n \pm j\omega_n \sqrt{1 - \zeta_r{}^2}$$

Therefore, from equation (2, 44) the frequency response function from excitation at location q and response at location *p* is:

$$H_{pq}(j\omega) = \sum_{\substack{r=1 \\ p,q}}^{2N} \frac{\psi_{pr}\psi_{qr}}{a_r(j\omega - \lambda_r)} + \frac{\psi_{pr}{}^*\psi_{qr}{}^*}{a_r(j\omega - \lambda_r{}^*)} \tag{2,45}$$

Or,

$$H_{pq}(s) = \sum_{\substack{r=1 \\ p,q}}^{2N} \frac{A_{pq}{}^r}{(s - \lambda_r)} + \frac{A_{pq}{}^{*r}}{(s - \lambda_r{}^*)} \tag{2,46}$$

Where $A_{pq}{}^r = \frac{\psi_{pr}\psi_{qr}}{a_r}$ is the residue at pole λ_r ; and s=jω is the Laplace variable.

The result in equation (2, 46); which is called modal superposition equation is the key of experimental modal analysis, is an extremely valuable relationship between frequency response function and modal constant, it relates motion at any point p due to a force at point q.

Notice an important implication of equation (2, 45) and (2, 46) is that the frequency response matrix *[H]* is symmetric; so the following expression can be written [11]:

$$H_{pq}(j\omega) = H_{qp}(j\omega) \tag{2,47}$$

Then it can be noted that the frequency response function (FRF) between two points is the same if an excitation occurs e in point q and the response is measured in point p as if the force and response points are reversed.

The residues can easily be formulated in matrix A_r as follow:

$$[A_r] = Q_r\{\psi_r\}\{\psi_r\}^T = Q_r \begin{bmatrix} \psi_{1r}\psi_{1r} & \psi_{1r}\psi_{2r} & \psi_{1r}\psi_{3r} & \cdots \\ \psi_{2r}\psi_{1r} & \psi_{2r}\psi_{2r} & \psi_{2r}\psi_{3r} & \cdots \\ \psi_{3r}\psi_{1r} & \psi_{3r}\psi_{2r} & \psi_{3r}\psi_{3r} & \cdots \\ \vdots & \vdots & \vdots & \cdots \end{bmatrix} \quad (2,48)$$

Which is a matrix of Rank one (since it is composed only of linear combination of one vector $\{\psi_r\}$). It should be noted that each column in $[A_r]$ is the mode shape $\{\psi_r\}$, scaled by the modal constant Q_r and the mode shape coefficient corresponds to the column, that is.

$$A_r = Q_r[\ \psi_{1r}\psi_r \ \ \psi_{2r}\psi_r \ \ \psi_{3r}\psi_r \ \cdots]$$

With the expression for the residue matrix, the entire frequency response matrix *[H(jω)]* can be written compactly as:

$$[H(j\omega)] = \sum_{r=1}^{2N} \frac{[A_r]}{s - \lambda_r} \qquad (2,49)$$

For the synthesizing frequency response function from modal parameters, and the basic expression used for modal parameters extraction it should be noted that equation is valid for any type of damping. An important implication in the equation of the residues (2, 48) for experimental modal analysis is found by observing that any row or column in the residue matrix *[Ar]* contains the mode shape $\{\psi_r\}$, therefore it can be deduced from this, the minimum data to be able to extract a mode shape from a measurement of a frequency response matrix, is one row or column.

In the experimental modal analysis the equation is often written using inverse pole matrix [Λ⁻¹] but expanding to a size 2N; and renumbering the poles to λ_r , r=1, 2, 3, ….., 2N. thus the inverse poles matrix are :

$$[\Lambda^{-1}(s)] = \begin{bmatrix} \dfrac{1}{j\omega - \lambda_1} & 0 & 0 & \cdots \\ \cdots & \dfrac{1}{j\omega - \lambda_2} & 0 & \cdots \\ & & & \cdots \\ \cdots & \cdots & \ddots & 1 \\ \cdots & \cdots & \cdots & \dfrac{1}{j\omega - \lambda_{2N}} \end{bmatrix} \qquad (2,50)$$

23

Now if the 2N is redefined by 2N mode shape matrix $[\psi']$ including the complex conjugate mode in columns, equation (2, 49) can be written more compactly as:

$$[H(j\omega)] = [\psi'][\Lambda^{-1}][\psi']^{T} \qquad (2,51)$$

When the poles and the modes shapes of all modes are known; the frequency response function between any two points on the structure can be synthesized.

The examination of a multi degree-of-freedom frequency response permits to determine its characteristics. In the Figure 2.4 in particular the change of phase through resonance, the peak in magnitude and imaginary parts, and the zero crossing in the real part can be clearly detected. If the real versus imaginary part is plotted the frequency response take shapes of several circles for MDOF as illustrated in Figure 2.3. In addition to the shape of the frequency response in the vicinity of the resonance, the natural frequency and damping can be estimated. Similarly for the multi degree-of-freedom system, the mode shape can also be estimated.

It is possible in many situations to reasonably apply SDOF theory. Notice that there are several differences between SDOF and MDOF frequency response function. One important difference is that there is now more than one frequency response function for the system. Additionally, notice that there are now multiple peaks and the phase is no longer restricted 0, -π. As a result the phase at resonance can be ±π/2.
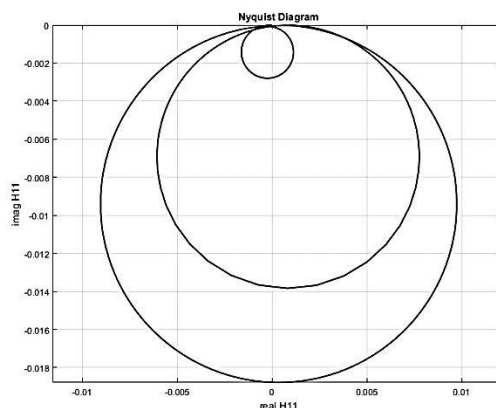

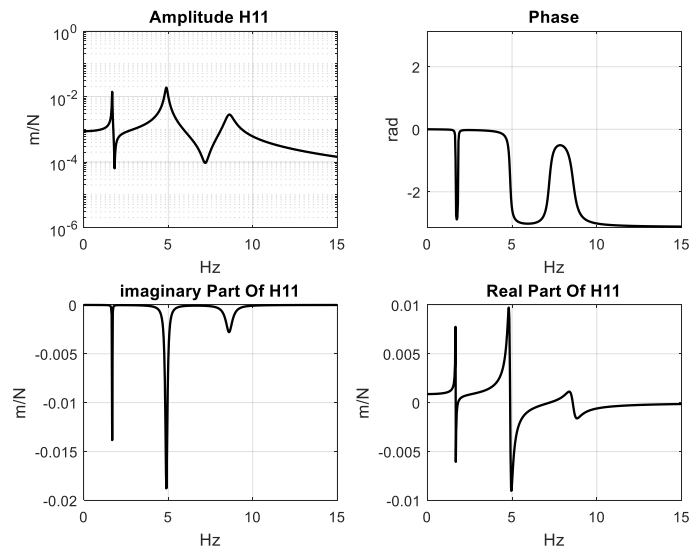*Fig 2.3: Nyquist diagram for 3DOF system*

Figure 2.4: Amplitude, phase, real part, imaginary part of the Receptance H11 driving point versus frequency (3DOF)

2.1.5 Plot of the Mode Shape

A simple approach to analyze the complexity of the vector mode shape consists in plotting its components in the complex plane as illustrated in the Fig 2.5. One can then easily determine if these components [12] [13] tend to be aligned according to a specific direction. One can also visually assess the vector whereas the second one is really a complex vector.
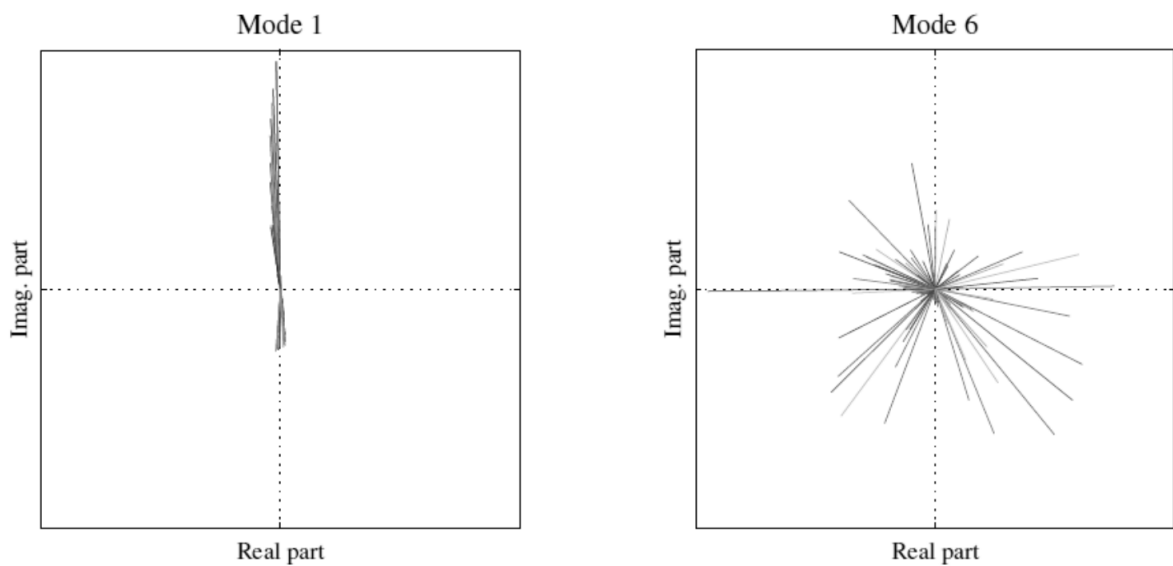

Fig 2.5: Plot of the mode shape

25

2.2   EXPERIMENTAL MODAL ANALYSIS & OPERATION MODAL ANALYSIS.

2.2.1   EXPERIMENTAL MODAL ANALYSIS

Experimental Modal Analysis (EMA) [6] [7] [14] is based on the measurement of the frequency response function (FRF), it is defined as the ratio between of the output response and the input excitation force. This measurement is typically acquired using a dedicated instrument such as a FFT (Fast Fourier Transform) analyzer or data acquisition system with software that performs the FFT. In addition, different excitation can be used in the estimation of the FRF. Modal parameter estimation methods are used to obtain modal parameters of the structure from measured frequency response functions. Figure 2.6 illustrates the process of a modal test [1].

Test structure

measure the frequency response function

Curve fit representation

Modal parameters

$$H_{pq}(s) = \sum_{r=1}^{2N} \frac{A_{pq}^{\ r}}{(s - \lambda_r)} + \frac{A_{pq}^{\ *r}}{(s - \lambda_r^{\ *})}$$

Frequency
Damping
Mode shapes
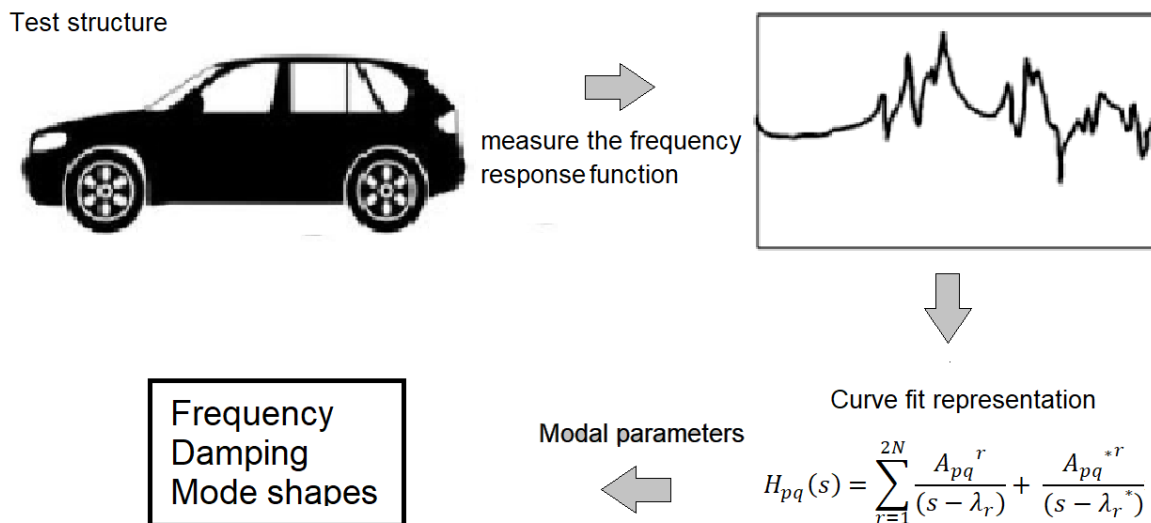
Fig 2.6: Modal Test

The structures have an infinite number of DOFs and infinite number of modes. From testing point of view, a real structure can be sampled spatially at as many DOFs as we like. There is no limit to the number of unique DOFs between which FRF measurements can be made. However, because of time and cost constraints,

we only measure a small subset of the FRFs that could be measured on a structure. This is illustrating in Fig 2.7 [13] [14].

Also, from this small subset of FRFs, we can define the modes that are within the frequency range of the measurements. Of course, the more we spatially sample the surface of the structure by taking more measurements, the more definition we will give to its mode shapes.
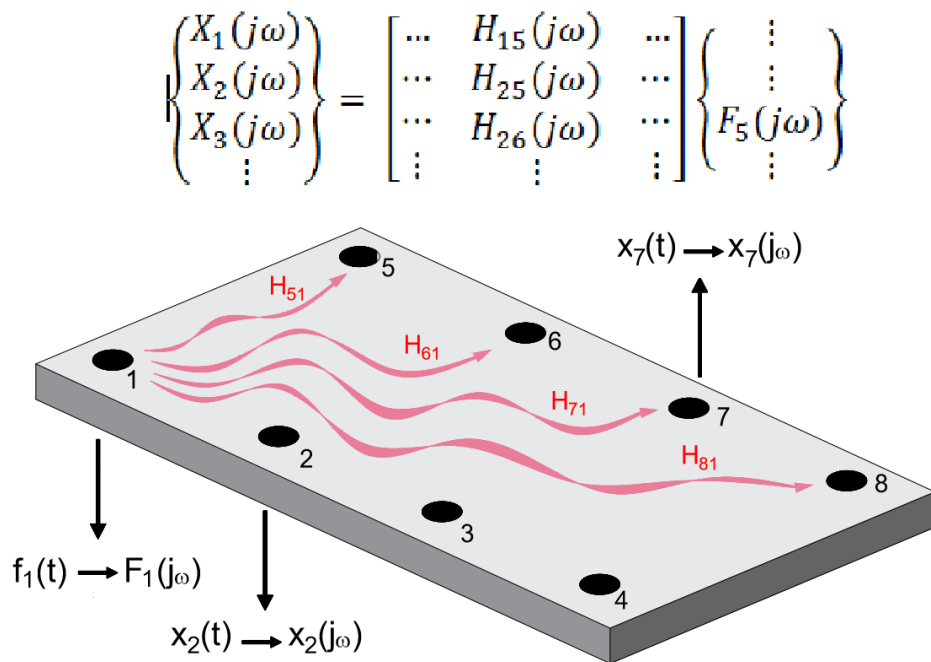
$$\begin{Bmatrix} X_1(j\omega) \\ X_2(j\omega) \\ X_3(j\omega) \\ \vdots \end{Bmatrix} = \begin{bmatrix} \cdots & H_{15}(j\omega) & \cdots \\ \cdots & H_{25}(j\omega) & \cdots \\ \cdots & H_{26}(j\omega) & \cdots \\ \vdots & \vdots & \vdots \end{bmatrix} \begin{Bmatrix} \vdots \\ \vdots \\ F_5(j\omega) \\ \vdots \end{Bmatrix}$$

Fig 2.7: Measuring FRFs on a structure.

Modal testing requires that FRFs be measured from at least one row or column of the FRF matrix. Modal frequency and damping are global properties of a structure, and can be estimated from any or all of the FRFs in a row or column of the FRF matrix. In the other hand, each modes shape is obtained by assembling together FRF numerator terms (called residues) [17] from at least one row or column of the FRF matrix. For the determination the row or column of the FRFs usually the structure will excited by a hammer or shaker.

The most common type of modal testing is done with either a single fixed input or a single fixed output. A roving hammer impact test using a single fixed motion

transducer is a common example of single reference testing. The single fixed output is called the reference in this case.

When the single fixed point input (such as a shaker) is used, this is called SIMO (Single Input Multiple Output) testing. In this case single fixed input is called the reference.

When two or more fixed input are used, and FRFs are calculated between each of the input and multiple output, then FRFs from multiple Reference or MIMO (Multiple Input Multiple Output) testing. In this case, the inputs are the references

Likewise, when two or more output are used, and FRFs are calculated between each output and multiple inputs, this is also multiple references testing, and the output are the references.

Multiple-reference testing is done for the following reasons.

- The structure cannot be adequately excited from one reference.
- All modes of interest cannot be excited by using one reference.
- The structure has repeated roots; closely coupled modes need more than one reference in order to be identified.

2.2.2   Exciting Modes with Impact Testing.

Impact testing is a fast, convenient, and low-cost way of finding the modes of machines and structures.
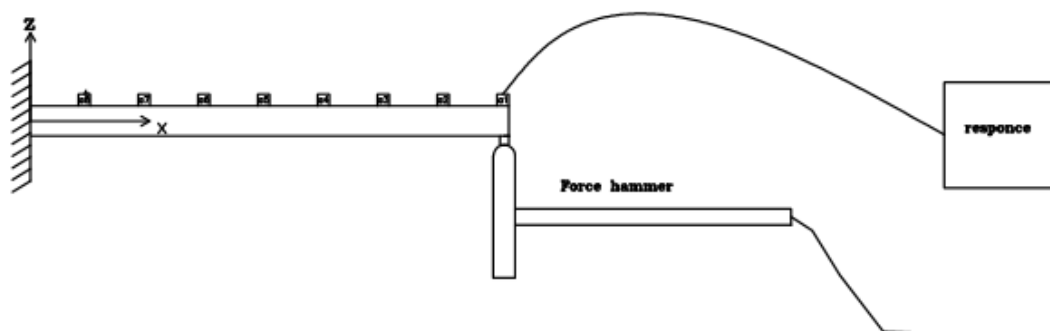
Fig 2.8: Impact testing

Impact testing is depicted in Fig 2.8. The following equipment is required to perform an impact test,

- An impact hammer with load cell attached to its head to measure the input force.
- A sensor for measuring the response acceleration at a fixed point and direction.
- A FFT analyzer to compute FRFs.
- Post-processing modal software for identifying modal parameters and displaying the modes shapes in animation.

A wide variety of structures and machines can be impact tested. of course different hammers are required to provide the appropriate impact force, depending on the size of the structures; small hammers for small structures, large hammers for large structures.

2.2.3 Shaker Measurements

Not all structures can be impact tested, For instance, structure with delicate surface cannot be impact tested. Or because of its limited frequency range or low energy density over a wide spectrum, the impacting force is not be sufficient to adequately excite the modes of interest.

When impact testing cannot be used, FRF measurements must made by providing artificial excitation with one or more shakers, attached to the structure. A typical shaker test is depicted in Fig 2.9.
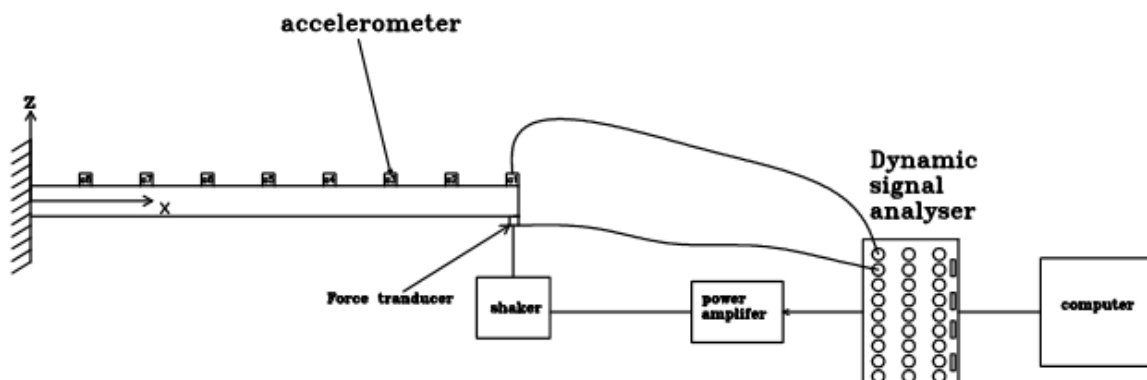
Fig 2.9: Shaker test setup.

At least a 2-channel FFT analyzer and single axis accelerometer are required to make FRF measurements using a shaker. If analyzer with 4 or more channels is used, then a tri-accelerometer can be used and 3D motion of the structure measured at each test point.

In SIMO test, one shaker is used in this case the single fixed input is called the reference. In a MIMO test, multiple shakers are used, and the shakers are the multiple references.

2.2.4 Operation Modal Analysis

Since the first application of this alternative testing procedure, many new powerful algorithms for modal parameter identification have been developed. Still, most of them are based on techniques previously established for EMA. As modal information is derived from structural responses (outputs) while the structure is in operation, this process is usually called Operation Modal Analysis (OMA) [18] [19] or Output-only Modal Analysis (in opposition to input-output modal analysis). That because the real loading conditions to which a structure is subjected often differs considerably from those used in laboratory testing. However, all real-world systems are to certain extent non-linear, the models obtained under real loading will be linearized for much more representative working points. Additionally, environmental influences on system behavior will be taken into account.

OMA permit the identification of natural frequencies, damping ratios and mode shapes of relevant modes of vibration and the characterization of the vibration amplitude associate with normal operation conditions or motivated by recreated load scenarios [20], as for instance controlled rain passages or test in footbridges with crowds trained to walk with predefined pacing rate wind turbine, Airplane.

Also it is the case where large in-operation data sets are measured for other purposes such as operating field shapes analysis, level verification…Thus if procedures of the classical operating data analysis were extended with modal parameter identification capabilities, better utilization of these data will be permitted.

2.3   FRF estimation

As described above the various analytical techniques differ according to the type of excitation, number of excitation points and modal parameter extraction methods. There are two main categories of excitations; the first includes random excitations. The second includes sinusoidal excitations [7] [21] [22] which gives a good quality of FRF measured. Hence, the information about structure obtained by this way is more accurate and contains more details.

A further difference between the methods used is the number of excitation points, using a multiply excitation points will allow to measure energy more uniformly in the structure and obtain more uniform response, eliminate the possibility to lose the own modes if they are excited in their nodes.

The FRF is calculated using the Auto-Correlation [6] and Cross-Correlation functions applied to the response of the structure having an *x(t)* as a signal. The Auto-Correlation function is defined as:

$$R_{xx}(\tau) = \lim_{T\to\infty} \frac{1}{T} \int_{-T/2}^{T/2} x(t).x(t+\tau)dt \qquad (2,52)$$

This will always be a real and even function of time.

The Fourier Transform of $R_{xx}(\tau)$ is called Spectral Density, in this case the Auto-or Power Spectral Density (PSD); $S_{xx}(\omega)$ is defined as:

$$S_{xx}(\omega) = \mathcal{F}\{R_{xx}(\tau)\} = \int_{-\infty}^{+\infty} R_{xx}(\tau)e^{-j2\pi\omega\tau}d\tau \qquad (2,53)$$

The PSD is a real and even the function of frequency. The function $S_{xx}(\omega)$ is linked to the Fourier Transform of *x(t)* from the relation:

$$S_{xx}(\omega) = X^*(\omega).X(\omega) = |X(\omega)|^2 \qquad (2,54)$$

It is a real function that contains information about frequencies present in *x(t)* except the phase. It is defined as the Cross-Correlation and Cross Spectral Density functions. (CSD) of two signals *x(t)* and *y(t)* as:

$$R_{xy}(\tau) = \lim_{T\to\infty} \frac{1}{T} \int_{-T/2}^{T/2} x(t).y(t+\tau)dt \qquad (2,55)$$

Which indicates how much these two signals *x(t)* and *y(t)* are correlated.

The Cross Spectral Density (CSD) is defined as its Fourier Transform:

$$S_{xy}(\omega) = \mathcal{F}\{R_{xy}(\tau)\} = \int_{-\infty}^{+\infty} R_{xy}(\tau)e^{-j2\pi\omega\tau}d\tau \qquad (2,66)$$

The function $S_{xy}(\omega)$ is linked to the Fourier Transform of *x(t)* and *y(t)* by the following expression:

$$S_{xy}(\omega) = X^*(\omega).Y(\omega) \qquad (2,57)$$

That is a complex function which *f(t)* is the excitation of the structure and *x(t)* its response as illustrated in the Fig 2.12, now the FRF will be defined in frequency domain as the ratio of their Fourier Transform:
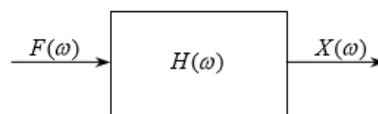
Fig 2.12: Simple Model Of H(ω)

In order to minimize the error during the measurement various estimators will be used to estimate *H(ω)* from the measured input and output signals.

2.3.1 Estimator H₁

$$H_1 = \frac{S_{fx}(\omega)}{S_{ff}(\omega)} \qquad (2{,}58)$$

Assuming that the input [1] can be measured without any noise, only the output has noise in the system, where all measurements of *x* are accurate. It minimizes the noise on the output using the Least Square.

This estimator tends to give underestimate the FRF and has a good fit in anti-resonances. Best results are obtained with this estimator when the input is uncorrelated as shown Fig 2.13:

In the Frequency domain it exists:

$$Y(\omega) = H(\omega)X(\omega) + N(\omega) \qquad (2{,}59)$$
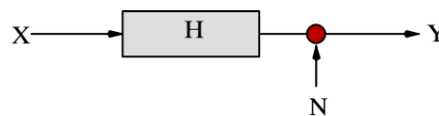
Fig 2.13: Estimator H1

2.3.2 Estimator H₂

$$H_1 = \frac{S_{xx}(\omega)}{S_{xf}(\omega)} \qquad (2{,}60)$$

This assumes that there is no noise on the output as can be seen in Fig 2.14, then all the *Y* measurements are accurate. The noise is minimized by the Least Square.

This estimator tends to give an overestimate of the FRF. This estimator estimates the resonance better than the anti-resonance. In the frequency domain there is:

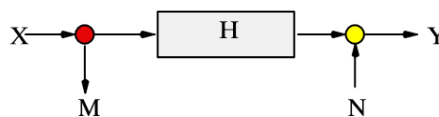$$Y(\omega) = H(\omega)[X(\omega) - M(\omega)] \qquad (2,61)$$
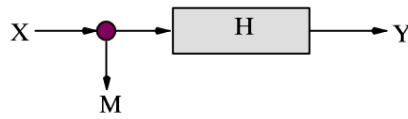
Fig 2.14: Estimator H2

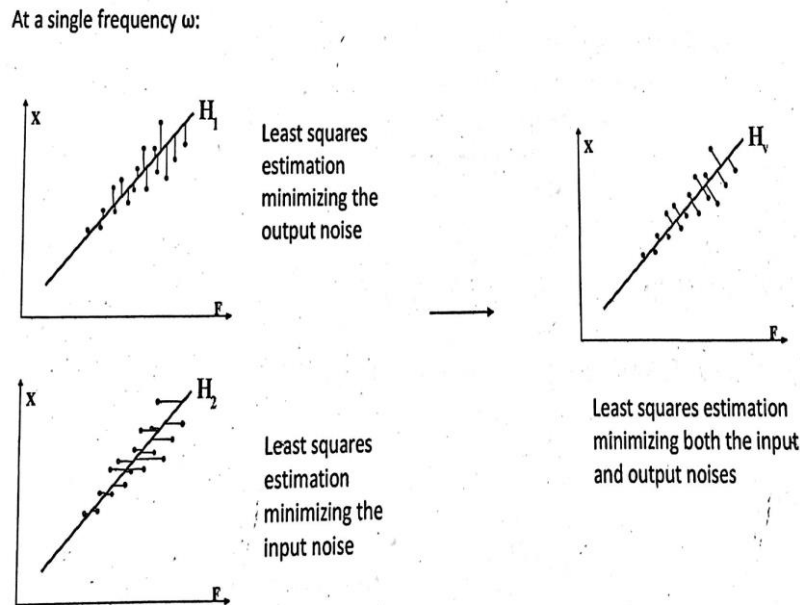### 2.3.3   Estimator H_v

H(ω) is calculated from the Eigenvector corresponding to the smallest Eigenvalue of a matrix $\left(S_{ffx} \right)$:

$$S_{ffx} = \begin{pmatrix} S_{ff} & S_{fx} \\ S_{xf} & S_{xx} \end{pmatrix} \qquad (2,62)$$

This estimator minimizes the global noise contribution in a Total Least Square sense as illustrated in the Fig 2. 16.

This estimator as depicted in the Fig 2.15 provides the best overall estimate of the FRF. It approximates to the H_2 estimator at the resonance and the H_1 at the anti-resonance. In the frequency domain exists:

$$Y(\omega) - N(\omega) = H(\omega)(X(\omega) - M(\omega)) \qquad (2,63)$$

Fig 2.15: Estimator H_v

At a single frequency ω:

Least squares estimation minimizing the output noise

Least squares estimation minimizing the input noise

Least squares estimation minimizing both the input and output noises

Fig 2.16: FRF Estimation with Graphical interpretation

2.3.4 Coherence Function

Coherence in used to check the quality of the data:

$$\gamma(\omega)^2 = \frac{H_1(\omega)}{H_2(\omega)} = \frac{|S_{fx}(\omega)|^2}{S_{ff}(\omega) \cdot S_{xx}(\omega)} \leq 1 \qquad (2,63)$$

If all well measured, the coherence should be unity.

Pure noise: $\gamma(\omega)^2 \rightarrow 0$

Not contaminated with noise: $\gamma(\omega)^2 \rightarrow 1$

Poor coherence can be eliminated by taking great many averages. But this is only possible if the reason is due to random noise, which can be averaged out over a period of time. In practice, data with a coherence of less than 0.75 are not used and indicate that the test should be done over. Usually the Anti-resonances it is difficult to estimate as shown in the Fig 2, 17.
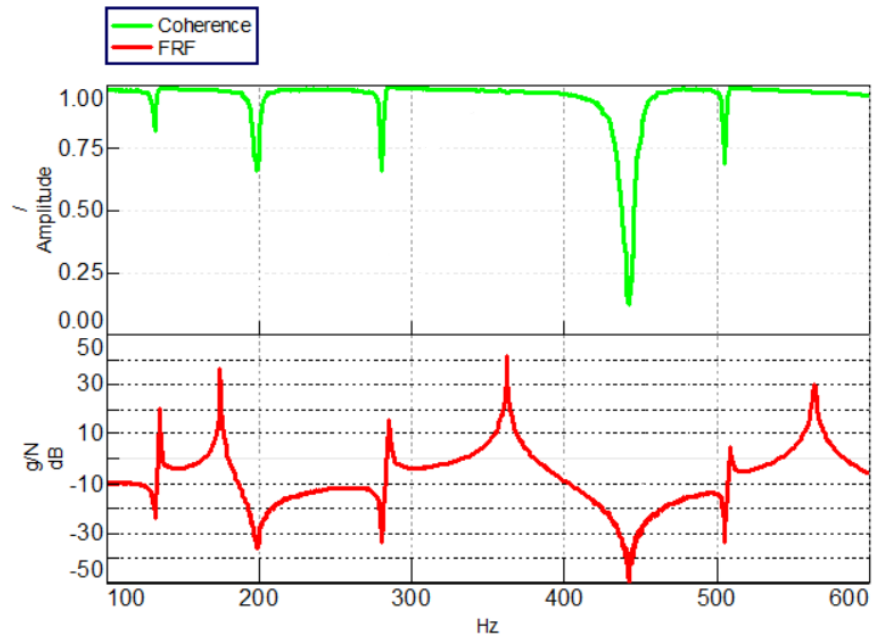
Fig 2.17: FRF Estimation- Coherence

2.3   Impulse Response Function.

The analysis is based on the general excitation/response relationship in the time domain. This relationship takes the form of a convolution integral [6].

$$y(t) = \int_{-\infty}^{+\infty} x(\tau)h(t - \tau)d\tau \qquad (2,64)$$

h(t) is determined using the inverse Fourier Transform of the Frequency Response Function as shown below:

$$h(t) = \mathcal{F}^{-1}[H(\omega)] \qquad (2,65)$$

Chapter 3

Modal parameter estimation

Introduction

The modal parameter estimation is one of the most important parts of the experimental modal analysis; it is the key step to finally reveal the modal properties. Parameter estimation process relies on employing the measurements as data in many of the numerous methods developed to find the natural frequencies, the damping factors and the mode shapes.

There is a great amount of modal parameter estimation methods expanded and improved throughout the decades, and the technical literature is full of papers that document many different approaches. However none of these methods is perfect and none can cover all types of cases, each works on it won domain. The methods are divided in two major categories, the time domain and the frequency domain methods. In addition, there are certain methods developed to works on SDOF only and others that are composed of more complex algorithms to operate on MDOF.

A good implementation in Matlab of these methods depends strongly on a profound understanding of the theory in order to perceive the operation and performance of each method. Having deep insight on the methods permits to simplify the materials and create the most adequate implementation in Matlab. Chapter 6 will provide detailed information about the method applied in this study.

3.1.1   Peak Amplitude

This method is sometimes referred also as a Peak-Picking [6] method or 3 dB method and it is SISO and it is the simplest of the modal parameter estimation methods. However, this method has some great limitation. First of all, it works well just for structures with the well separated modes and second for the structures with a good damping. For heavily damped system, the response at the resonance is influenced by more than one mode and on the other hand the accurate measurements at the resonances are difficult to obtain for light damped structure.

The method is applied as follows:

Considering the amplitude of the Receptance for one DOF with a proportional damped:

$$|\tilde{\alpha}(\omega)| = \frac{1/k}{\sqrt{\left(1 - \frac{\omega^2}{\omega_n^2}\right)^2 + (\frac{2\zeta\omega}{\omega_n})^2}} \tag{3,1}$$

After the plotting of $|\tilde{\alpha}(\omega)|$ its maximum is $\omega = \omega_d = \omega_n\sqrt{1 - 2\varsigma^2}$ if from this value decreases by 3 dB are intercepted [5] on the curve in two points where the amplitude decreases of $10^{3/20} \cong \sqrt{2}$ compared to the maximum. The two points that identified as ω_a and ω_b are the half-power points see Fig 3.1. Assuming $r = \frac{\omega}{\omega_n}$ the intersection between the $|\tilde{\alpha}(\omega)|$ and $|\tilde{\alpha}(\omega_n)|/\sqrt{2}$ is:
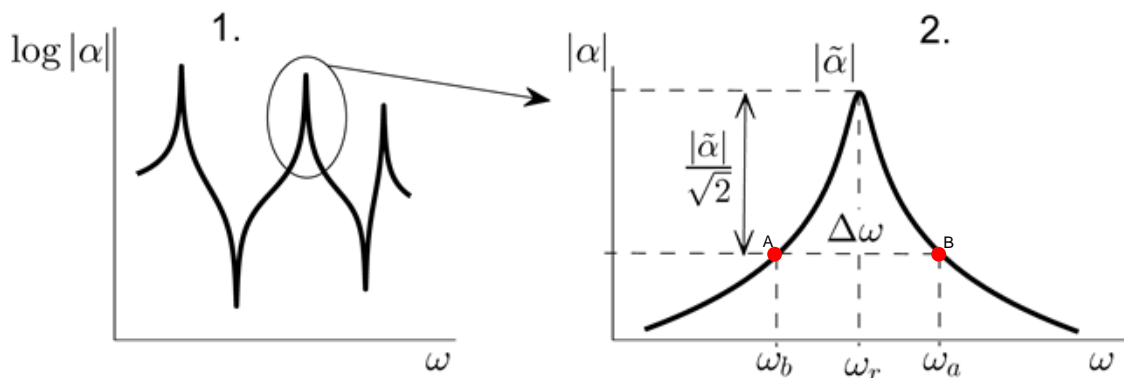
Fig 3.1: FRF and resonance detail

$$\frac{1/k}{\sqrt{(1-r^2)^2 + (2\zeta r)^2}} = \frac{1/k}{\sqrt{2}(2\zeta)^2} \qquad (3,2)$$

Developing the calculations we are reduced to biquadratic equation.

$$r^4 - 2(1 - 2\zeta^2)r^2 + 1 - 8\zeta^2 = 0 \qquad (3,3)$$

Thus,

$$r_{1,2}{}^2 = (1 - 2\zeta^2) \mp 2\zeta\sqrt{\zeta^2 + 1} \qquad (3,4)$$

Considering $\zeta \ll 1$ we can write $r_{1,2}{}^2 \cong 1 \mp 2\zeta$.

$$\frac{\omega_a{}^2 - \omega_b{}^2}{\omega_n{}^2} = 4\zeta \qquad (3,5)$$

The peak close to the natural frequency is symmetric respect the ω_a and ω_b that we can consider.

$$\omega_n \cong \frac{\omega_a + \omega_b}{2} \qquad (3,6)$$

Hence, the damping factor of the mode can now be estimated from the following formula:

$$\zeta = \frac{\omega_a{}^2 - \omega_b{}^2}{4\omega_b{}^2} \cong \frac{\omega_a - \omega_b}{2\omega_n} \qquad (3,7)$$

The sign of the mode shape value is directly given by the imaginary part of the FRF but its value has to be computed from a modal constant. The real modal constant, for the given mode index r and FRF index pq , is estimated by:

$$A_{pq}{}^{r} = 2|\tilde{\alpha}|\zeta\omega_{r}{}^{2} \tag{3,8}$$

This step will be repeated for each FRF's that measured. Then will obtain one value into a matrix of the modal constants. The mode shapes can be computed from the matrix of the modal constant as:

$$p \equiv q \rightarrow \psi_{pr} = \sqrt{A_{pq}{}^{r}} \tag{3,9}$$

Or,

$$p \neq q \rightarrow \psi_{pq} = \frac{A_{pq}{}^{r}}{\psi_{pr}} \tag{3,10}$$

The mode shapes in this form are unscaled so it is appropriate to scale them. There are several methods of the scaling possible further information can be seen in the reference [7]

The natural frequencies and the damping factors of the given mode should be the same for every analysis of FRFs, but it's understandable they are not because of the influence of the noise during a measurement. Therefore modal parameters have to be averaged. These averaged values of the natural frequencies and the damping factors will be taken as the final estimation.

3.1.2   Circle Fit.

One of the most widely used frequency domain modal analysis methods [5] [6], the Circle-Fit method, will be mathematically derived and discussed in detail. This method uses the fact and it is SISO, that the FRF is close to a circle in the Nyquist plot. The method fits a circle on the experimental data and derives the modal properties from the properties of the fitted circle. According to the algorithm of the Circle-Fit method can be described by the following sequence:

- Select points to be used
- Fit circle basing of these points, and calculate the quality of fit.
- Locate natural frequency, obtain damping estimate.
- Calculation of multiple damping estimates and their mean and scatter.

- Determination of the modal constant.

The step 1 can be perform by selecting a fixed number of points around the maximum FRF in the frequency range of interest, however, better results can be effected by the operator, so the points which are nor influence by the measured noise and neighbor modes can be selected. In general, more point available for the circle fit should produce better results. Not less six point should be used.

The second step the fitting of the circle [10] is made. This can be done by various numbers of the numerical techniques, usually based on the least square curve fitting method. The result of this step are the coordinates of the circle which are the center and diameter, then the optimal case of the information about the quality of the circle is when its shape fit a perfect circle.as can show the Fig 3.2
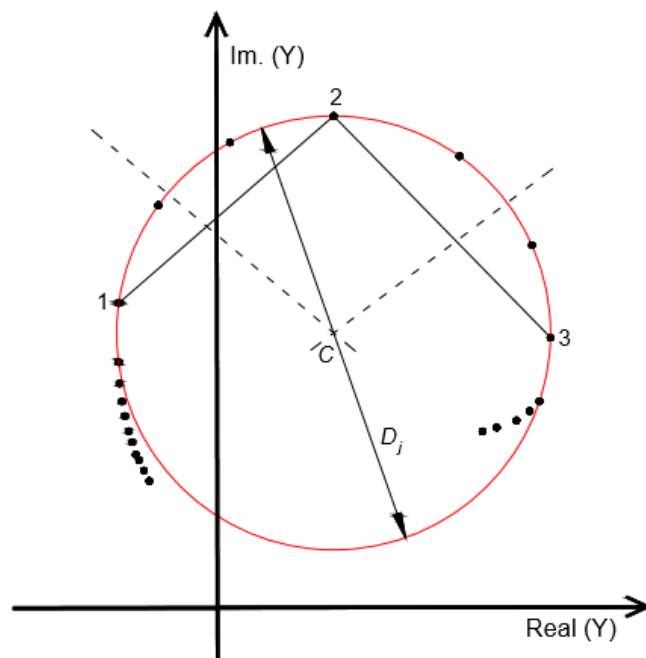
Fig 3.2: Fitting a circle.

The role of step 3 is to estimate the natural frequency of the fitted mode. This is done by a construction of the radial lines from the circle center to the frequency points around the resonance and by the calculation the angles they subtend with each other. The frequency at which this angle reaches its maximum can be taken as the natural frequency. All this process is performed numerically. Fig 3.3 illustrates this step.

The alternative way of the estimation of the natural frequency can be done from following these sequences:

      a) The maximum magnitude of the response.

      b) Maximum imaginary part of the response.

      c) Zero real part of the response.
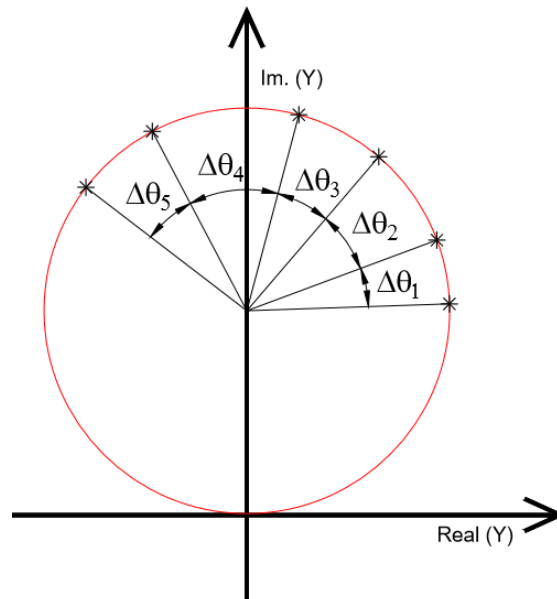
Fig 3.3: Location of the natural frequency

Next, in step 4 damping estimates are computed using every possible combination from selected set of points below and above resonance as shown in Fig 3.4 using the equation (3, 11) for all cases of FRF.

$$\zeta_r = \frac{\omega_a^2 - \omega_b^2}{2\omega_r \left(\omega_a \tan\left(\frac{\theta_a}{2}\right) + \omega_b \tan\left(\frac{\theta_b}{2}\right)\right)} \qquad (3,11)$$

This formula is expressed in Fig 3.4. From this process we can estimate a great amount of the damping factors.
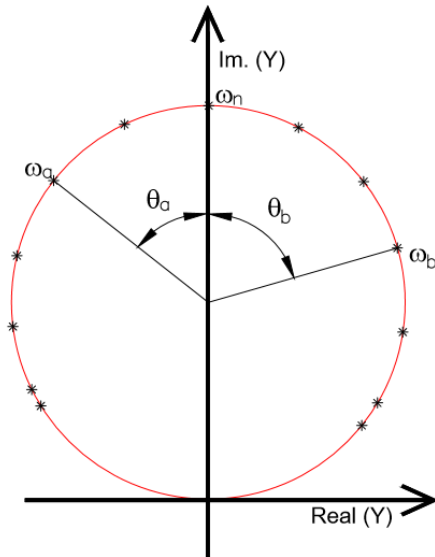
Fig 3.4: damping estimates

It is convenient to plot these data into a 3D graph. Where x-axis represents the frequencies below the resonance, y-axis represents frequencies above the resonance and the z-axis is for the damping factor. An example of this graph is given in Fig 3.5.

This graph should be extracted for every FRF. This graph is very useful in diagnosing the quality of the total analysis. More about these practices is written [1]. As the final estimate of
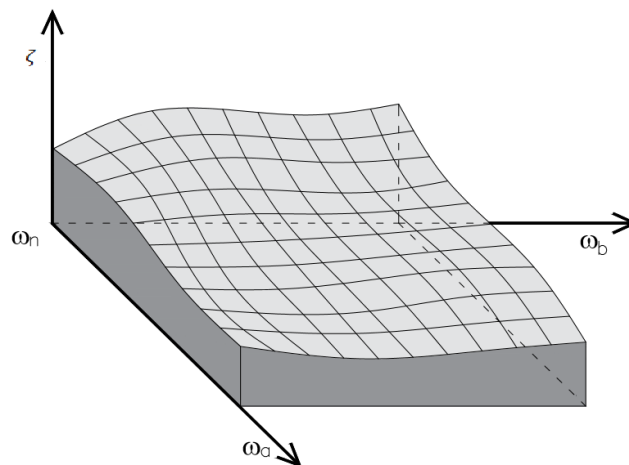
Fig 3.5: plot of damping estimates

The final estimate of damping factor is taken as the mean of all values together. Along with its deviation. If the deviation reach less than 5%, then the analysis. However, the scatter around 20% [6] or more can indicate a serious error in the

44

measured data or the analyzing process itself. Therefore, special caution should be paid in these cases.

The final, step involves a determination of the modal constant. This is done in two sub-steps. First the magnitude of the modal constant is calculated from.

$$A_{pq}{}^r = 2D_{pq}{}^r \omega_r{}^2 \zeta \quad \text{Receptance} \tag{3,12}$$

$$A_{pq}{}^r = 2D_{pq}{}^r \omega_r \zeta \quad \text{Mobility} \tag{3,13}$$

$$A_{pq}{}^r = 2D_{pq}{}^r \zeta \quad \text{Inertance} \tag{3,14}$$

If these three cases are scaled by ω_r or $\omega_r{}^2$, their result will be the same Modal constant.

Second, the sign of the Modal constant depends on the sign of the imaginary part of the FRF

Demonstration

By considering the mobility with a viscous damping case, then selecting a small range of frequency in the vicinity of the natural frequency of mode r, the following formulae is obtained:

$$Y(j\omega) = \frac{j\omega}{k - \omega^2 m + j\omega c} = \frac{\omega^2 c + j\omega(k - \omega^2 m)}{(k - \omega^2 m)^2 + (\omega c)^2} \tag{3,15}$$

With,

$$Re(Y) = \frac{\omega^2 c}{(k - \omega^2 m)^2 + (\omega c)^2} \tag{3,16}$$

And

$$Im(Y) = \frac{\omega(k - \omega^2 m)}{(k - \omega^2 m)^2 + (\omega c)^2} \qquad (3,17)$$

Thus the following expression is considered.

$$U = \left(Re(Y) - \frac{1}{2c}\right) \quad \text{and} \quad V = Im(Y) \qquad (3,18)$$

The relation between U and V holds:

$$U^2 + V^2 = \frac{((k - \omega^2 m)^2 + (\omega c)^2)^2}{4c^2((k - \omega^2 m)^2 + (\omega c)^2)^2} = \left(\frac{1}{2c}\right)^2 \qquad (3,19)$$

Therefore, a plot of $Re(Y)$ vs. $Im(Y)$ for $\omega = 0 \rightarrow \infty$ will trace out a circle of radius $\frac{1}{2c}$ and with center$\left(\frac{1}{2c}; 0\right)$, as illustrated clearly in Fig 3.6.
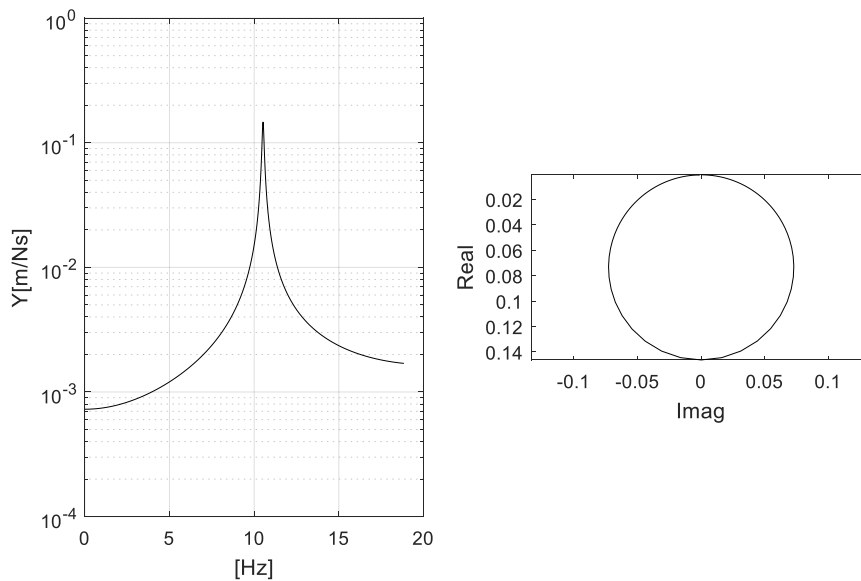
Fig 3.6: Mobility FRF of viscously damped SDOF system- Nyquist plot.

Now with considering the Mobility FRF with MDOF system and viscously damping, the assumption is expressed as follows:

$$Y_{ij}(j\omega) = \sum_{s=1}^{N} \frac{j\omega A_{pq}{}^{s}}{\omega_s{}^2 - \omega^2 + 2j\zeta\omega_s\omega} \tag{3,20}$$

Or can be rewritten as:

$$Y_{ij}(j\omega) = \frac{j\omega A_{pq}{}^{r}}{\omega_r{}^2 - \omega^2 + 2j\zeta_r\omega_r\omega} + \sum_{\substack{s=1 \\ \neq r}}^{N} \frac{j\omega A_{pq}{}^{s}}{\omega_s{}^2 - \omega^2 + 2j\zeta_s\omega_s\omega} \tag{3,21}$$

Now, the so-called SDOF assumption is that if one considers only a frequency range in the close vicinity of a resonance frequency of a MDOF system, the FRF will be strongly dominated by the term corresponding to the mode under examination with the collective contribution of all the other modes remaining nearly constant throughout the considered frequency range.

Mathematically this assumption can be defined by the following:

$$Y_{pq}(j\omega)_{\omega=\omega_r} \cong \frac{j\omega A_{pr}{}^{r}}{\omega_r{}^2 - \omega^2 + 2j\zeta_r\omega_r\omega} + B_{pq}{}^{r} \tag{3,22}$$

In Fig 3.7 an example explains this equation. Using a 3DOF system, the mobility has been computed. The vicinity of the second mode marked in the figure was illustrated in the first term, it is related by the mode under examination that describes a circle in the complex plan scaled and rotated by multiplication with a complex number $A_{pq}{}^{r}$. Similarly, the two other modes were separately illustrated in the second term representing the combination of all other modes describe a single point in the complex plan.

47
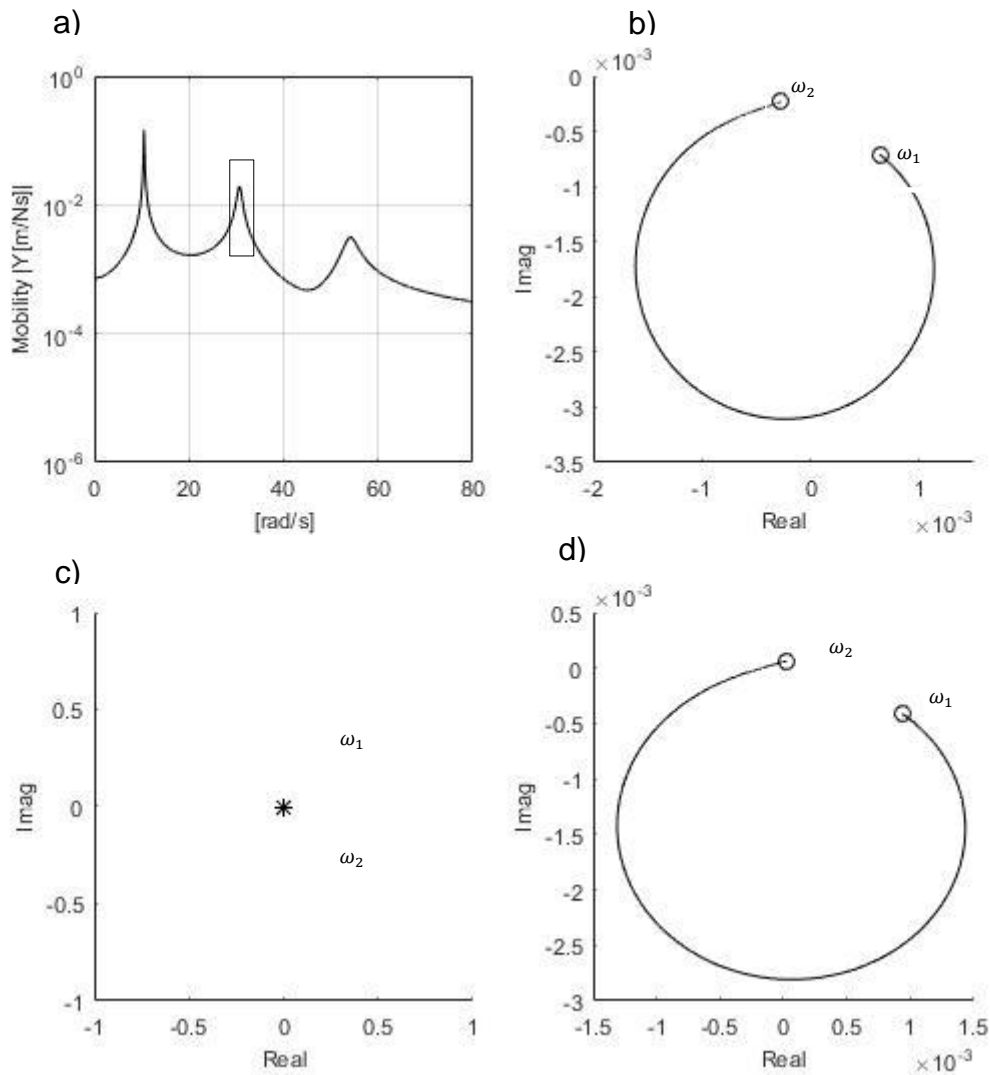
Fig 3.7 : a) Amplitude of 3 DOF system, b) Nyquist plot of the first term, c) second term and d) represent the whole eq. 2,22 when $\omega \sim \omega_r$.

As mentioned before, the Fig 3.7 represent the Mobility of a viscously damped system, and the equation (3, 22) describes a circle disposed in the complex plan by adding the complex constant $B_{pq}{}^r$ as well as scaled and rotated by the modal constant $A_{pq}{}^r$. Obviously the basic property of the modal circle did not change by the operations of scaling, rotating and displacing in the complex plan. Therefor if the Mobility FRF of SDOF by equation (3, 15) and equations (3, 16), (3, 17) are considered, the first step can be done (Fitting a circle) using Least Square method. Further information is given in appendix A.
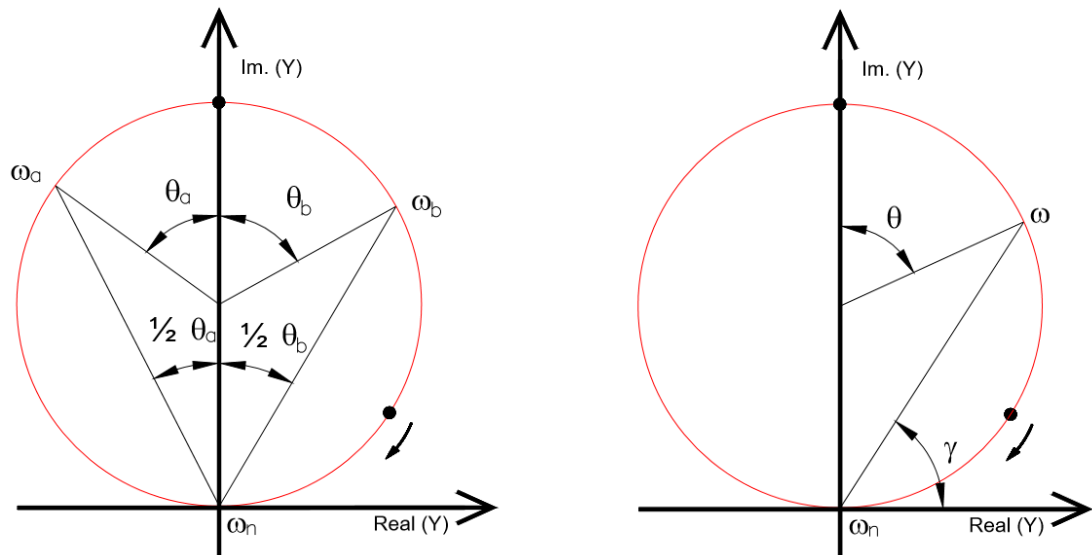
Fig 3.8: Geometric properties of modal circle

For the determination of natural frequency, the Receptance for a structural damping should be used. For this step, the following expressing is considered.

$$\alpha_{pq}(j\omega) = \frac{1}{\omega_r{}^2 - \omega^2 + j\eta_r\omega_r{}^2} \tag{3,23}$$

Basing on the Fig 3.8 the following expression was extracted:

$$tan(\gamma) = \frac{\eta_r}{\left(1 - \left(\frac{\omega}{\omega_r}\right)^2\right)} \tag{3,24}$$

The relation between γ and θ is:

$$90° - \gamma = \frac{\theta}{2} \tag{3,25}$$

Thus,

$$tan\left(\frac{\theta}{2}\right) = \frac{\left(1 - \left(\frac{\omega}{\omega_r}\right)^2\right)}{(\eta_r)} \qquad (3,26)$$

From which we obtain:

$$\omega^2 = \omega_r^2 \left(1 - \eta_r \tan\left(\frac{\theta}{2}\right)\right) \qquad (3,27)$$

If one derived with respect to θ the equation (3, 27). Then, for obtaining the maximum frequency, it must be differentiated respecting to ω as expressed below::

$$\frac{d\theta}{d\omega}\left(\frac{d\omega^2}{d\theta}\right) = 0 \quad \text{when} \quad \omega^2 - \omega_r^2 = 0 \rightarrow \omega = \omega_r \qquad (3,28)$$

For the determination of the natural frequency for a structural damped the Receptance was used, since in this way an exact estimation can be achieved . As for a viscously damped system, the Receptance can merely give an estimation of the natural frequency.

For the determination of damping factor recalling equation (3, 16) and (3, 17) :

$$tan\left(\frac{\theta}{2}\right) = \frac{Im(Y)}{Re(Y)} = \frac{\omega(k - \omega^2 m)}{\omega^2 c} = \frac{\left(1 - \left(\frac{\omega}{\omega_r}\right)^2\right)}{\left(\frac{2\zeta\omega}{\omega_r}\right)} \qquad (3,29)$$

If one takes two points *a* and *b* from the Fig.3.8 with $\omega_a > \omega_r$ and $\omega_b < \omega_r$ we obtain the following equations:

$$tan\left(\frac{\theta_a}{2}\right) = \frac{\left(\left(\frac{\omega_a}{\omega_r}\right)^2 - 1\right)}{\left(\frac{2\zeta\omega_a}{\omega_r}\right)}$$

(3,30)

In a similar fashion;

$$tan\left(\frac{\theta_b}{2}\right) = \frac{\left(1 - \left(\frac{\omega_b}{\omega_r}\right)^2\right)}{\left(\frac{2\zeta\omega_b}{\omega_r}\right)}$$

(3,31)

From equations (3, 30) and (3, 31) the following expression is formulated:

$$\zeta = \frac{\omega_a{}^2 - \omega_b{}^2}{2\omega_r\left(\omega_a \tan\left(\frac{\theta_a}{2}\right) + \omega_b tan\left(\frac{\theta_b}{2}\right)\right)}$$

(3,32)

Basing on different estimation of ω_a and ω_b, the damping factor ζ can be determined, then the scatter of the damping factor will be calculated by the following formulae:

$$\sigma = \sqrt{\frac{1}{N}\sum_{i=1}^{N}(\zeta_i - \bar{\zeta})^2}$$

(3,33)

With,

$$\bar{\zeta} = \frac{1}{N}\sum_{i=1}^{N}\zeta_i$$

(3,34)

The best estimation of the damping factor is when the σ is minor to 5%, and for an improvement in the estimation of the damping, it should be calculate that for all the

FRF (each FRF has been used to determine the frequency and the damping, following the procedure explained before).

As for the constant modal, it can be easily determined by substituting ω=ω$_r$ in the amplitude of the equation (3, 15) ($|Y(i\omega)|$). The following expression is obtained:

$$A_{pq}{}^r = 2D_{pq}{}^r \omega_r \zeta$$

This procedure has been repeated for each FRF, therefore, we can determine the whole vector of the mode shape, reminding that the modal constant sign depends of the imaginary part sign of the FRF.

This method has some limits because, it can gives erroneous answer when the modal coefficient is approximate to zero, also the modes should be well separated., the damping must be a proportional, and the mode shapes values are given as real numbers [1].

3.1.3   Rational Fraction Polynomial.

The Rational Fraction Polynomial method was first presented in 1982 [14], and is the most popular method and widely used in MDOF. This method works in the Frequency Domain, and it is SISO MDOF. The Rational Polynomial Method(RFP). Is a special version of the general Curve-Fitting [6], but it is based on the FRF which is expressed in the Rational fraction form. Thus the FRF requires an expression of the frequency response function as the ratio of two polynomials, with the roots of numerator permitting to determine the modal constant while the roots of the denominator yielding the poles (frequency, damping). Generally the numerator and the denominator orders are independent one of the others. The denominator is considered as the characteristic polynomial of the system. By Curve-Fitting FRF against the analytical form in equation (3, 36), and then solving the roots of both the numerator and the characteristic polynomials, the zeros and poles of the FRF can be determined [21] [23].

Curve- Fitting in the RFP consists of finding the unknown a_k (k=0,1.....2N-1) and b$_k$ (k=0,1.....2N), when the error between the analytical expression (3,36) and FRF is minimized in the chosen frequency range, the result of the liner equation often

involves ill conditioned matrices [24] [25]. The initial estimate to obtain the modal parameters is usually done using the Least Square Method.

The FRF in term of the Receptance, for a linear system with N-DOF and viscous damping can be giving by the partial fraction form [1].

$$\alpha(j\omega) = \sum_{r=1}^{N} \frac{A_r + \omega B_r j}{\omega_r^2 - \omega^2 + 2\zeta_r \omega_r \omega j} \tag{3,35}$$

Where A_r and B_r are constants, the expression can be written as the ratio of two polynomials in $j\omega$.

$$\alpha(j\omega) = \frac{\sum_{k=0}^{2N-1} a_k (j\omega)^k}{\sum_{k=0}^{2N} b_k (j\omega)^k} \tag{3,36}$$

The difference between the analytical FRF $\alpha(j\omega)$ and the experimental FRF $\tilde{\alpha}(j\omega)$ is the error function given by:

$$e_i = \frac{\sum_{k=0}^{2N-1} a_k (j\omega)^k}{\sum_{k=0}^{2N} b_k (j\omega)^k} - \tilde{\alpha}(j\omega) \tag{3,37}$$

The error function is linearized by working with the following modified error function:

$$e_i' = e_i \sum_{k=0}^{2N} b_k (j\omega_i)^k \tag{3,38}$$

And take $b_{2N}=1$;

$$e_i' = \sum_{k=0}^{2N-1} a_k (j\omega_i)^k - \tilde{\alpha}(j\omega) \left[\sum_{k=0}^{2N} b_k (j\omega_i)^k + (j\omega_i)^{2N} \right] \tag{3,39}$$

Now, an error vector for all the *L* measured frequencies can be defined.

$$\{E\} = \begin{pmatrix} e'_1 \\ e'_2 \\ . \\ . \\ . \\ e'_L \end{pmatrix} \quad\quad (3,40)$$

Basing on the equation (3, 39) the following expression was developed:

$$\{E\} = \begin{pmatrix} 1 & (j\omega_1)^1 & (j\omega_1)^2 & \dots & (j\omega_1)^{2N-1} \\ 1 & (j\omega_2)^1 & (j\omega_2)^2 & \dots & (j\omega_2)^{2N-1} \\ \vdots & \vdots & \vdots & \dots & \vdots \\ 1 & (j\omega_L)^1 & (j\omega_L)^2 & \dots & (j\omega_L)^{2N-1} \end{pmatrix} \begin{pmatrix} a_0 \\ a_1 \\ \vdots \\ a_{2N-1} \end{pmatrix} - \quad (3,41)$$

$$\begin{pmatrix} \breve{\alpha}(j\omega_1) & \breve{\alpha}(j\omega_1)(j\omega_1) & \dots & \breve{\alpha}(j\omega_1)(j\omega_1)^{2N-1} \\ \breve{\alpha}(j\omega_2) & \breve{\alpha}(j\omega_2)(j\omega_2) & \dots & \breve{\alpha}(j\omega_2)(j\omega_2)^{2N-1} \\ \vdots & \vdots & \dots & \vdots \\ \breve{\alpha}(j\omega_L) & \breve{\alpha}(j\omega_L)(j\omega_L) & \dots & \breve{\alpha}(j\omega_L)(j\omega_L)^{2N-1} \end{pmatrix} \begin{pmatrix} b_0 \\ b_1 \\ \vdots \\ b_{2N-1} \end{pmatrix} -$$

$$\begin{pmatrix} \breve{\alpha}(j\omega_1)(j\omega_1)^{2N} \\ \breve{\alpha}(j\omega_2)(j\omega_2)^{2N} \\ \vdots \\ \breve{\alpha}(j\omega_L)(j\omega_L)^{2N} \end{pmatrix} .$$

Or

$$(3,42)$$

$$\underbrace{\{E\}}_{(Lx1)} = \underbrace{[P]}_{(Lx2N)} \times \underbrace{\{a\}}_{(2Nx1)} - \underbrace{[T]}_{(Lx2N)} \times \underbrace{\{b\}}_{(2Nx1)} - \underbrace{\{W\}}_{(Lx1)}$$

In the intention to calculate *a* and *b*, the equation (3, 43) will be minimized by the Least Square Method, minimizing a squared error function **J**:

$$(3,43)$$

$$J = \{E^*\}^T\{E\}$$

Substituting equations (3, 42) in (3, 43) and after performing some development [3], the following formula was obtained:

$$J = \{a\}^T Re([P^*]^T[P])\{a\} + \{b^T\}Re([T^*]^T[T])\{b\} \quad (3,44)$$
$$+ \{W^*\}^T\{W\} - 2\{a\}^T Re([P^*]^T[T])\{b\}$$
$$- 2\{a\}^T Re([P^*]^T\{W\}) + 2\{b\}^T Re([T^*]^T\{W\})$$

To minimize **J**, it was derived respecting to **a** and **b** and set these equal to zero:

$$\frac{\partial J}{\partial\{a\}} = 0 \; ; \; \frac{\partial J}{\partial\{b\}} = 0 \qquad (3,45)$$

Solving these equations, the result became:

$$Re([P^*]^T[P])\{a\} - Re([T^*]^T[T])\{b\} - Re(\{P^*\}^T\{W\}) = \{0\} \quad (2,46)$$

Also,

$$Re([T^*]^T[T])\{b\} - Re([T^*]^T[P])\{a\} + Re([T^*]^T\{W\}) = \{0\} \quad (3,47)$$

In matrix form,

$$\begin{pmatrix} [Y] & [X] \\ [X]^T & [Z] \end{pmatrix} \begin{pmatrix} \{a\} \\ \{b\} \end{pmatrix} = \begin{pmatrix} \{G\} \\ \{F\} \end{pmatrix} \qquad (3,48)$$

Where,

$$[Y] = Re([P^*]^T[P])$$

$$[X] = -Re([P^*]^T[T])$$

$$[Z] = Re([T^*][T])$$

$$\{G\} = Re([P^*]^T\{W\})$$

$$\{F\} = -Re([T^*]\{W\})$$

It is possible from this equation to calculate **a, b**, but both the matrices [P] and [T] are found to be ill conditioned. Hence, to solve this, another refinement of the method will be used like *Gradient method* [26] or the *orthogonal polynomial;* the most popular method used that is counseled by Richardson and Formenti [24] [25]. These methods improve the numerical calculation of the resulting coefficient estimates beneficial to extract the natural frequencies, damping ratio and mode shapes. In this case better conditioned equations are developed. Once the coefficients a_0, a_1 . . . . etc b_0, b_1 . . . . . etc has been calculated, the modal parameters will be obtained. This is usually done by solving the two polynomial expressions; from the denominator the roots were determined. then the poles of the system were known, and from the numerator the zeros (Modal Constant) were determined using the partial fractions method. . More information regarding the orthogonal polynomial can be found in [14] [24] [25].

For the application of this method a stabilization diagram shall be constructed increasing the number of order step by step, and then the poles for each iteration will be calculated, hence; the cluster of poles can be chosen after rejecting all the unwanted poles corresponding to the non-physical modes. If a good cluster for a high number of order is unclear, re-run the analysis for slightly different frequency range selection all of which embrace the modes of interest.

After the cluster of poles were obtained, for checking the modals parameters, the Curve-Fitting was regenerated and compared by the original FRF, using a modal validation Known in the literature likewise, Frequency Response Assurance Criterion (FRAC).

3.1.4   Least Square Complex Exponential Method

Firstly the complex exponential method (CE) was introduced by the University of Cincinnati [10] [27], Structural Dynamics Reasearch Lab (UC-SDRL) in 1974 and it is SISO. After the Least Square Complex Exponential Method was developed jointly by the UC-SDRL and the University of Leuven, Belgium in 1977 basing on the theory of CE, and it is SIMO. Then the Polyreference Time Domain (PTD) was created as an extention of the LSCE and it is MIMO. This alghorithm was

developed by Vold at SRDC. All these methods work in the time domain, and are used the impulse response function as data. These algorithms are still the most commonly used algorithms today.

In this thesis we will describe in detail the theory of LSCE and its implementation in Matlab. This method starts using the FRF receptance [6] [7] of a general MDOF system with a general viscous damping.

$$\alpha_{ij}(j\omega) = \sum_{r=1}^{2N} \frac{A_{ij}^{\ r}}{j\omega - \lambda_r} \tag{3,49}$$

The CE works with the corresponding impulse response function(IRF), obtained by an inverse Fourier Trasformation of equation (3, 49) as follow:

$$h_{ij}(t) = \sum_{r=1}^{2N} A_{ij}^{\ r} e^{\lambda_r t} \tag{3,50}$$

With, $t=[0, \Delta t, 2\Delta t, \ldots, (N-1)\Delta t]$;

It is convenient to use an abbreviation notion, as follows:

$$\begin{cases} C_r = A_{ij}^{\ r} \\ V_r = e^{\lambda_r t} \end{cases}$$

Thus, for the lth-Sample, we have:

$$h_l = \sum_{r=1}^{2N} C_r V_r^{\ l} \quad l = 0, 1, \ldots, N-1 \tag{3,51}$$

Which, when extended the equation (3, 51) to the full data set of l samples, gives:

$$\left\{\begin{array}{l} h_0 = h(0.\Delta t) = C_1 + C_2 + \ldots + C_{2N} \\ h_1 = h(1.\Delta t) = C_1 V_1 + C_2 V_2 + \ldots + C_{2N} V_{2N} \\ \vdots \\ h_l = h(l.\Delta t) = C_1 V_1{}^l + C_2 V_2{}^l + \ldots + C_{2N} V_{2N}{}^l \end{array}\right.$$

In matrix form;

$$\begin{bmatrix} 1 & 1 & 1 & \cdots & 1 \\ V_1 & V_2 & V_3 & \cdots & V_{2N} \\ \vdots & \vdots & \vdots & \vdots & \vdots \\ V_1{}^l & V_2{}^l & V_3{}^l & \cdots & V_{2N}{}^l \end{bmatrix} \begin{bmatrix} C_1 \\ C_2 \\ \vdots \\ C_{2N} \end{bmatrix} = \begin{bmatrix} h_0 \\ h_1 \\ \vdots \\ h_{2N} \end{bmatrix}$$

Or,

(3,53)

$$[V][C] = [h]$$

We know the values of h_i, but we don't know C_r and V_r ;

This equation will be solved using Prony's Method, the roots λ_r for a under damped system that always occurs in complex conjugate pairs regardless the values of the modified variable V_r . There will always exist a polynomial in Vr of order l with a real coefficients β, called the autoregressive [16] coefficient such that the following relative equation is verified:

$$\beta_0 + \beta_1 V + \beta_2 V^2 + \ldots + \beta_l V^l = 0 \qquad (3,54)$$

Or,

(3,55)

$$\sum_{i=0}^{l} \beta_i V^i = 0$$

For which the roots are V_1 , V_2 , $\ldots$, V_l ;

Now considering the *l* the number of data points from Impulse Response Function (IRF); it is convenient to take *l* = 2N, (the number of DOF N is equal the number of simple points).

Substituiting the roots in equation (3, 55) we can write the following equation:

$$\sum_{i=0}^{2N} \beta_i V_r^i = 0 \tag{3,56}$$

In order to calculate the coefficient β to evaluate the V_r , multiply both sides of equation (3, 51) by β_0 to β_l, Thus :

$$\sum_{i=0}^{2N} \beta_i h_i = \sum_{i=0}^{2N} \left(\beta_i \sum_{r=1}^{2N} C_r V_r^i \right) = \sum_{r=1}^{2N} \left(C_r \underbrace{\sum_{r=1}^{2N} \beta_i V_r^i}_{=0} \right) \tag{3,57}$$

Thus every term of the equation (3, 57) becomes zero

$$\sum_{i=0}^{2N} \beta_i h_i = 0 \tag{3,58}$$

Or,

$$\sum_{i=0}^{2N-1} \beta_i h_i = -h_{2N} \qquad \text{by setting } \beta_{2N} = 1 \tag{3,59}$$

In matrix form the equation (3, 59) can be written as:

$$[h_0 \quad h_1 \quad \dots \quad h_{2N-1}] \begin{bmatrix} \beta_0 \\ \beta_1 \\ \vdots \end{bmatrix} = -h_{2N}$$

Now, the entire process can be repeated from equation substituting t_0 by t_1.

$$[h_1 \quad h_2 \quad \dots \quad h_{2N}] \begin{bmatrix} \beta_0 \\ \beta_1 \\ \vdots \end{bmatrix} = -h_{2N+1}$$

Successive applications of this procedure lead to a full set of 2N equation.

(3,60)

$$\begin{bmatrix} h_0 & h_1 & h_2 & \cdots & h_{2N-1} \\ h_1 & h_2 & h_3 & \cdots & h_{2N} \\ \vdots & \vdots & \vdots & \vdots & \vdots \\ h_{2N-1} & h_{2N} & h_{2N+1} & \cdots & h_{4N-1} \end{bmatrix} \begin{bmatrix} \beta_1 \\ \beta_2 \\ \vdots \\ \beta_{2N-1} \end{bmatrix} = - \begin{bmatrix} h_{2N} \\ h_{2N+1} \\ \vdots \\ h_{4N-1} \end{bmatrix}$$

Or,

(3,61)

$$\underbrace{[h]}_{2N\text{x}2N} \underbrace{[\beta]}_{2N\text{x}1} = \underbrace{[\tilde{h}]}_{2N\text{x}1}$$

It should be noted that noise disturbances can be averaged out by considering a number of measured values much greater than the model order (the number of rows 2N for [h] >> the number of columns n), in this case we end up with an overdetermined system to solve.

$$\beta = -([h]^T[h])^{-1}[h][\tilde{h}] \tag{3,62}$$

Knowing the coefficient $\beta_0, \beta_1, \dots \beta_{2N-1}$, the equation (3, 62) can be solved to yield the V_r roots. Then the poles λ_r can be calculated as.

$$\lambda_r = \frac{\ln(V_r)}{\Delta t} \tag{3,63}$$

Then, the natural frequency ω_r and the damping ratio ζ_r can be determined, as following:

$$\omega_r = \frac{|\lambda_r|}{2\pi} \; and \; \zeta_r = \frac{-Re(\lambda_r)}{|\lambda_r|} \tag{3,64}$$

The modes shapes of the system can be calculated by substituting the [V] in the equation (3, 53).

$$\tag{3,65}$$

$$
\begin{bmatrix}
1 & 1 & 1 & \cdots & 1 \\
V_1 & V_2 & V_3 & \cdots & V_{2n} \\
\vdots & \vdots & \vdots & \vdots & \vdots \\
V_1{}^{2N-1} & V_2{}^{2N-1} & V_3{}^{2N-1} & \cdots & V_{2n}{}^{2N-1}
\end{bmatrix}
\begin{bmatrix}
C_1 \\ C_2 \\ \vdots \\ C_{2n}
\end{bmatrix}
=
\begin{bmatrix}
h_0 \\ h_1 \\ \vdots \\ h_{2N-1}
\end{bmatrix}
$$

In matrix form;

$$\underbrace{[V]}_{2N\mathrm{x}2n} \; \underbrace{[C]}_{2n\mathrm{x}1} = \underbrace{[h]}_{2N\mathrm{x}1} \tag{3,66}$$

The system matrix *[V]* has dimension *(2N) X (2n)* with *2N > 2n* and is complex. Equation (3, 66) also to be solved in a Least –Square sense.

$$[C] = ([V]^T[V])^{-1}[V][h] \tag{3,67}$$

The LSCE is the extension of the previous procedure to SIMO method. Processing several IRFs from response locations simultaneously is the straightforward. In the

sense the coefficients β$_i$ do not [depend on the particular IRF considered. *p* response locations the following system is to be solved:

$$\begin{bmatrix} [h_{11}] \\ [h_{12}] \\ \vdots \\ [h_{1p}] \end{bmatrix} \begin{bmatrix} \beta_0 \\ \beta_0 \\ \vdots \\ \beta_{2n} \end{bmatrix} = \begin{bmatrix} [\tilde{h}_{11}] \\ [\tilde{h}_{12}] \\ \vdots \\ [\tilde{h}_{1p}] \end{bmatrix}$$

(3,68)

Or,

$$\underbrace{[H]}_{2N \times 2n} \underbrace{[\beta]}_{2n \times 1} = \underbrace{[\tilde{H}]}_{2N \times 1}$$

(3,69)

Now the least square solution can be found as the following;

$$\beta = -([H]^T [H])^{-1} [H][\tilde{H}]$$

(3,70)

Knowing β we can find the V_r and then we can find the poles λ$_r$

For the modal constant we can find it following procedure.

$$\begin{bmatrix} 1 & 1 & 1 & \cdots & 1 \\ V_1 & V_2 & V_3 & \cdots & V_{2n} \\ \vdots & \vdots & \vdots & \vdots & \vdots \\ V_1^{2N-1} & V_2^{2N-1} & V_3^{2N-1} & \cdots & V_{2n}^{2N-1} \end{bmatrix} \begin{bmatrix} C_{11}^{1} \\ C_{11}^{2} \\ \vdots \\ C_{11}^{2n} \end{bmatrix}$$

(3,71)

$$= \begin{bmatrix} h_{11}(0.\Delta t) \\ h_{11}(1.\Delta t) \\ \vdots \\ h_{11}(N\Delta t) \end{bmatrix}$$

Or,

$$[V][C_{11}] = [h_{11}]$$

(3,72)

Knowing the [V] and the [h_{11}] we can find the first rows of the modal constant matrix by the LS. Then the whole vector of the modal constant will be obtained repeating this procedure for each IRFs.

A stabilization diagram will be construct for determine the poles and the modes shapes, starting by number of order 1 to 2n.

3.1.5   Eigen system Realization Algorithm.

Eigensystem Realization Algorithm (ERA) was developed by Juang & Pappa at the Nasa Langely Research Center in 1985 [14] [20] [22] [28]. The ERA works in the time domain and it's MIMO. This method begins with the definition of the Markov parameter of a state-space modal.

Consider a discrete time state space model described previously in the chapter two:

$$x(k+1) = Ax(k) + Bu(k) \qquad\qquad (3,73)$$
$$y(k) = Cx(k) + Du(k)$$

Let consider the response as an impulse at *k=0*, and the first input a Delta Dirac:

$$(3,74)$$

$$\begin{cases} u(0) = 1; \\ u(k) = 0, \qquad k > 0 \\ D = 0 \end{cases}$$

Assume an impulse force at *k=0*, with 0 initial conditions. Thus by iterating system of equation (3, 73) in time. We have the following parameters:

$$x(0) = 0; \qquad\qquad\qquad \rightarrow\ y(0) = 0; \qquad\qquad (3,75)$$
$$x(1) = Ax(0) + Bu(0) = B \quad \rightarrow\ y(1) = CB;$$
$$x(2) = AB; \qquad\qquad\qquad \rightarrow y(2) = CAB;$$
$$x(3) = Ax(2) = A^2B \qquad\quad \rightarrow y(3) = CA^2B;$$

In general

$$y(k) = \underbrace{[C]}_{(p \times 1)} \underbrace{[A]^{k-1}}_{(p \times 2N)} \underbrace{[B]}_{(2N \times 2N)} \quad (2N \times 1)$$ (3,76)

Considering the impulse at all the *q* location, the expression obtained is;

$$Y(k) = \underbrace{[C]}_{(p \times q)} \underbrace{[A]^{k-1}}_{(p \times 2N)} \underbrace{[B]}_{(2N \times 2N)} \quad (2N \times q)$$ (3,77)

By constructing the Hankel matrix of the Markov parameters *Y(k).*

$$\underbrace{H(k-1)}_{(\alpha p \, \times \, \beta q)} = \begin{bmatrix} Y(k) & Y(k+1) & \dots & Y(k+j) \\ Y(k+1) & Y(k+2) & \dots & Y(k+j+1) \\ \vdots & \vdots & \ddots & \vdots \\ Y(k+i) & Y(k+i+1) & \dots & Y(k+i+j) \end{bmatrix}$$ (3,78)

Where *i*= 1, ... , α-1 and *j*= 1, ... , β-1, α and β are arbitrary integers. And *k>0*;

The matrix *H(k-1)* is equivalent to the matrix product; if there is an initial state response measurement , *H(k-1)* must be simply replaced by *H(k).* Substituting eq (3, 77) in (3, 79) the resulting expression is:

$$\underbrace{\begin{bmatrix} C \\ CA \\ CA^2 \\ \vdots \\ CA^{\alpha-1} \end{bmatrix}}_{Q} \underbrace{[B \quad AB \quad A^2B \quad \dots \quad A^{\beta-1}B]}_{W} = H(k);$$ (3,79)

Thus;

$$H(k) = [Q][A]^k[W] \; with \; k \geq 0$$ (3,80)

[Q] and *[W]* are called observability and controllability matrices respectively. The objective is to reconstruct the *Hankel* matrix *H(k),* from the experimental data. Thus the system matrices become known from the responses of the structure. There can be found an infinite number of the state space matrices *A, B, C* and *D* where each has different dimensions, but the dimension of the system remain unknown Since the number of the modes in the signal is unknown, therefore, there

64

is an infinite number of realizations. In the modal analysis the matter is to determine the matrices *A* and *C*, where the eigenvalues of A consist of the complex conjugates poles of the system. From each poles the natural frequency and the damping ratio can be obtain. The mode shapes is related to the matrix *C*.

The objective is to obtain a minimum realization, the realization corresponding to the minimum order of the state space formulation.

Assume that there exists a matrix $[H]^+$ satisfying the relation.

$$\underbrace{[W]}_{(2Nxq\beta)} \underbrace{[H]^+}_{(q\beta xp\alpha)} \underbrace{[Q]}_{(p\alpha x2N)} = \underbrace{[I]}_{2Nx2N} \tag{3,81}$$

Let us pre-multiply and post-multiply equation (3, 81) by *[Q]* and *[W]* respectively:

$$[Q][W][H]^+[Q][W] = [Q][W] \tag{3,82}$$

Using equation (3, 80) and consider k=0 we have;

$$[H(0)] = [Q][W] \tag{3,83}$$

Thus;

$$[Q][W][H]^+[Q][W] = [H(0)] \tag{3,84}$$

Hence;

$$[H(0)][H]'[H(0)] = [H(0)] \tag{3,85}$$

From equation (3, 85) we can note the *[H]'* is the pseudo-inverse of *[H(0)]*:

$$\tag{3,86}$$

$$[H]' = [H(0)]^+$$

Using the singular values decomposition (SVD) for determine the pseudo-inverse of *[H(0)]*. Thus;

$$\underbrace{[H(0)]}_{p\alpha xq\beta} = \underbrace{[U]}_{p\alpha x2N} \underbrace{[\Sigma]}_{2Nx2N} \underbrace{[V]^T}_{2Nxq\beta} \tag{3,87}$$

[U] and *[V]* are orthonormal matrices of singular vector an $[\Sigma]$ is diagonal matrix of singular values, the pseudo inverse of *[H]⁺*:.

$$[H(0)]^+ = [V][\Sigma]^{-1}[U]^T \qquad (3,88)$$

To obtain the realization with $k \geq 0$; let consider the equation (3, 77).

$$Y(k+1) = [C][A]^k[B] \qquad (3,89)$$

Using the identity:

$$Y(k+1) = [E_p]^T[H(k)][E_q] \qquad (3,90)$$

By defining the

$$\underbrace{E_p{}^T}_{\text{pxpα}} = \left\{ \underbrace{[I]}_{[pxp]} \quad \underbrace{[0]}_{[pxp]} \quad \cdots \quad \underbrace{[0]}_{[pxp]} \right\} \qquad (3,91)$$

And

$$\underbrace{E_q}_{\text{qβxq}} = \left\{ \begin{array}{c} \underbrace{[I]}_{qxq} \\ \underbrace{[0]}_{qxq} \\ \vdots \\ \underbrace{[0]}_{qxq} \end{array} \right\} \qquad (3,92)$$

By using equations (3, 80), and (3, 90) a minimum order of realization can be obtained:

$$Y(k+1) = [E_p]^T[Q][A]^k[W][E_q] \qquad (3,93)$$

Substituting eq (3, 81) and (3, 82) in (3, 93);

$$Y(k+1) = [E_p]^T[Q][[W][H]'[Q]][A]^k[[W][H]'[Q]][W][E_q] \qquad (3,94)$$

Substituting eq (3, 83) in (3, 94);

$$Y(k + 1) = [E_p]^T [H(0)] [H]' \left[[Q][A]^k[W]\right] [H]'[H(0)] [E_q] \quad (3,95)$$

$$= [E_p]^T [H(0)] \left[[V_{2N}][\Sigma_{2N}]^{-1}[U_{2N}]^T\right] \left[[Q][A]^k[W]\right] \left[[V_{2N}][\Sigma_{2N}]^{-1}[U_{2N}]^T\right]$$

$$[H(0)][E_q]$$

After some manipulating we can obtain the following expression, for more detail see [3][16];

$$Y(k + 1) = \left[[E_p]^T [U_{2N}][\Sigma_{2N}]^{\frac{1}{2}}\right] \left[[\Sigma_{2N}]^{-\frac{1}{2}}[U_{2N}]^T[H(1)][V_{2N}][\Sigma_{2N}]^{-\frac{1}{2}}\right]^k \quad (3,96)$$

$$\left[[\Sigma_{2N}]^{1/2}[V_{2N}]^T[E_q]\right]$$

Comparing equation (3, 96) and (3, 89) we can determinate the *[C], [A]* and *[B]*:

$$[C] = [E_p]^T [U_{2N}][\Sigma_{2N}]^{\frac{1}{2}} \quad (3,97)$$

$$[A] = [\Sigma_{2N}]^{-\frac{1}{2}}[U_{2N}]^T[H(1)][V_{2N}][\Sigma_{2N}]^{-\frac{1}{2}} \quad (3,98)$$

$$(3,99)$$

$$[B] = [\Sigma_{2N}]^{1/2}[V_{2N}]^T[E_q]$$

Using the matrix *[A]* and by solving the Eigen-problem:

$$(3,100)$$

$$[A][\psi_u] = \Lambda[\psi_u]$$

To determine the modes shapes in terms of the physical coordinate of system, we must use the equation (3, 73). Thus;

$$\underset{px1}{\psi} = [C][\psi_u]$$

<div style="text-align: right">(3,101)</div>

With $\Lambda = \{\Lambda_1, \ \Lambda_2, \ldots, \Lambda_n\}$, is the eigenvalues and $[\psi_u]$ is the eigenvector. Then we can determine the poles as follow:

$$\lambda_i = \frac{\ln(\Lambda_i)}{\Delta t}$$

<div style="text-align: right">(3,102)</div>

Then we can determine the natural frequency and the damping ratio.

3.2   Model Order

In the modal parameter study filed, finding an accurate estimation of model order that corresponds to the physical number of modes presented in the system has always been the main concern of researches. To determine the model order in this thesis, several trusted methods were chosen from the theoretical achieve of this domain [5][7][27]. The simplest method consists of finding the number of peaks in the Frequency Response Function in the frequency band of analysis. In some situation it is difficult to visualize the number of peaks especially where the modes are closely spaced. A more practical procedure for including the peaks present in various FRFs is to determine the summation the functions represented the auto power of the FRFs, represented by the following expression.

$$H_{power} = \sum_{p=1}^{N_0} \sum_{q=1}^{N_i} H_{pq}(\omega) H_{pq}(\omega)^*$$

<div style="text-align: right">(3,103)</div>

These simple techniques are still useful but do not provide an accurate estimate of the model order when there is a vicinity of modes in frequency range

In order to determine a reasonable estimate of the model order presented in the system, some of the commonly used techniques are; measurement synthesis and comparison, rank estimate, Error chart, singular values decomposition, and stability diagram, this thesis focuses only on the last three method

3.2.1 Error Chart

The error chart is a plot of the error in the modal as a function of increasing model order, when the modal order is insufficient this model error will be high, but when the model error has the correct value, the error drops dramatically as can show in the Figure 3.9:
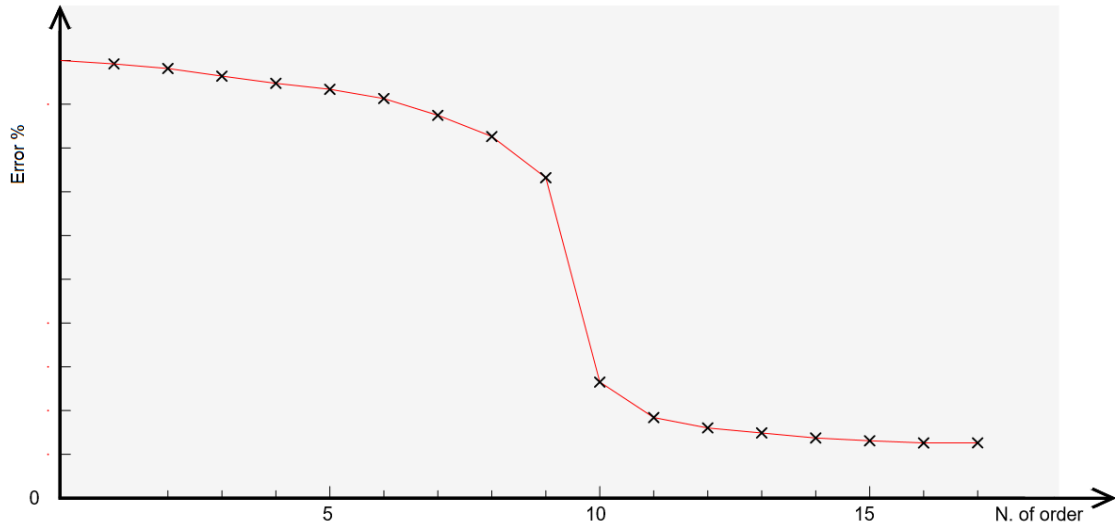
Fig 3.9: Model Order Determination Error Chart.

3.2.2 Singular Values Decomposition

The singular values decomposition serves for the same purpose. The plot of singular values of the Hankel matrix [7]:

$$H = [U][\Sigma][V] \tag{3,104}$$

Where $[U]$ and $[V]$: are orthonormal matrices

$[\Sigma]$: Diagonal matrix of *n_0 singular values :*

$$\sigma_1 \geq \sigma_2 \geq \cdots \geq \sigma_n \geq \sigma_{n+1} \approx \sigma_{n+2} \approx \cdots \cong \sigma_{n_0} \approx 0 \tag{3,105}$$

Indicates the number of present modes n by the fact that σ_{n+1} is close to zero or that the ratio σ_n / σ_{n+1} is very large as show in the Fig 3.10
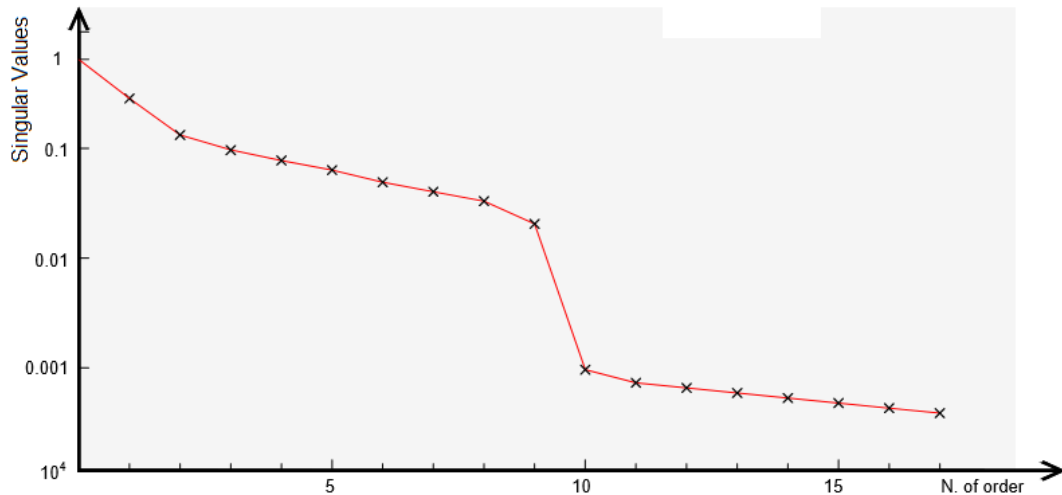
Fig 3.10: Diagram of singular values

3.2.3   Stabilization Diagram

One of the most common methods for [27] [30] determining the number of modes present in the measurement data is the use of stability diagram. This tool used to discriminate physical pole from the spurious. It is obtained by repeating the poles calculation for increasing model order. Each set of poles calculated for a certain model order is compared with the set of poles calculated for the lower model order. If the rth pole at i^{th} model order is not found for the order below *(i-1)* is labeled as new or unstable pole in the stabilization diagram. A pole is considered not fount when there is no pole in a 1% frequency tolerance for lower order.

The Fig 3.11 [10] represents an example for a stabilization diagram that in the vertical axis yields the number of order in the horizontal axis represents the frequency vector.
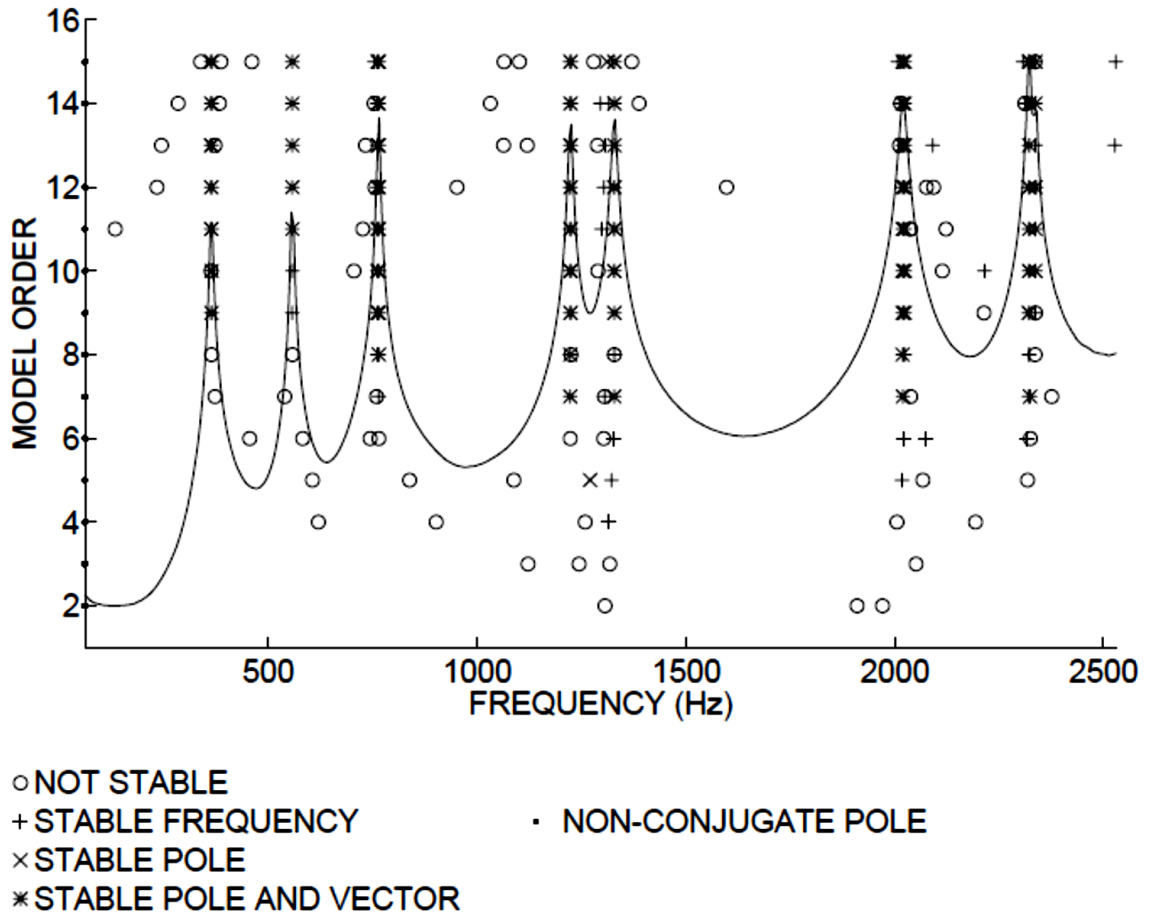
Fig 3.11: Stability diagram [10]

In general the stability diagram has been used for a high number of order [30], but if the concept of stability was expanded to include consistency, a stability diagram can be constructed for almost any modal parameter estimation. In this thesis the stability diagram will be used in three methods LSCE, ERA RFP and Polymax.

The tolerances that were used regarding the frequency and damping ratio in this thesis are:

$$\frac{|f_{i+1} - f_i|}{f_{i+1}} \leq 1\ \% \ (stable\ frequency) \qquad (3,106)$$

$$\frac{|\zeta_{i+1} - \zeta_i|}{\zeta_{i+1}} \leq 5\ \% \ (stable\ damping) \qquad (3,107)$$

$if\ \Delta f \leq 1\%\ and\ \Delta\zeta \leq 5\% \rightarrow (stable\ pole)$. For determining the stable vector a *MAC* will be used.

$$MAC(\psi_{i+1}, \psi_i) =\leq 90\% \tag{3,108}$$

3.3 Modal Assurance Criterion.

Modal Assurance Criterion (MAC) is used widely to compare two modal vectors. MAC values oscillate between 0 and 1. A unitary meaning a perfect correlation. In practice [12], two vector are considered correlated when the MAC is greater than 0.9. The modal Assurance Criterion can only indicate consistency, not validity or orthogonality [29]. It can be used to check the relation between modes within the same set as well, and then it is called auto-MAC.

$$MAC(\psi_{i+1}, \psi_i) = \frac{|\{\psi_{i+1}\}^T\{\psi_i\}^*|^2}{(\{\psi_{i+1}\}^T\{\psi_{i+1}\}^*)(\{\psi_i\}^T\{\psi_i\}^*)} \leq 90\% \tag{3,109}$$

3.4 Frequency Response Assurance Criterion (FRAC).

This criterion is used to compare two frequency response functions. The simple case is a validation procedure that compares the FRF regenerated from the modal parameters extracted with the measured FRF data. The FRFs can be compared over the full or partial frequency range of the FRFs as long as the same discrete frequencies are used in the comparison. It is possible to define the FRAC with the following expression:

$$FRAC_{pq} = \frac{\left|\sum_{\omega=\omega_1}^{\omega_2} H_{pq}(\omega)\widetilde{H}_{pq}^{*}(\omega)\right|^2}{\sum_{\omega=\omega_1}^{\omega_2} H_{pq}(\omega)H_{pq}^{*}(\omega) \sum_{\omega=\omega_1}^{\omega_2} \widetilde{H}_{pq}(\omega)\widetilde{H}_{pq}^{*}(\omega)} \tag{3,110}$$

As MAC a values of one gives perfect correlation, a low values indicate a poor correlation.

Chapter 4

Modal Parameter Estimation Results & Comparisons

Introduction

This chapter is separated in two major sections, the first treats the simulated analytical data and the second discusses the experimental data, it also includes the Experimental Modal Analysis (EMA) and Operation Modal analysis. The necessary plots are shown in order to demonstrate and discuss how the modal parameters are affected with respect to specific parameters. The results of the analytical and the experimental procedures are discussed along with showing how the accuracy of the extracted modal analysis is affected. It is evident that the analytical data result is found more precised because of the acquisition of FRFs without any noise. In this case the error of the modal parameters can be found with a comparison between the analytical case results and the other Methods implemented in MATLAB.

In order to calculate the error of the frequency and the damping, the formulae of equations used are (4, 1) and (4, 2):

$$error\ \% = \frac{\left|f_{analytical} - f_{exctracted}\right|}{f_{analytical}} \cdot 100 \qquad (4,1)$$

$$error\ \% = \frac{\left|\zeta_{analytical} - \zeta_{exctracted}\right|}{\zeta_{analytical}} \cdot 100 \qquad (4,2)$$

For a comparison between the mode shapes in the analytical case employing the LSCE and ERA, only the real part of the mode shapes will be taken into consideration. Afterwards the MAC will be utilized as described in detail formerly in the chapter three:

$$MAC = \frac{|\{\psi_{an}\}^T\{\psi_{ex}\}^*|^2}{(\{\psi_{an}\}^T\{\psi_{an}\}^*)(\{\psi_{ex}\}^T\{\psi_{ex}\}^*)} \qquad (4,3)$$

ψ_{an} : Mode shape extracted by analytical method.

ψ_{ex} : Mode shape extracted by experimental method.

In the Experimental data, for the acquisition of the FRFs the LMS Test-Lab software will be used employing a periodic excitation and the free response from the structure under test (random excitation) [6][7]. In addition, the *Polymax* method will be applied to extract the modal parameters in both cases

In the Experimental Modal Analysis (EMA) (Periodic excitation), the first experiment will be held on a steel plate in condition free-free that will be excited in z direction by a shaker in 15 points as illustrated in the Fig 4.3.1 in order to then measure the FRF's. The second case consider a gearbox in condition free-free. Its system will be excited by a *hammer* in 34 points in x, y, and z direction as shown in Fig 4.4.1.

In the Operation Modal Analysis (OMA) (Random Excitation) an airplane is used. The free responses are measured in the 15 points as displayed in the Fig 4.5.1.

In the Analytical case a system with 3 DOFs will be examined knowing the *M, K, and C* matrices in two states: with modes close to each other and with well separated modes. Subsequently the PP, CF, LSCE, ERA, and RFP Methods will be applied to extract the *frequency, damping and modes shapes.* Thus the results of Frequency and Damping will be reported in the tables numerated from 4.1; to 4.12. Following that the stabilization diagram of the LSCE, ERA and RFP will be plotted for identifying the physical modes.

In the LSCE Method the stable poles that have stability in frequency and damping in the stabilization diagram were plotted. Normally a tolerance, in percentage is given for the stability of each of the modal parameters that are being evaluated. In the LSCE stability diagram the vectors are not engaged, because the non-physical poles appear with the increase of the number of order consequently it will be hard to reach a good estimation of mode shapes. In this state, the best to do is to detect only the stable poles that correspond to physical modes, thus the mode shapes will be determined using equation (3, 53).

Hence to find the physical modes in the ERA the stability of vector (modes shapes) and the stable poles were schemed. In order to compare the mode shapes between the iterations, the MAC was used with a tolerance 90% to identifying the stability of vectors($MAC \geq 90\%$).

Applying the RFP Method, the stability of the vector can be rarely found because when the number of order is increased the ill conditioning problem start to appear. In the Analytical case the stable of vector can be probably seen but this is usually hard to do in the experimental case, this is why its plot was eliminated in the stabilization diagram by RFP. The selection of the most advantageous mode shapes is carried out according to the highest values of the FRAC resulting of a comparison between the FRF synthesized for each mode and the FRF measured.

For the synthesis of the FRF in the analytical case H_{12} was chosen to use, because the mode shapes were normalized respecting to the first element in the column. In this way some information can be collected about the validity of the mode shapes.

Now seeking more precision in the physical modes present in the system, two new strategies will be followed only where the LSCE and ERA are applied.

In the LSCE Method, the error of the *Least Square* for the block-*Hankel* data matrix was calculated [6], to be plotted later in function of the number of order, this offers certain information concerning the number of physical modes presented in the system. Observing the graph, the exact number of modes can be defined where the error chart of least square drops drastically. Similarly in the ERA, the Singular Values Decomposition of the block-*Hankel* matrix was calculated for the same purpose [1], [11].

In the experimental case, in addition to the previously used methods, the LSCE Tool box MATLAB will be employed, the results extracted from this method are to be compared with the LSCE implemented in MATLAB, in the same process used on the results acquired in the analytical case from the other methods applied. At this stage the focus will be laid on the stabilization diagram to extract the physical modes and consequently their modal parameters that will be compared to the modal parameters of the LSCE that have been already implemented. The modes shapes will be compared using the MAC where a histogram will be plotted to see if the mode shapes are similar. In the experimental case, in intent to reach further accuracy in the analysis the Auto-MAC will be used. In this Auto-MAC a set of modes are correlated with themselves, this criterion gives the opportunity to see if a mode of family 1 may appear to correlate equally well with several modes of family 2. All the results from these methods will be validated in comparison with

the Polymax method by Test-Lab software. In this thesis, the Polymax is applied only to determine the diagram of stabilization for the sake of calculating the modal parameters. The Auto-Mac and the synthesis of FRF will be omitted since their results were verified in prior.

In the EMA Method the modes shapes were not normalized in the previously used methods because the modes shapes extracted by Polymax were not normalized, then FRF that has been fitted is H_{11} and the FRAC was determined between the FRF H_{11} measured and H_{11} fitted.

Then all the modes shapes extracted will be plotted, in the Argand plan (Complex Plan) real vs. imaginary part. The last step consist of comparing all the modes shapes already estimated with the mode shapes determined by Polymax method using the MAC.

In the OMA the same procedures were carried out but the application of PP and the CF methods was skipped because the free response presents a high level of noise that makes it difficult to identify the Peaks of the physical modes.

The description of the procedure is illustrated in the Fig 4.1:

First step: report the values of the frequency and the daming ratio in the tables for each method.

Second step: show how the modal paramters are extracted from the PP and CF method in 3 Figures, then the stabilizatian diagram for each methods will be plotted,then the least square error in the LSCE and the Singular Values Decomposition in the ERA will be plotted.

Third step: - comparing the modes shapes using MAC in the analytical case.

- write the Auto-MAC in the experimental case for the LSCE, ERA and RFP.

Foufth step: synthesis of the FRF.

Fifth step: plot the modes shapes.

Seventh step:(only for the experimental case) Compare the modes shapes extracted by Polymax and the modes shapes extracted by LSCE,ERA, and RFP.

Fig 4.1: The procedure applied when the modal analysis methods are used.

4.1   Analytical 3DOFs Vicinity Modes.

Considering a three DOFs system with mass spring and proportional damped, in this section all the procedures of the five methods described in the initial chapter 4 will be applied. Now consider the three matrixes of M, K, and C as follow:

$$M = \begin{bmatrix} 1 & 0 & 0 \\ 0 & 1 & 0 \\ 0 & 0 & 12 \end{bmatrix}; K = \begin{bmatrix} 1800 & -1000 & 0 \\ -1000 & 2000 & -1000 \\ 0 & -1000 & 2100 \end{bmatrix}; C = \begin{bmatrix} 1.801 & -1 & 0 \\ -1 & 2.001 & -1 \\ 0 & -1 & 2.112 \end{bmatrix}.$$

	Frequency [Hz]	Damping factor %
Mode 1	1.675	0.53
Mode 2	4.886	1.54
Mode 3	8.6	2.7

Table 4.1.1: Frequency and damping ratio for system with 3DOF for the analytical method.

	Frequency [Hz]	Damping factor %	Error	
			Freq %	Damp %
Mode 1	1.675	0.54	0.03	1.85
Mode 2	4.885	1.54	0.02	0.04
Mode 3	8.62	2.7	0.23	0.08

Table 4.1.2: Frequency and damping ratio for system with 3DOFfo the PP method.

	Frequency [Hz]	Damping factor %	Error %	
			Freq %	Damp %
Mode 1	1.675	0.534	0.08	0.74
Mode 2	4.885	1.54	0.02	0.05
Mode 3	8.62	2.68	0.23	0.74

Table 4.1.3: Frequency and damping ratio for system with 3DOF for the CF method.

LSCE	Frequency [Hz]	Damping factor %	Error %	
			Freq %	Damp %
Mode 1	1.675	0.507	0.005	4.33
Mode 2	4.885	1.54	0.02	0.04
Mode 3	8.59	2.7	0.11	0.007

Table 4.1.4: Frequency and damping ratio for system with 3DOF for the LSCE method.

	Frequency [Hz]	Damping factor %	Error %	
			Freq %	Damp %
Mode 1	1.625	0.546	2.98	2.93
Mode 2	4.836	1.55	1.02	0.64
Mode 3	8.55	2.7	0.58	0.03

Table 4.1.5: Frequency and damping ratio for system with 3DOF for the ERA method.

RFP	Frequency [Hz]	Damping factor %	Error %	
			Freq %	Damp %
Mode 1	1.675	0.53	5.3e-14	5.37e-12
Mode 2	4.886	1.54	1.63e-13	6.43e-12
Mode 3	8.6	2.7	1.55e-12	6.91e-11

Table 4.1.6: Frequency and damping ratio for system with 3DOF for the RFP method.

Second step: this step clarifies through Fig 4.1.1, 4.1.2, 4.1.3, 4.2.1, 4.2.2 and 4.2.3 how to extract in detail the modal parameters from the PP and the CF Methods, then presents the plots of the stabilization diagrams for LSCE, ERA and *Least square Error, Singular Values Decomposition* respectively.
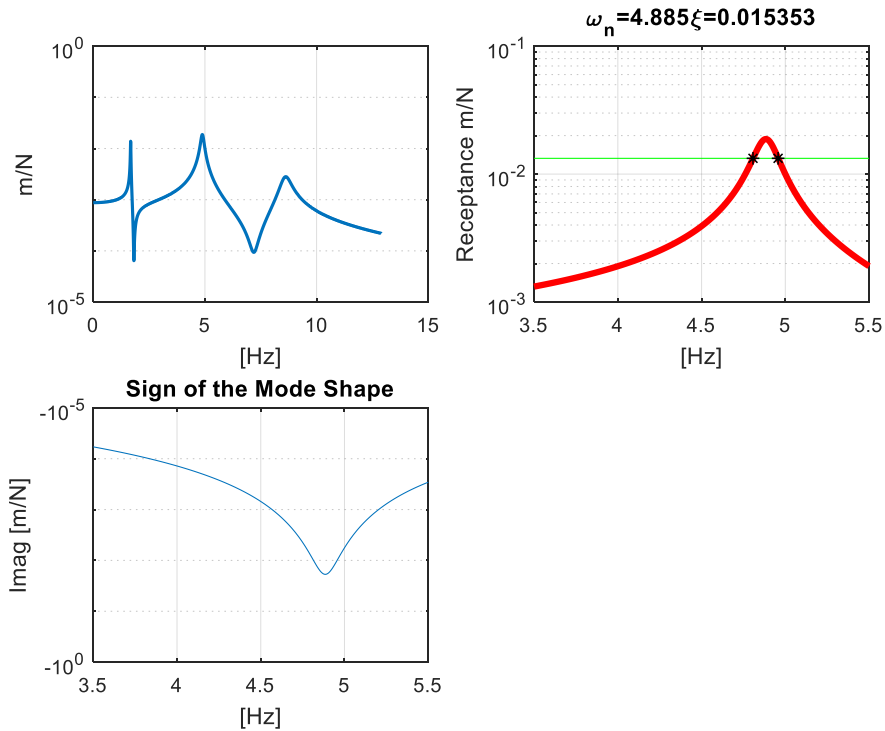
Fig 4.1.1: Estimation the modal parameters of one mode by PP method.

In the figure 4.1.1 the details about the method *PP* are clarified in order to calculate the modal parameter. This figure is composed of three sub-figures, the first on top left illustrate the Receptance for three DOF, the second graph on top right shows the result delivered by the *PP* method when applied to the second mode of the testing system, the red function represent the contribution of the second mode of the FRF, the green line is the function of $H(\omega_n)\big/\sqrt{2}$, the two asterisks in black are the half-power points, then as explained in the Chapter 3, the estimate of the natural frequency correspond to the maximum of the red function and the estimation of the damping depends of the two half-power points that have been used in the equation (3, 7). The third graph permits to determine the sign of the modal constant, then knowing the frequency, the damping and the sign of the second mods, the model parameters can be calculated through the equation (3, 8). To identify the other modal parameters, this procedure will be repeated for each mode.
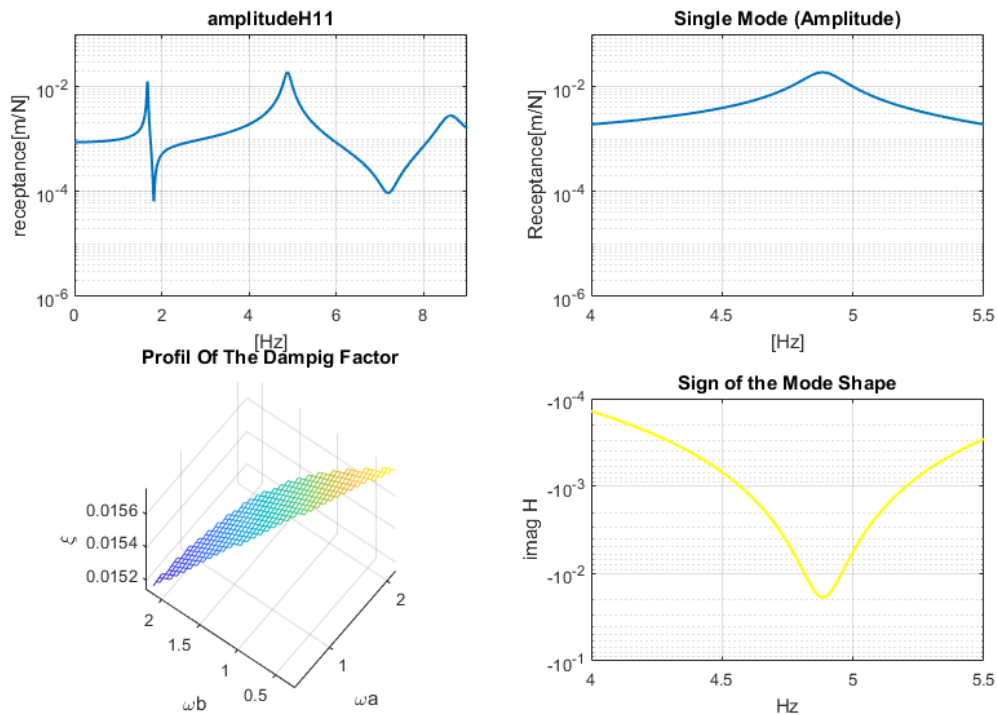
Fig 4.1.2: Estimation the modal parameters of one mode by CF method.

This figure is composed of four sub-figures, the fist on top left represents the Receptance for three DOF, the second on top right presents an isolation of the

single mode for this FRF, the third plots the scatter of the damping values estimated by a set of points (that will be showed in the upcoming figure) below and above the resonance using equation (3, 11). The deviation of this estimate was found equal to 0.0204%.
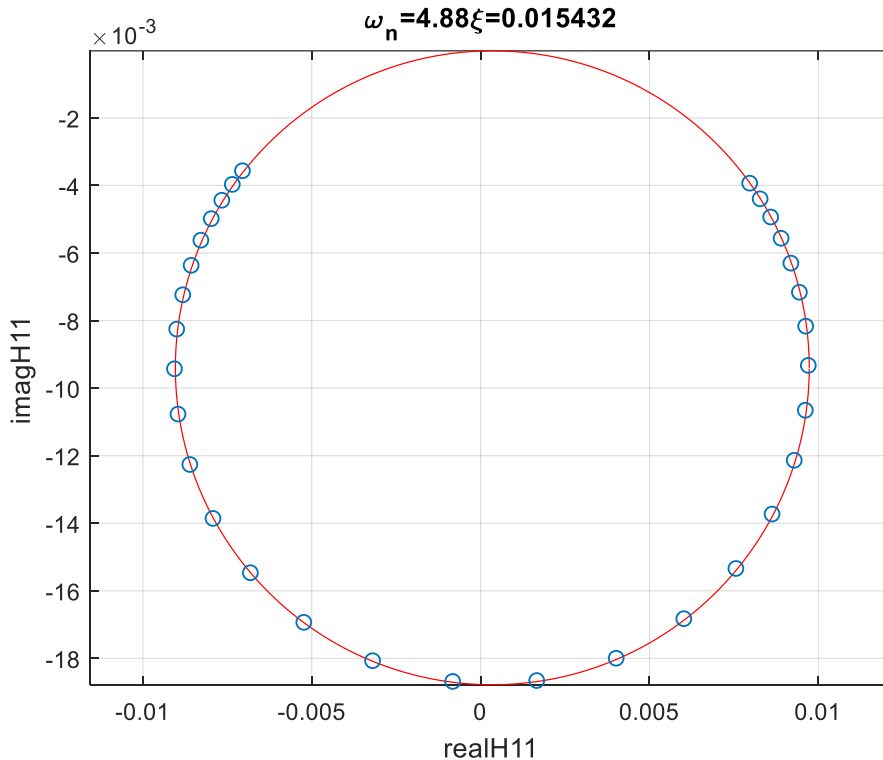
Fig 4.1.3: Fitted a Circle selecting Sets of point.

In the figure 4.1.3, a set of points was considered to obtain the circle fit using the Least Square Method, afterwards this circle was plotted in the complex plane passing through all the points that correspond to a very perfect shaped circle as can be seen and this reflect the high degree of accuracy. In this figure on top, the value of the natural frequency and the damping factor were calculated using the equations (3, 28) and (3, 11) respectively.

The last graph on the bottom right in the Figure 4.1.2 allows identifying the sign of the modal constant that was determined in the same way described above in the method *PP.* In order to evaluate the other modal parameters, this procedure will be repeated for each mode.
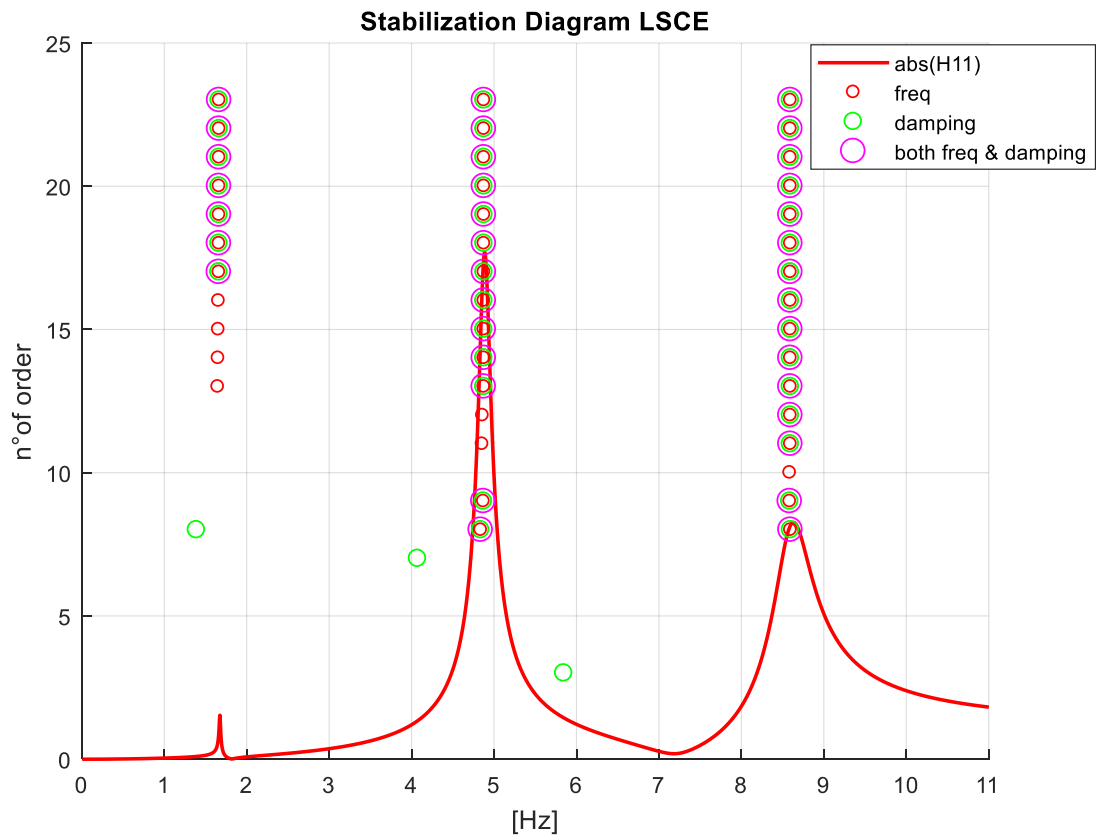
Fig 4.1.4: Stabilization diagram by LSCE method.

The Fig 4.1.4 represents the stabilization diagram of the method LSCE. In this diagram, only the modes that have stability in frequency and damping marked in red rings and green rings respectively were plotted. The other poles that present neither a conjugate part nor stability in frequency and damping were rejected. The stable poles that have stability in frequency and damping were plotted by magenta colored rings. Through this diagram, the presence of three cluster can be corresponding to each peak can be detected, and through these clusters the three physical modes can be obtained.
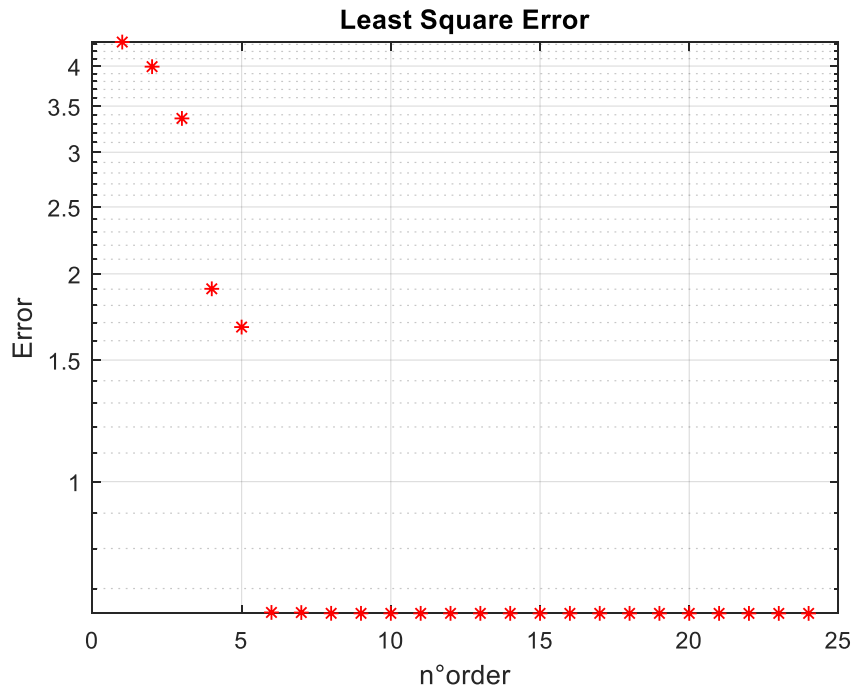
Fig 4.1.5: Least square error

The figure 4.1.5 illustrates the plot of the Least Square Error Method in function the number of order; it can be noticed here that the error drops severely when the number of order reaches 5. This number corresponds theoretically to the number of physical modes presented in the system.
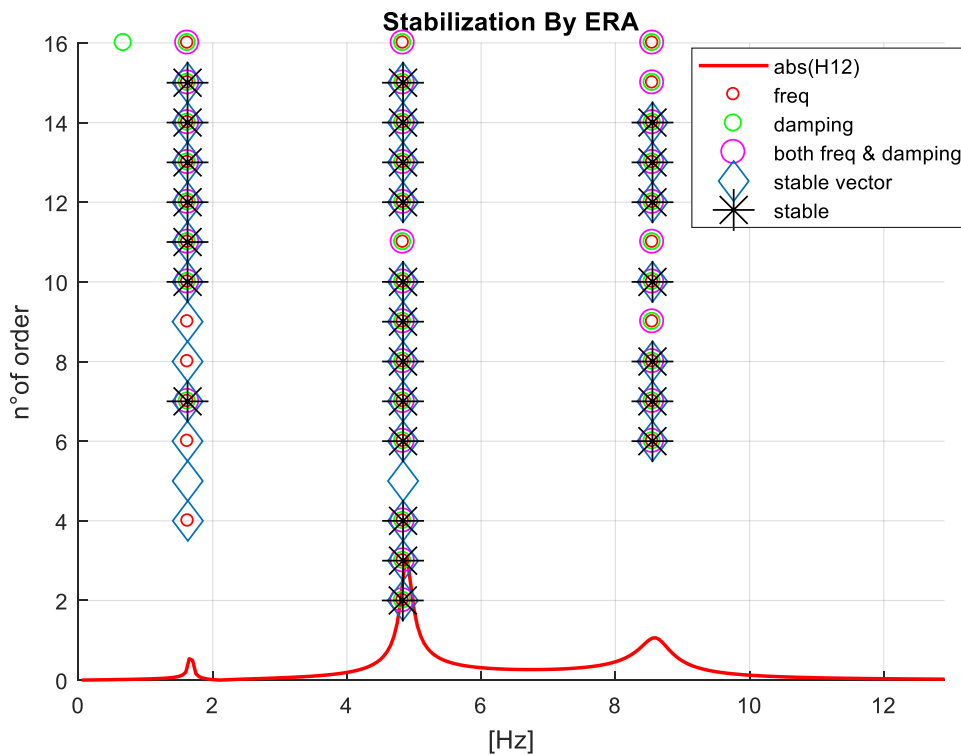
Fig 4.1.6: Stabilization diagram by ERA method.

The figure 4.1.6 shows the stabilization diagram determined by the ERA method, where, comparing to the previous stabilization diagram corresponding to the LSCE, few elements were added which are a stable vector symbolized by a diamond shape and a stable of pole and vector represented by a black asterisk. It can clearly be seen in this diagram the presence of three clusters that correspond to the tree physical modes in the system.
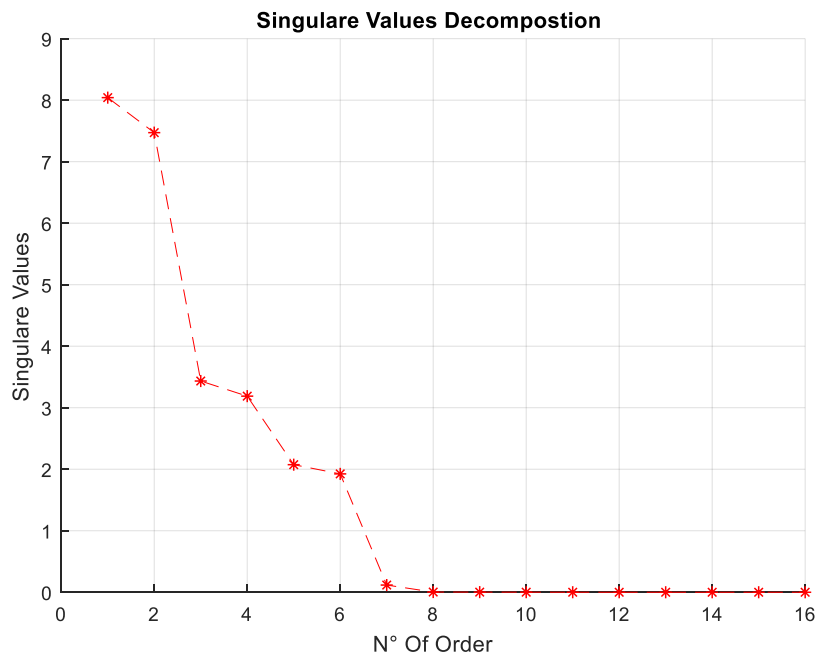
Fig 4.1.7: Singular Values of the Hankel Matrix H_0

The figure 4.1.7 displays the plot of the Singular Value Decomposition Method in function the number of order; it can be observed that the first value of the *SVD* is very high that means the system is near to the singular matrix then by increasing the number of order, the *SVD* drift away from the singular matrices. Thus, it can be noticed that the magnitude of the SVD decreases rapidly when the number of order is 6. This number corresponds theoretically to the number of physical modes presented in the system. Only one part of the physical mode will be considered, and then the number of order taken is $n = 3$ from $2n = 6$.
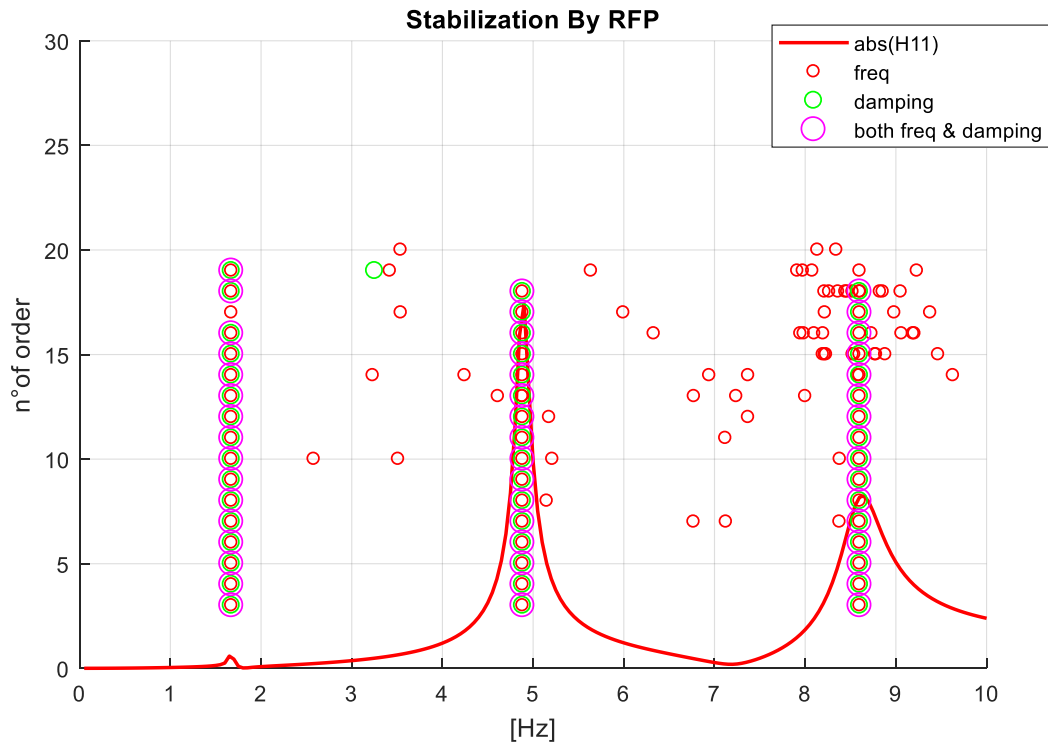
Fig 4.1.8: Stabilization diagram by RFP method.

The stabilization diagram in figure 4.1.8 was determined using the RFP Method, it present some similarity to the LSCE graph. However it was better to use in this diagram a low number of orders to prevent the appearance of the ill-conditioning problem. In comparison to the two previous diagrams calculated by LSCE and ERA, in this case many randomly spared poles that have stability in frequency were found not corresponding to any physical mode, the presence of three clusters is clearly visible, this indicates the existence of three physical modes in this system. In the theoretical case, it can be seen that the selection of a large frequency range allows the plot of a stability diagram that can give good results for the estimation of the modal parameters.

Third step: Compare between the modes shapes extracted by experimental method and the analytical method.

Modal Assurance Criterion (MAC) Matrix
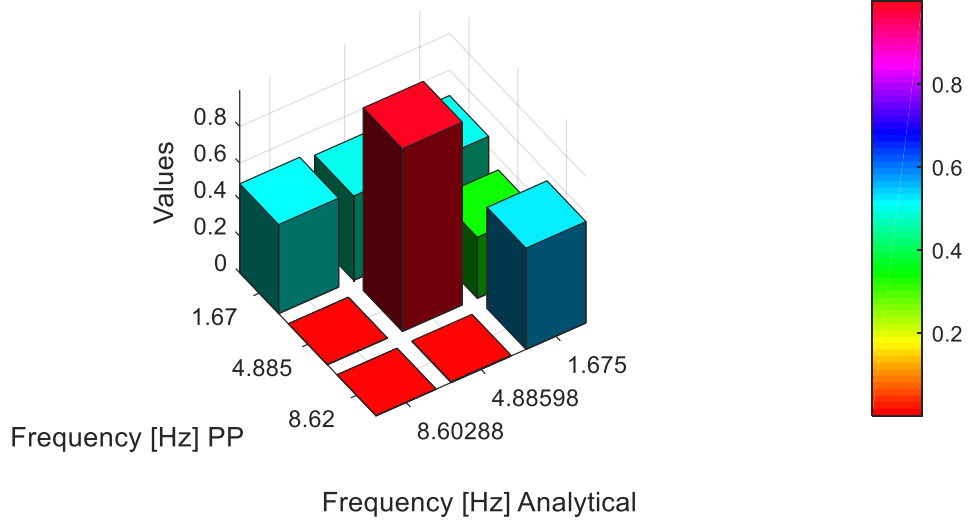
Fig 4.1.9: Compare the modes shapes PP Vs. analytical

Modal Assurance Criterion (MAC) Matrix
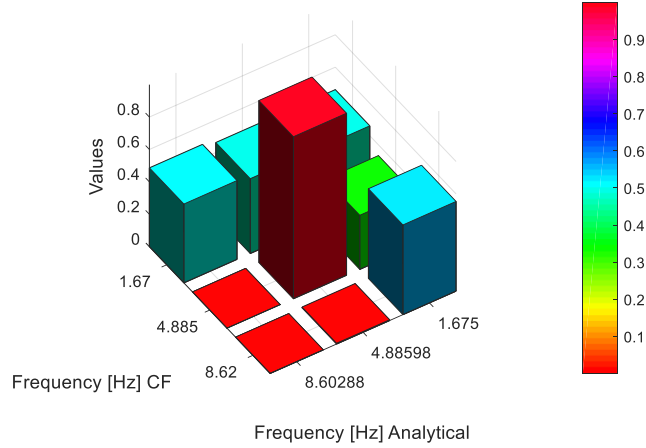
Fig 4.1.10: Compare the modes shapes CF vs. Analytical

Modal Assurance Criterion (MAC) Matrix
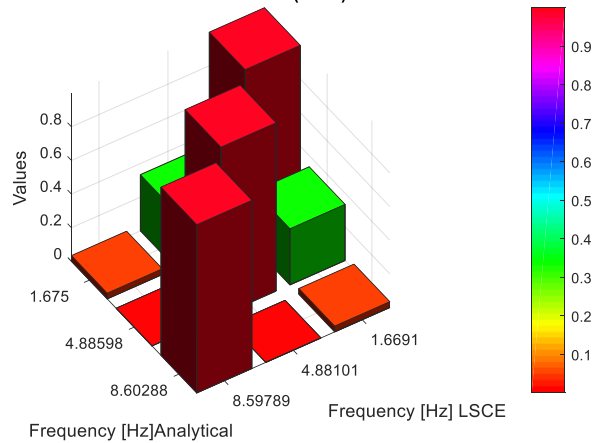
Fig 4.1.11: Compare the modes shapes LSCE Vs Analytical
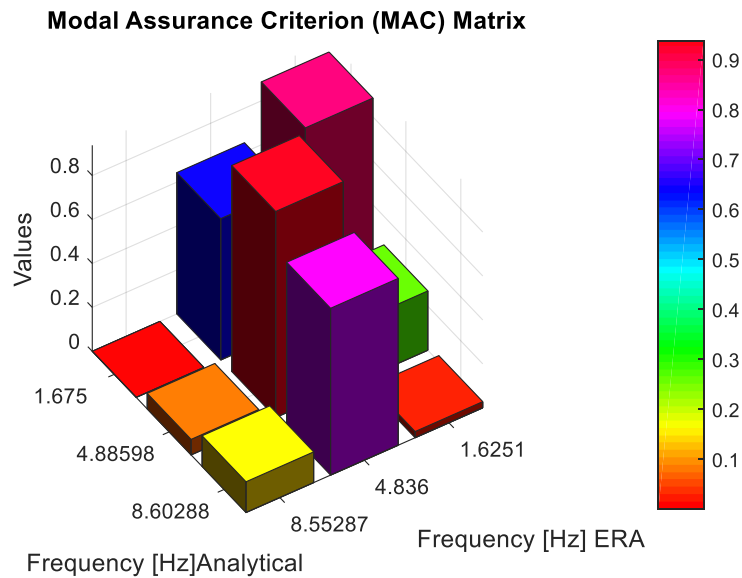
Fig 4.1.12: Compare the modes shapes ERA Vs Analytical
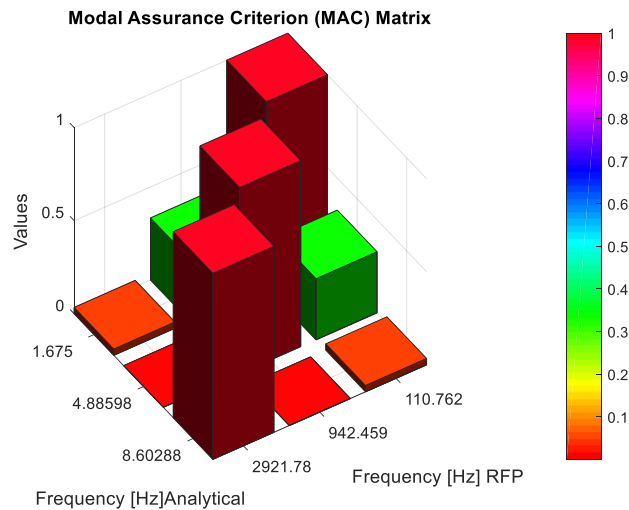
Fig 4.1.13: Compare the modes shapes RFP Vs Analytical

In the figures 4.1.9 and 4.1.10 the mode shapes resulted from the analytical case were compared to the others obtained by the PP and CF methods using Modal Assurance Criterion. When the PP and CF were used almost the same result ere given, the second mode offer a high value for the MAC, but the first and the third modes were badly estimated since low values of mac were obtained; in the first mode it was worth almost 50% and in the third it dropped below the 2%. In the figure 4.1.11 the mode shapes resulted from the analytical case and the LSCE case were compared. From the LSCE, only the real parts of the mode shapes were considered the condition that permitted to obtain very satisfying results, and develop a high correlation, this is why a high value of MAC was detected (>90%)

The figure 4.1.12 consists of a comparison between the analytical Method and the ERA Method, it can be clearly seen that a good estimation for mode shapes was given on the first and the second modes that presented high values of MAC (>90%), but regarding the third mode, a bad estimation and a very low value of MAC that went down to less than 20 % were received.

Similarly the figure 4.1.13 consists of a comparison between the analytical Method and the RFP method, it can be clearly seen that all mode shapes were very good estimated, and as précised these results are, high values for MAC that hit 100% were obtained.

Fourth step: Fitting the curve for H_{12} and determine the FRAC values.
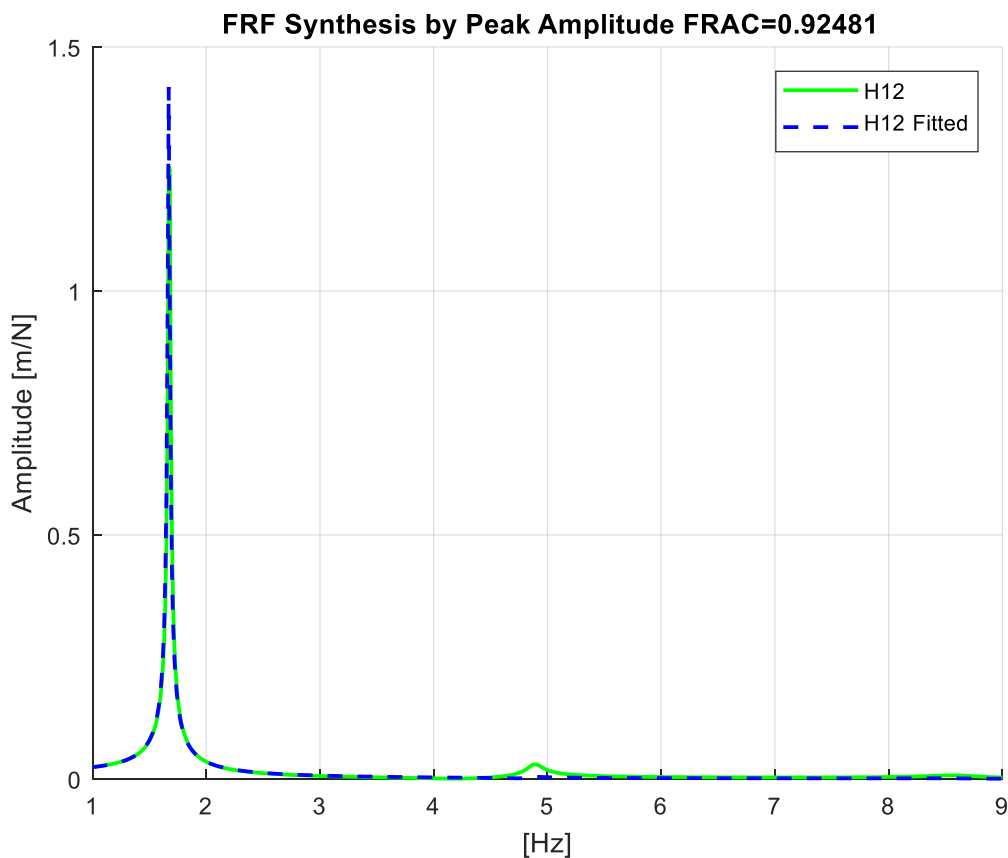
Fig 4.1.14: Fitting the FRF H12 by PP
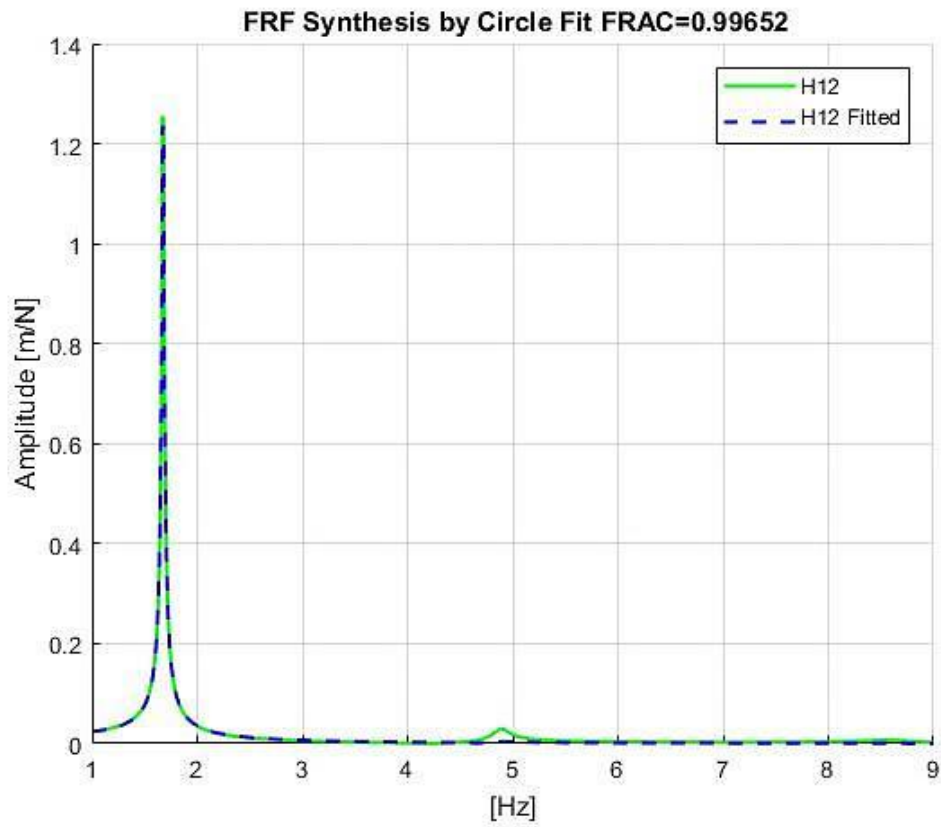
Fig 4.1.15: Fitting the FRF H12 by CF
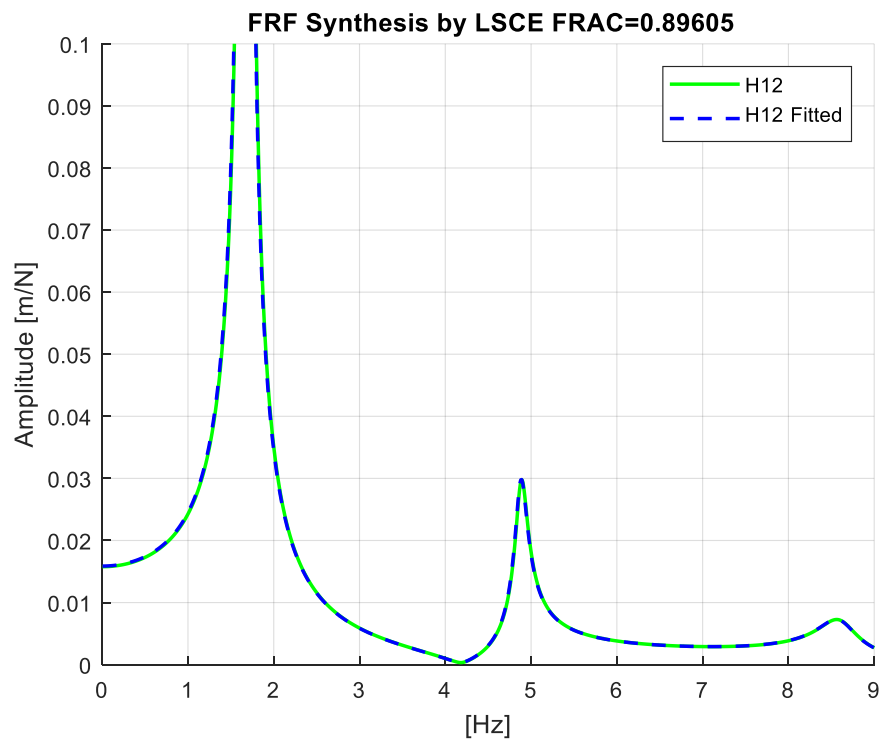
Fig 4.1.16: Fitting the FRF H12 by LSCE.
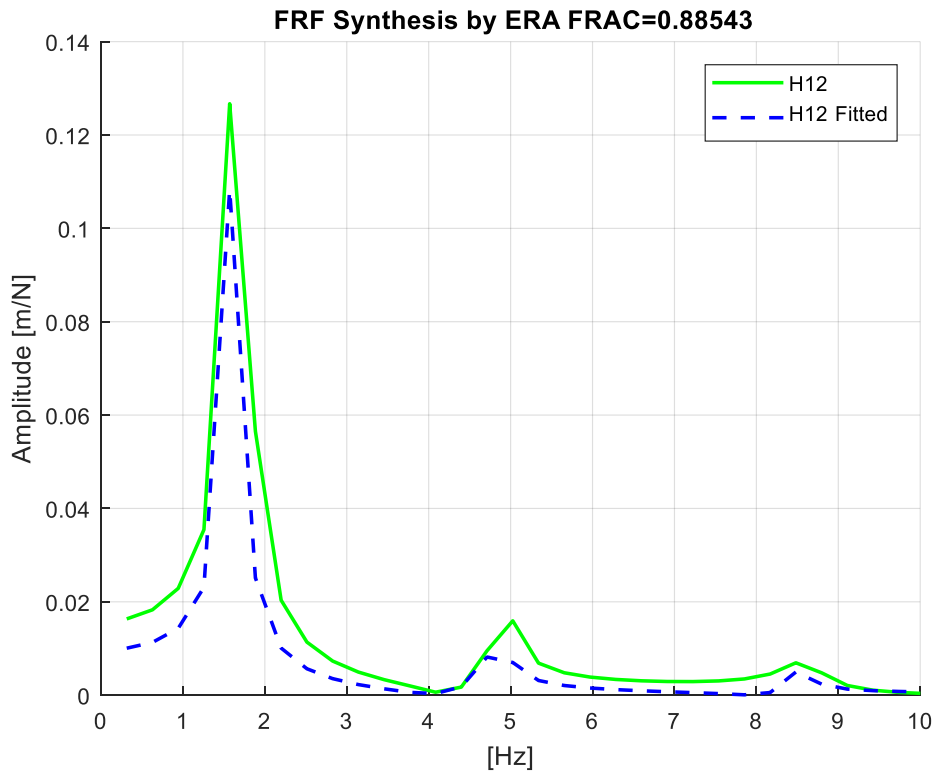
Fig 4.1.17: Fitting the FRF H12 by ERA
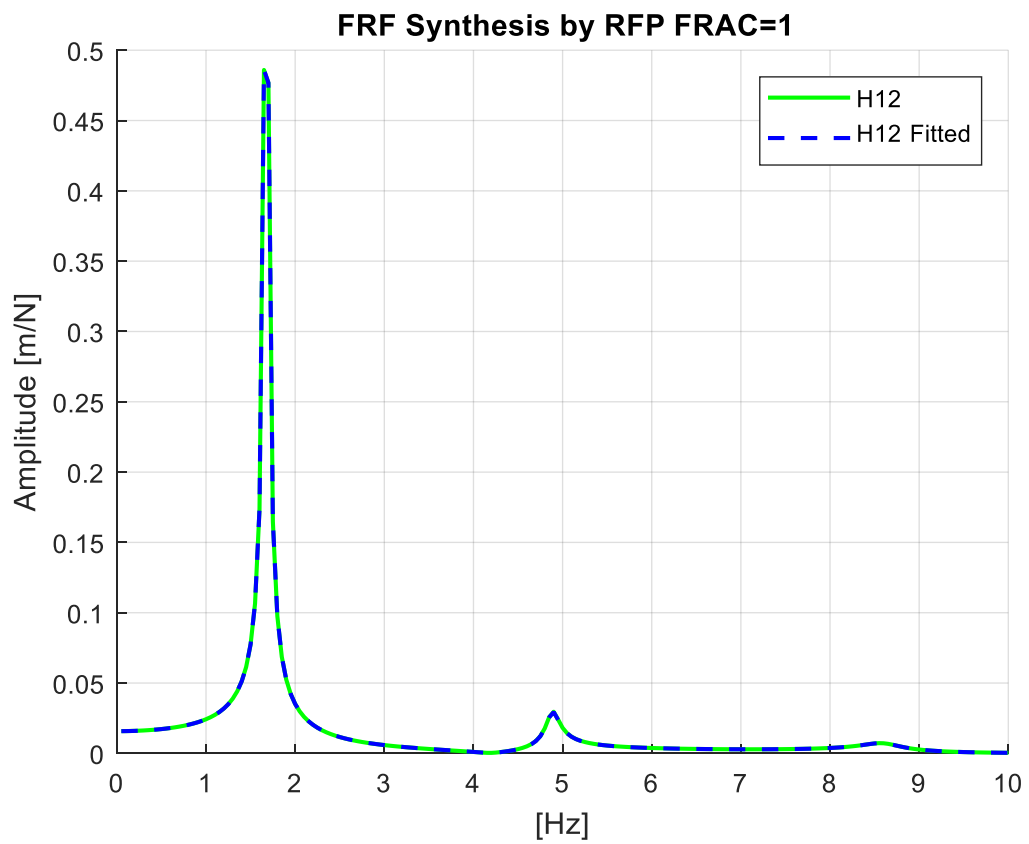
Fig 4.1.18: Fitting the FRF H12 by RFP.

In this step, as it can be shown from figure 4.1.14 to the figure 4.1.18, the FRF Receptance was regenerated for the methods. The FRF H_{12} was the chosen for each FRF because the modes shapes were normalized respecting to the first element of each from their columns. Following that, there was a comparison between the H_{12} extracted for the different methods with the H_{12} determined from the analytical case throughout the frequency vector.

Almost in all the figures mentioned above, high values of the FRAC were obtained, among these results, the lowest values can be detected in the figure 4.1.16 and 4.1.7, they were determined respectively by the ERA and the LSCE methods, and a higher value of the FRAC can be spotted in the Fig. 4.1.14, obtained from the method PP, and the highest value was resulted from the RFP and the CF methods. The best values of the FRAC that reached 100% were given by the RFP method.

Fifth step: Plot the modes Shapes extracted by each method.
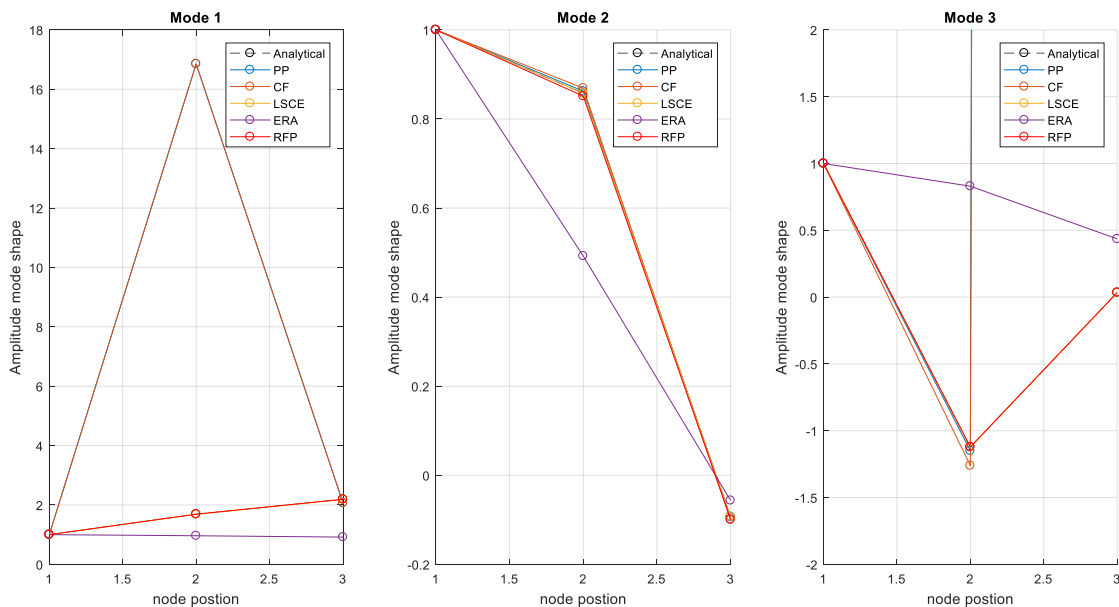
Fig 4.1.19: Plot the modes shapes of 3 DOF.

The figure 4.1.19 is composed of three subfigures representing the plot of the three mode shapes of all the methods. The first one on left belongs to the first mode shape; in this graph the ERA and the CF and the PP were found not matching with the analytical case, but the RFP and the LSHE match with it very well to the point that their graph hides the analytical cases trace. The middle subfigure represents the plot of the second mode shape; it shows that all the methods matched decently with the Analytical Case Method except for the ERA that presented the least degree of correspondence.

The third subfigure shows that the ERA, the PP and the CF graphs were far from meeting with the Analytical cases plot, but the RFP and the LSCE graphs correspond well with it.

4.2: Analytical 3DOFs well Separated Modes

Consider a new matrix M, K, and C, the same procedure described previously in the example 5.1 was repeated, then results were reported in table (4.2.1); (4.2.2); (4.2.3); (4.2.4); (4.2.5) and (4.2.6).

$$M = \begin{bmatrix} 1 & 0 & 0 \\ 0 & 1 & 0 \\ 0 & 0 & 1 \end{bmatrix} ; K = \begin{bmatrix} 237315 & -161000 & 0 \\ -161000 & 398315 & -161000 \\ 0 & -161000 & 398315 \end{bmatrix} ; C = \begin{bmatrix} 40 & 0 & 0 \\ 0 & 40 & 0 \\ 0 & 0 & 40 \end{bmatrix}$$

	Frequency [Hz]	Damping factor %
Mode 1	52.35	6.08
Mode 2	90.96	3.46
Mode 3	123.18	2.58

Table 4.2.1: Frequency and damping ratio for system with 3DOF for the analytical method.

	Frequency [Hz]	Damping factor %	Error	
			Freq %	Damp %
Mode 1	52.1	6.13	0.003	1.61
Mode 2	91	3.46	1.997e-4	0.28
Mode 3	123.1	2.9	0.002	11

Table 4.2.2: Frequency and damping ratio for system with 3DOF for the PP method.

Circle-Fit	Frequency [Hz]	Damping factor %	Error	
			Freq %	Damp %
Mode 1	52.3	6.2	0.095	1.97
Mode 2	90.96	3.15	0.001	8.6
Mode 3	123.1	2.68	0.06	3.5

Table 4.2.3: Frequency and damping ratio for system with 3DOF for the CF method.

	Frequency [Hz]	Damping factor %	Error	
			Freq %	Damp %
Mode 1	51.18	6.02	2.23	0.98
Mode 2	90.45	3.45	0.56	0.04
Mode 3	123.91	2.58	0.58	0.09

Table 4.2.4: Frequency and damping ratio for system with 3DOF for the LSCE method.

	Frequency [Hz]	Damping factor %	Error	
			Freq %	Damp %
Mode 1	52.30	6.08	0.09	0.001
Mode 2	90.91	3.48	0.05	0.86
Mode 3	123.13	2.58	0.04	0.15

Table 4.2.5: Frequency and damping ratio for system with 3DOF for the ERA method.

	Frequency [Hz]	Damping factor %	Error	
			Freq %	Damp %
Mode 1	52.35	6.08	8.14e-14	1.03e-12
Mode 2	90.96	3.45	3.12e-14	1.03e-12
Mode 3	123.18	2.584	8.07e-14	1.58e-12

Table 4.2.6: Frequency and damping ratio for system with 3DOF for the RFP method.
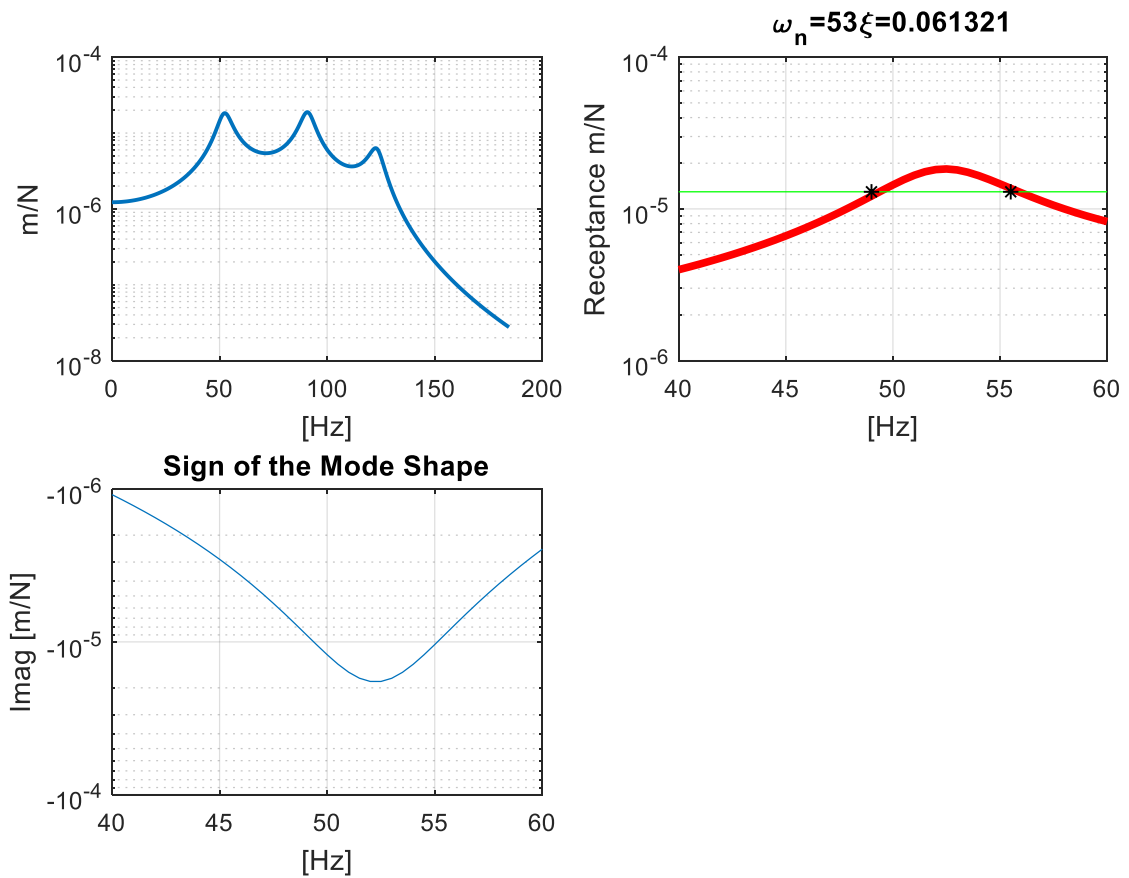
Fig 4.2.1: Estimation the modal parameters of one mode by PP method.

Figure 4.2.1 illustrates the plots of the modal parameter estimation for the first mode by PP, using the same procedure followed in the example represented in Fig.4.1.1.
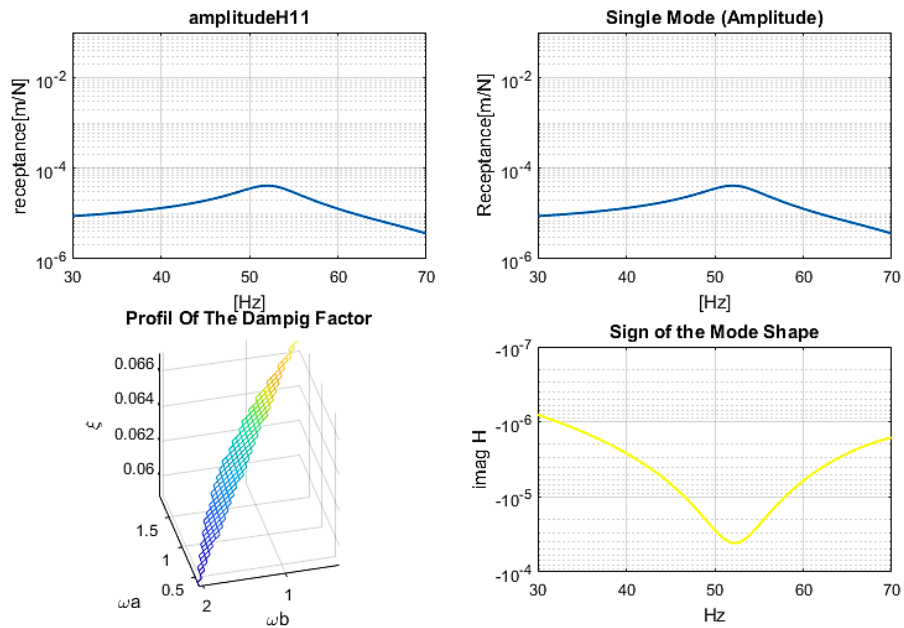
Fig 4.2.2: Estimation the modal parameters of one mode by CF method.

The Figure 4.2.2 above describes the estimation of modal parameter for the first mode using the CF in the similar process used in the example illustrated in Fig.4.1.2
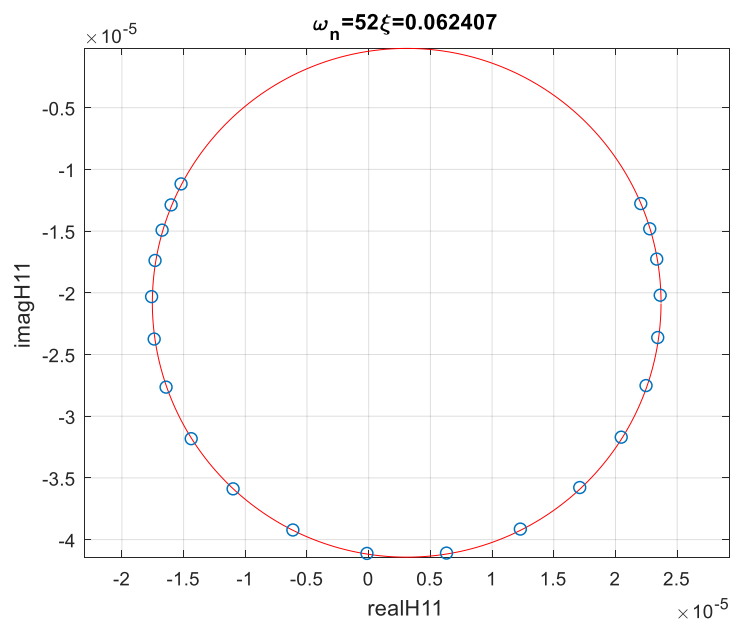
Fig 4.2.3: Fitting a circle selecting Sets of point.

Similarly to the example illustrated in the Fig 4.1.3, the figure above shows the fitting of a circle in a set of points selected from the Receptance of well separated FRF. In this example the deviation of this damping estimation was equal to 0.289%.
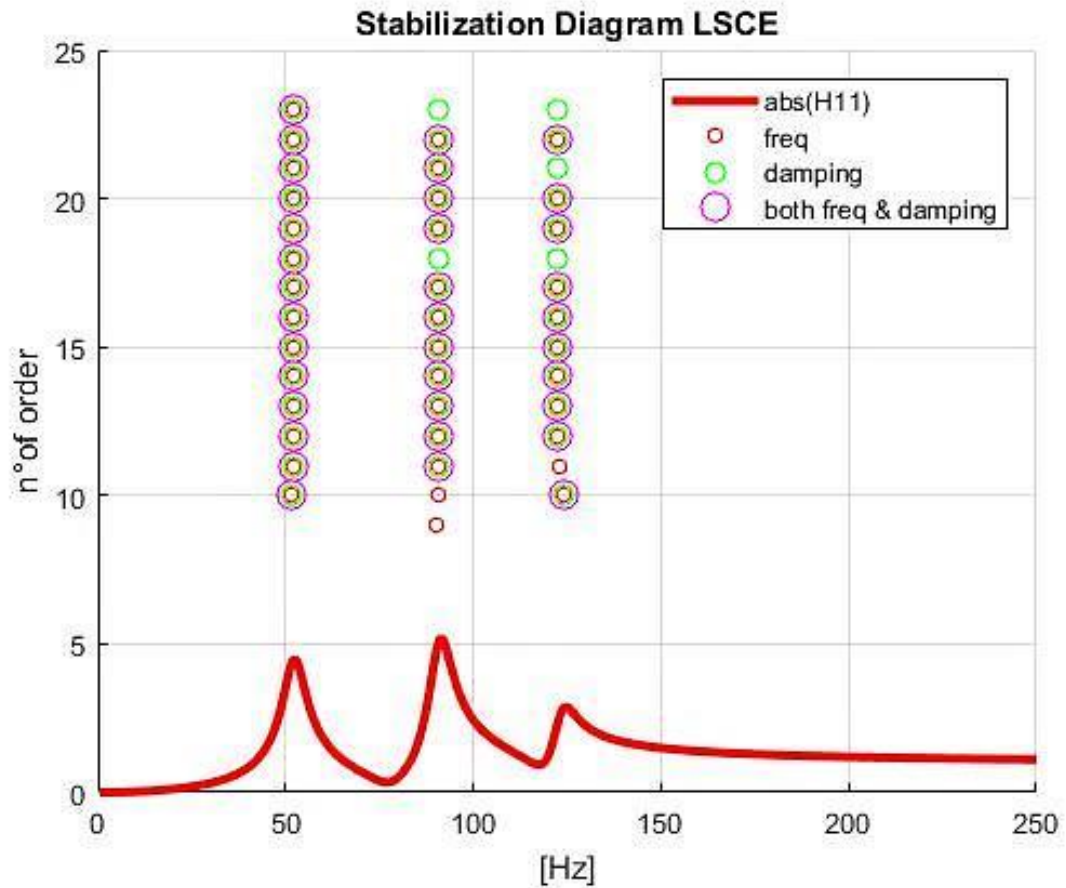
Fig 5.2.4: Stabilization Diagram by LSCE

In the Fig 4.2.4, the stabilization diagram of the method LSCE is displayed in the same manner as the example 4.1.4 was plotted. In this diagram equally three clusters corresponding to each peak can be distinguished. Through these clusters three physical modes can be derived.
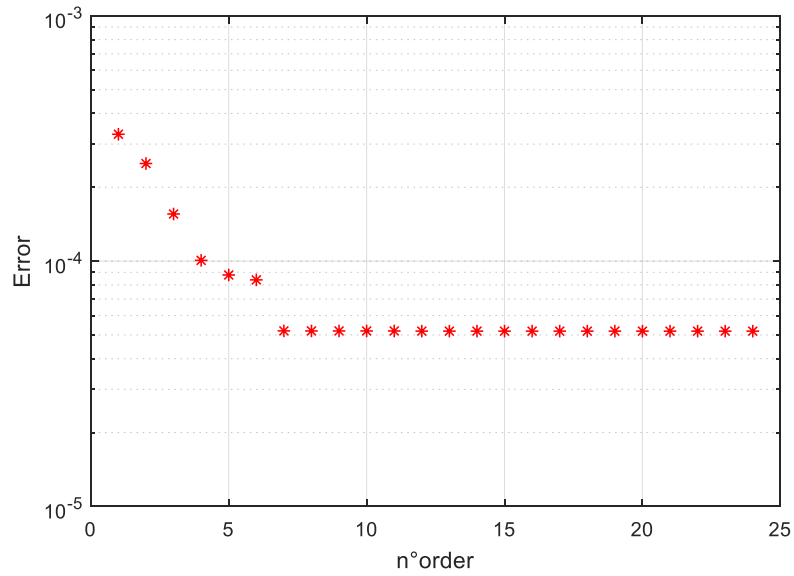
Fig 4.2.5: Least Square Error

The figure 4.2.5 represents the plot of the Least Square Method versus the number of order; it shows that the error decline significantly when the number of order is 6, this number consists of the number of physical modes existing in the system.
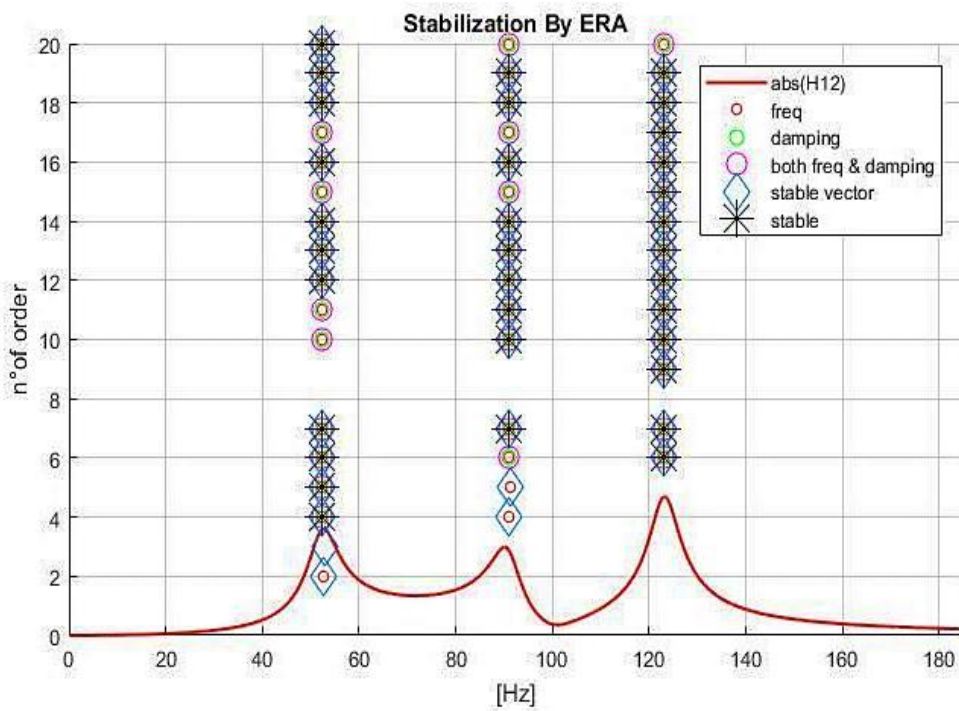
Fig 4.2.6: Stabilization Diagram By ERA

99

The figure 4.2.6 shows the stabilization diagram obtained by the ERA Method, illustrated similarly to the example in Fig.4.1.6. In this diagram, three clusters that correspond to the tree physical modes in the system can be identified.
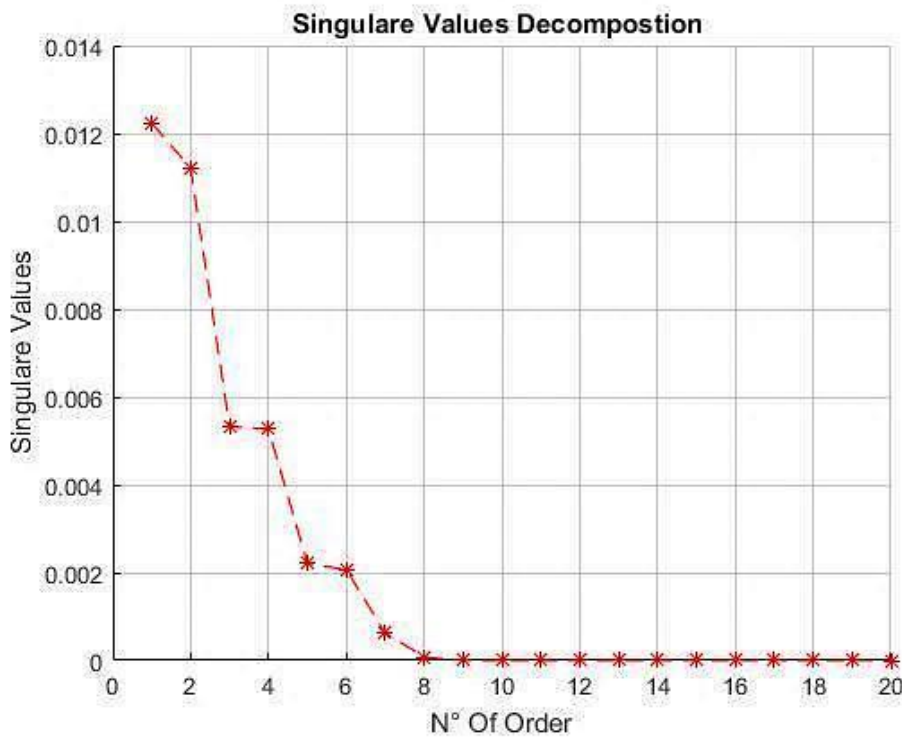
Fig 4.2.7: Singular Values of the Hankel Matrix H_0.

The figure 4.2.7 illustrates the plot of the Singular Value Decomposition Method; it was interpreted similarly to the example of the Fig 4.1.7. In the same manner here, the value of the SVD decreased drastically when the number of order became 6, indicating that the number of order considered is $n = 3$.
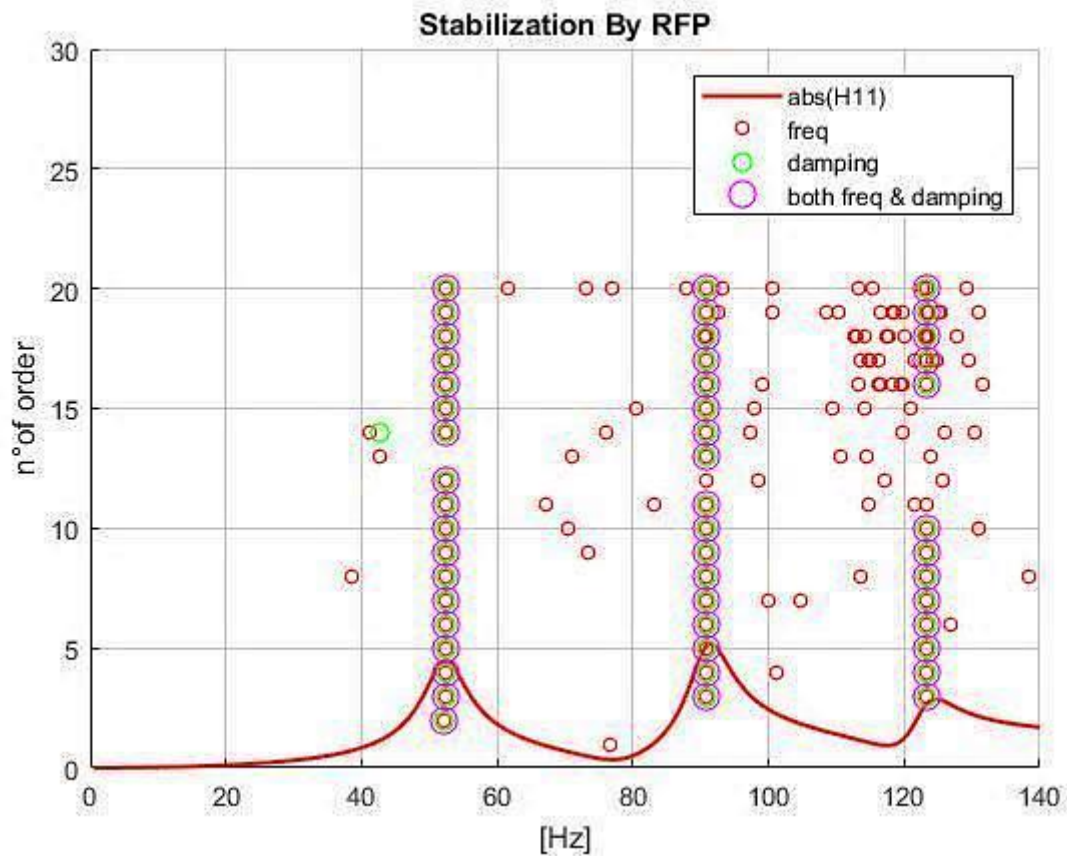
Fig 4.2.8: Stabilization diagram by RFP.

Figure 4.2.8 represents the stabilization diagram determined applying the RFP Method, it is similar to diagram explained in Fig 4.1.8. Also in this case, many randomly spared poles that have stability in frequency are found not corresponding to any physical mode. From this diagram three clusters can be noticed, they represent the three physical modes present in the system.

Third step: Compare between the modes shapes extracted by experimental method and the analytical method.
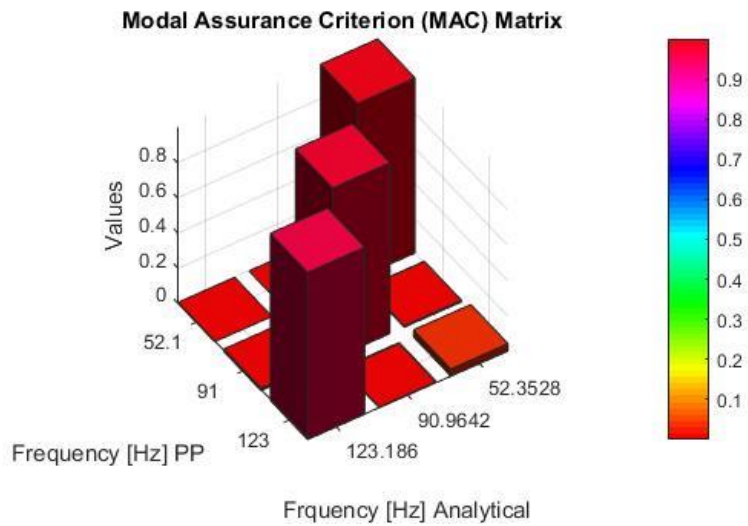
Fig 4.2.9: Compare the modes shapes PP Vs. analytical
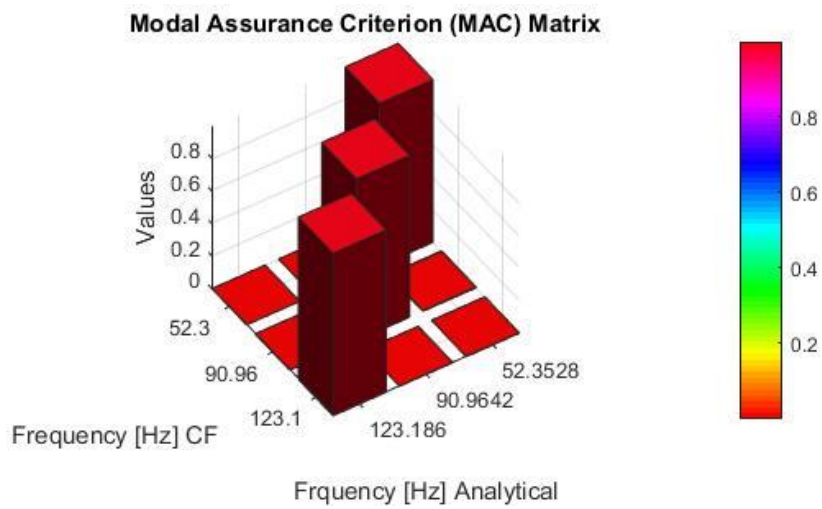
Fig 4.2.10: Compare the Modes Shapes CF Vs. Analytical
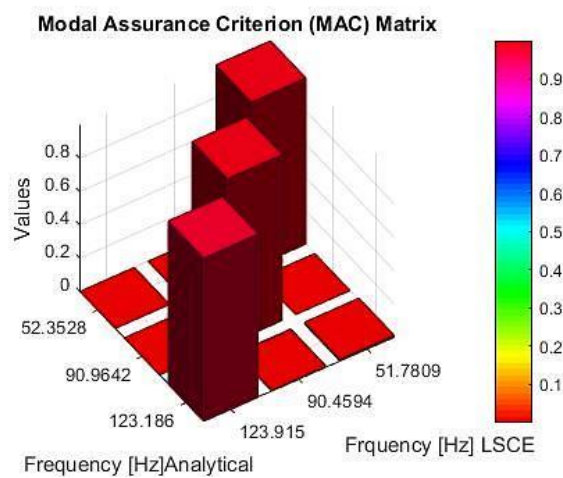
Fig 4.2.11: Compare the modes shapes LSCE Vs. analytical

102
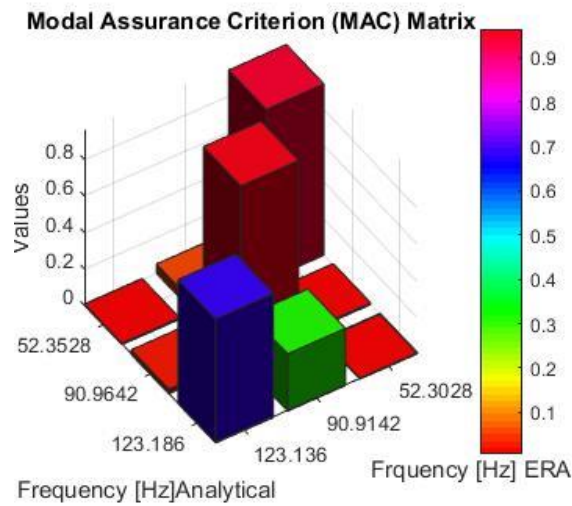
Fig 4.2.12: Compare the modes shapes ERA Vs. Analytical
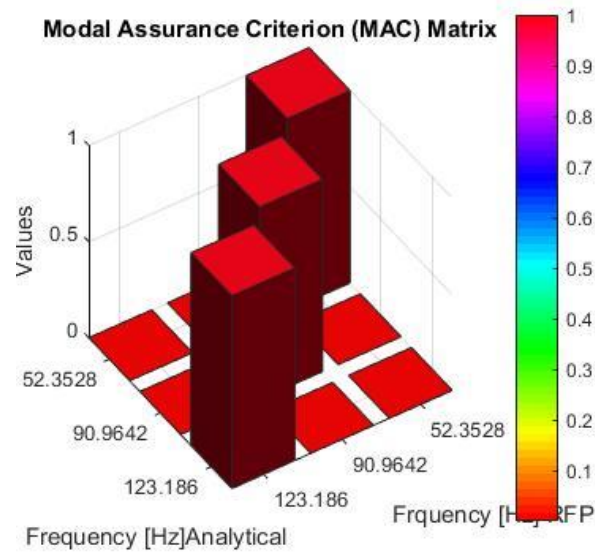
Fig 4.2.13: Compare the modes shapes RFP Vs. analytical.

Observing the figures arranged from Fig.4.2.9 to Fig.4.2.13, it can be noticed that all the methods provide with good results for the mode shapes since they gave high values of MAC, except for the ERA method from Fig.4.2.12 that result in a low value of MAC in the third mode (MAC < 70%). The best method that can be used for the estimation of mode shapes is the RFP that gave a 100% value for MAC.

Fourth step: Fitting the curve for H_{12} and determine the FRAC values.
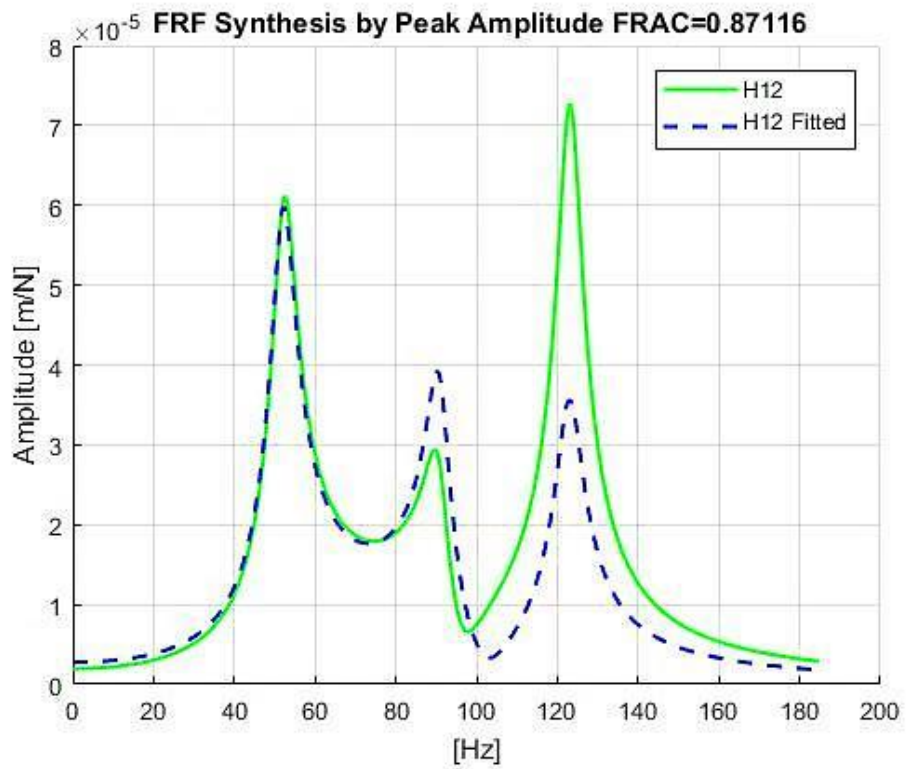
Fig 4.2.14: Fitting the FRF H12 by PP
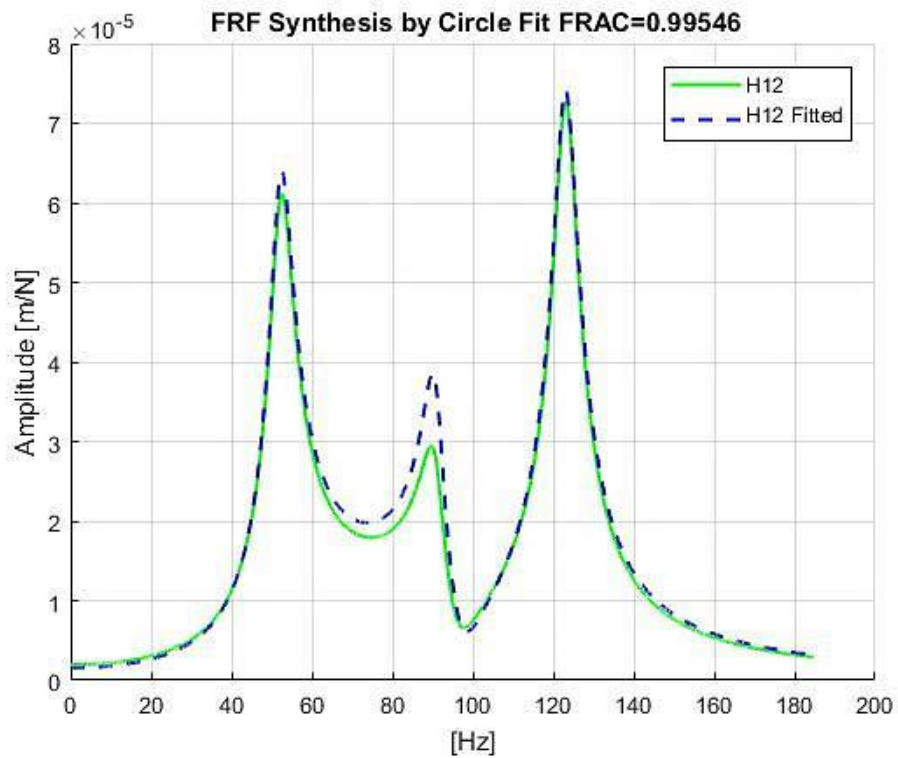
Fig 4.2.15: *Fitting the FRF H12 by C.F.*
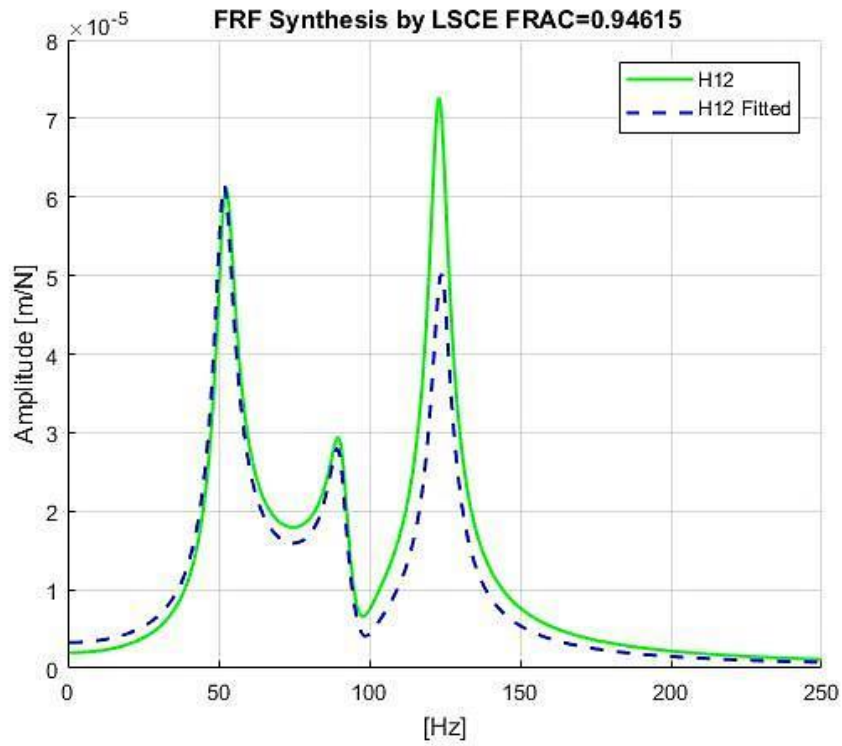
Fig 4.2.16: Fitting the FRF H12 by LSCE
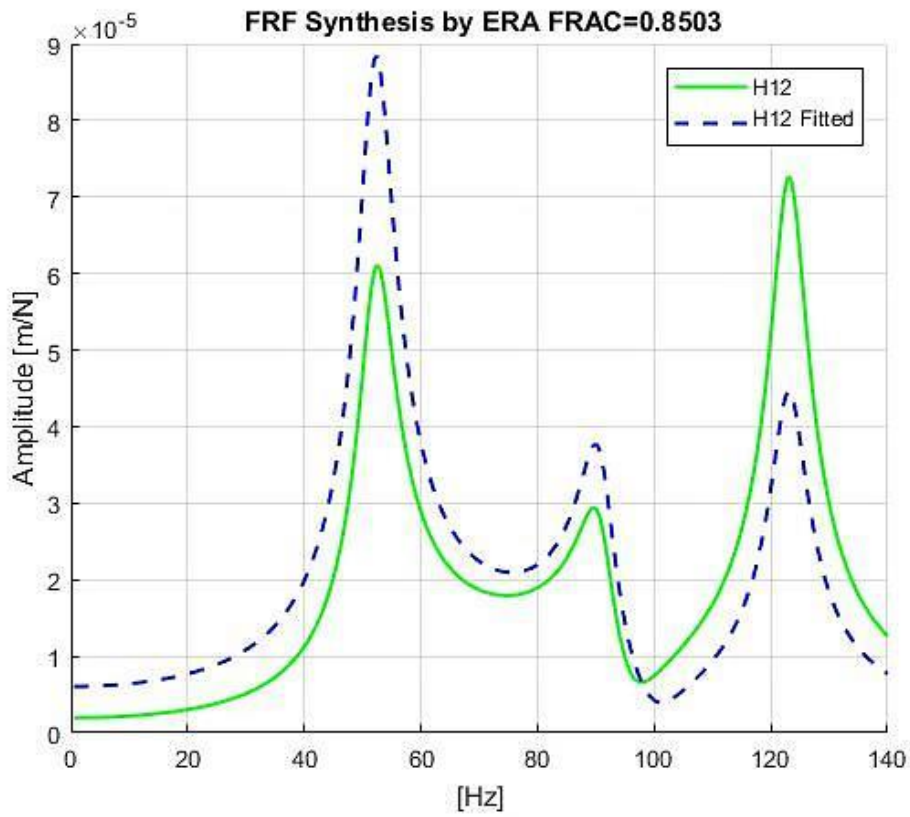
Fig 4.2.17: Fitting the FRF H12 by ERA
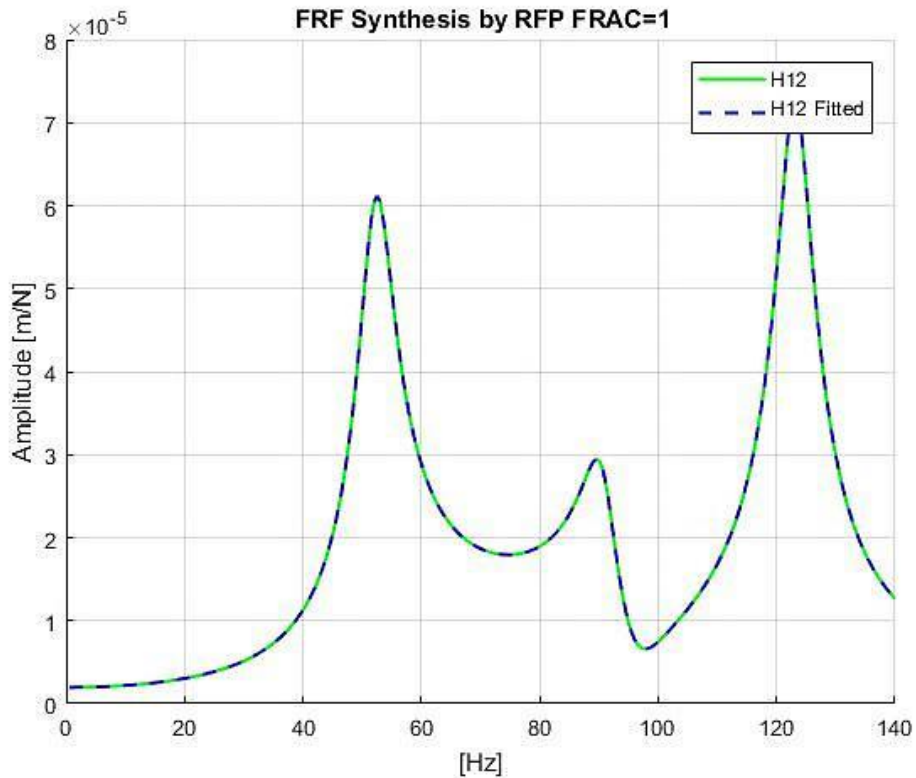
Fig 4.2.18: Fitting the FRF H12 by RFP.

The figures ranging from Fig.4.2.14 to Fig.4.2.18 represent the plots of the regeneration of the FRF H_{12} for each method compared to the analytical case as was operated for the modes close to each other; this comparison was made basing on the values of FRAC. Also in the case of well separated modes the values of FRAC obtained were high, and the ERA as seen in the Fig.4.2.14 continue to rate the lowest value of FRAC, and the rank remains the same for the other methods with the FRP staying in the lead by a 100% percentage of FRF fitting with the analytical case FRF as shown in the Fig.4.2.18.
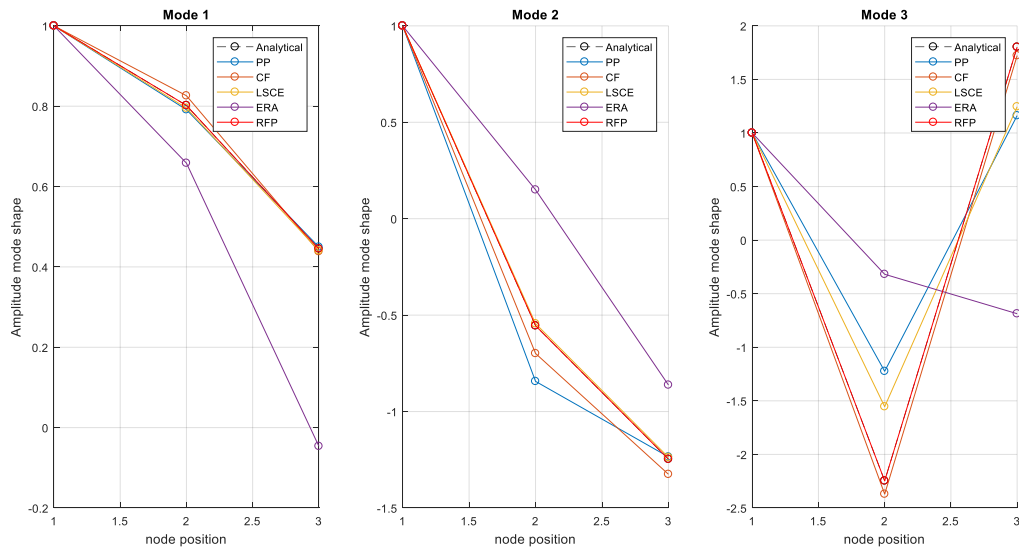
Fig 4.2.19: Plot the mode shapes of 3 DOF well separated modes.

The figure 4.2.19 shows the plot of the three mode shapes of each one of the methods in three subfigures as made in the case where the modes were close to each other in Fig.4.1.19.

From the graph corresponding to the first mode shape on the left, it can be realized that all the methods match well the analytical case except for the ERA that presents a lower degree of compatibility. In the second graph plotting the second mode, it can be noticed that the FRP and the LSCE have the best match with the analytical case, followed by the CF, then the PP that present an inferior affinity compared to the previous, and at the last stays the ERA ranking the lowest in compatibility. Also, the plot of the third mode shape in the last subfigure shows that the entire methods match with the analytical case, the RFP method meets perfectly with the analytical case like in the previous modes; however the ERA was found very far from matching with the analytical case.

Conclusions

All methods gave good results. The PP and the CF were the simplest methods and they are SISO, they presented slight errors when compared to the analytical frequency and damping as reported in the tables (Table.4.1.1, 4.1.2, 4.1.3, 4.2.1, 4.2.2 and 4.2.3.) above. As for the modes shapes in case of modes close to each other, using these methods the first and the third modes shapes presented low values of MAC as seen in the Fig 4.1.9 and Fig 4.1.10. It is important to mention here that in the first example a small values of Δf=0.01 Hz was considered, for this reason good results were obtained. In the second case the value of Δf was taken as 0.5 Hz, and good results were achieved when the PP and CF were employed in all modal parameters. When calculating the mode shapes using the ERA method, several problems occurred, as it can be seen in the Fig 4.1.12. First, low values of the MAC were obtained in the third mode, second, the diagonal off present a high number of MAC when the mode 1 and the mode 2 were compared, as between mode 3 and mode 2 the MAC surpassed 60%. For here it can be considered that the case 4.2 gave better results comparing to the first, but still the values of the MAC remain low in the third modes. Therefore, it can be deduced that the ERA does not yield the mode shapes in the Analytical case. The error values in the LSCE and the RFP have constantly been low; hence it is safe to consider here that the RFP is the best method to depend on since it was the least in giving error in frequency, damping and mode shapes. In the both occasions the exact same modes shapes values were resulted in, and the regeneration of the FRF was successful by the FRAC matching 100 % with the analytical case.

The stabilization of diagram was very clear in the LSCE and the ERA. In the RFP when the number of order is increased, a perturbation of the stability in the poles occurred, because the ill conditioning problem appeared with the rise of number of order. Observing Fig 4.1.8 and 4.2.8, it can be seen that the third cluster presents a less number of the stability of poles than the third cluster in both the LSCE and ERA methods. Noted that regardless further augmentation in the number of order these two methods can still give good cluster plot.

Referring to the Least Square Error and the Singular values decomposition, the number of physical modes presented in the system can be immediately found when the error chart drops drastically as shown in Fig 4.1.5 Fig 4.1.7, Fig 4.2.5 and Fig 4.2.7.

Experimental Data

In this part the methods PP, CF, LSCE, ERA and RFP will be applied, on the FRFs of a plate and gearbox, and the LMS Test-Lab will be used to validate the modal parameters extracted. Then the LSCE method will be reapplied using the toolbox in Matlab (*modalsd*, *modalfit)*, and the results of the LSCE method given in both ways are compared to study their compatibility.

In the experimental case new procedures which were not used in the analytical case will be added. In order to have more precision in modal parameters the Auto Mac will be implemented to the Modes Shapes extracted from the poles in the clusters. The Auto Mac Compares the Modes Shapes and evaluates their similarity to eliminate the repetitive unwanted mode.

4.3   Steel Plate Experimental Data.

In this example a plate with fifteen accelerometers was considered, as shown in the Fig 4.3.1, and the plate is excited by a shaker in point pt_2:1 in direction z. The fifteen FRFs that were measured represent one row of the matrix of FRF. The parameters of data are illustrated in the table 4.3:
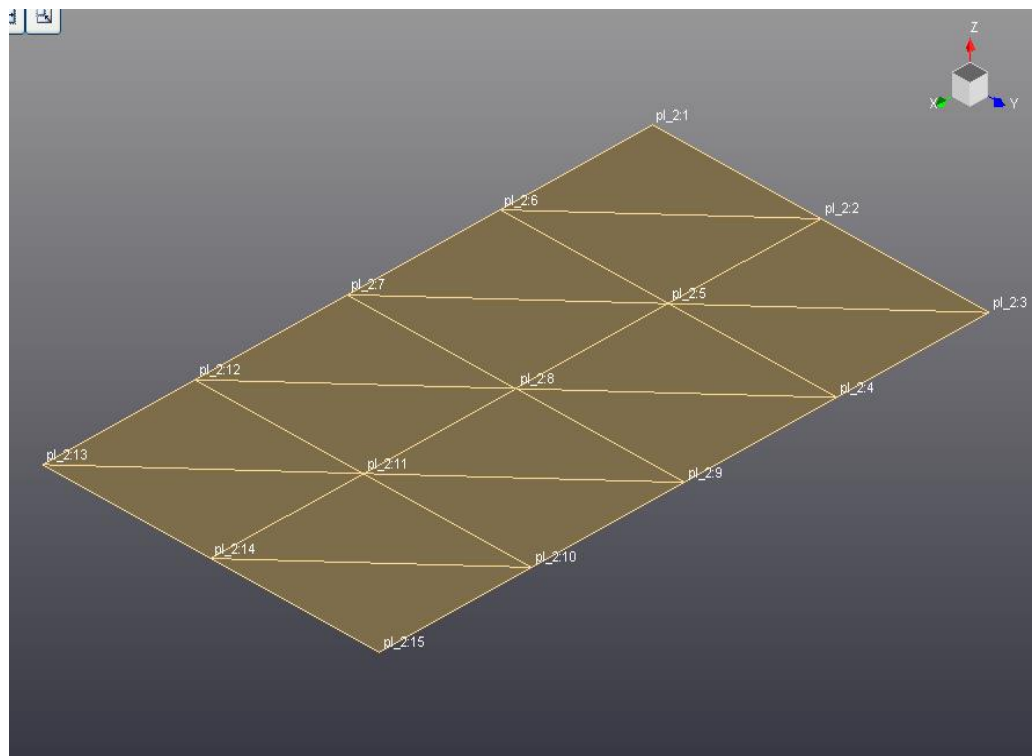
Fig 4.3.1: Modal of the plate.

Sample rate	2048 Hz
Number of samples	2048
Δf	1 Hz
Nyquist frequency	1024 Hz

Table 4.3: Parameters data of the plate.

	Mode 1	Mode2	Mode3	Mode4	Mode 5	Mode 6	Mode7
Frequency [Hz]	133,7	135,2	305	374,5	385,3	474,2	554,3
Damping Factor %	3.58	3.20	2.99	2.85	2.92	2.62	2.97

Table 4.3.1: Frequency and damping ratio for the 7 modes of the plate extracted by the Test-Lab polymax method .

Peak-Amplitude	Mode1	Mode2	Mode3	Mode4	Mode 5	Mode 6	Mode7
Frequency [Hz]	_____	136	307	_____	388	477	561
Damping Factor %	_____	3.67	2.9	_____	3	2.6	2.85

Table 4.3.2: Frequency and damping ratio for the 7 modes of the plate extracted by the PP method.

	Mode1	Mode2	Mode3	Mode4	Mode 5	Mode 6	Mode7
Frequency [Hz]	_____	136	307	_____	388	477	561
Damping Factor %	_____	3.3	2.9	_____	3	2.6	2.85

Table 4.3.3: Frequency and damping ratio for the 7 modes of the plate extracted by the CF method.

	Mode 1	Mode 2	Mode 3	Mode 4	Mode 5	Mode 6	Mode7
Frequency [Hz]	133.8	134.5	305.2	375.1	387.14	474.6	554.4
Damping Factor %	2.78	3.24	3.05	2.85	2.45	2.79	2.76

Table 4.3.4: Frequency and damping ratio for the 7 modes of the plate extracted by the LSCE method.

	Mode 1	Mode 2	Mode 3	Mode 4	Mode 5	Mode 6	Mode7
Frequency [Hz]	134.4	135.1	305.3	375	386	474.8	555
Damping Factor %	3.6	3.6	3	2.91	2.9	2.64	2.71

Table 4.3.5: Frequency and damping ratio for the 7 modes of the plate extracted by the LSCE Matlab toolbox.

	Mode 1	Mode 2	Mode 3	Mode 4	Mode 5	Mode 6	Mode7
Frequency [Hz]	133.9	135.2	305.3	375	386	474.8	555
Damping Factor %	4.6	3.35	3.16	2.97	2.92	2.69	2.72

Table 4.3.6 : Frequency and damping ratio for the 7 modes of the plate extracted by the
ERA method

	Mode 1	Mode 2	Mode 3	Mode 4	Mode 5	Mode 6	Mode7
Frequency [Hz]	133.3	135.1	306	376	387	475	555.3
Damping Factor %	1.84	3.52	2.98	2.76	2.74	2.63	2.7

Table 4.3.7: Frequency and damping ratio for the 7 modes of the plate extracted by the
RFP method.
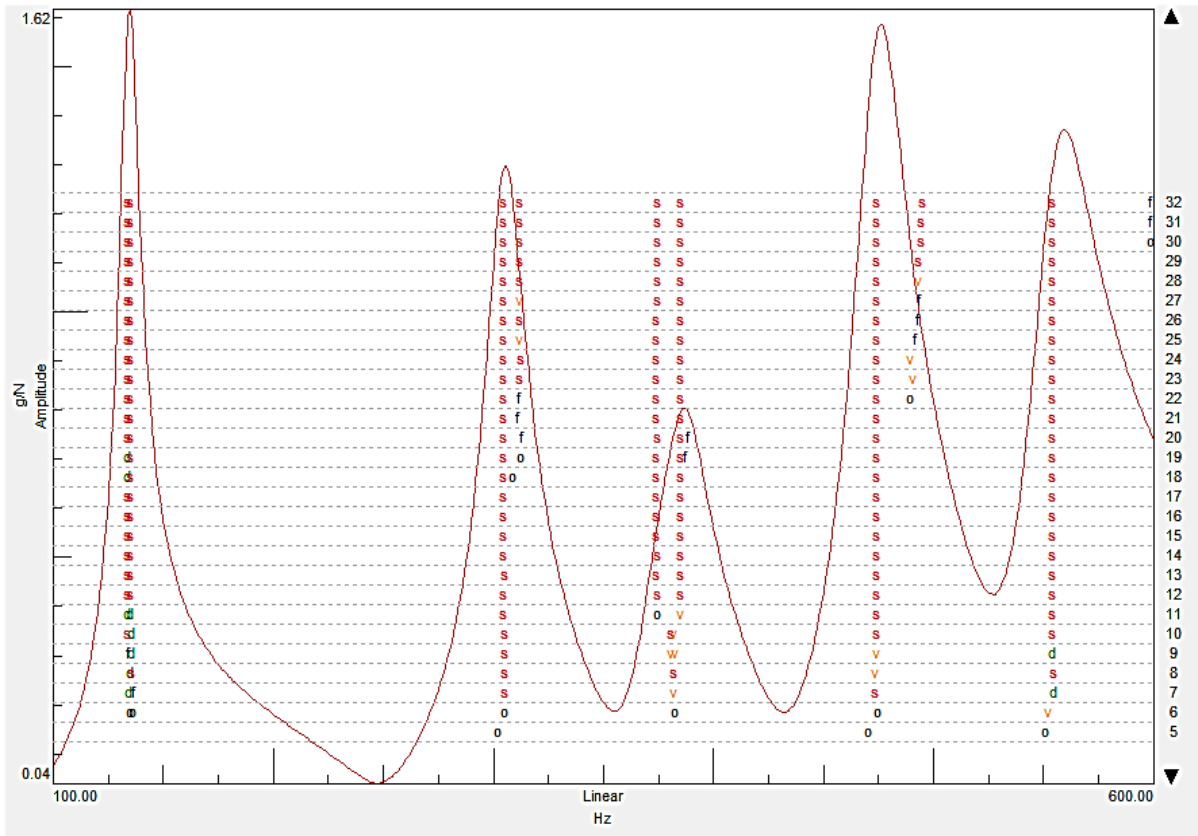
Fig 4.3.1: Stabilization diagram by *Test-Lab Polymax* method of the plate.

As the first step in the experimental case, the results calculated in the Polymax
Method were displayed, and the stabilization diagram present Fig.4.3.1 is also a
result of this method. In this diagram, multiple clusters can be detected, from these
cluster seven physical modes can be extracted. It actually presents more than

seven clusters as can be seen in the figure, but only seven were chosen because when the AutoMAC was determined the repetitive modes which are the fourth and the eighth clusters were eliminated.
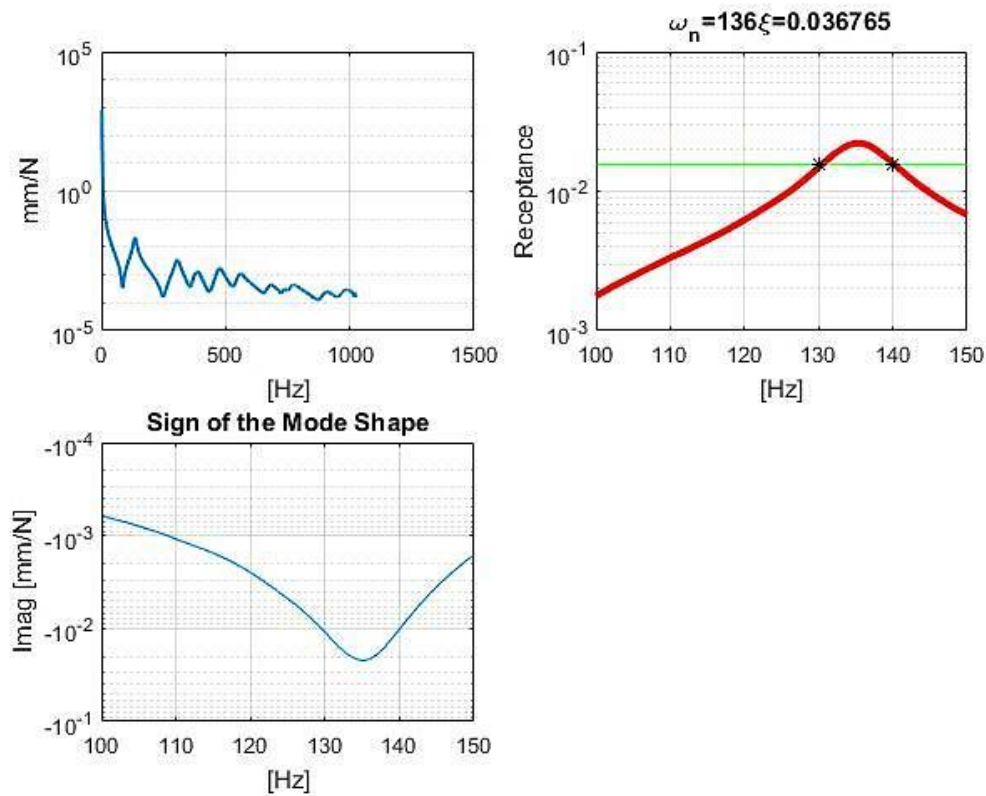
Fig 4.3.2: Estimation modal parameters of one mode by PP of the plate

In the Fig.4.3.2 the same procedure followed in the Analytical case was also used in the experimental case in order to extract the model parameters. At this stage it is impossible to determine the whole matrix of the modal constant by PP and CF methods, because as can be noted from the Fig 4.3.3, the H_{12} do not have the same peaks present in the H_{11}, it can be seen that near 305 Hz the H_{12} does not present a peak as in the H_{11}. Then the second row of the matrix cannot be found. In this case the H_{11} *is chosen* as the reference presenting the major part of the peaks. The operator observes and analysis the FRF carefully to choose the most adequate one that has less noise and presents a high number of peaks.

Noted, the first row of the modal constant matrix can be determined, and then the H_{11} reconstructed by the modal parameters is extracted and compared it with the Experimental H_{11}.
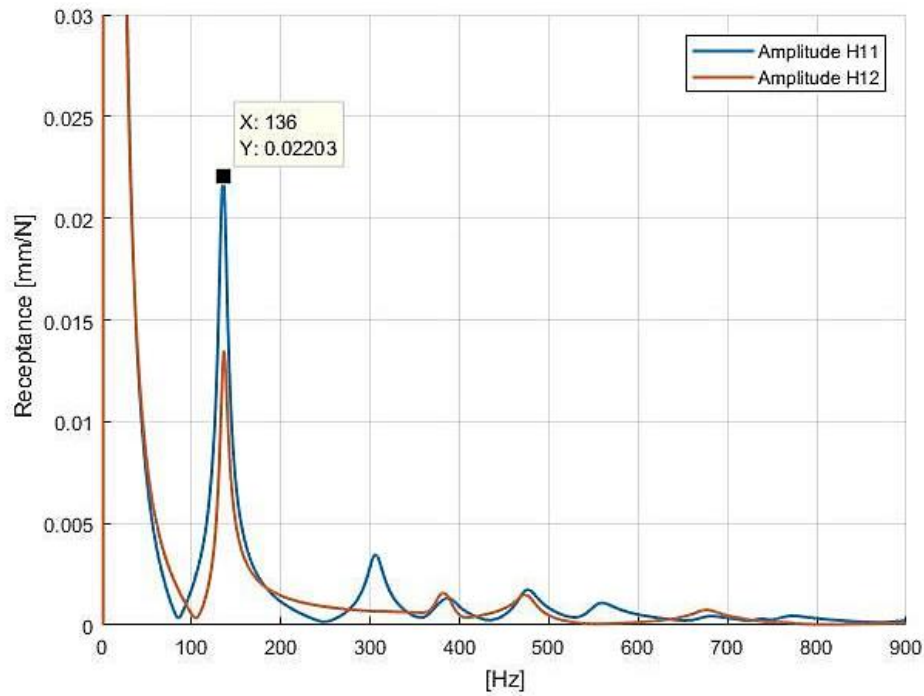
Fig 4.3.3:H_{11} and H_{12} for the plate under testing.
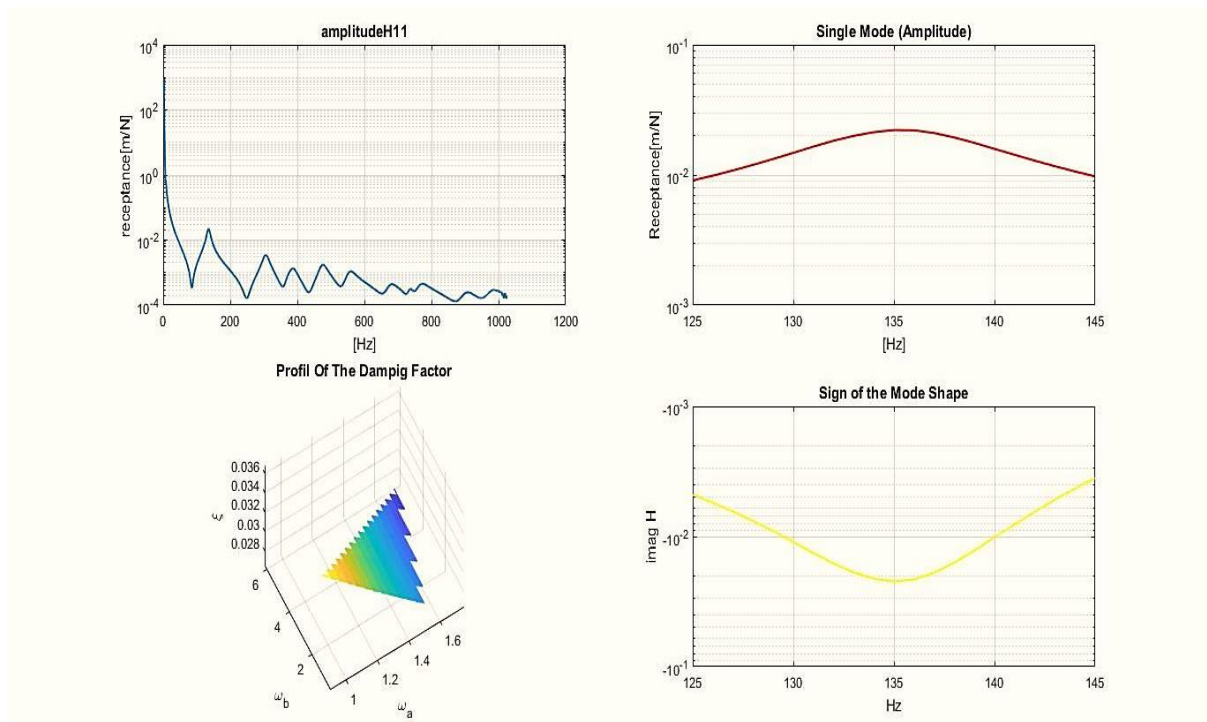
Fig.4 3.4: Estimation modal parameters by CF of the plate.

In the Fig.4.3.4 the models parameters were extracted from the experimental case following the same process applied in the Analytical case. The deviation of the damping factor in the first mode is 3.2%.

ω_n=136ξ=0.033356
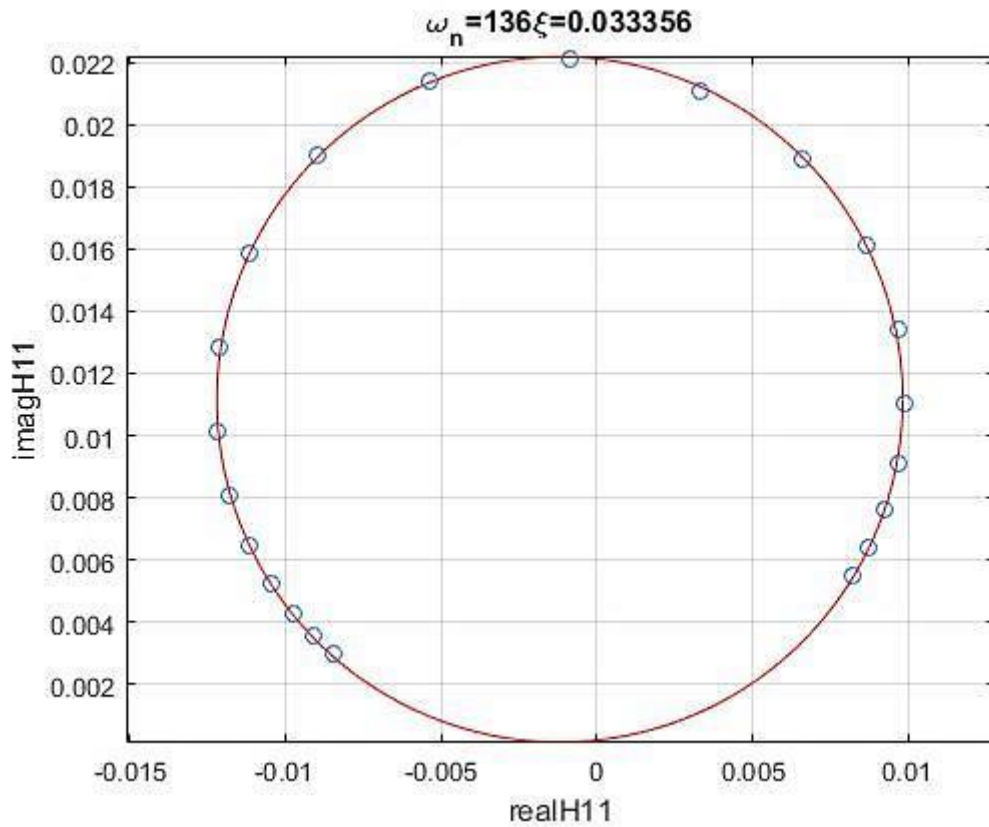
Fig 4.3.5: Fitting a circle selecting a Set of points.

In the Fig.4.3.5, 31 points were selected neighboring the resonance for the fitting of the circle, it can be seen that the circle fit well because it pass almost through all the points, this allows to estimate a damping factor with a low deviation and permit to say that the FRF acquired are well précised. Then of course the same procedure will be repeated for all the modes that can be calculated in the system.
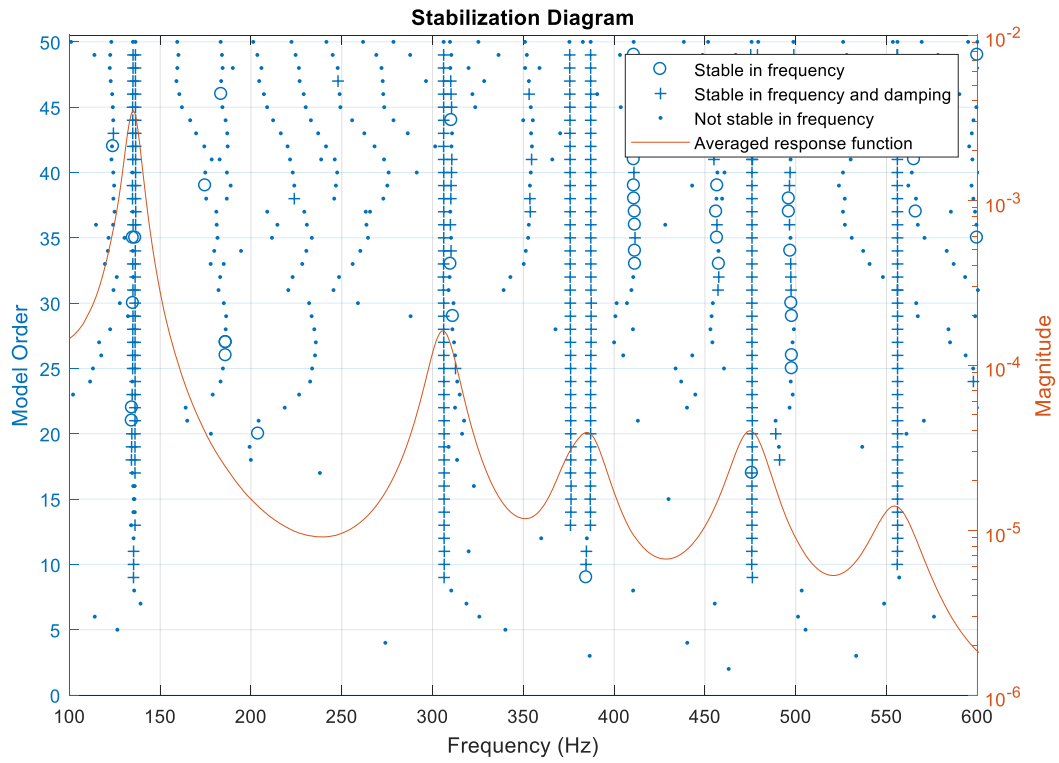
Fig 4.3.6: Stabilization diagram by LSCE Matlab toolbox of the plate.
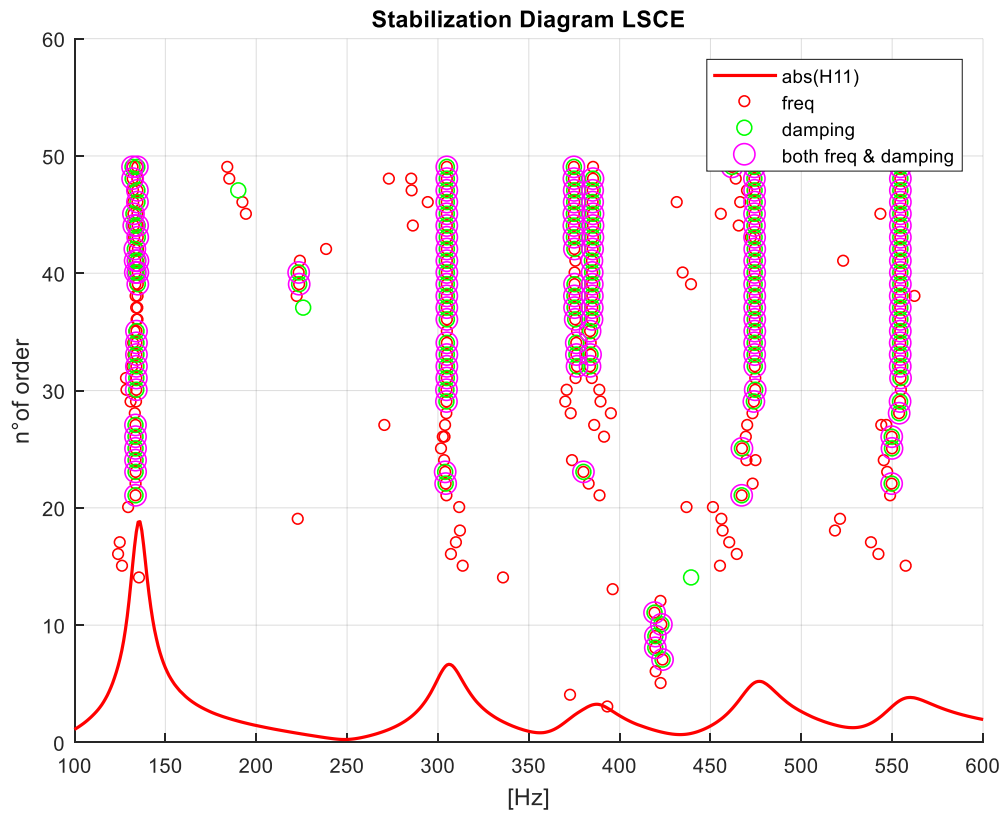
Fig 4.3.7: Stabilization diagram by LSCE of the plate
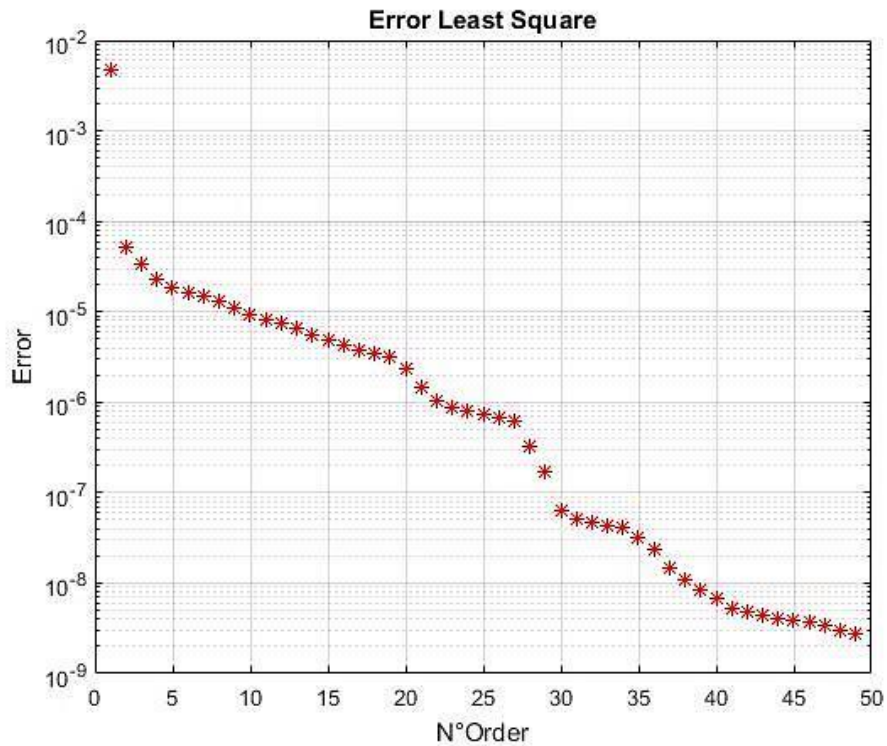
Fig 4.3.8: Least Square Error.

The Fig.4.3.6 represents the stabilization diagram issued from LSCE Toolbox, the clarity of this diagram permit to easily notice the presence of seven physical modes, thus the model parameters can be extracted immediately. In the Fig.4.3.7 illustrating the stabilization diagram determined by the LSCE Implemented, the presence of seven physical modes it can be evidently seen; therefore the modal parameters can be derived. In this figure the stability of poles start to show when the number of order exceed 20 however, in Fig.4.3.6 the appearance of the stability of poles begin when the number of order becomes higher than 10. In the Fig.4.3.8, the Least Square Error has failed to identify the number of physical modes existing in the system; and as can be seen the error drops rapidly when the number of order became 30, this can lead to identify the number of modes as 15 which is false.

117
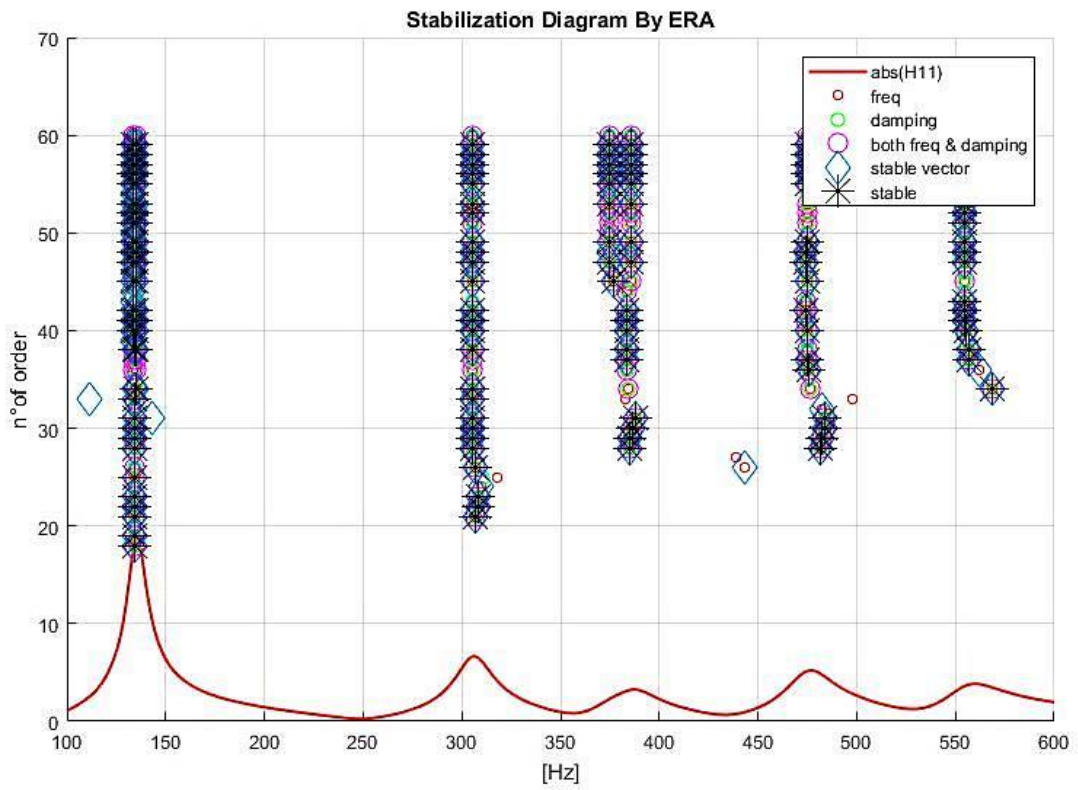
Fig 4.3.9: Stabilization diagram by ERA of the plate
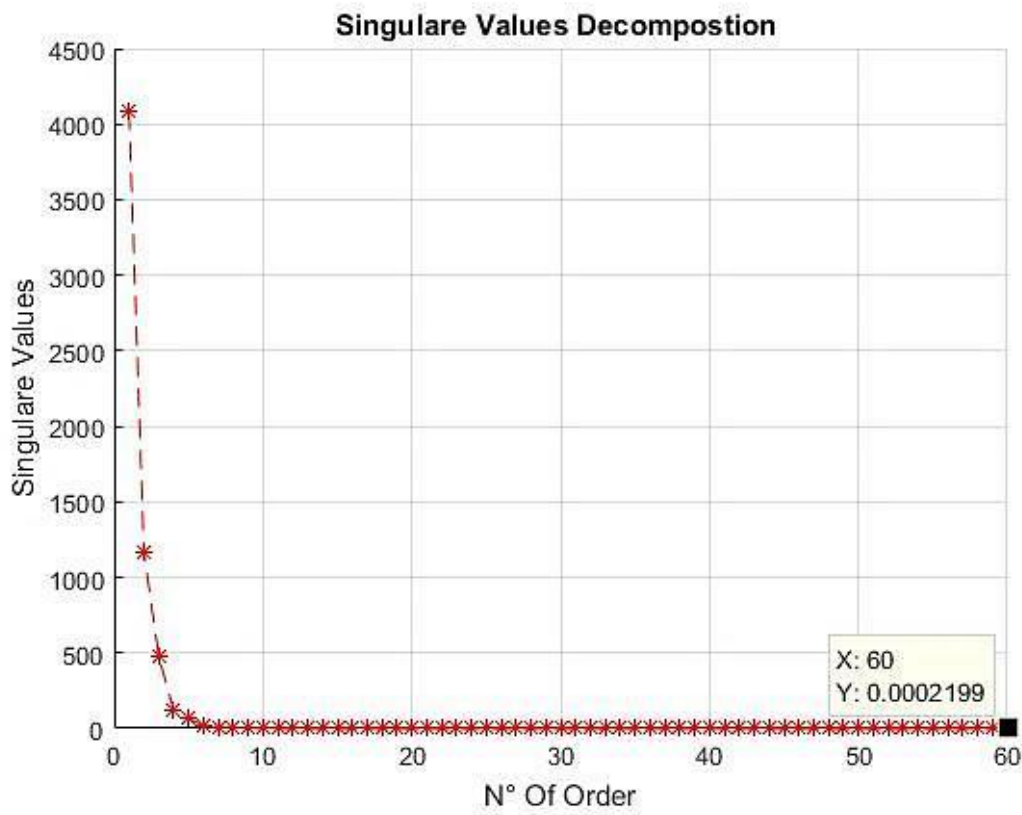
Fig 4.3.10: Singular Values of the Hankel Matrix H_0 .

The Fig.4.3.9 shows the stabilization diagram determined by the ERA Method, its clarity permits to recognize the presence of seven clusters to consequently determine the model parameters of these seven modes. In this diagram of stabilization the stable poles appeared when the number of order surpassed 20. However from the Fig.4.3.10 representing the plot of the Singular Values Decomposition in function of number of order, it can be noticed that this method failed to estimate the number of physical modes present in the system, and that the amplitude of the *SVD* drops drastically when the number of order is equal to 3. When the number of order is one the *SVD* is found very high, this means that the Hankel of matrix is very close to the singularity. Increasing the number of order, this amplitude decrease, and when it goes down the stable poles start to be visible in the stabilization diagram, this indicates that the Hankel of matrix became distance from the singularity.
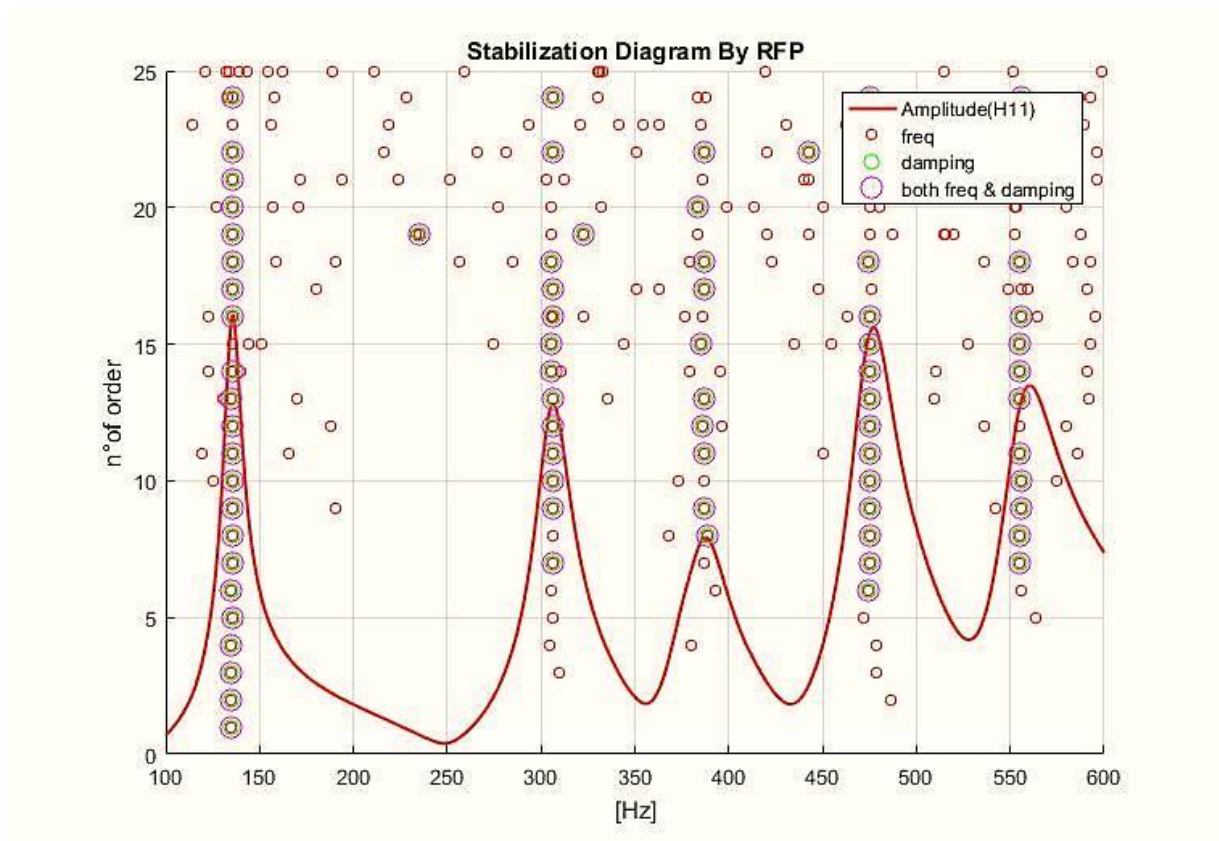
Fig4.3.11: Stabilization diagram by RFP of the plate.

The stabilization diagram determined by RFP illustrated in the Fig.4.3.11 shows that when a large bandwidth of frequency is selected, only four physical modes

appeared and each mode correspond to a single cluster. In this case many physical modes did not appear, thus if the bandwidth of the frequency is narrowed on the sides of the peak, others modes that were not present in the stabilization diagram plot above can be found. If it is restricted around the first and the third modes, a new stable pole can be found as shown in the Fig 4.3.12 a new pole that has 133.3 Hz as frequency can be obtained, also in Fig 4.3.13 a new cluster that has a 375 Hz as a frequency can be acquired.
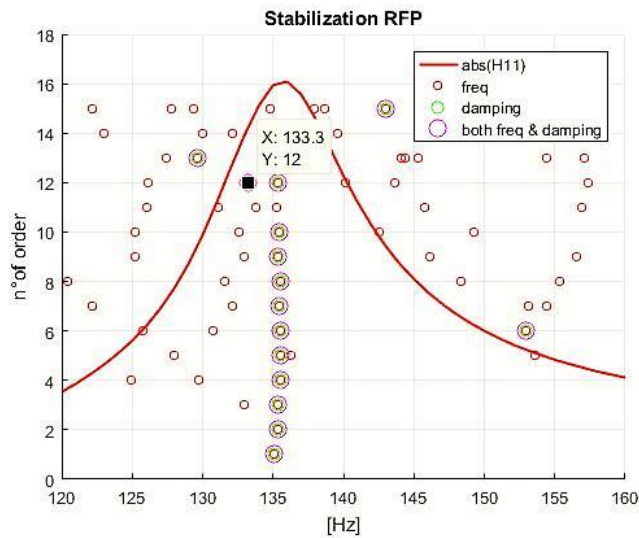
Fig 4.3.12: Stabilization diagram of the first mode surrounding
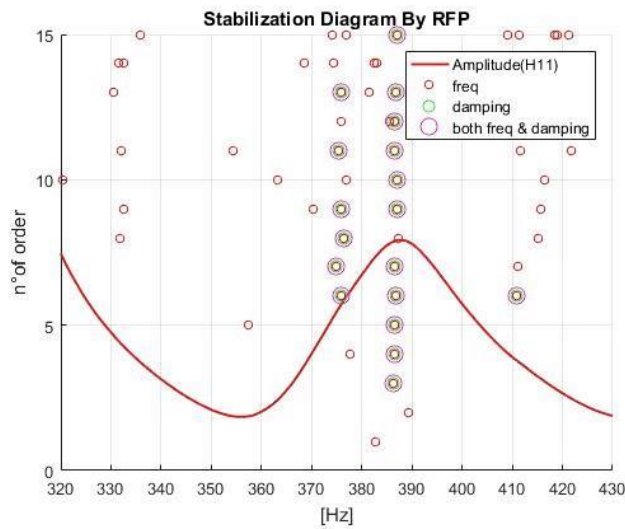
Fig 4.3.13: Stabilization diagram of the third mode surrounding
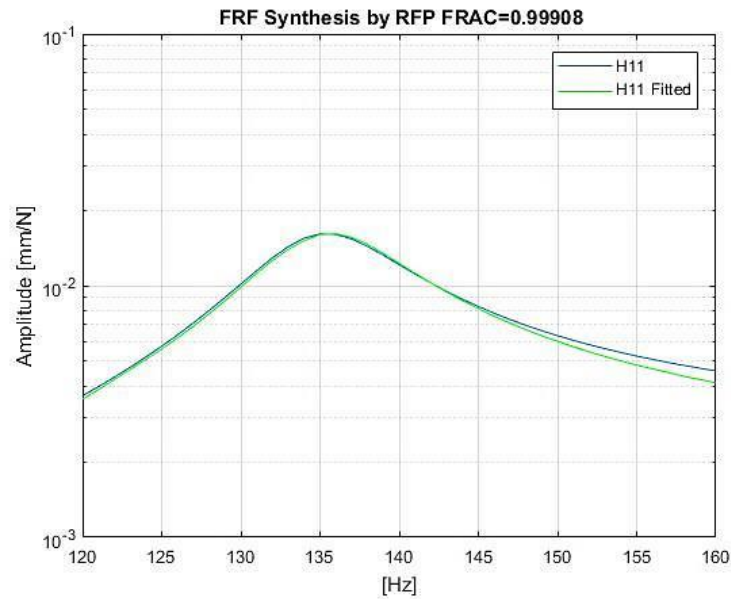
Fig 4.3.14: Synthesis of the FRF of the first modes by RFP.
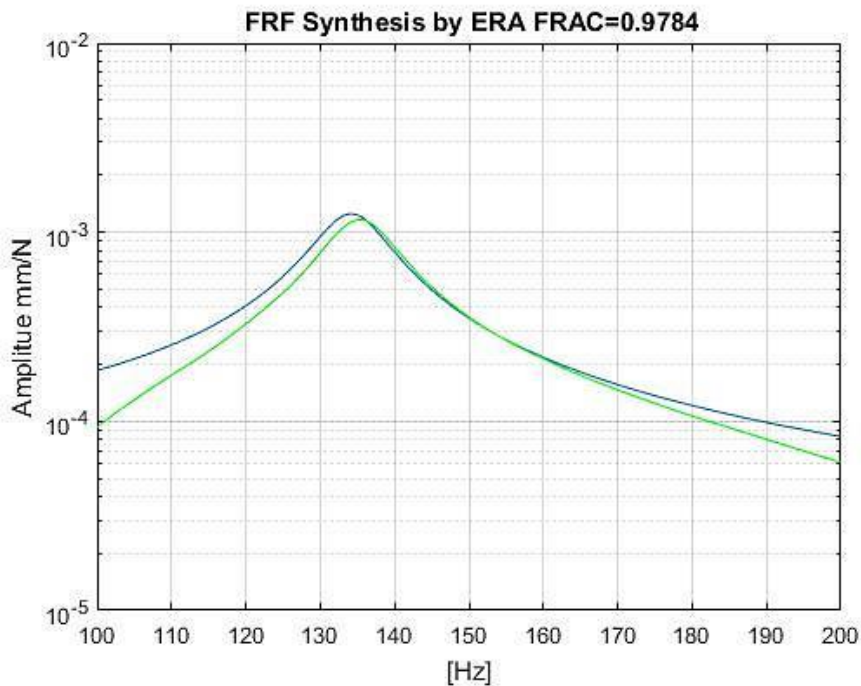
Fig4.3.15: Synthesis of the FRF close to the first modes by ERA

In order to choose the best pole in the cluster, each mode in the FRF is divided, as showed in the Fig 4.3.12 and Fig 4.3.13 and since clusters has multiple poles, to choose the best pole using ERA and RFP methods, the FRF were reconstructed in the bandwidth for each mode then it is compared in the bandwidth selected using the FRAC as seen in Fig 4.3.14 and Fig 4.3.15. This procedure will be repeated in all the poles present in the cluster. Basing on the results, the FRAC that has the highest value correspond to the best pole.

After choosing the best pole for each mode, FRF is fitted on the bandwidth that contains all the modes. This can be seen in the Fig 4.3.24 and Fig 4.3.25. .
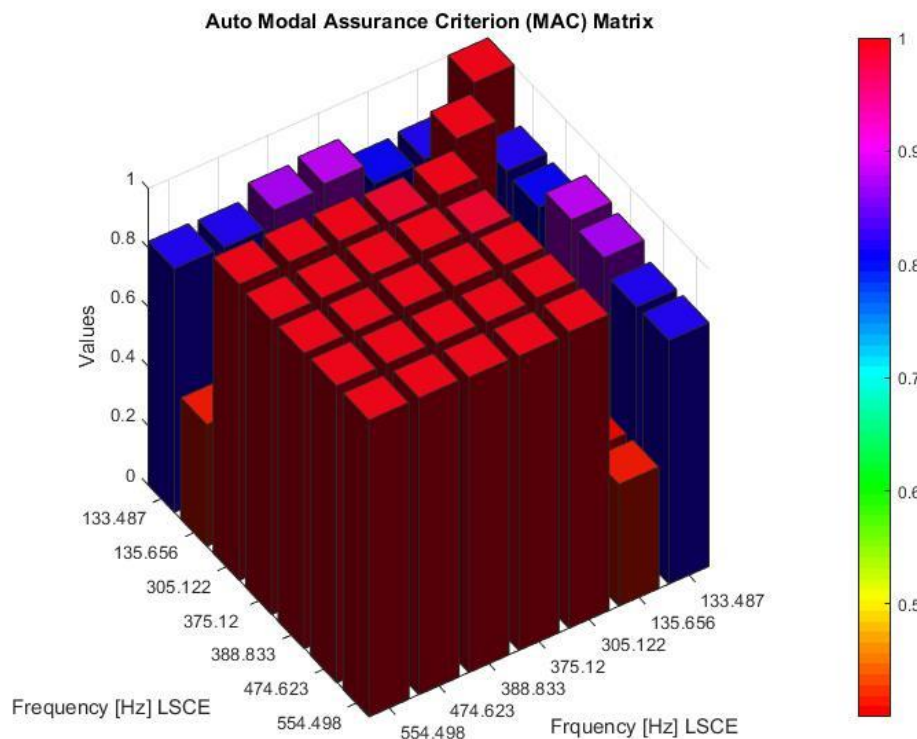
Fig 4.3.16: Auto-Modal Assurance Criterion of Modes extracted by the LSCE

The Fig.4.3.16 displays a comparison between the mode shapes extracted by the LSCE. As can be seen all the mode shapes are found similar, this demonstrates that the AutoMAC is not suitable to determinate whether there are insufficient degree-of-freedom in order to discriminate between the different modes. The same issue can be noticed in the Fig.4.3.17 when the mode shapes were extracted from the LSCE Toolbox. In the Fig.4.3.18 the modes shapes obtained by the LSCE and the others extracted by the LSCE Toolbox were compared using *MAC.* In this figure a similarity between the mode shapes was detected indicating that LSCE does not provide a good estimation for mode shapes in the plate using 15 FRFs Receptance.
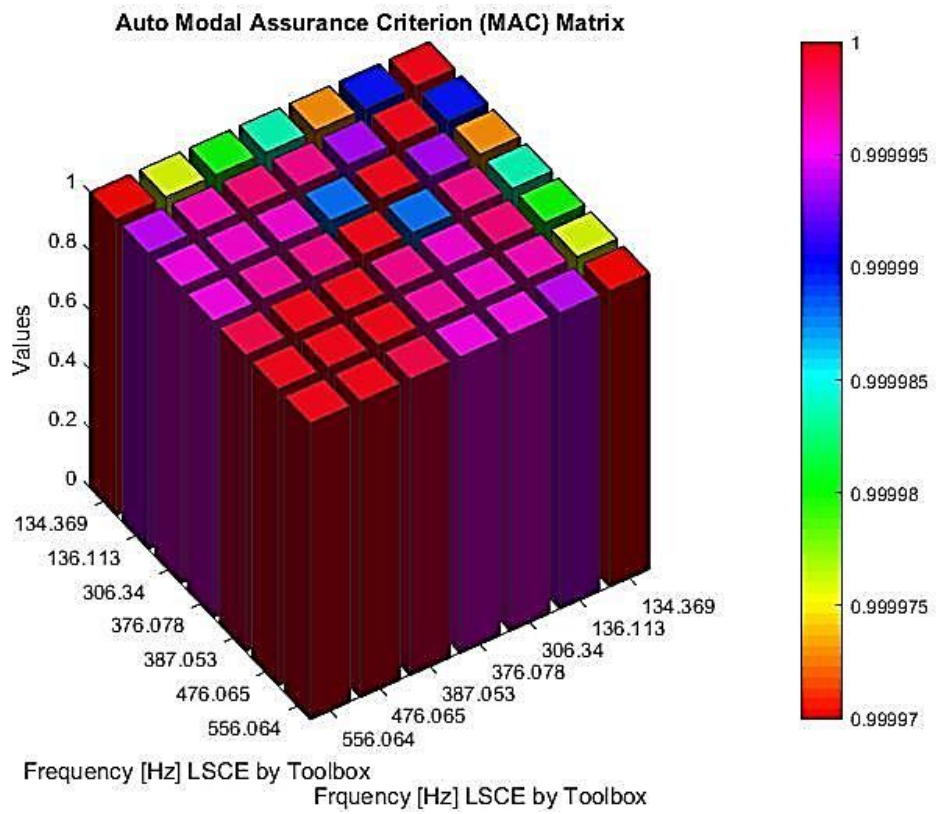
Fig 4.3.17: Auto-Modal Assurance Criterion of modes extracted by the LSCE Matlab toolbox.
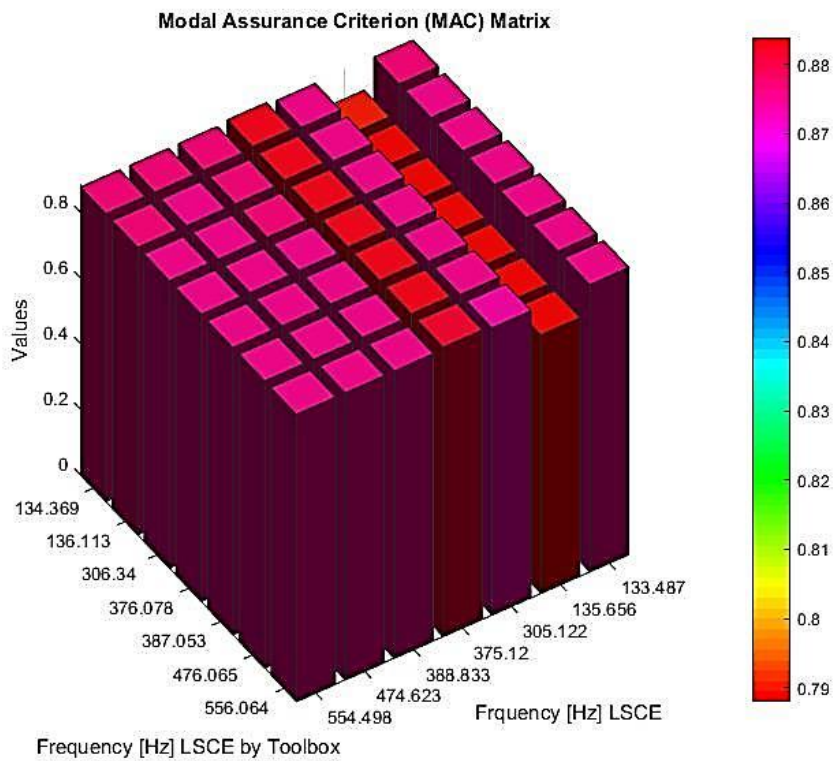
Fig 4.3.18: MAC of modes extracted by the LSCE Matlab toolbox and LSCE.
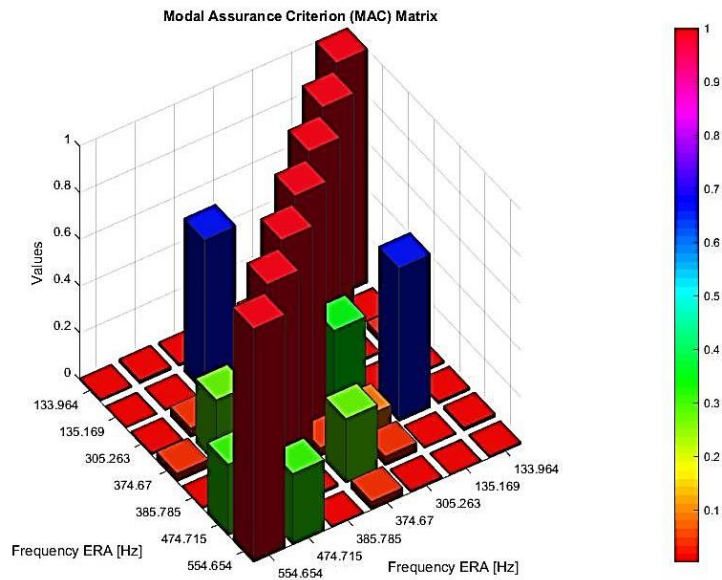
Fig 4.3.19: Auto-Modal Assurance Criterion by modes extracted by ERA.
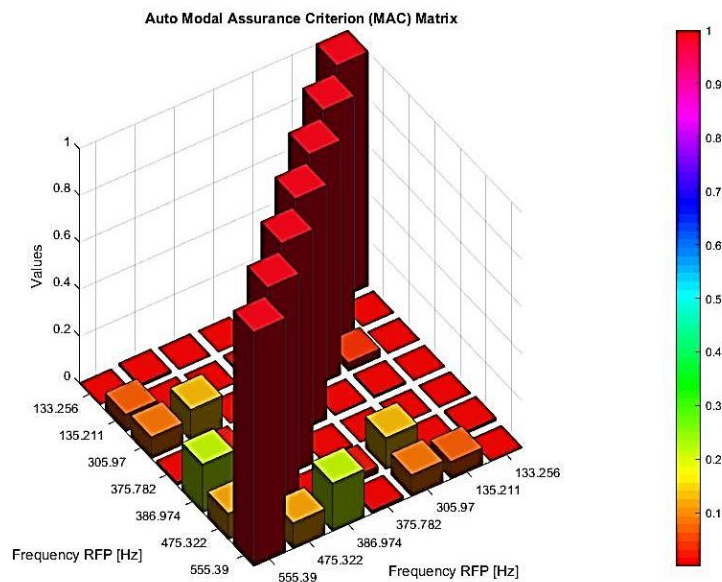
Fig 4.3.20: Auto-Modal Assurance Criterion by modes extracted by RFP.

The comparison between the mode shapes extracted from the ERA Method is shown in the Fig.4.3.19, the terms existing on the diagonal in this figure have a value of AutoMAC equivalent to one, the off-diagonal terms are not too high indicating except on the second and the fifth modes where the AutoMAC indicates a slightly high number (about 70%), in this case, it is possible to say that not enough sensors have been considered. However in the Fig.4.3.20 representing the comparison between the modes shapes extracted from the RFP, it can be

seen that the off-diagonal are not too high indicating, hence this method verify the opposite, it ensures that sufficient sensors have been considered in this state.
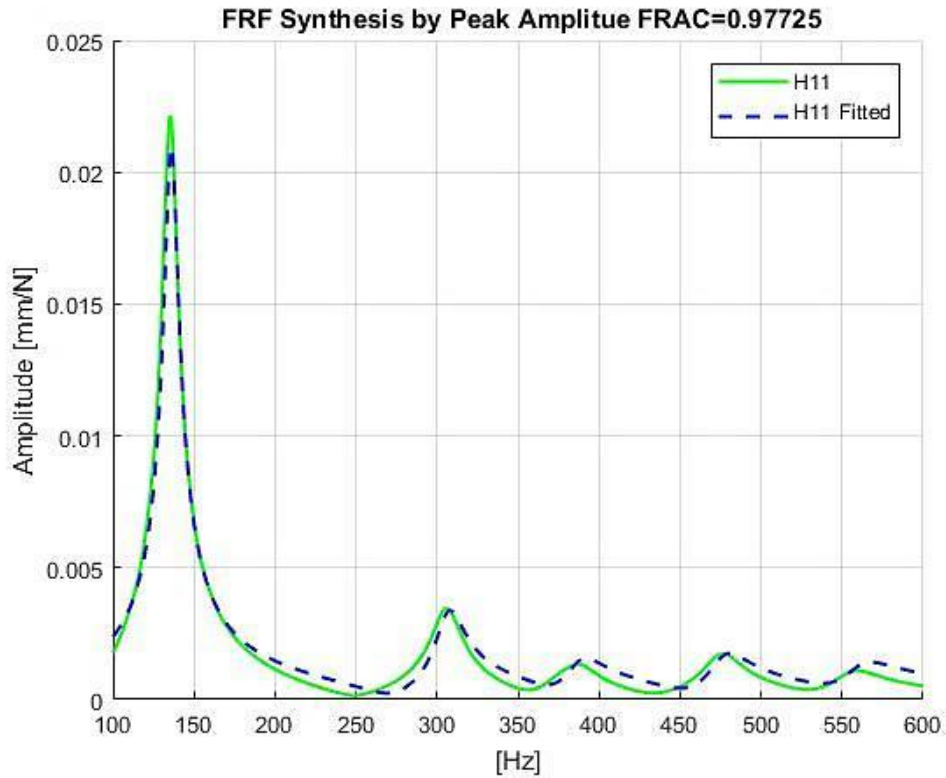
Fig 4.3.21: Fitting the FRF H11 by PP of plate.
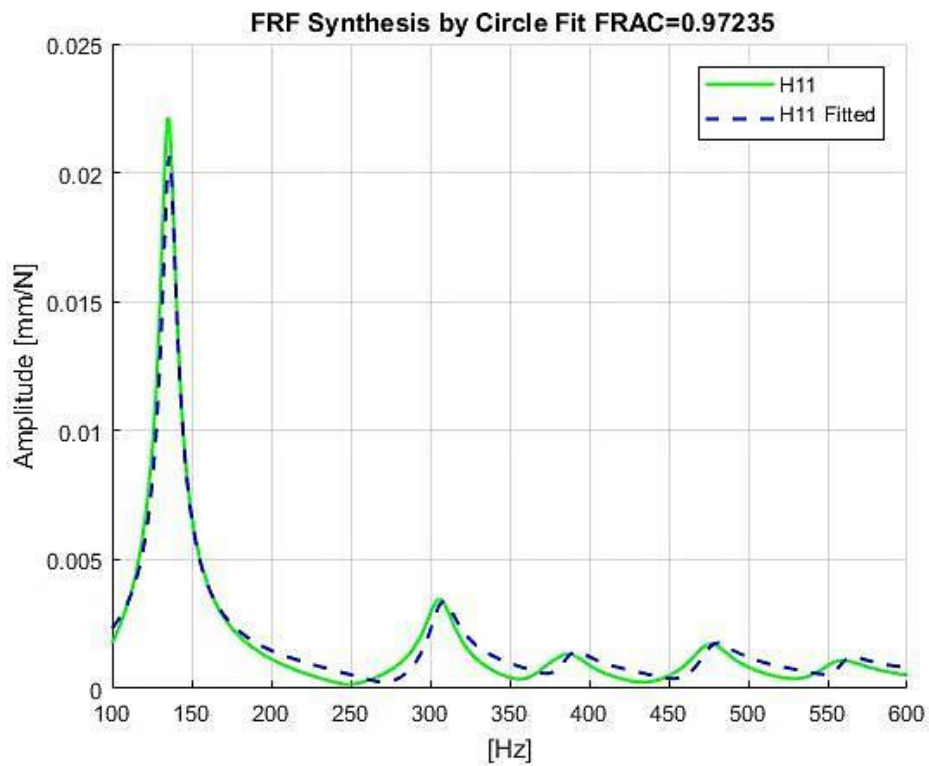
Fig 4.3.22: Fitting the FRF H11 by CF of plate.
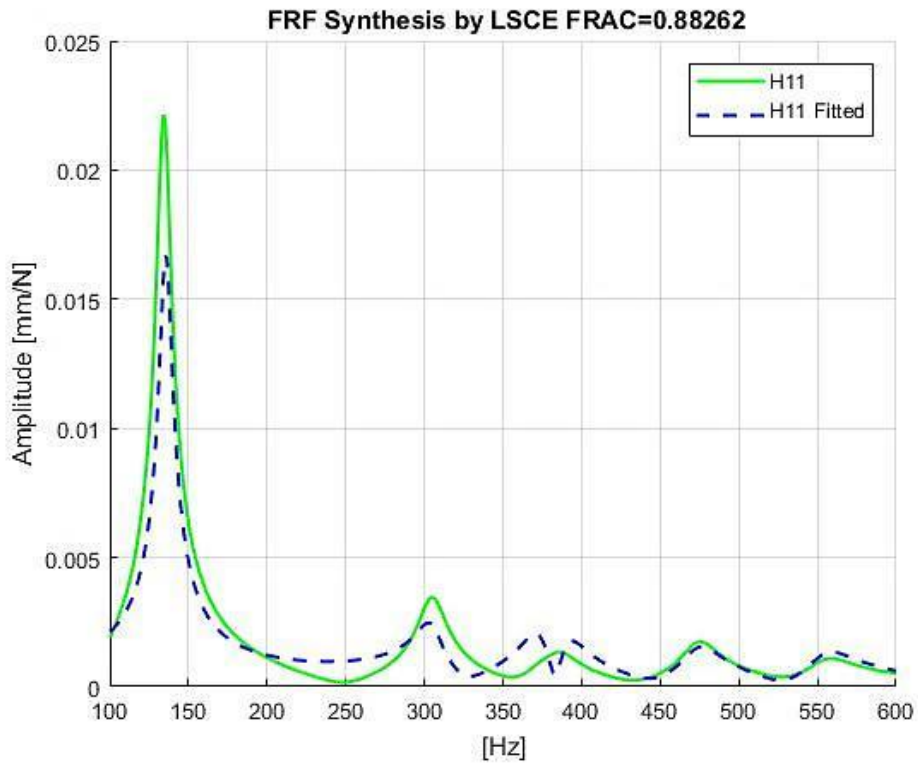
Fig 4.3.23 : Fitting the FRF H11 by LSCE plate.
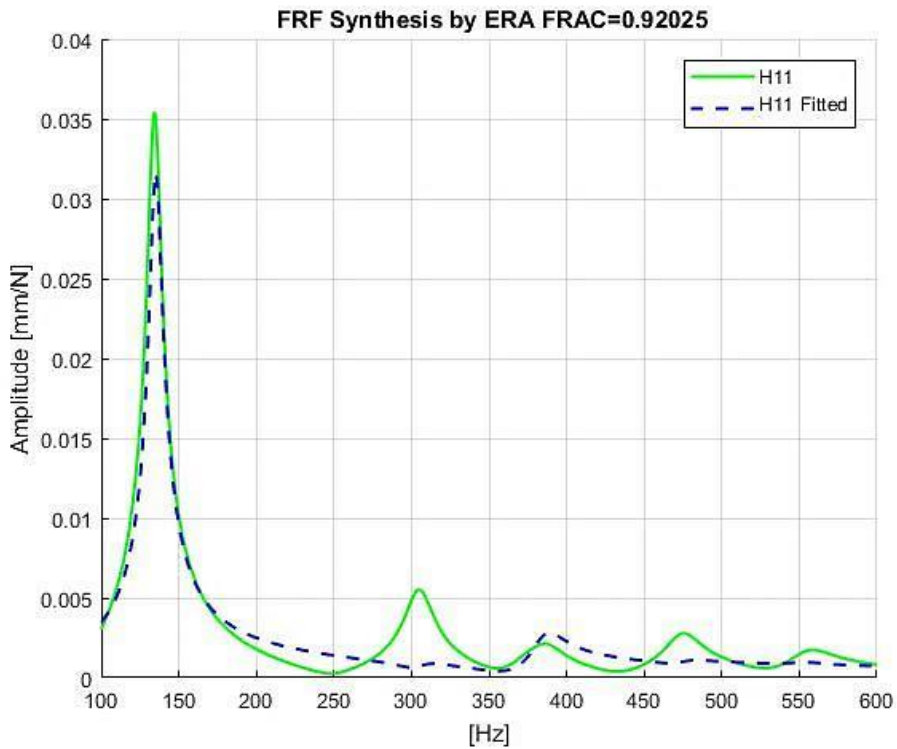
Fig 4.3.24: Fitting the FRF H11 by ERA of plate.
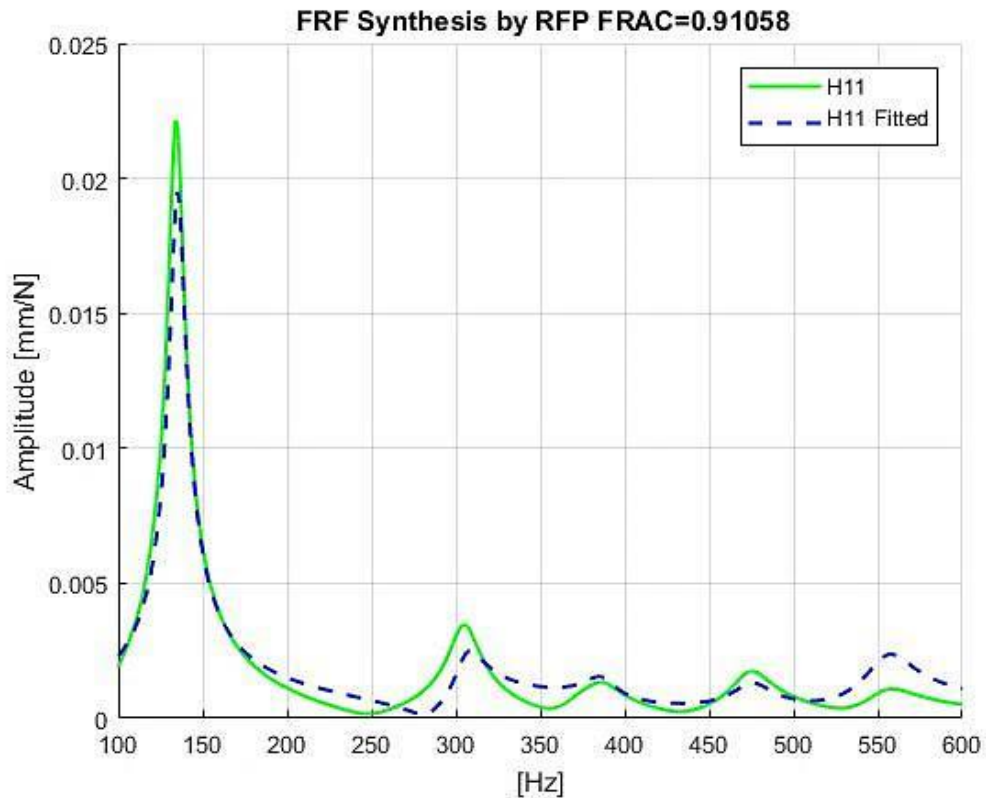
Fig 4.3.25 : Fitting the FRF H11 by RFP of plate.

In the figures ranging from Fig.4.3.21 to the Fig.4.3.25 there was a comparison between the chosen H_{11} from the FRFs Receptance measured with the H_{11} regenerated by the modal parameters extracted. In this case, the highest value for the FRAC was obtained from the *PP* Method followed by the *CF* Method that gave lower values, next comes the ERA, then the FRP, and the lowest values were obtained by the LSCE Method. This result allows saying that the plate has a proportional damping that led to consider that the PP and the CF Methods are the one to provide a good estimation for the modal parameters. Despite the fact that two physical modes could not be estimated, this estimation still deems to be considered advantageous. The LSCE gave the lowest value for the FRAC and it was the worst to estimate the mode shapes, even though it served well in estimating the frequency and the damping. Regarding the results gave by ERA Method, here and in all the previous cases, it can be said that it succeeded in delivering a good estimation for all the modal parameters.

Plot the mode shapes:

In this step the modes shapes of the Plate extracted by Polymax, LSCE, LSCE Toolbox, ERA and RFP will be plotted in the Argand Plan (Real vs Imaginary Part).
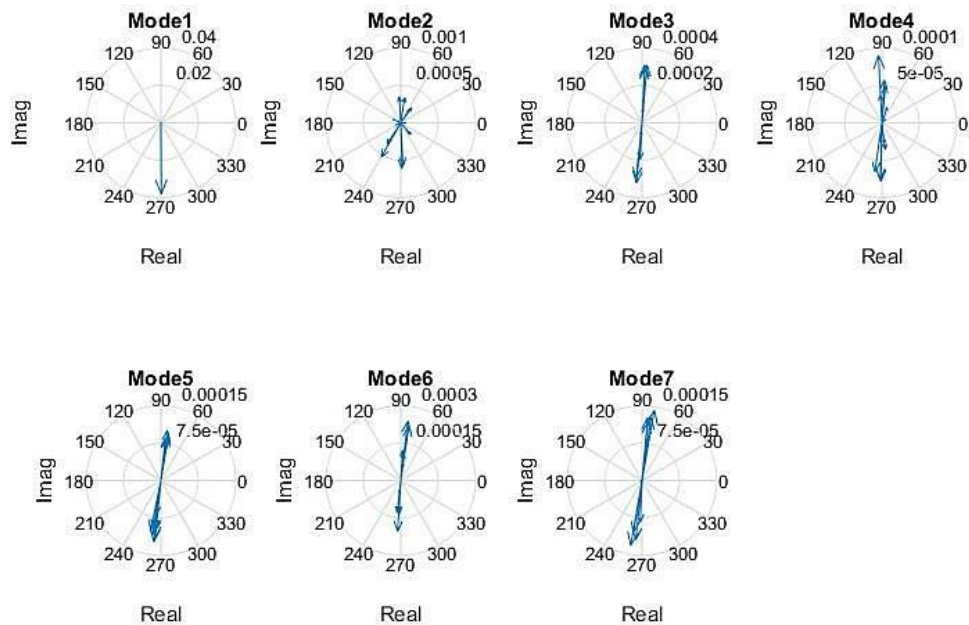
Fig 4.3.26: mode shapes extracted by Test-Lab Polymax method of the plate.
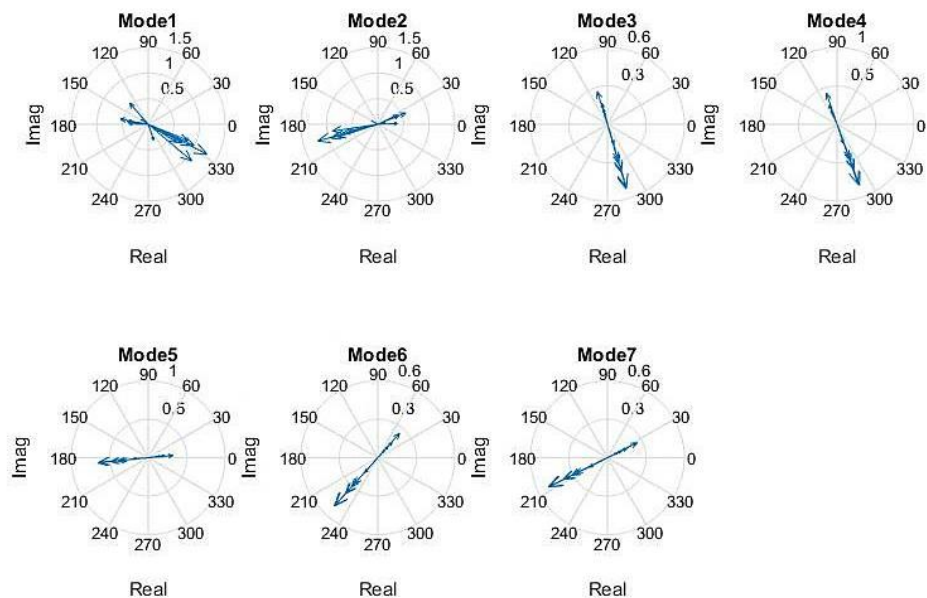
Fig 4.3.27: mode shapes extracted by LSCE of the plate.
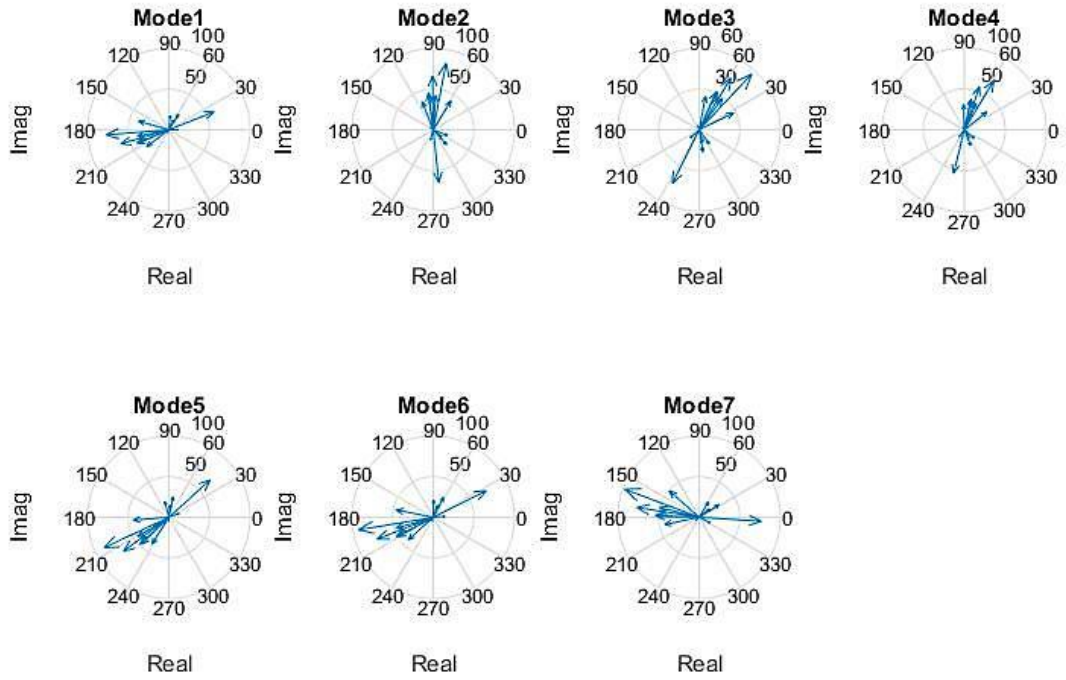
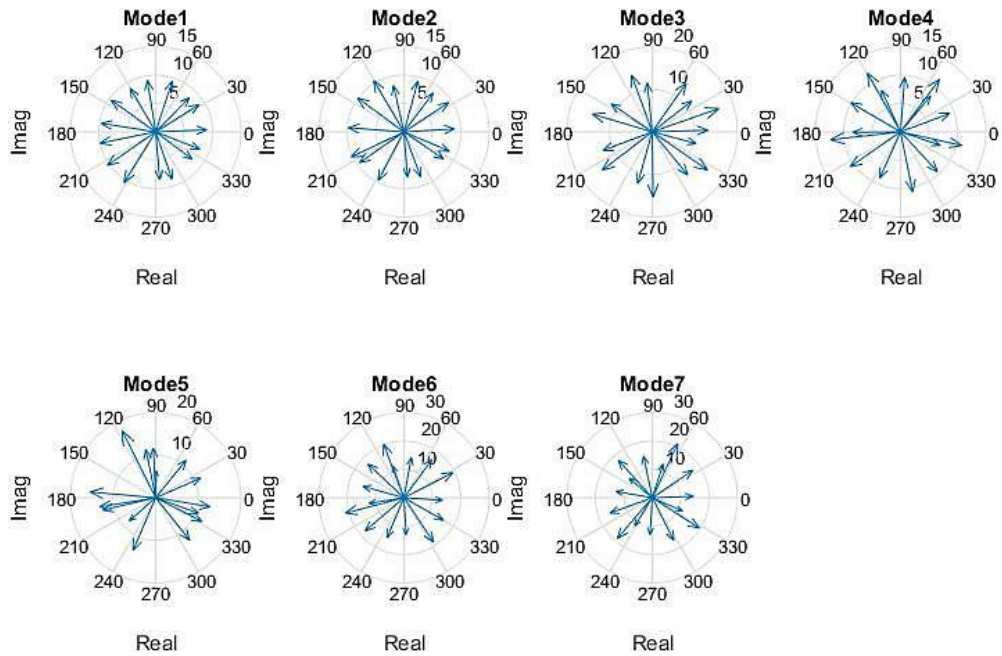*Fig 4.3.28: mode shapes extracted by LSCE Matlab toolbox of the plate .*
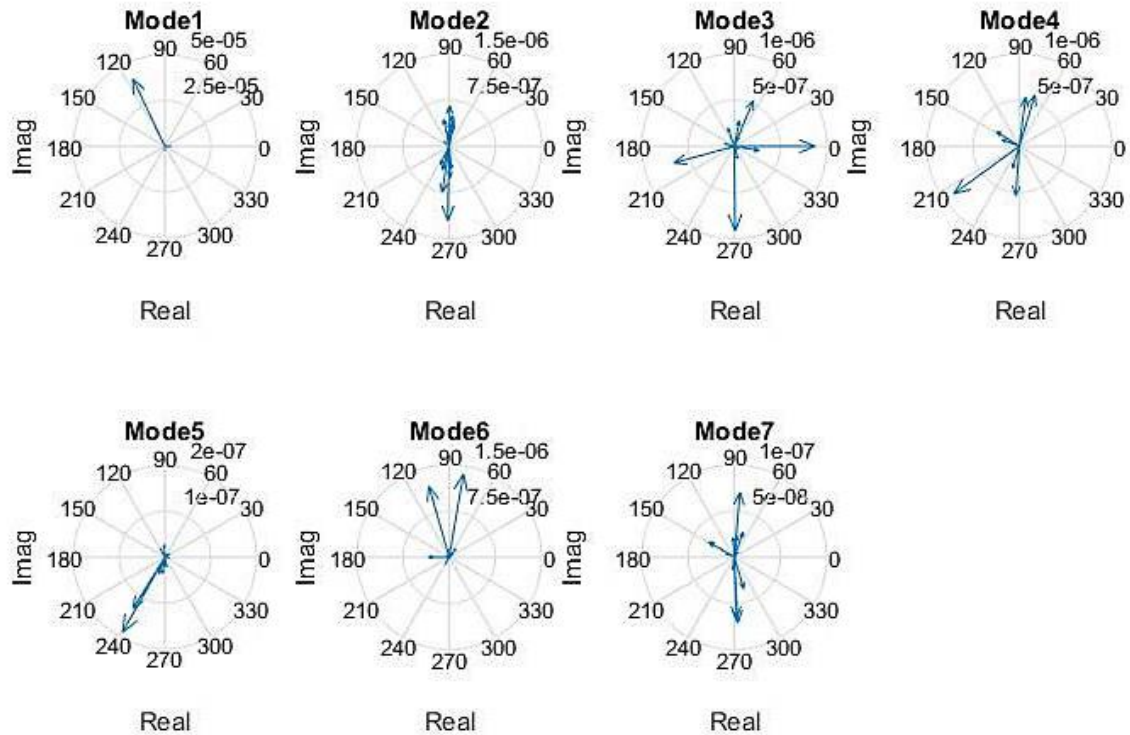

Fig 4.3.29: mode shapes extracted by ERA of the plate.

Fig 4.3.30: mode shapes extracted by RFP of the plate

The figures arranged from Fig.4.3.26 to Fig.4.3.30 illustrate the design of the vibration modes in term of amplitude and phase. In the Fig.4.3.26 representing the mode shapes calculated in the Polymax Method, all the mode shapes have a phase close to 90°, if they are scaled by j (complex number), a phase close to 0° or 180° can be obtained, except for the second mode that has an angle and phase arbitrary sparred. If the focus is laid on the other modes, it can be stated that this case is close to be a proportional damping. Observing the Fig.4.3.27 and Fig.4.3.28 that represent the mode shapes extracted respectively by the LSCE implemented and the LSCE Toolbox, it can be seen immediately and clearly that the mode shapes are dispersed in the same manner but rotated by an angle α. From the Fig.4.3.29 showing the mode shapes extracted by ERA, it can be detected that the mode shapes angles range between 0° and 360°. In this method it can be noted that the mode shapes are not close to be real, this permits to say that the modes extracted by the ERA Method are not similar to those extracted by the Polymax Method. The Fig.4.3.30 displays the mode shapes extracted by the RFP. It reveals that their phase ranges between 0° and 360°.
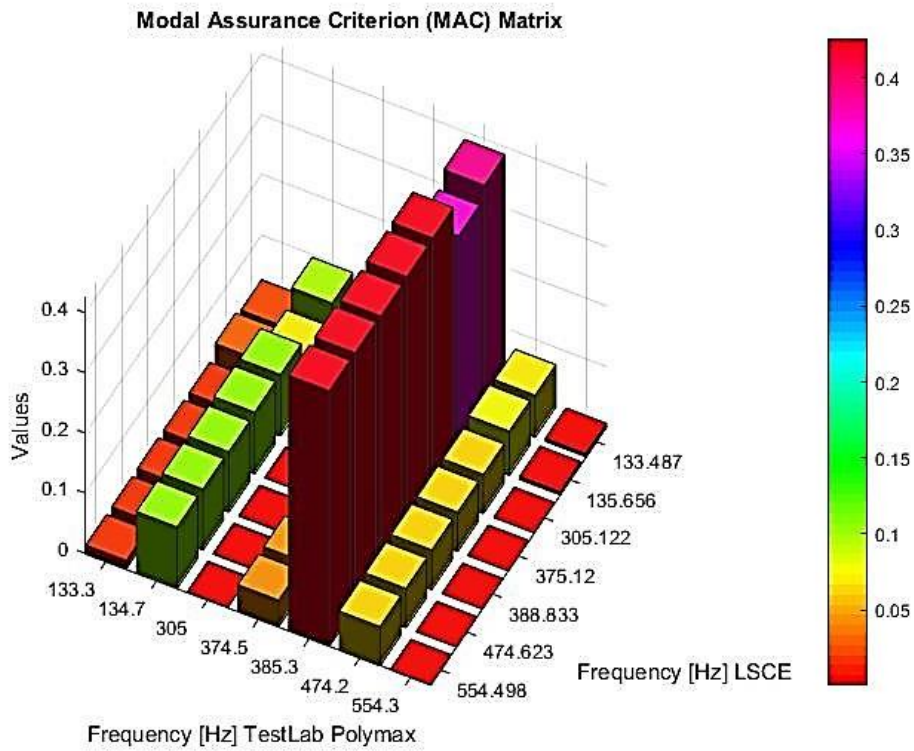
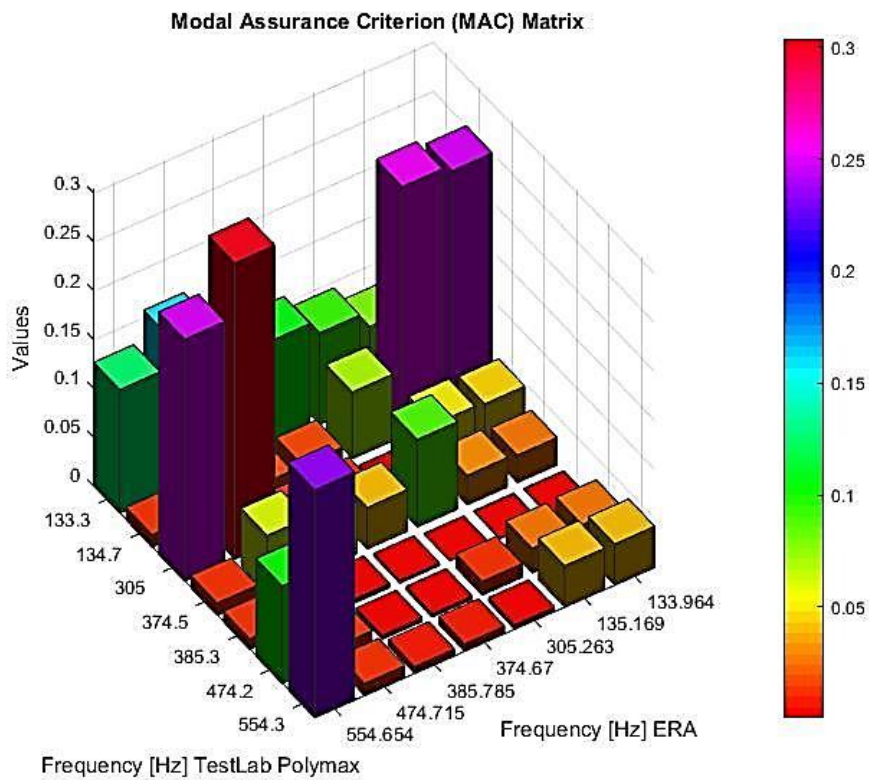*Fig 4.3.31: MAC of the mode shapes extracted by LSCE and Test-Lab Polymax.*

Fig 4.3.32: MAC of the mode Shapes extracted by ERA and Test-Lab Polymax.
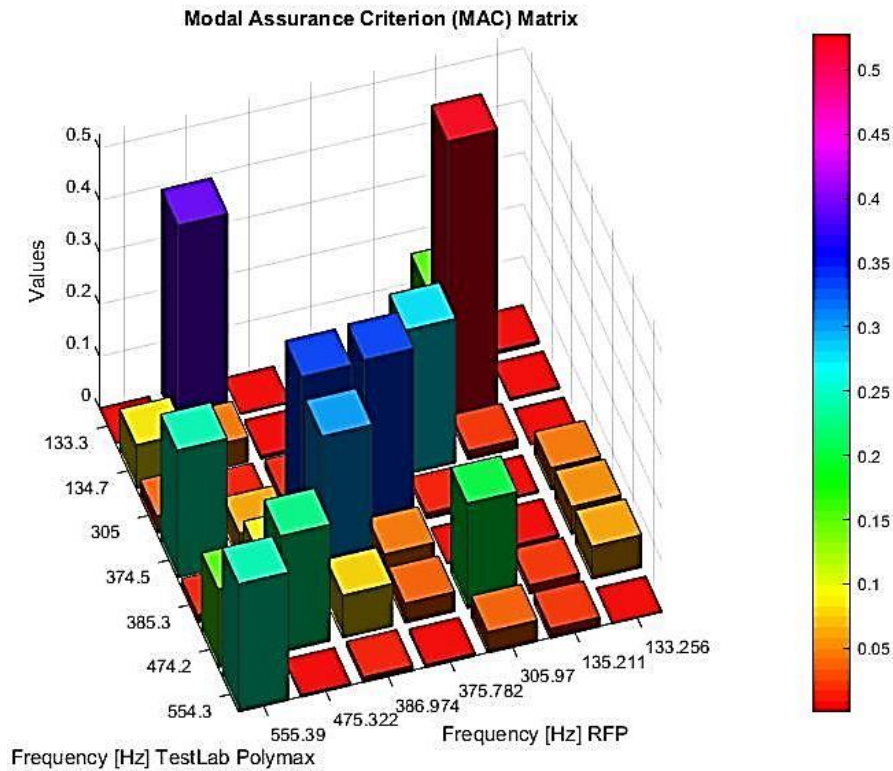
Fig 4.3.33: MAC of the Mode Shapes extracted by RFP and Test-Lab Polymax.

The Fig.4.3.31, Fig.4.3.32 and Fig.4.3.33 represent comparisons between the mode shapes extracted respectively by the LSCE, ERA and RFP with the mode shapes obtained from Polymax Method using MAC. In all these cases the values of MAC were very low; which indicated the non-correlation between the mode shapes calculated using the three methods and the modes shapes calculated by Polymax. The highest value of MAC was obtained through the mode shapes extracted by the RFP. As the diagonal in the Fig.4.3.33 shows, the second mode extracted by the FRP and the Polymax reached 50%, and the other modes had values ranging between the 25% and 40%. In the two previous figures, the worst modes shapes are those calculated using the LSCE, since the values of the diagonals were very low. The results of the MAC in the ERA Method were slightly better comparing to the LSCE.

132

4.4   Gearbox Experimental Data.

In this example a gearbox with 34 accelerometers has been considered, as shown in the Fig 4.4.1, and the gearbox will be excited by a hammer in point pt 1 in direction x, y and z. then the 34 FRF which represent one row of the matrix of FRF will be measured. The parameters of data are described in the table 4.4:
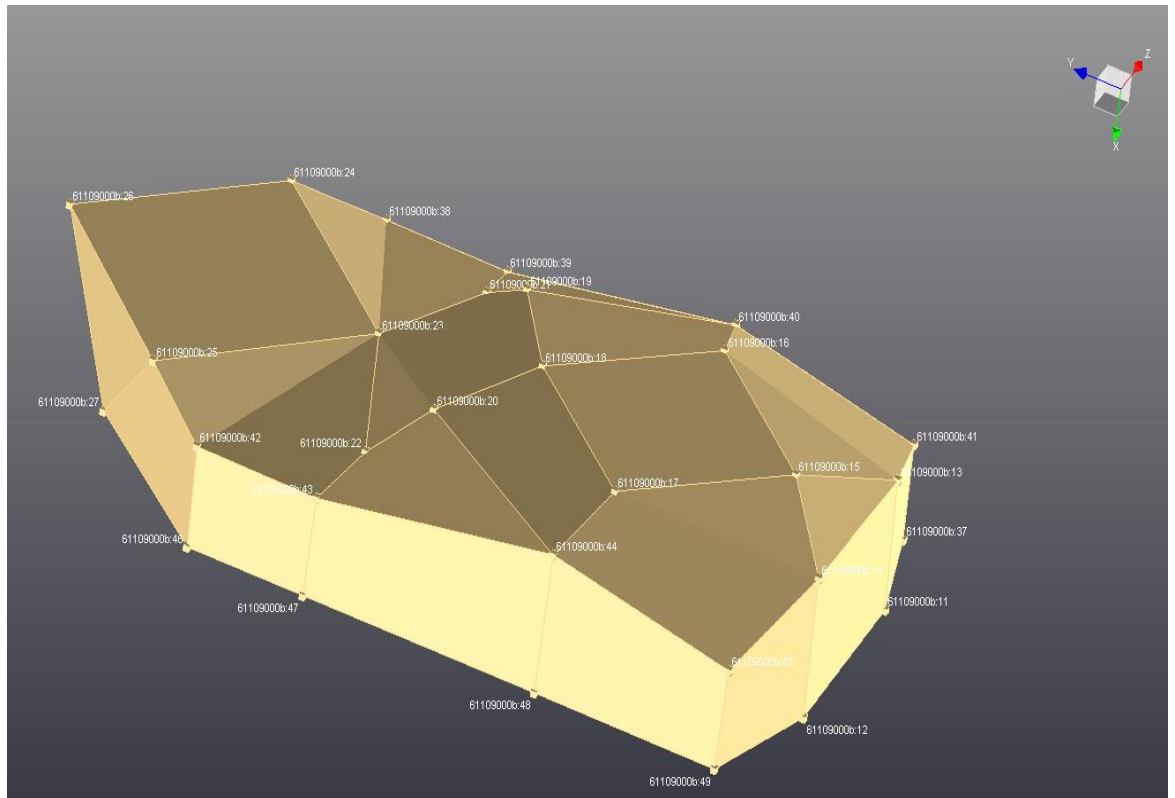

Fig 5.4.1: Model of the Gearbox.

Sample rate	25600 Hz
Spectral lines	16384
Δf	1.5625 Hz
Nyquist frequency	12800 Hz

Table 4.4: Parameters data of the gearbox.

	Mode 1	Mode 2	Mode 3	Mode 4	Mode 5
Frequency [Hz]	1705	2118	3413	3966	4339
Damping Factor %	0.18	0.53	0.28	0.45	0.74

Table 4.4.1: Frequency and damping ratio for the 5 Modes of the gearbox extracted by Test-Lab Polymax.

133

	Mode 1	Mode 2	Mode 3	Mode 4	Mode 5
Frequency [Hz]	1709	2125	3415	3964	4343
Damping Factor %	0.27	0.55	0.44	0.45	0.74

Table 4.4.2: Frequency and damping ratio for the 5 Modes of the gearbox extracted by the PP method.

	Mode 1	Mode 2	Mode 3	Mode 4	Mode 5
Frequency [Hz]	1707	2123	3414	3963	4342
Damping Factor %	0.23	0.5	0.53	0.47	0.74

Table 4.4.3: Frequency and damping ratio for the 5 modes of the gearbox extracted by the CF method.

	Mode 1	Mode 2	Mode 3	Mode 4	Mode 5
Frequency [Hz]	1706	2116	3340	3962	4348
Damping Factor %	0.19	0.53	0.29	0.45	0.78

Table 4.4.4 : Frequency and damping ratio for the 5 modes of the gearbox extracted by the LSCE method.

	Mode 1	Mode 2	Mode 3	Mode 4	Mode 5
Frequency [Hz]	1706	2117	3414	3966	4340
Damping Factor %	0.48	0.13	0.153	0.153	0.153

Table 4.4.5 : Frequency and damping ratio for the 5 modes of the gearbox extracted by the LSCE Matlab toolbox.

	Mode 1	Mode 2	Mode 3	Mode 4	Mode 5
Frequency [Hz]	1706	2118	3413	3964	4341
Damping Factor %	0.23	0.62	0.31	0.47	0.76

Table 4.4.6: Frequency and damping ratio for the 5 modes of the gearbox extracted by the ERA method.

	Mode 1	Mode 2	Mode 3	Mode 4	Mode 5
Frequency [Hz]	1705	2122	3408	3967	4330
Damping Factor %	0.19	0.69	0.26	0.47	0.84

Table 4.4.7: Frequency and damping ratio for the 5 modes of the gearbox extracted by the RFP method
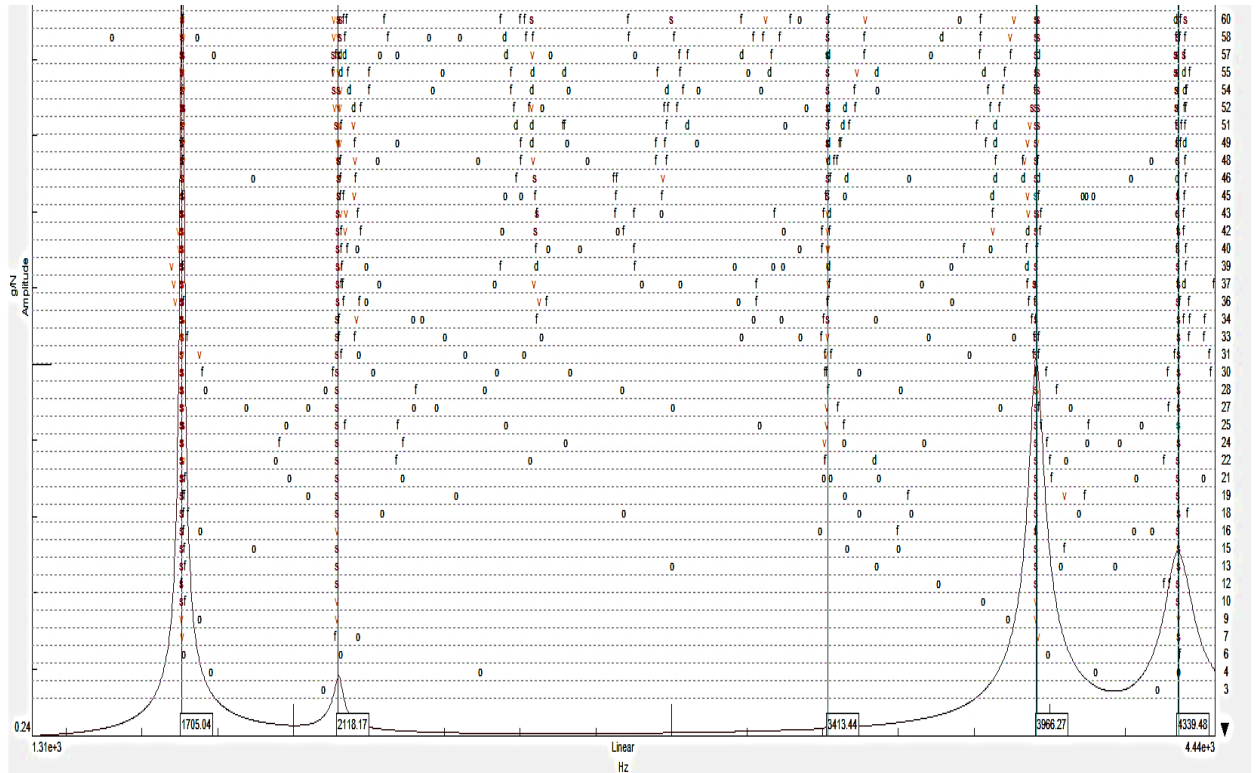
Fig 4.4.2: Stabilization diagram by Test-Lab Polymax method of the gearbox.

From the stabilization diagram of the Gearbox extracted by the Polymax Method showed in the Fig.4.4.2, the existence of five physical modes can be detected in this bandwidth, as the figure clarify, a high number of order was chosen because the third mode appears very distinctly when the number of order surpassed 45. This diagram is not as clear as the other extracted by the same method in the plate case, because the stable poles in this diagram appear discontinuous at some points when the number of order increases but in the plate case and through the Fig.4.3.2 it can be noticed that almost all the stables poles appeared when the number of order surpassed the 12 up to 32.
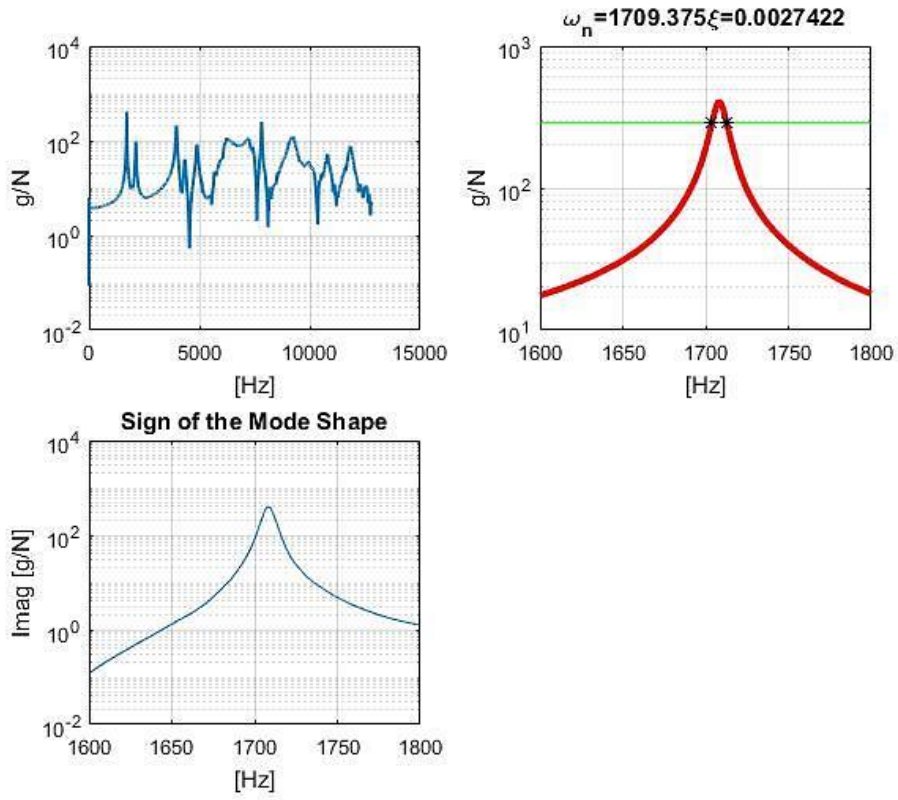
Fig 4.4.3: Estimation a modal parameters of one Mode By PP
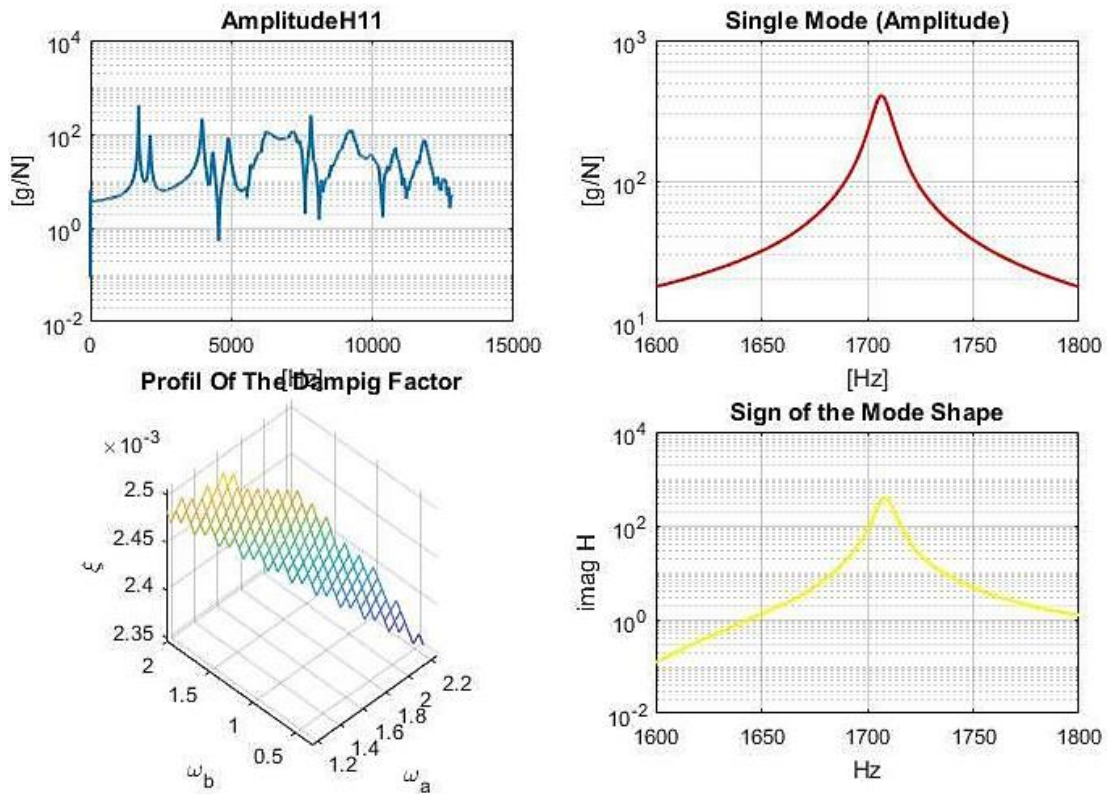
Fig 4.4.4: Estimation modal parameters by CF
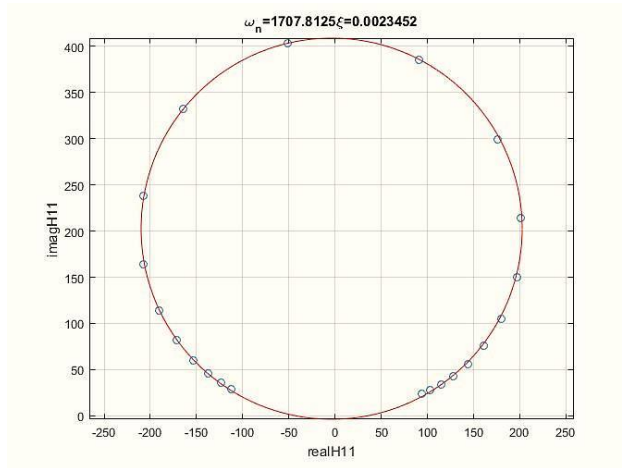
Fig 4.4.5: Fitting a circle selecting sets of points.

In the Fig.4.4.3 the Peak Amplitude Method was used for the extraction of the model parameters, it shows that the first physical mode was isolated in the same process applied in the Analytical case and the plate case. In the Fig.4.4.4 the CF Method was exerted on the first mode, then the model parameters were extracted in the same procedure used in the Analytical case and the plate case. The Fig.4.4.5 illustrating the fitting of circle using a set of point, shows that some point don't perfectly fit the circle and the deviation in this case when the system is excited by a hammer was equivalent to about 4,2%, which is still considered a good estimation.
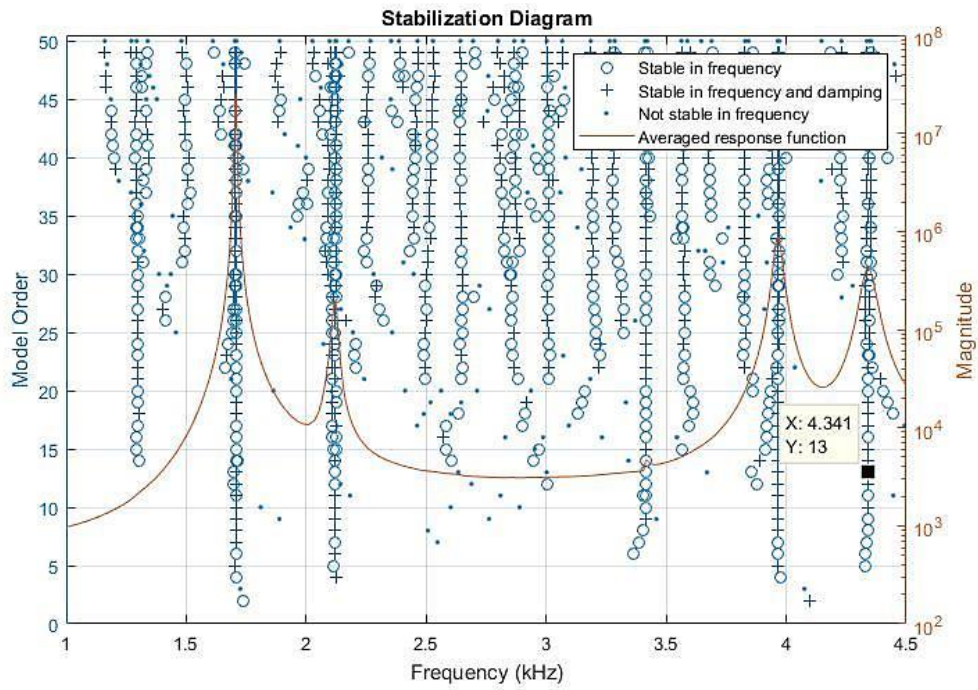
Fig 4.4.6: Stabilization diagram by LSCE Matlab Toolbox of the gearbox.
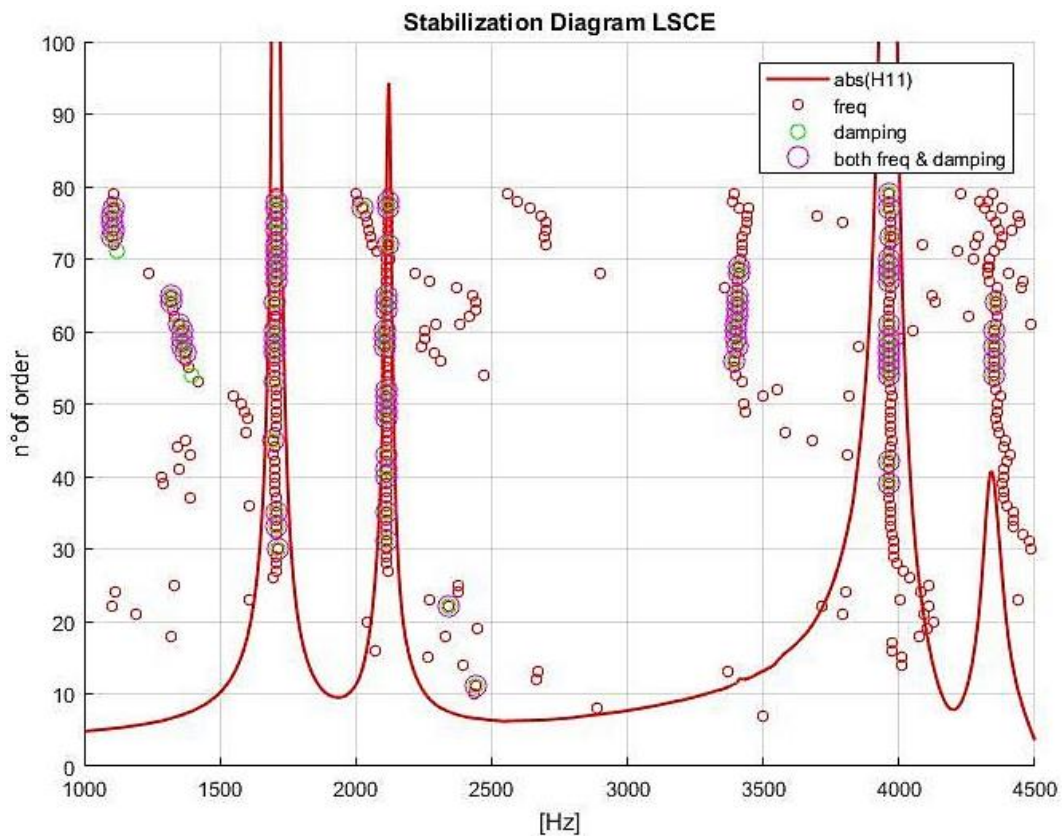
Fig 4.4.7: Stabilization diagram by LSCE of the gearbox.
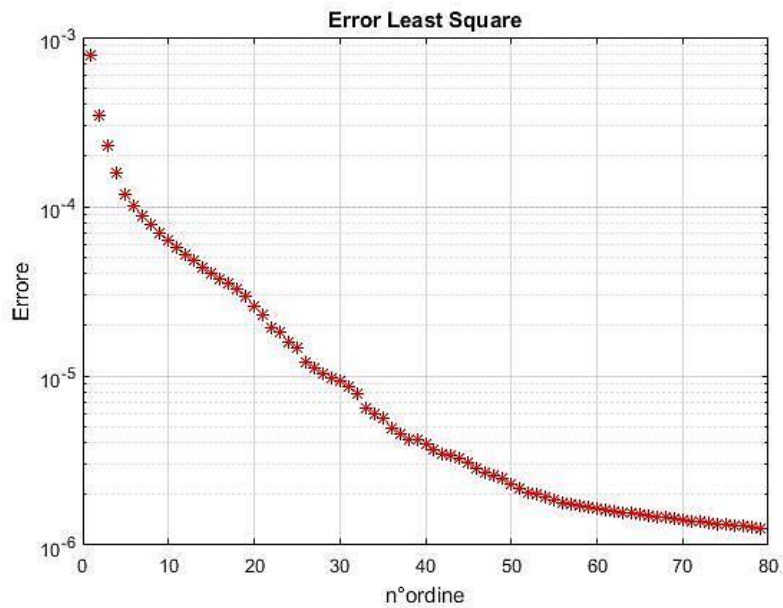
Fig 4.4.8: Least Square Error.

The Fig.4.4.6 illustrates the stabilization diagram extracted by the LSCE Toolbox, this stabilization diagram is not coherent, it presents a high number of cluster distributed chaotically many of which do not correspond to the physical modes. Through this diagram it is hard to indicate which the adequate physical modes are.

However the stabilization diagram of the Plate case was much clearer as can be seen in the Fig.4.3.6, since the stable poles started to appear for lower number of order comparing to this case. The Fig.4.4.7 represents the stabilization diagram extracted by the LSCE Method in the Gearbox case, it show that there are five clusters relatively clear that each correspond to a peak in the graph, and two small other clusters not correspond to any peak that can almost be noticeable. If compared to the stabilization diagram in the Plate case, it can be noted that this diagram is not as clear and the ability to determinate of physical modes is harder.

In this case the Least Square Error has again failed to identify the number of physical modes present in the system, as can be seen in the Fig.4.4.8; the error decreased gradually throughout the interval of numbers order, and no sharp decrease was witness as in the Plate case
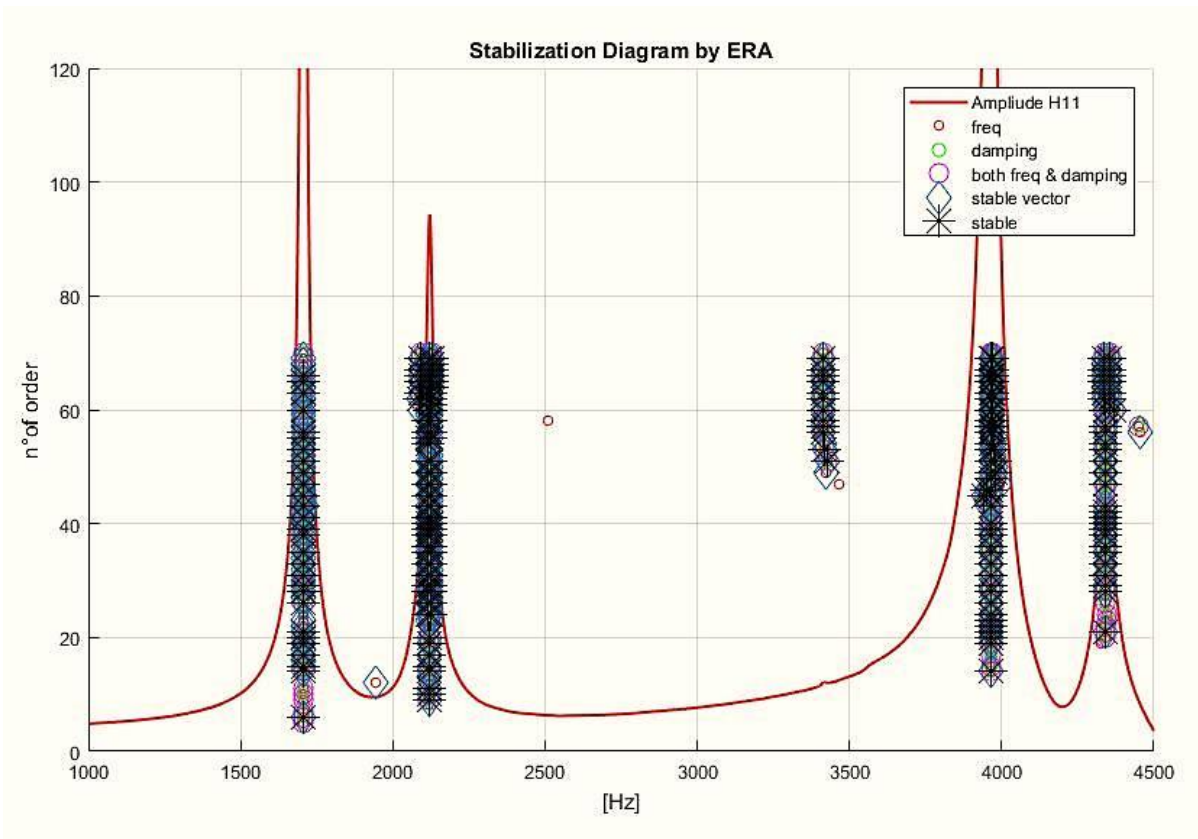
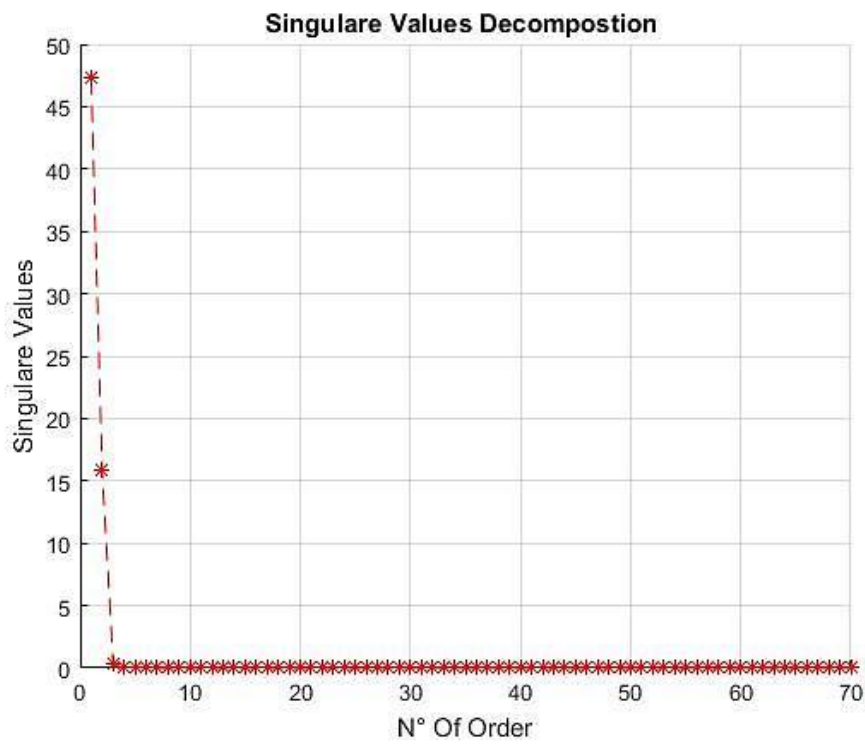*Fig 4.4.9: Stabilization diagram by ERA of the gearbox.*

Fig 4.4.10: Singular Values of the Hankel Matrix H_0.

The Fig.4.4.9 illustrates the stabilization diagram of the Gearbox extracted by the ERA Method. This diagram shows the presence of five physical modes, this diagram of stabilization is very clear and the stable poles appear only around the Peaks of the FRF function.

In the Fig.4.4.10 representing the plot of the Singular Values Decomposition in versus the number of order also, it was possible to determine he number of physical modes presented in the system from the diagram, since the *SVD* declined significantly when the number of order was equal to three.
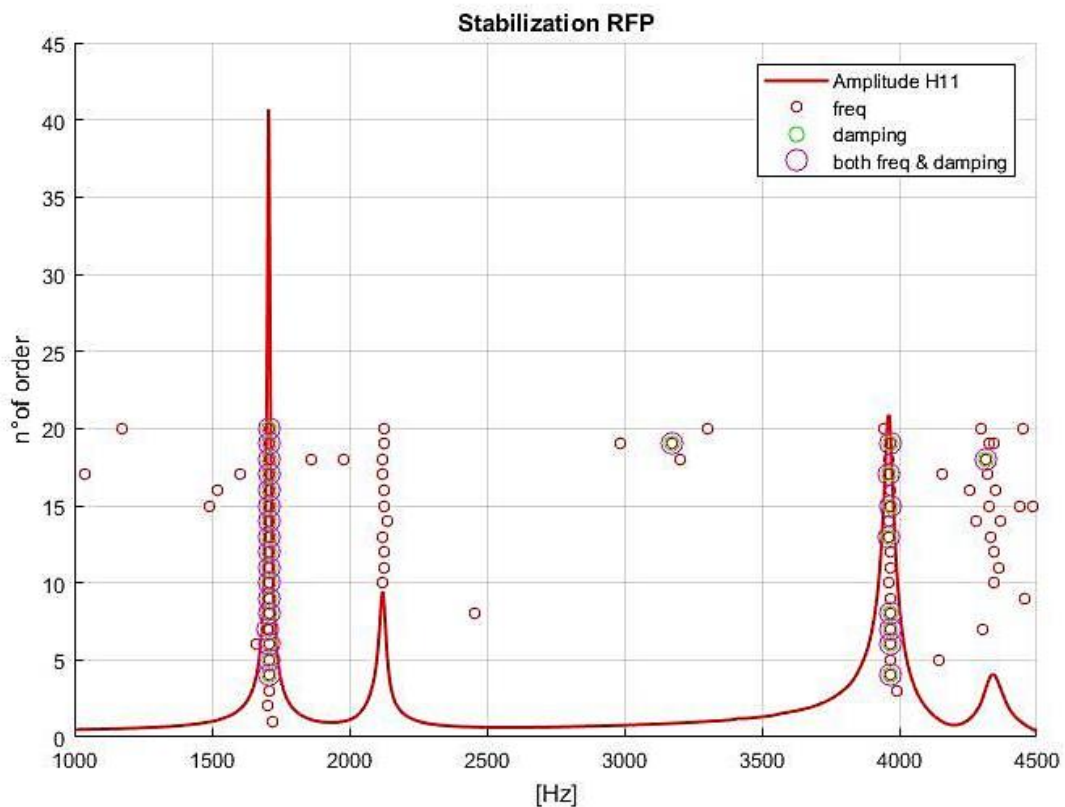
Fig 4.4.11: Stabilization diagram by RFP of the gearbox.
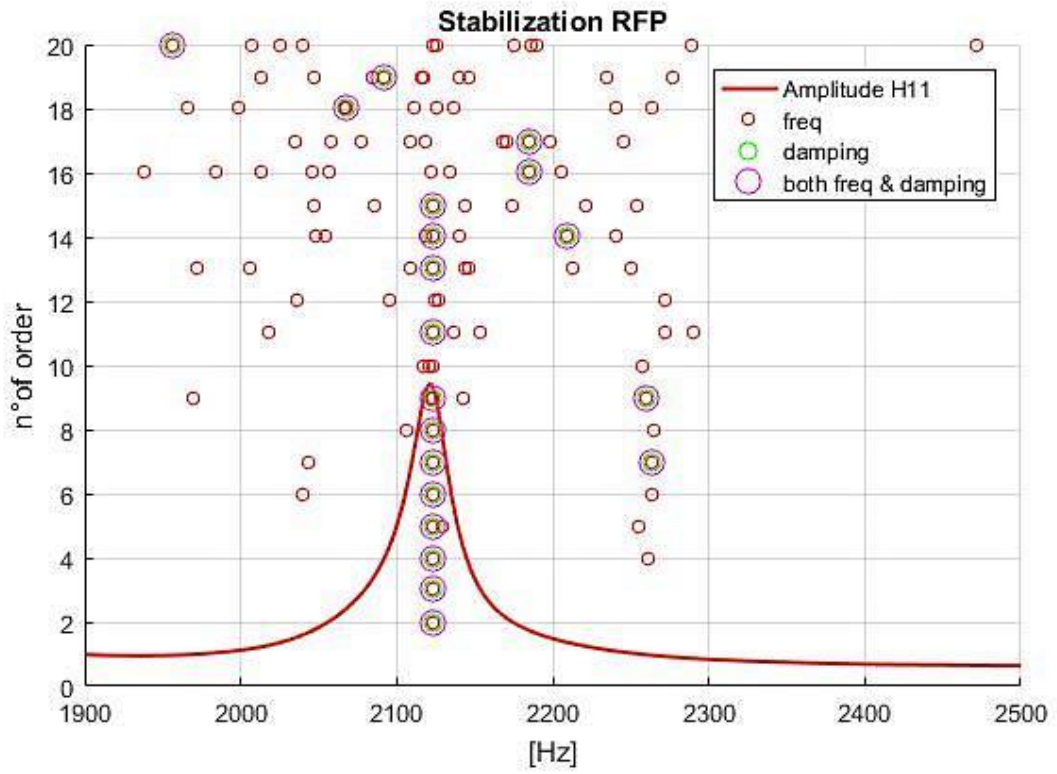
Fig 4.4.12: Stabilization diagram close to the second mode
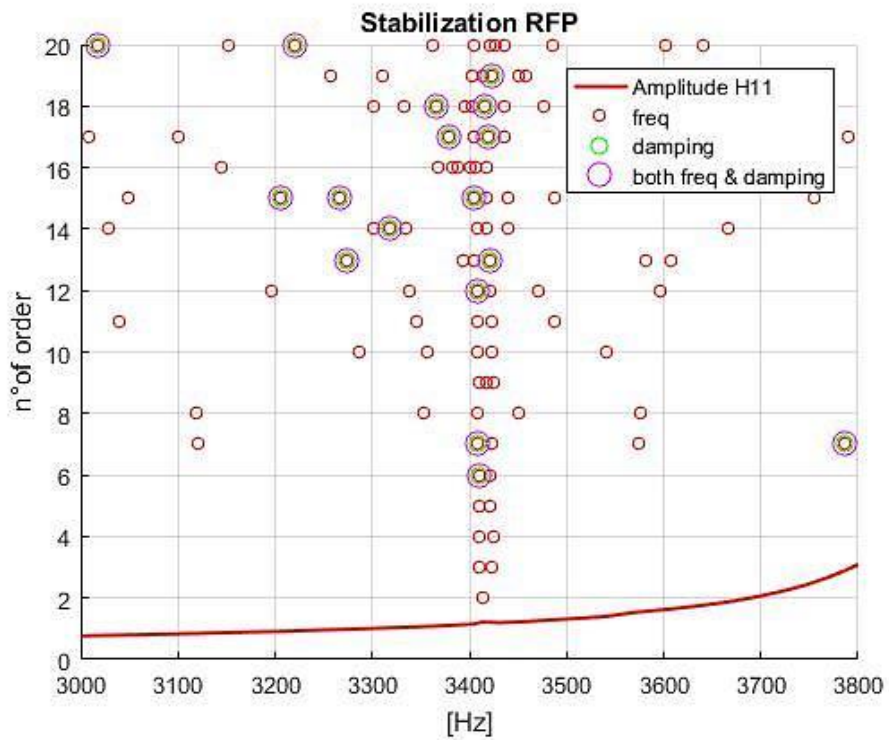
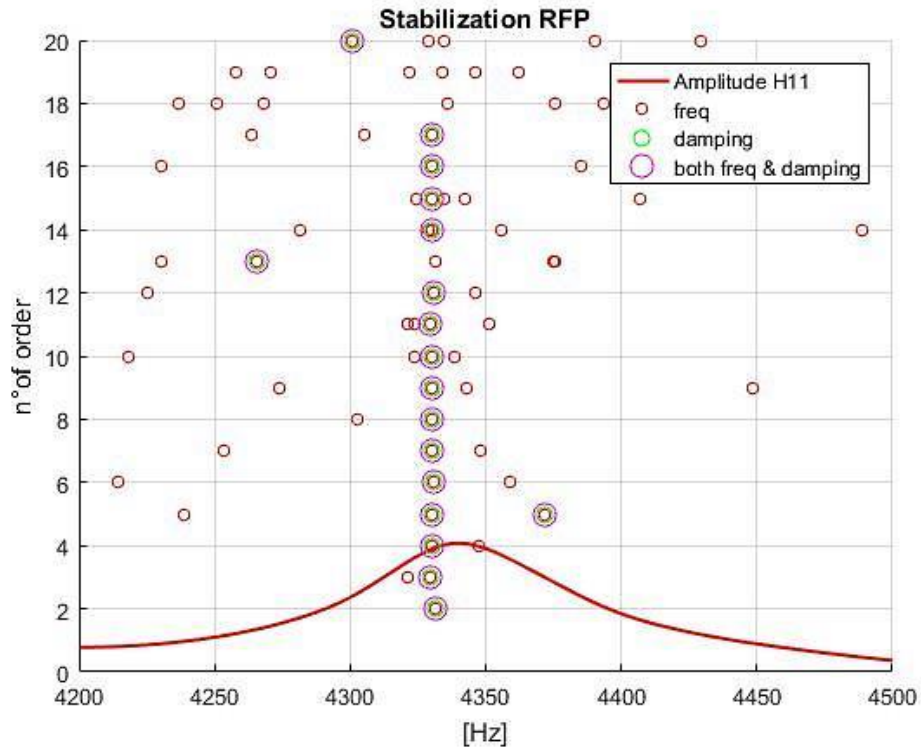*Fig 4.4.13: Stabilization diagram close to the third mode*

Fig 4.4.14: Stabilization diagram close to the fifth mode.

The Fig.4.4.11 represents the stabilization diagram of the Gearbox extracted by the RFP. This graph is not clear and as it can be seen that only the first and the fourth physical modes appear in this diagram selecting a large bandwidth. This leads to the ill-conditioning problem. Thus, in order to reduce the ill-conditioning the second, the third and the fifth modes were isolated as clarified in the Fig.4.4.12, Fig 4.4.13 and the Fig.4.4.14. Narrowing the bandwidth frequency around the Peaks, these modes immediately appear and their estimation becomes more accurate.

At this step, for choosing the best pole for each cluster The same procedure is describe above in the plate case by the ERA and the RFP Methods was reapplied. Then the FRF regenerating and the FRF measured for each mode were plotted in the Fig 4.4.15 and Fig 4.4.16, in this case the procedure of the isolation for the first mode was illustrated. Subsequently, the FRF was reconstructed for all the poles corresponding to each cluster one by one. The results will be compared with the FRF measured previously, thus the highest value of FRAC obtained is considered to be the best for estimating the modal parameters.
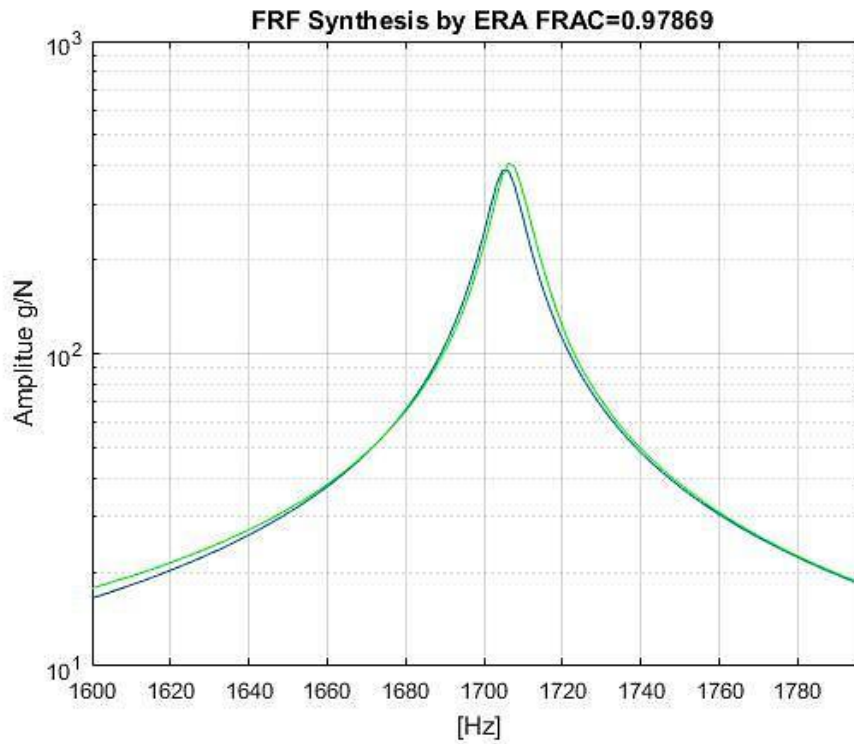
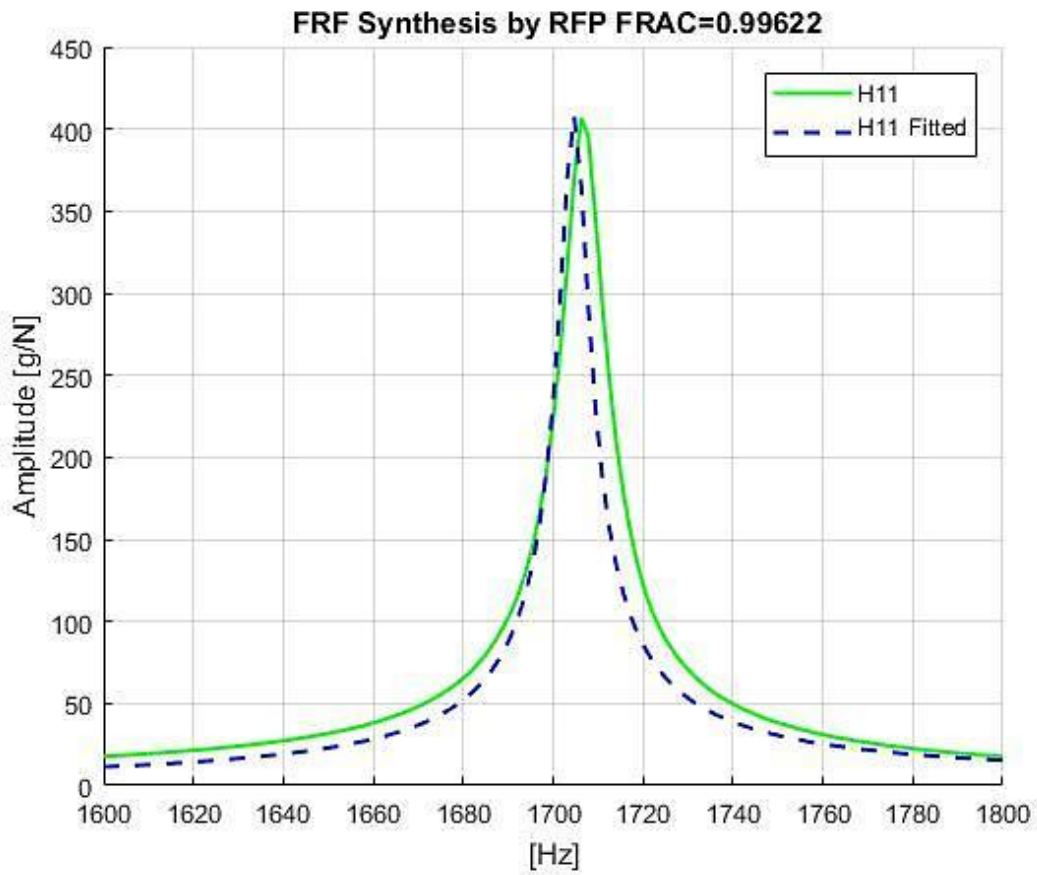*Fig 4.4.15: Synthesis of the FRF close to the first mode by ERA*

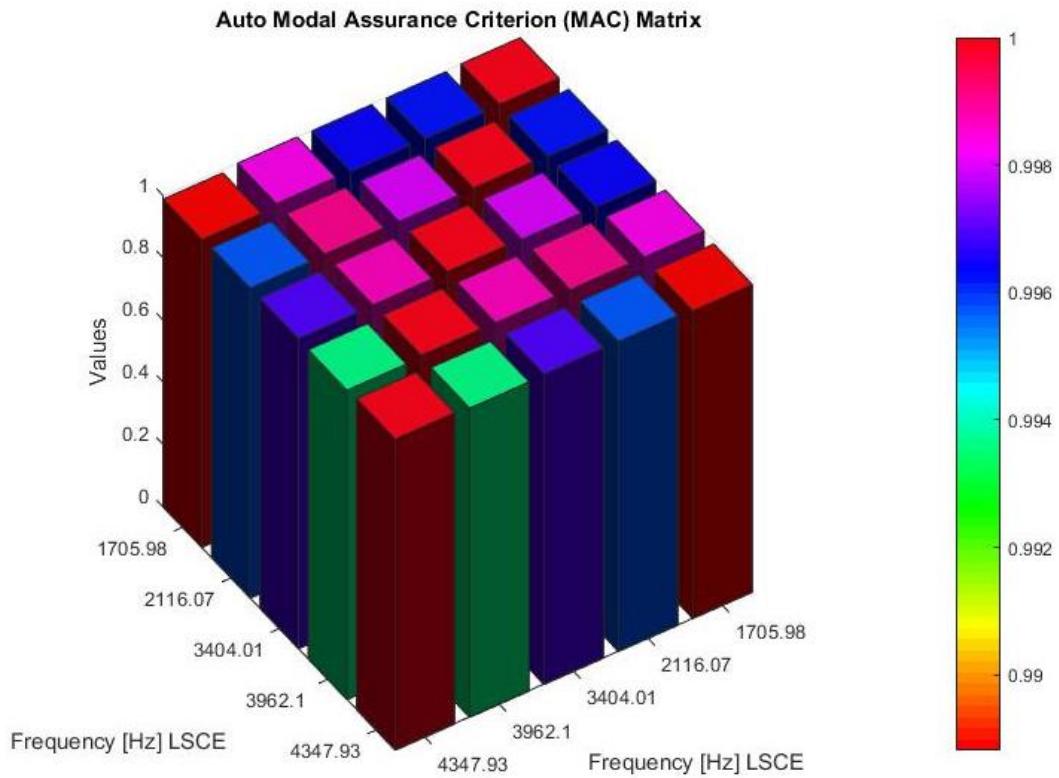*Fig 4.4.16: Synthesis of the FRF close to the first mode by RFP.*

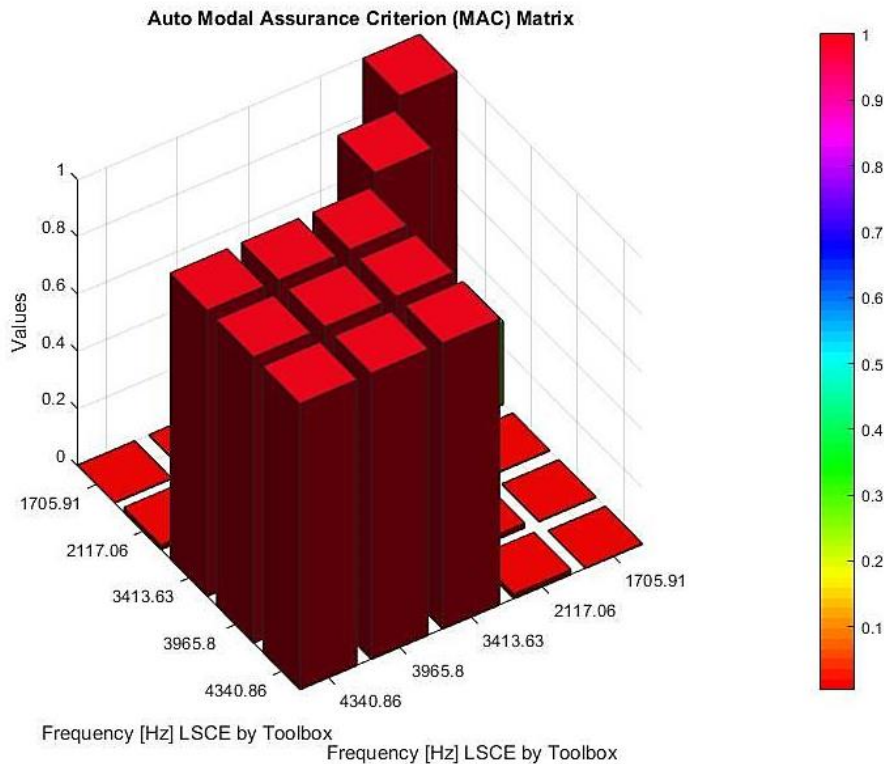*Fig 4.4.17: Auto-Modal Assurance Criterion of modes extracted by LSCE*

Fig 4.4.18: Auto-Modal Assurance Criterion of modes extracted by the LSCE Matlab toolbox.
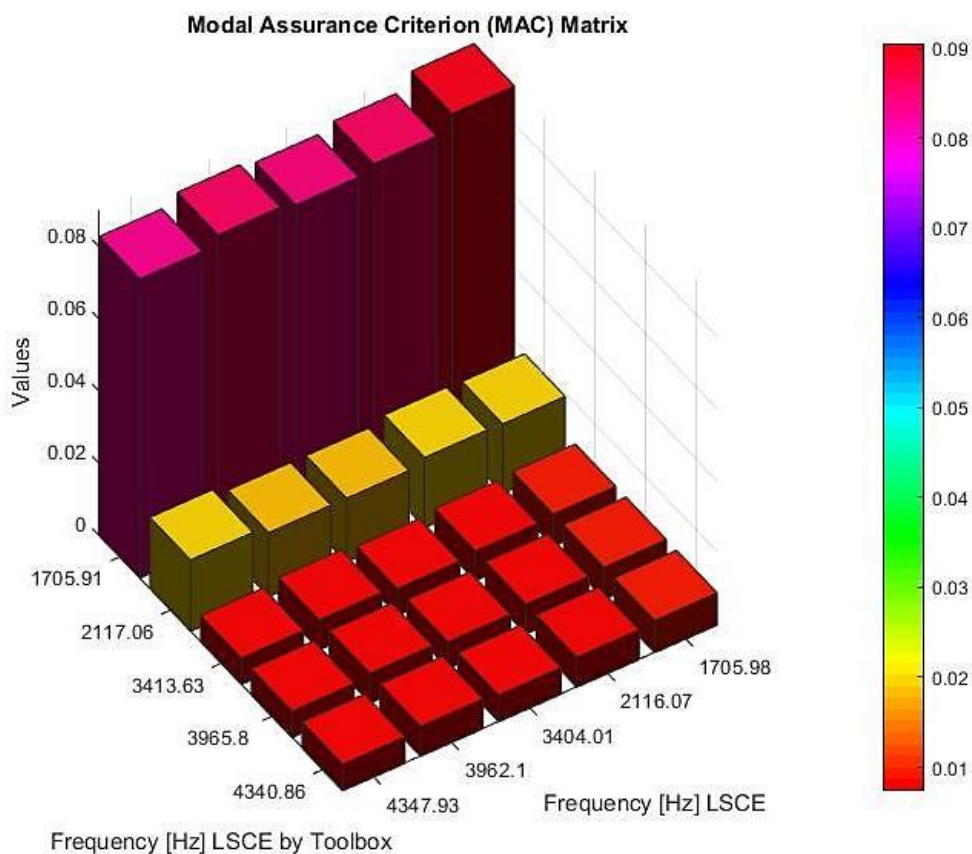
145

Fig 4.4.19: MAC of modes extracted by the LSCE Matlab toolbox and LSCE

In the Fig.4.4.17 the mode shapes extracted by the LSCE were compared to each other, all the mode shapes were found similar, likewise, the same situation that occurred in the Plate case. The Fig.4.4.18 shows the comparison of the mode shapes extracted by the LSCE Matlab toolbox, only the last three modes were similar, but when mode shapes extracted by the LSCE were compared to the mode shapes extracted by the LSCE Matlab toolbox in the Fig.4.4.19 it can be noticed that the values of MAC were very low what means that the all mode shapes were found different.

After the stable poles have been extracted from the stabilization diagram estimated by the LSCE Matlab toolbox, and using the *modalfit* command, the damping ratio and the mode shapes were calculated, it can be seen in the table 4.4.5; that the last three modes have present the same natural frequency and the same damping ratio, the reason why in this case it is not advised to use the modalfit command because it presents some problems.
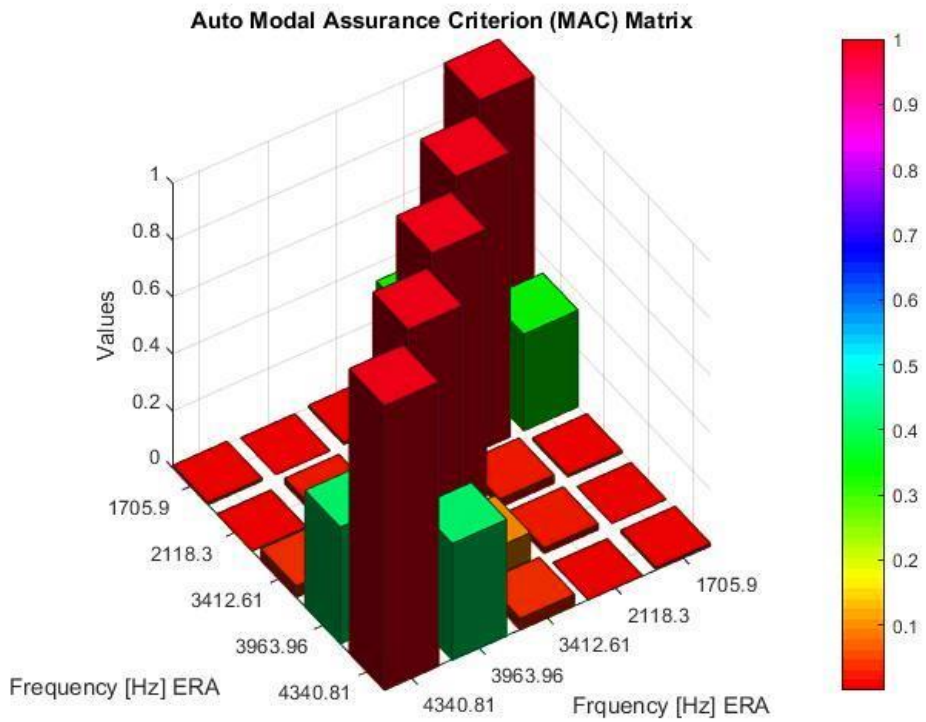
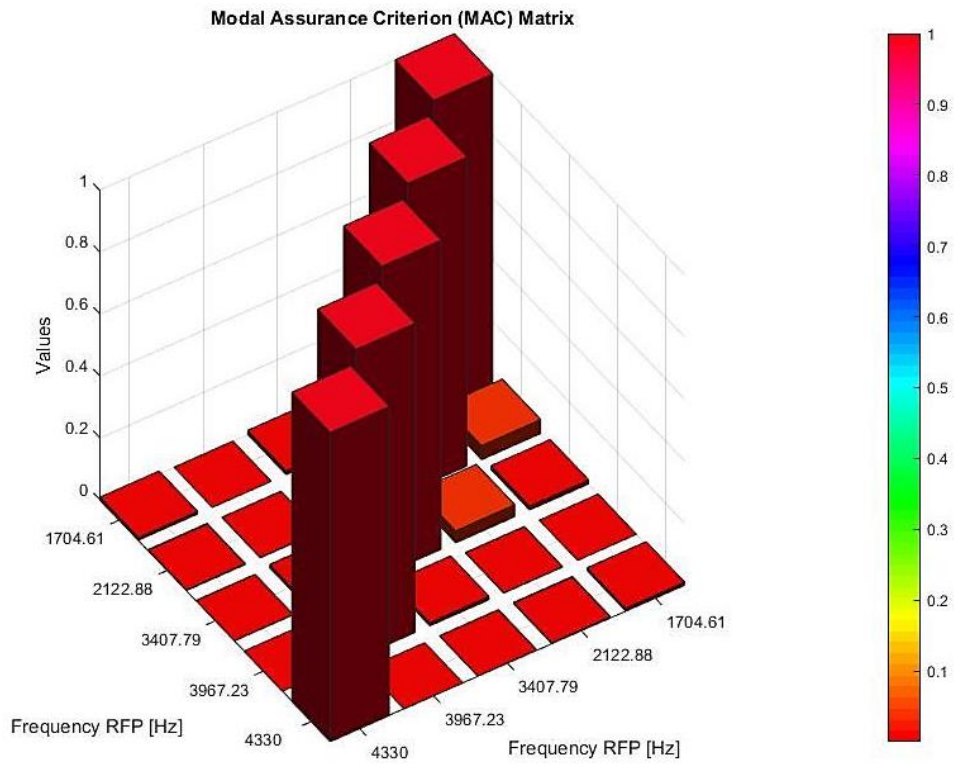*Fig 4.4.20: Auto-Modal Assurance Criterion of modes extracted by ERA.*

Fig 4.4.21: Auto-Modal Assurance Criterion by modes extracted by RFP.

The Fig.4.4.20 display the comparison between the mode shapes extracted by the ERA Method, this diagram shows that the off-diagonal terms are low and the maximal values in this term range varies between the 40% and 50%. In the Fig.4.4.21 representing the comparison between the FRF extracted by the RFP Method, it is noticeable that the off-diagonal terms are very low; this means that enough sensors have been considered in both cases.
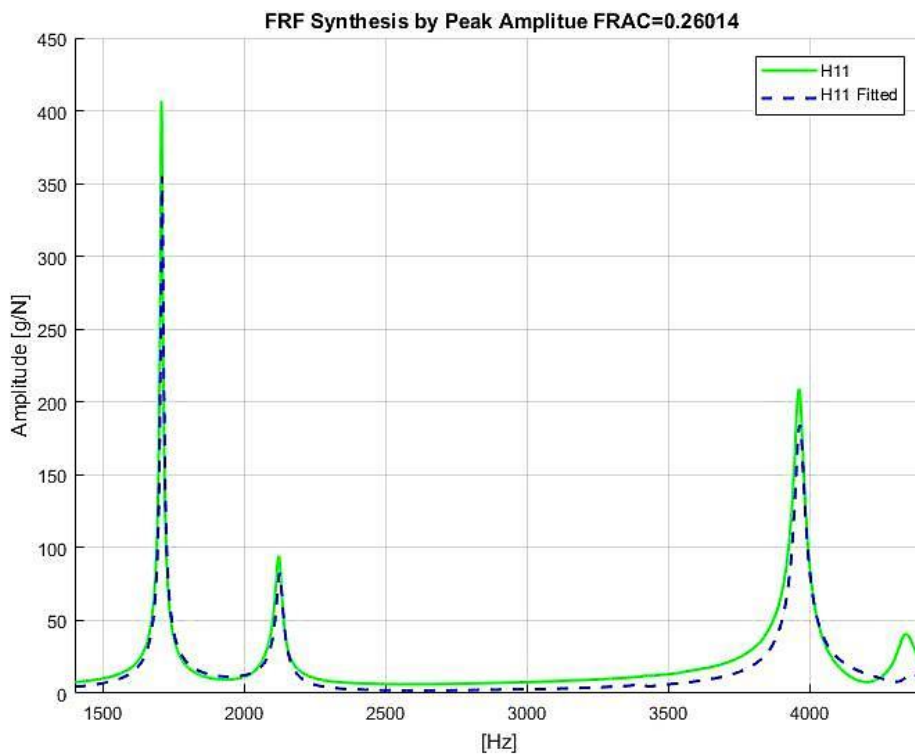

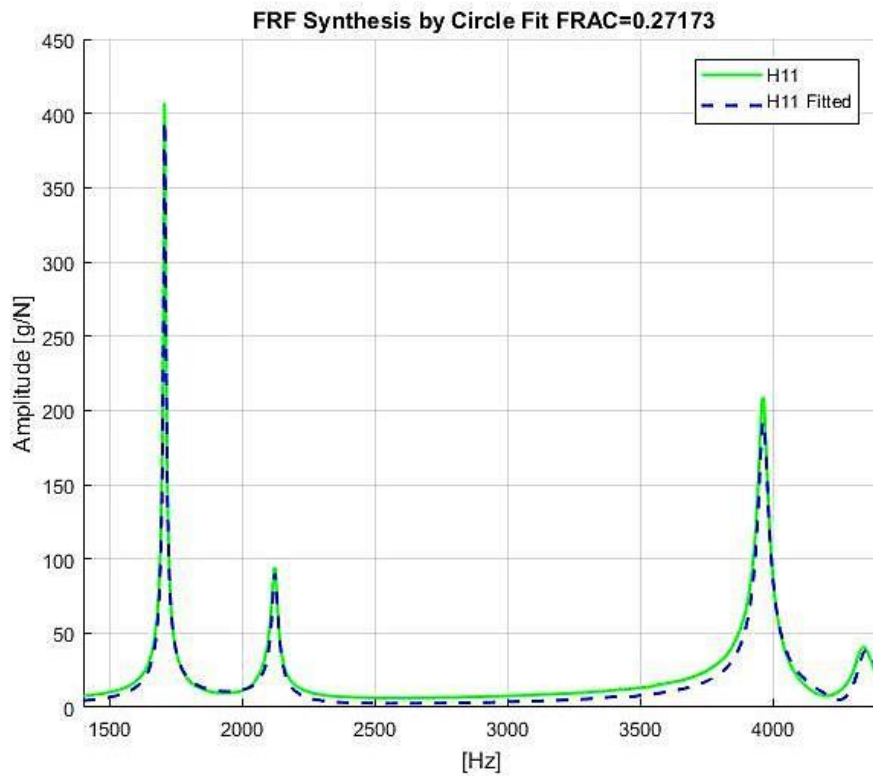*Fig 4.4.22: Fitting the FRF H11 by PP.*
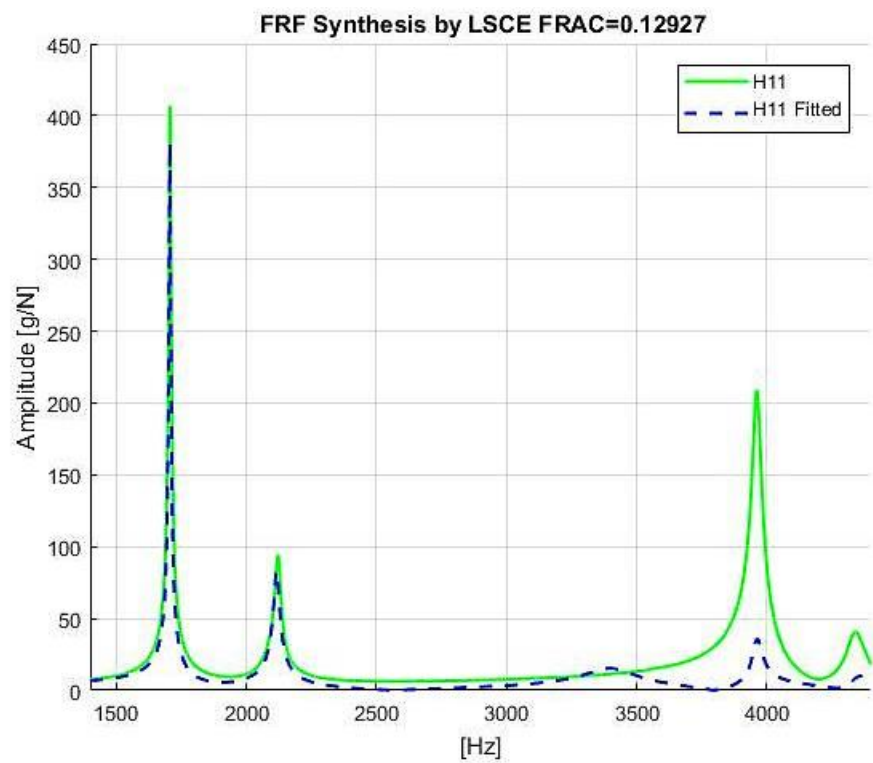
Fig 4.4.23: Fitting the FRF H11 by CF.

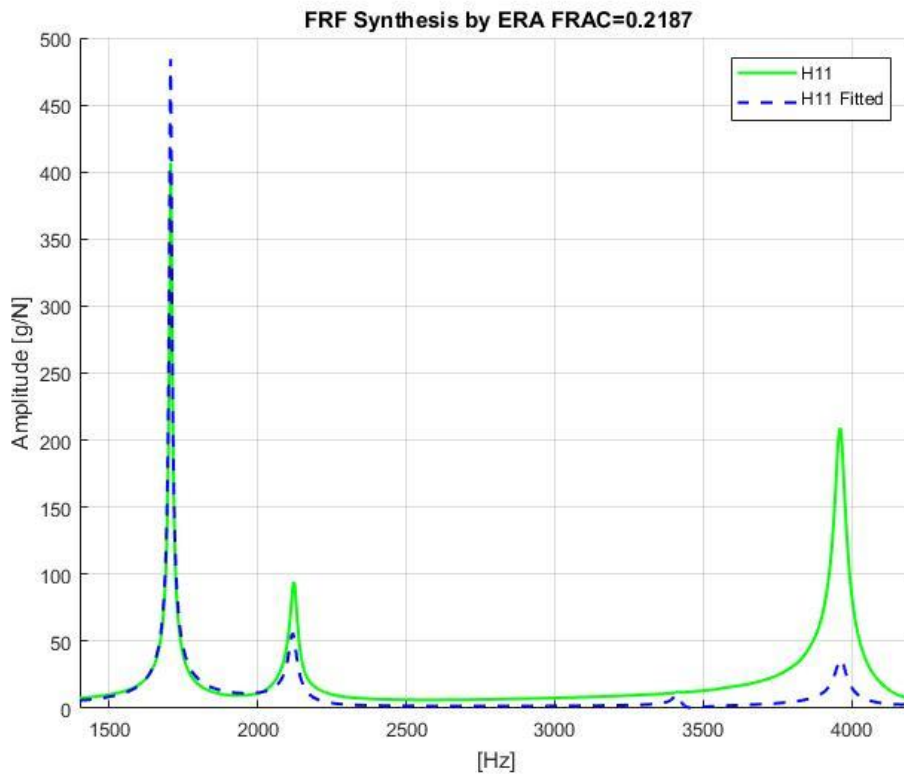*Fig 4.4.24: Fitting the FRF H11 by LSCE.*

Fig 4.4.25: Fitting the FRF H11 by ERA.
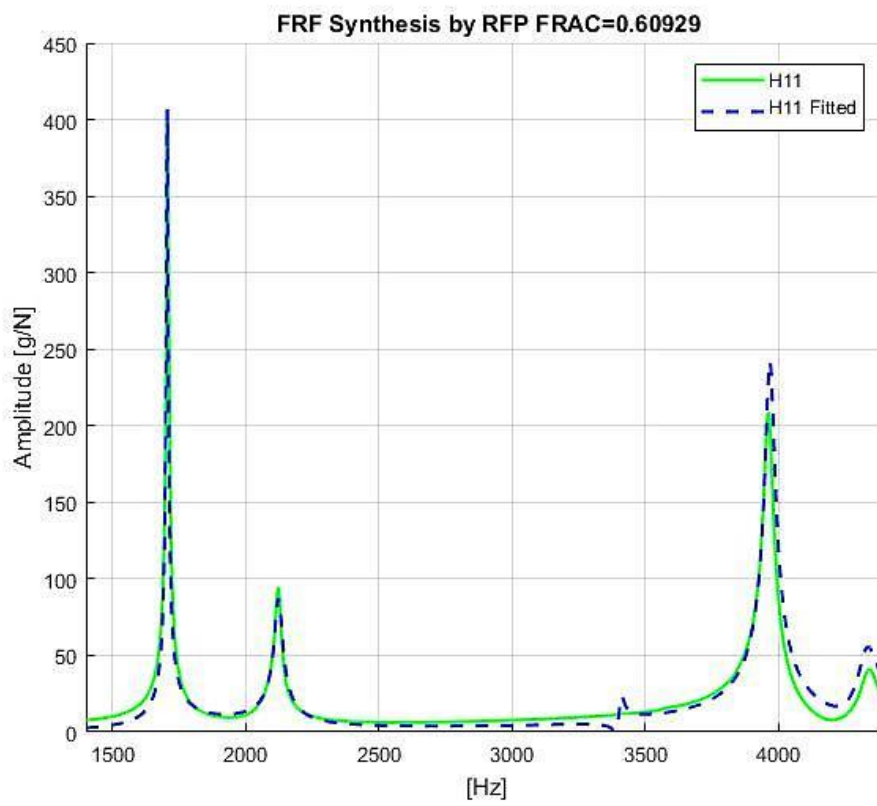
Fig 4.4.26: Fitting the FRF H11 by RFP.

150

The figures ranging from Fig.4.4.21 to the Fig.4.4.26 represent a comparison in the bandwidth [1000, 4500] Hz between the chosen H_{11} from the FRFs Inertance measured with the regenerated H_{11} by the modal parameters extracted. In all the methods used the FRAC values were very low, and then the maximum value was reached by the RFP, this means that the best estimation for the modal parameters was achieved using this method, it is important to mention here that in all the methods the FRAC values were low because the frequency range is very wide. If the bandwidth was restricted on each mode, high values of the FRAC can be obtained.

Fig 4.4.27: mode shapes extracted by Test-Lab Polymax method of the gearbox.

151

Fig 4.4.28: mode shapes extracted by LSCE of the gearbox.

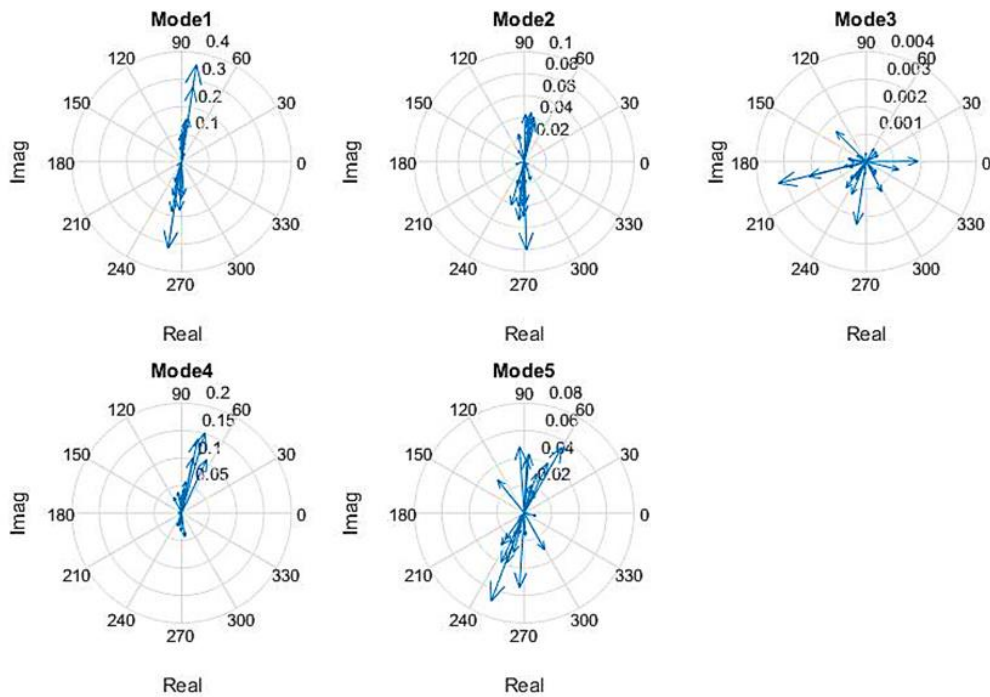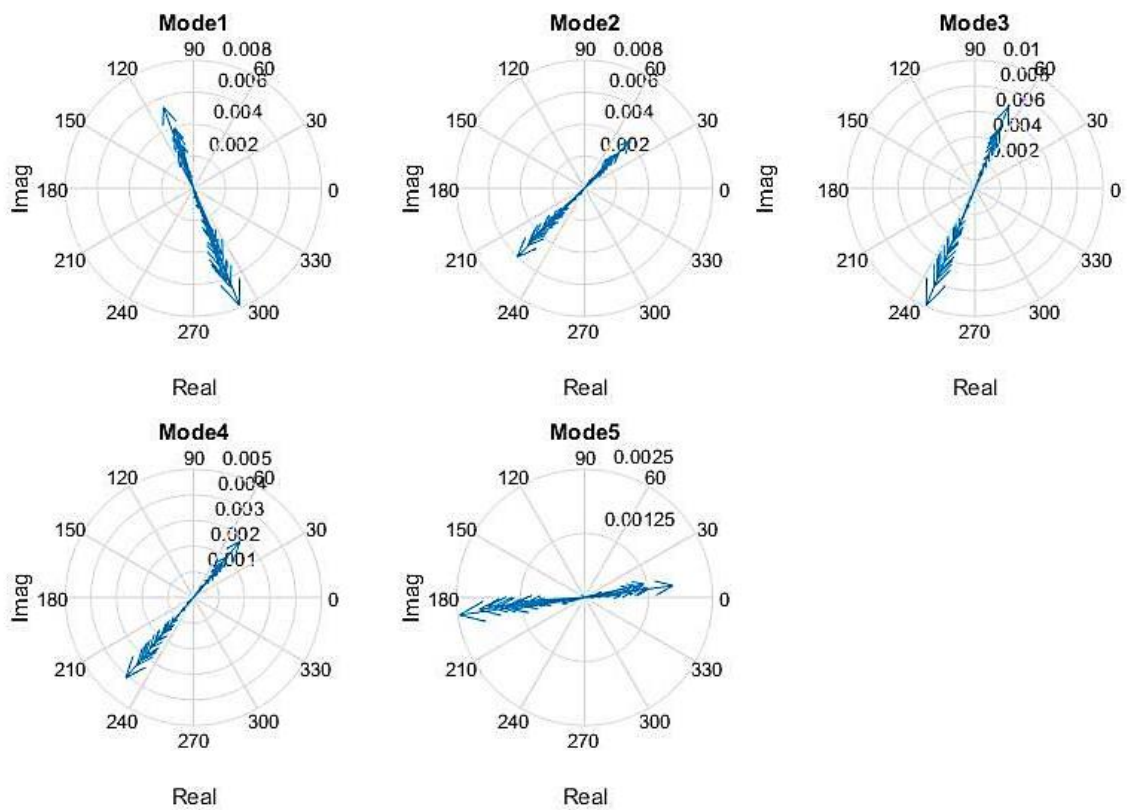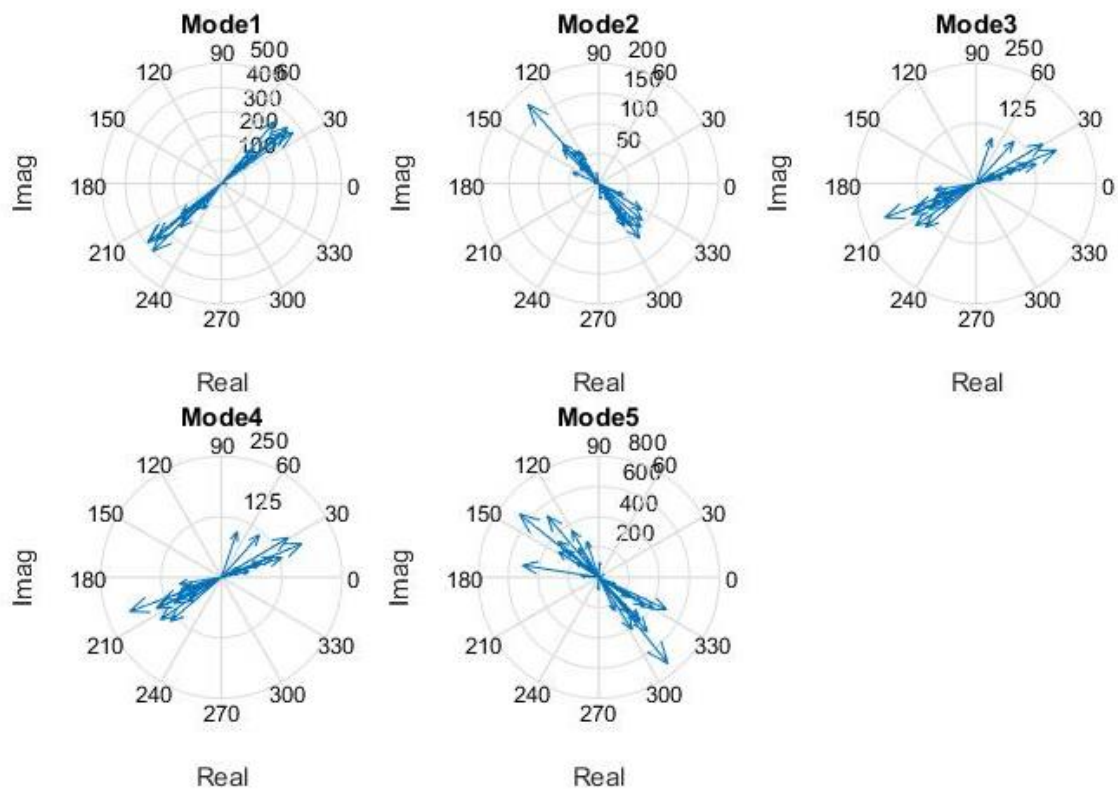
Fig 4.4.29: mode shapes extracted by LSCE Matlab toolbox of the gearbox.

152
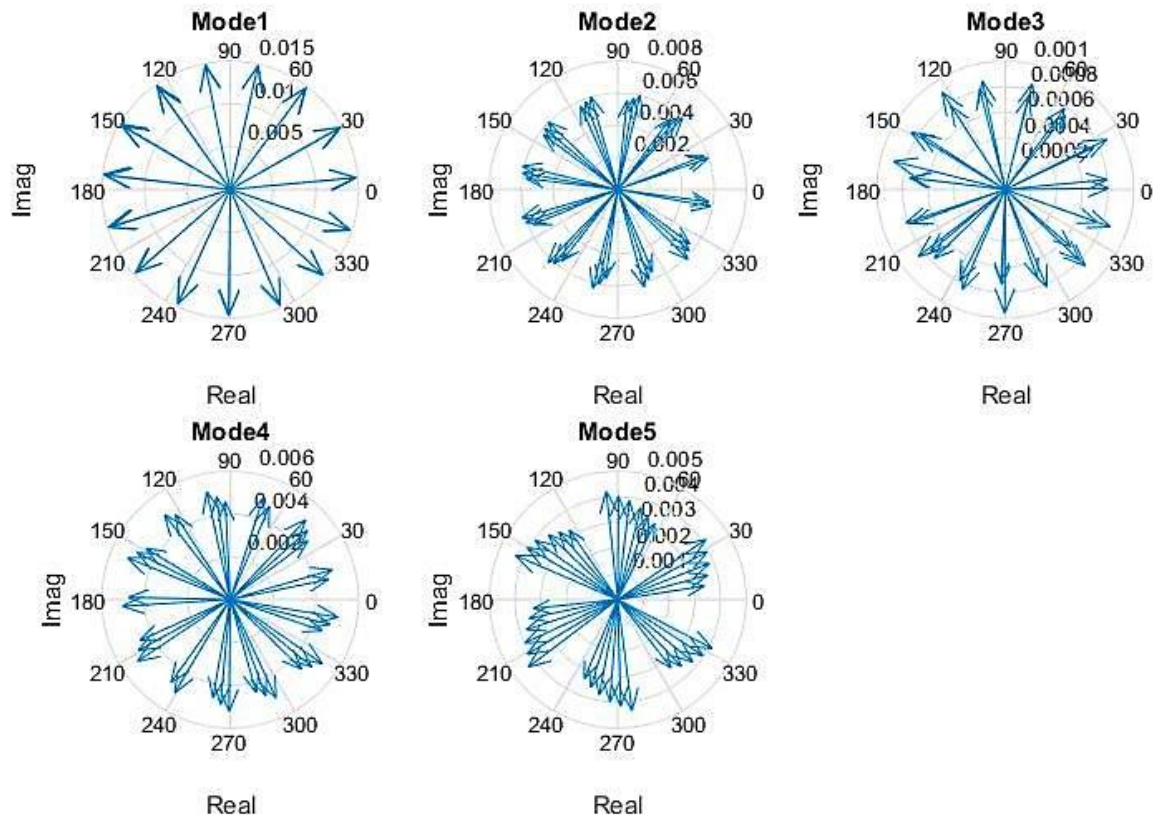
Fig 4.4.30: mode shapes extracted by ERA of the gearbox.
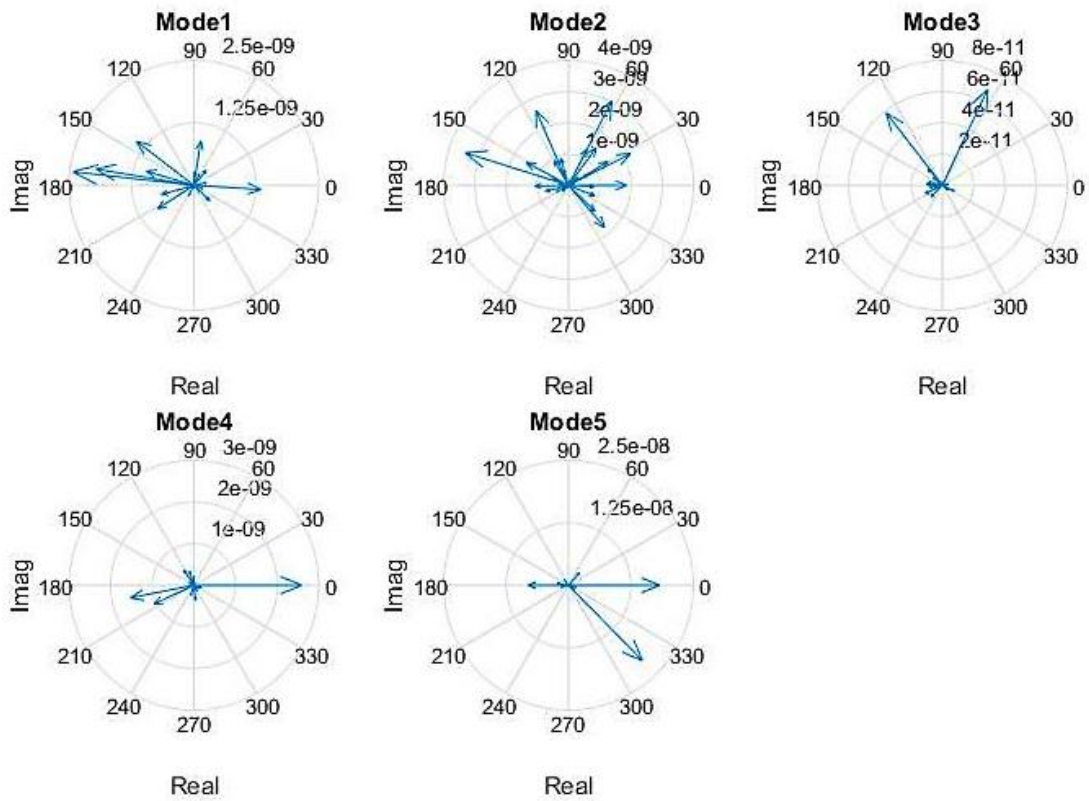
Fig 4.4.31: mode shapes extracted by RFP of the gearbox.

153

The figures arranged from the Fig.4.4.27 to the Fig.4.4.31 display the plots of the mode shapes in the complex plane (real part vs. imaginary part). In the Fig.4.4.27 when the polymax Method was used, the mode shapes appeared far from being real having phases dispersed chaotically ranging between the 0° and 360°. In the Fig.4.4.28 representing the mode shapes extracted by the LSCE implemented, it can be noted that if the modes are rotated by an angle α they will be similar. In the Fig.4.4.29 presenting the plot of the mode shapes extracted by LSCE Toolbox, it can be seen that the last three modes are similar. In the Fig.4.4.30 and Fig.4.4.31 showing the mode shapes respectively extracted by the ERA and the RFP Methods, it is detectable that the mode shapes are dispersed chaotically in the complex plane. If these figures are visually skimmed through, it can be noted that they are not similar, this will be demonstrated in the next part when these methods are compared using the MAC.

Fig 4.4.32: *MAC of mode shapes extracted by LSCE and Test-Lab Polymax.*

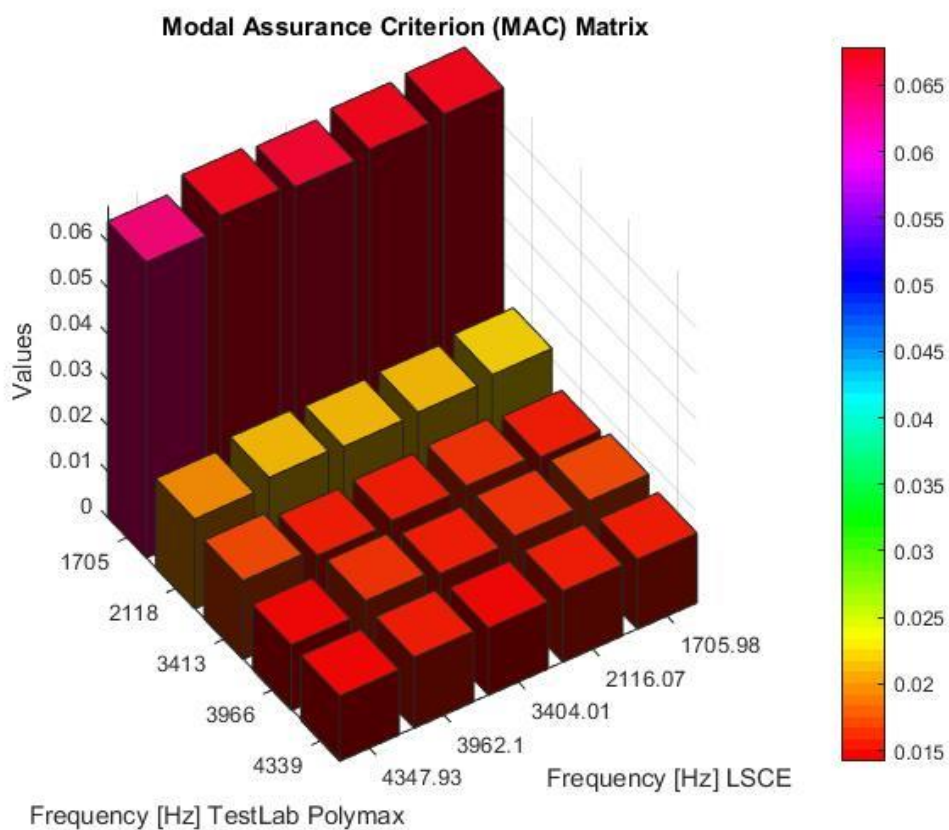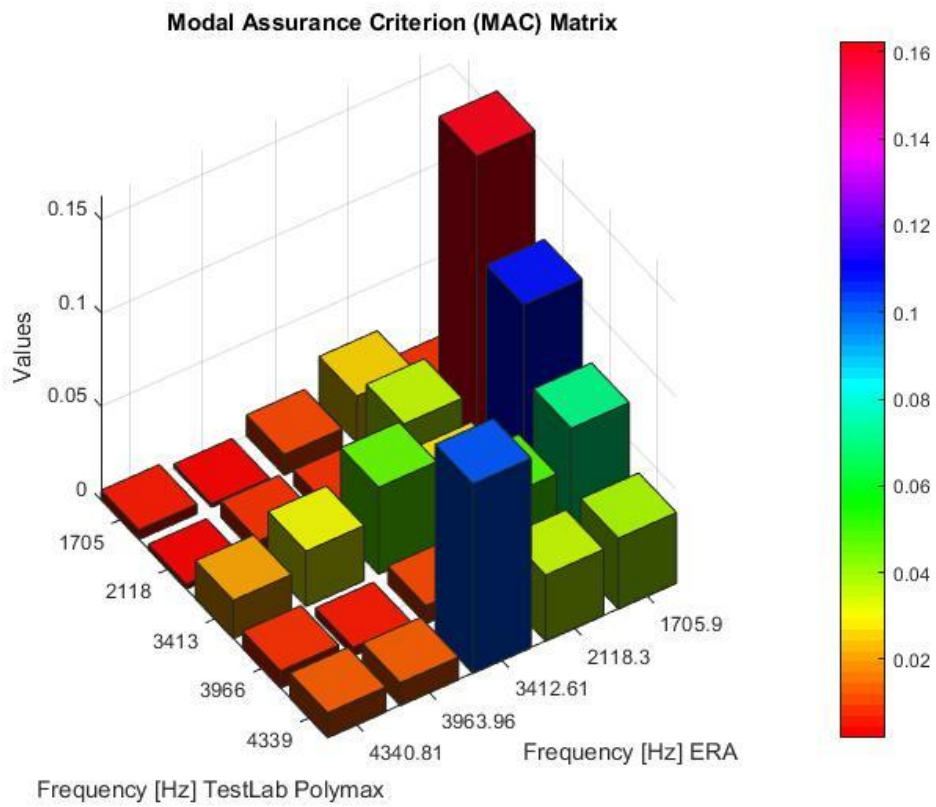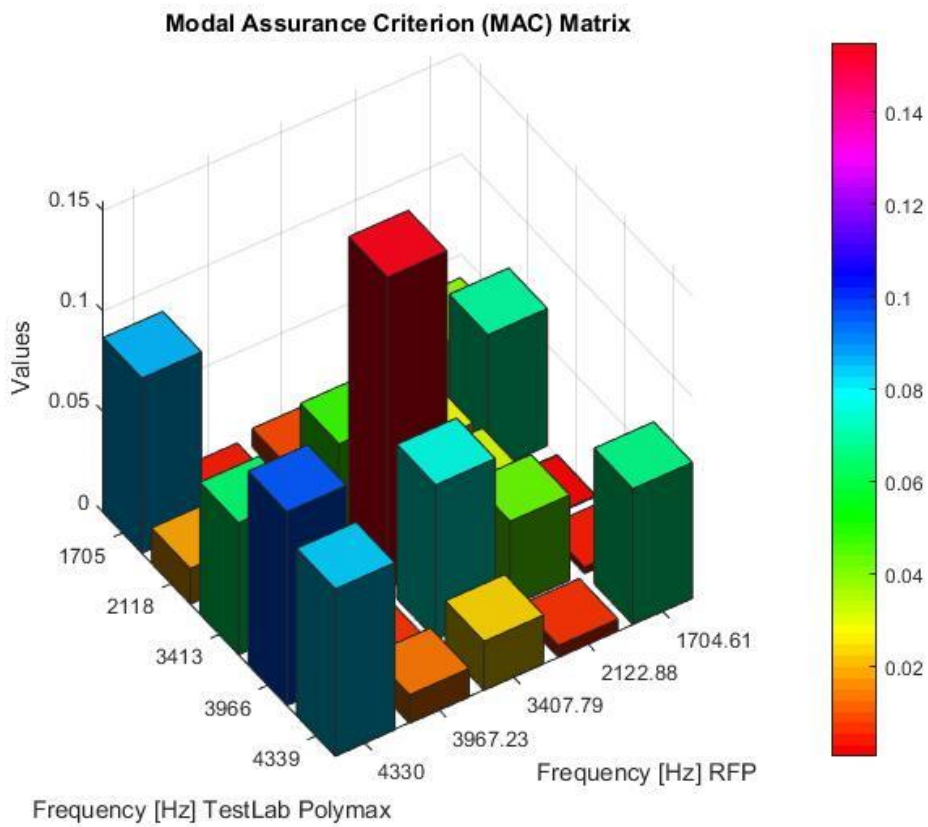Fig 4.4.33: *MAC of the mode shapes extracted by ERA and Test-Lab Polymax.*

Fig 4.4.34: *MAC of the mode shapes extracted by RFP and Test-Lab Polymax.*

From the Fig.4.4.32, Fig.4.4.33 and Fig.4.4.34 show the comparison between the mode shapes extracted respectively by the LSCE, ERA and RFP with the mode shapes extracted by Test-Lab Polymax Method using MAC. In all cases the modes shapes were badly estimated since the values of MAC obtained were very low, and there was no correlation between the mode shapes when compared to each other.

Conclusions

In the plate example in both cases of modes close to each other and well separated modes in the range 0-600 Hz, the PP and CF methods gave good results continuously as can be seen in the tables 4.3.2 and 4.3.3. In a particular situation, on the first and the third modes, the vicinity mode limited the extracting of their modal parameters; this issue that also appeared in this experimental case was described in the chapter 3. However the other modes had good estimation of the damping ratio because the values of damping and frequency were very close to the Test-Lab Polymax results. In fact, in the case of heavy damping the results of the PP and the CF Methods tend to be more accurate. Regarding the second example, the Gearbox, the damping was light (ζ< 2%) and the modes were well separated. In the physical modes present in the range 0-4500 Hz, the tables 4.4.2 and 4.4.3.show that on the first and the third modes the damping values extracted by PP and CF methods, are distant from the ones obtained by Test-Lab Polymax. The mode shapes in these methods are real and it's difficult in some cases to find the whole vector for each mode as seen in the case of plate.

When the LSCE and LSCE Matlab toolbox were applied in the plate case, good results were obtained comparing to when the PP and CF were used. All the modes shapes have been extracted with good estimation of the damping ratio in both cases as seen in the table 4.3.4 and table 4.3.5. Their values were very close to the Test-Lab Polymax Values, and even between them the results were very similar. In the Gearbox case as shown in the table 4.4.4, the LSCE continue to give good results since they appeared very close to the Test-Lab Polymax values. In the LSCE Matlab toolbox case, table 4.4.5 shows that the last three modes looked similar, also this method gave same values for the damping and same frequencies for these last three modes. Despite that if the LSCE and the LSCE

156

Matlab toolbox presented a similar cluster in the stabilization of diagram, the *modalfit* command presented a problem when the damping and the mode shapes were extracted. In this case in the table 4.4.5 only the frequencies extracted by the stabilization diagram and not by the *modalfit* command were reported.

Regarding the stabilization diagram, comparing its clarity between the LSCE and the LSCE Matlab toolbox, it can be deduced that the diagram obtained by the LSCE toolbox was not clear and this was noticeable in the Gearbox case as the Fig.4.4.8 shows where it was difficult to identify the physical modes. While the LSCE diagram seemed clearer, it was easy to identify the modal parameters of the physical modes, and this can be seen in the two cases.

The LSCE and LSCE Matlab toolbox did not succeed in yielding the modes shapes. In addition, the Auto-MAC could not be applied to verify the repetition of the modes shapes and the insufficiency of measured degree-of-freedom hence it was difficult to discriminate between the different modes. This was detected in the both examples of plate and Gearbox

As for the FRAC, high values were only obtained in the plate case in all cases, contrarily to in the Gearbox case when all FRAC values were low. The highest values in both cases were obtained using the modal parameters extracted by the RFP method. Thus, this means that calculating FRAC on a large frequency bandwidth is not enough to judge the estimation of the modal parameters. The FRAC values were influenced by other parameters such as noise, upper residual, lower residual, etc...

The ERA Method gives a very clean stabilization diagram in both cases as cloud be seen in the Fig 4.3.9 and Fig 4.4.9, and good results of the damping were obtained as the table 4.3.4 and table 4.4.6 can show. In this case it's possible to apply the Auto-MAC to verify if a mode of family 1 may appear to correlate equally well with several modes of family 2 in order to eliminate the non-physical mode as illustrated in the Fig 4.3.19 and Fig 4.4.20.

The RFP is very sensible of the noise, and it was discovered that not all the physical modes appear when working in a large bandwidth as the Fig 4.3.11 and Fig 4.4.11 showed when some of the modes were missing. In the plate example the first and the third mode could not be found similarly to the second, third, and

the fifth modes in the second example. Thus if a large bandwidth was selected the ill conditioning problem appear, here the influence of frequency range width on poles estimation have been observed. using a very narrow frequency ranges implies to overlooking stables poles as illustrated in the Fig 4.3.12, Fig 4.3.13, Fig 4.4.12, Fig 4.4.13 and Fig 4.4.14. Hence, narrowing the frequency range, the number of equations is reduced as describe in the chapter 3, then the possibility of ill conditioning problem appearance decreases.

As for the mode shapes, the best estimation was achieved through the RFP Method. This could be seen in the comparison with the Test-Lab Polymax method using the *MAC* in the Fig.4.3.33, the *MAC* (2,2) surpassed the 50% and the diagonal MAC gave the highest numbers in comparison to the previous methods

Concerning the Least Square error in Fig 4.3.7 and Fig 4.4.8 and the singular Value Decomposition Fig 4.3.10 and Fig 4.4.10 it's impossible to determine the physical modes presented in the system. In the least square error any brisk decrease in the error can be seen in both cases, The amplitude of the *SVD* dropped rapidly for a number of order that does not correspond to any physical mode.

4.5   Airplane Experimental Data.

In this part the modal parameters were estimated by the operation modal analysis method (OMA). In this situation the free response was considered from the structure under test and only the Test-Lab Polymax, LSCE, ERA, RFP Methods were applied. Since the free response has a high level of noise, it is not convenient to begin the study using the PP and CF methods, because the operator cannot identify immediately which of the peaks need to be selected in the bandwidth of the frequency range. Hence only these three methods can be used.

In order to gain some insight into the practical application of the methods, they were applied to a benchmark structure built to simulate the dynamic behavior of an airplane.

The measurement have been carried out using fifteen accelerometers; three accelerometers positioned on the tail and 12 on the wings as marked in red in the Fig 4.5.1. The parameter of data will illustrate in table 4.3.
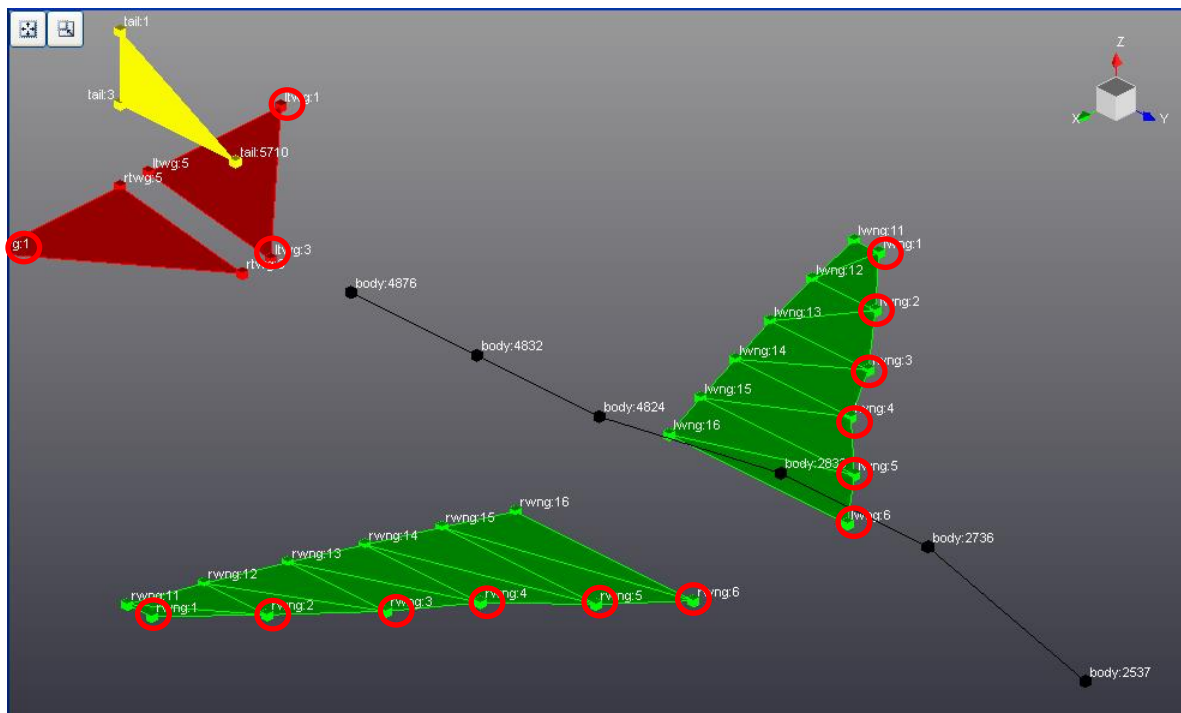

Fig 4.5.1: Model of the airplane.

The study is limited in the 0-90 Hz range. Thus only the first six modes will be extracted.

Sample rate	400 Hz
Number of samples	512
Δf	0.78125 Hz
Nyquist frequency	200 Hz

Table 4.3: Parameters data of the airplane .

	Mode 1	Mode 2	Mode 3	Mode 4	Mode 5	Mode 6
Frequency [Hz]	9.34	25.58	39.23	74,6	75.31	86.44
Damping Factor %	8.77	3.38	3.4	1.83	2.82	1.96

Table 4.5.1:Frequency and damping ratio for the 6 modes of the airplane extracted by
Test-Lab Polymax.

	Mode 1	Mode 2	Mode 3	Mode 4	Mode 5	Mode 6
Frequency [Hz]	9.14	25.45	39.35	74.26	75.84	86.74
Damping Factor %	8.54	3.49	3.26	2.63	2.8	2.04

Table 4.5.2: Frequency and damping ratio for the 6 modes of the airplane extracted by the
LSCE method.

	Mode 1	Mode 2	Mode 3	Mode 4	Mode 5	Mode 6
Frequency [Hz]	9.44	25.74	39.35	74.26	75.84	86.74
Damping Factor %	17.43	3.94	3.51	_____	2.54	3.18

Table 4.5.3: Frequency and damping ratio for the 5 modes of the airplane extracted by the
LSCE Matlab toolbox.

	Mode 1	Mode 2	Mode 3	Mode 4	Mode 5	Mode 6
Frequency [Hz]	9.44	25.74	39.35	74.26	_____	86.74
Damping Factor %	9.33	4.06	3.42	2.19	_____	1.71

Table 4.5.4: Frequency and damping ratio for the 5 modes of the airplane extracted by the
ERA method.

	Mode 1	Mode 2	Mode 3	Mode 4	Mode 5	Mode 6
Frequency [Hz]	9.3	_____	39.35	74.71	_____	86.29
Damping Factor %	8.63	_____	3.66	1.88	_____	1.74

Table 4.5.5: Frequency and damping ratio for the 5 modes of the airplane extracted by the
RFP method
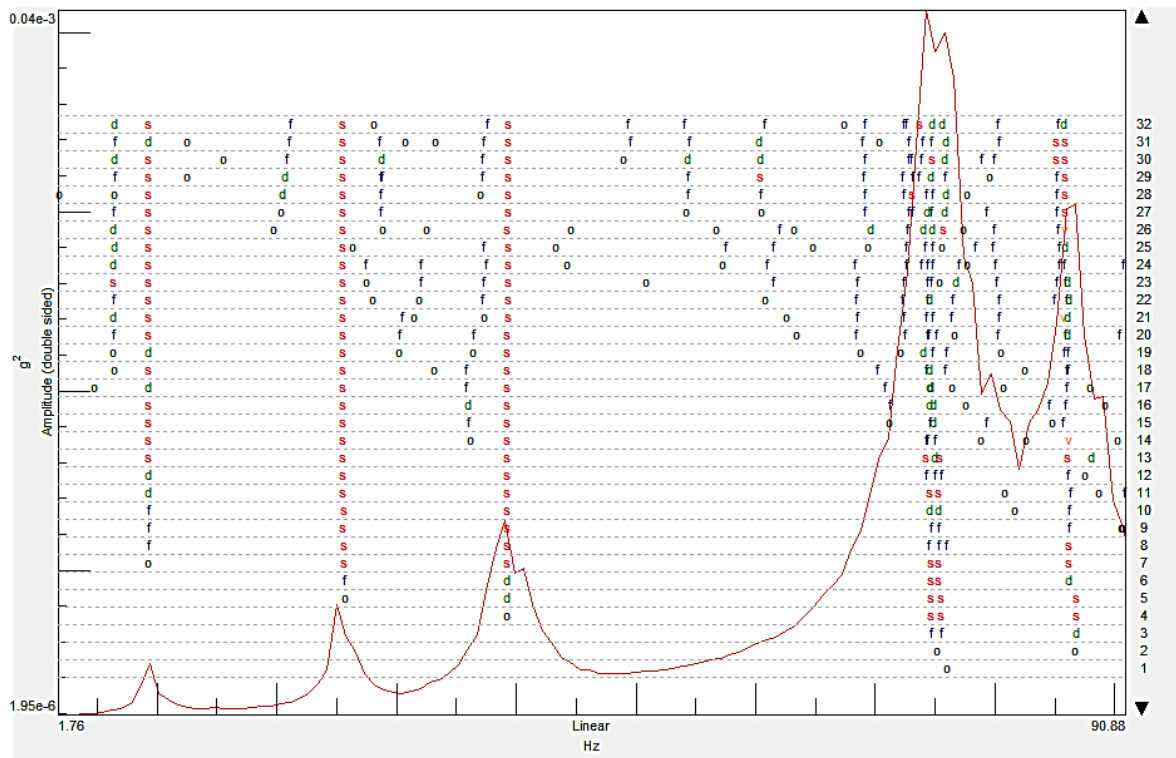
Fig 4.5.2: *Stabilization diagram by Test-Lab Polymax method of the airplane.*

In The Fig.4.5.2 illustrating the stabilization diagram extracted by the Polymax Method, the existence of six clusters that correspond to six physical modes is detected, three clusters seemed very clear and having a high number of stable poles, the other three were less evident and presented a lower number of stable poles. In these poles as the figure shows when the number of order surpass 13 the last three modes disappear until the number of order reaches 27, the last modes start to be visible, the forth and the fifth start to appear discontinuously.

161

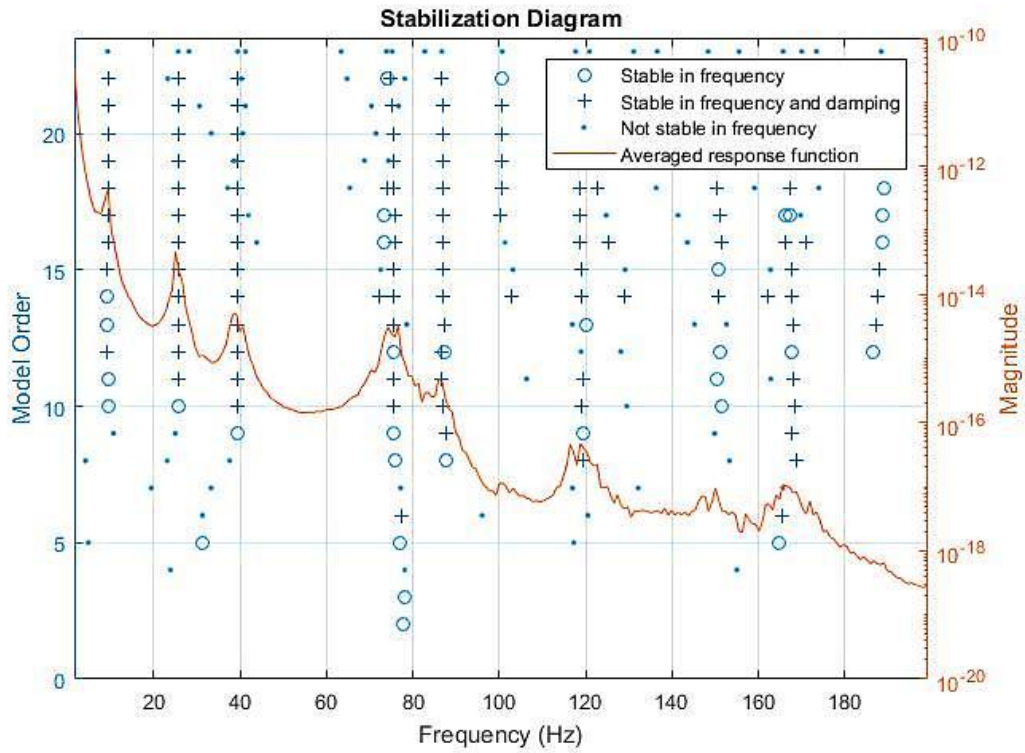*Fig 4.5.3: Stabilization diagram by LSCE Matlab toolbox of the airplane.*
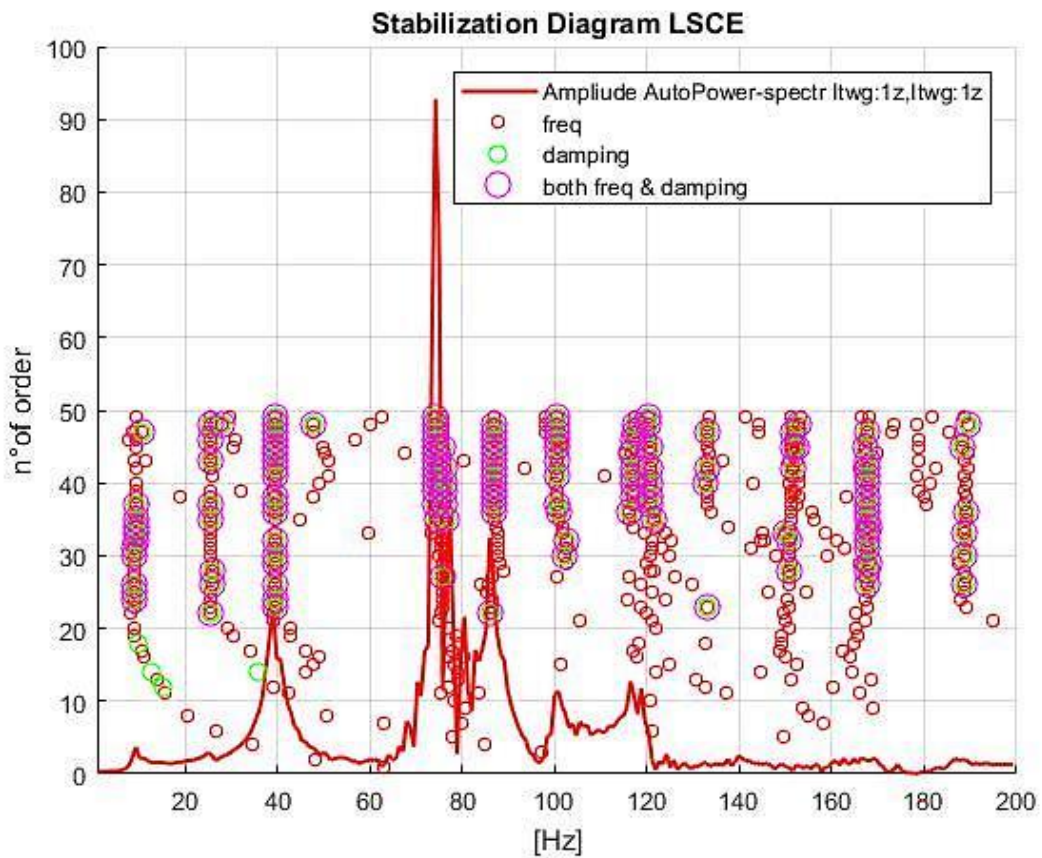

Fig 4.5.4: Stabilization diagram by LSCE of the Airplane.
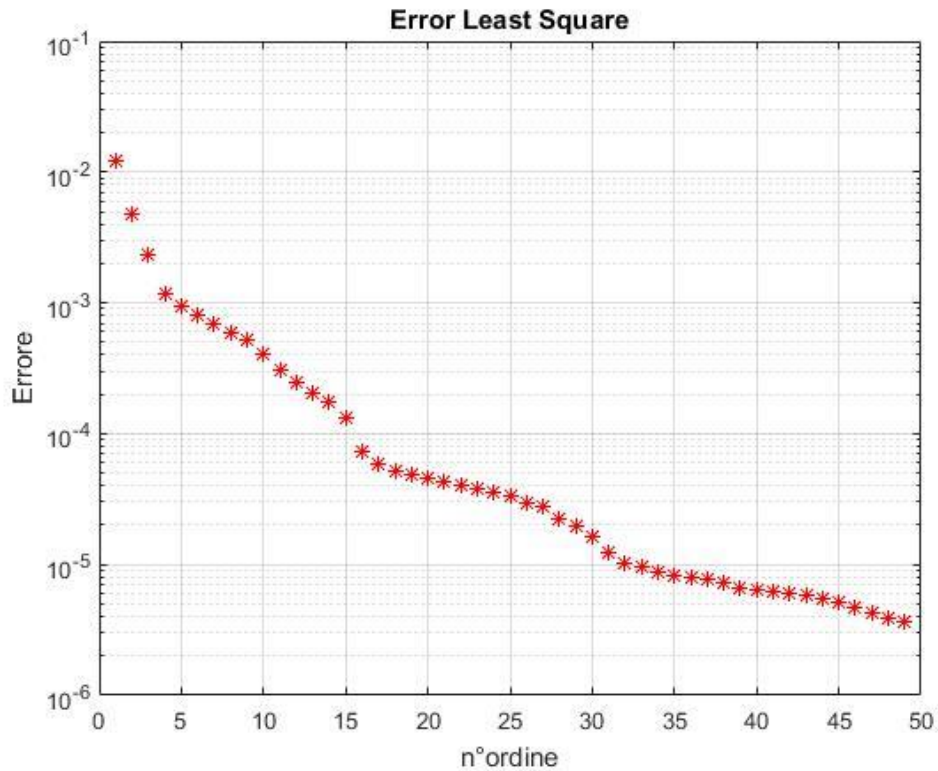
Fig 4.5.5: Least Square error.

The Fig.4.5.3 and Fig.4.5.4 represent the stabilization diagram extracted respectively by LSCE Toolbox and LSCE implemented. In these diagrams the focus is laid on the range 0-90 Hz. The first diagram was clear, it enclosed six clusters that were legible except for the fourth cluster corresponding to the fourth mode that was less defined. The stable poles begin to appear evidently when the number of order is superior to 12. In this stabilization diagram, the maximal number of order that can be reached is 23, because this number of order cannot be exceeded in LSCE Toolbox. The Fig.4.5.4 indicates that the system has six physical modes by the presence of six clusters in the diagram. In this case the stable poles appear when the number of order is higher than 20.

In the Fig.4.5.5 the Least Square Error was plotted in function of the number of order, it is not possible through this diagram to find the number of physical modes since the error did not show a brisk decrease.
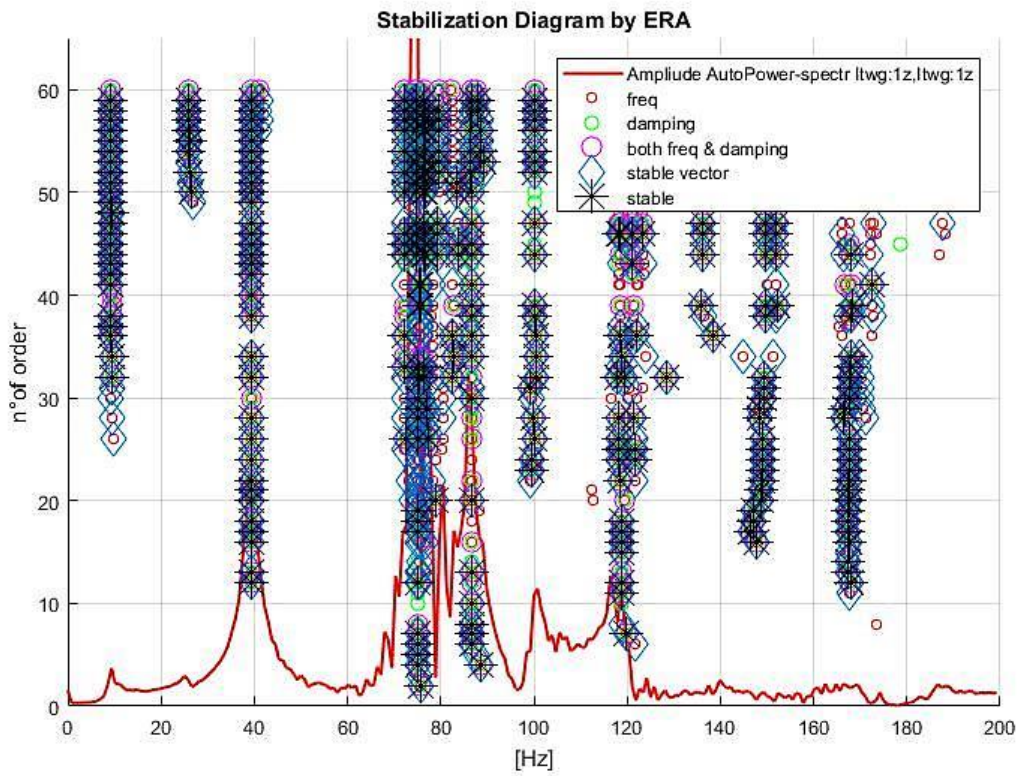
Fig 4.5.6: Stabilization diagram by ERA of the airplane.
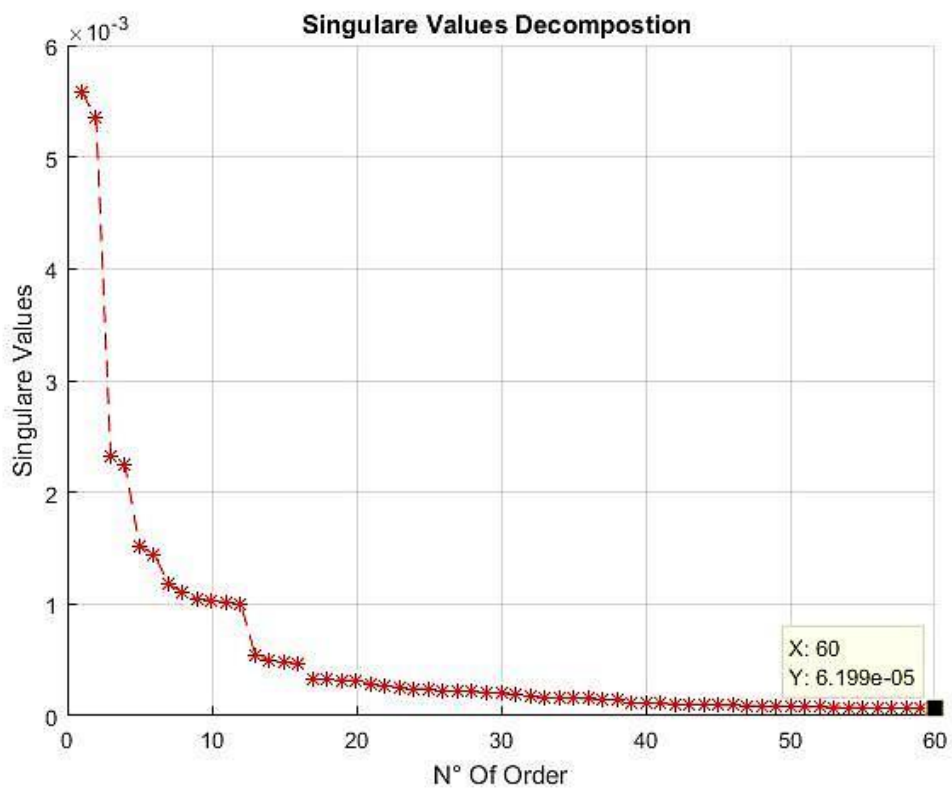
Fig 4.5.7: Singular Values of the Hankel matrix H_0 .

The Fig.4.5.6 illustrate the stabilization diagram extracted by ERA, eleven clusters, which is considered a high number, can be detected in this diagram, the first three clusters were very clear, but the others need other refinement as Auto-MAC to determine whether they correspond to any physical mode or not, this will be seen in the upcoming section.

From the Fig.4.5.7 representing the plot of the Singular Values Decomposition in function of number of order, it can be noted that also in this case, the method failed to identify the number of physical modes, the amplitude of the *SVD* went down rapidly for a number of order that does not correspond to the physical modes.
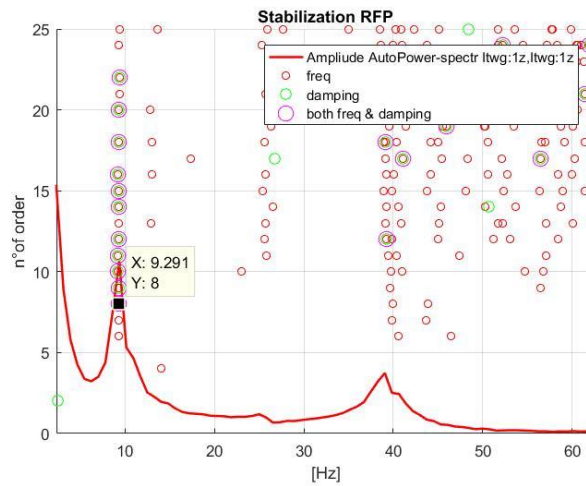
Fig 4.5.8: Stabilization diagram close to the first mode
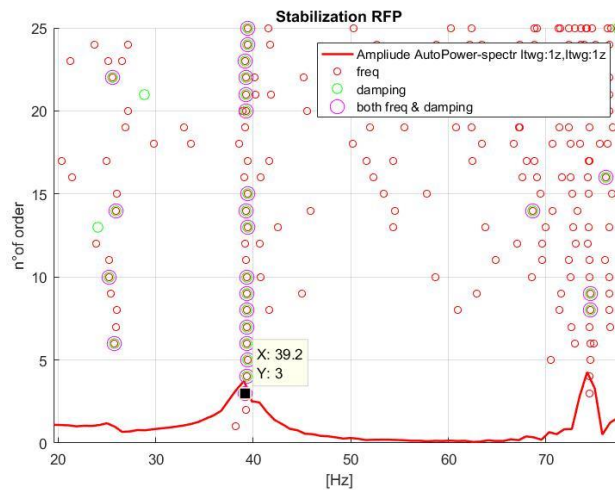
Fig 4.5.9: Stabilization diagram close to the third mode
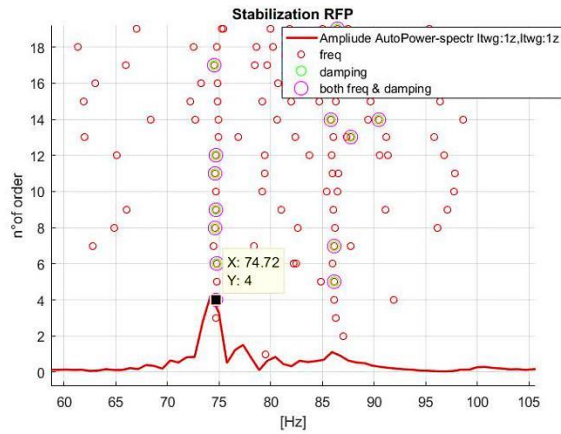
Fig 4.5.10: Stabilization diagram close to the fifth mode
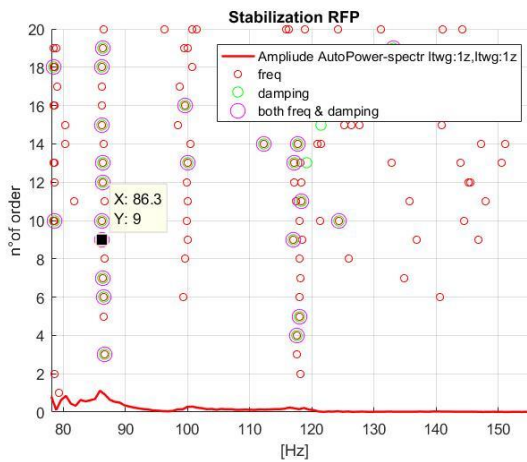
Fig 4.5.11: Stabilization diagram close to the sixth mode

The figures ranging from the Fig.4.5.8 to the Fig.4.5.11 display the stabilization diagram of the single modes extracted by RFP, it is difficult to find the bandwidth that serves to extract the physical modes in this case, and here it was a strain in determining the physical modes that have already been obtained in the previous methods. The stabilization diagram was not clear enough, and the second and the fourth modes could not be identified with this method. After several attempts, it was possible to obtain few clear clusters that were used to extract the model parameters. This indicates that the RFP method when applied on the operation model analysis, it make it very difficult to estimate the modal parameters.

Fig 4.5.12: Auto-Modal Assurance Criterion of modes extracted by LSCE.
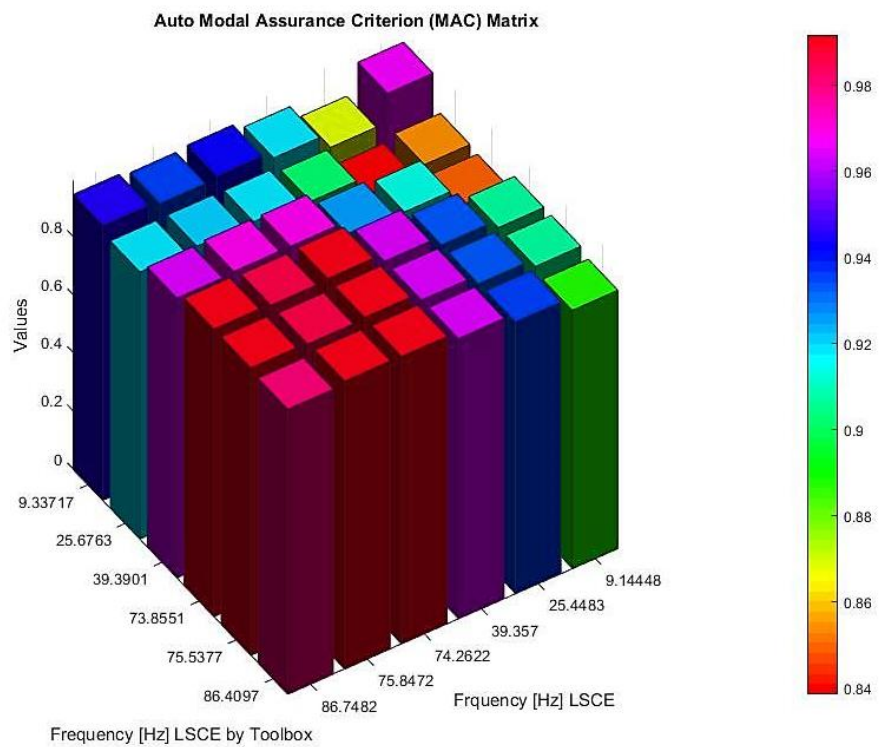
Fig 4.5.13: Auto-Modal Assurance Criterion of modes extracted by the LSCE Matlab toolbox.

167
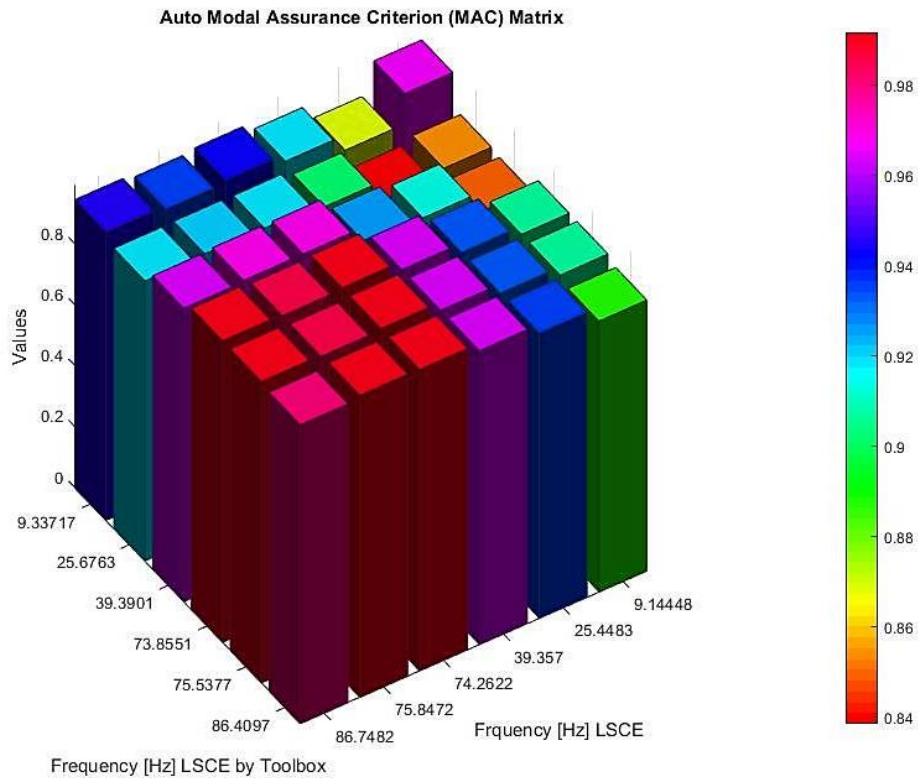
Fig 4.5.14: MAC of modes extracted by the LSCE Matlab toolbox and LSCE.

Fig.4.5.12 and Fig.4.5.13 represent the comparison between the mode shapes extracted respectively by LSCE implemented and LSCE Toolbox using AutoMAC, it can be noted that all the mode shapes are similar in both cases. In the Fig.4.4.14 representing the comparison between the mode shapes extracted by LSCE implemented and LSCE Toolbox using the MAC, it can be seen that these two methods have the same modes. In this situation of operation modal analysis happened previously in the plate example, similarly, in this case the application of AutoMAC in the LSCE Method do not give any information when the degrees of freedom measured are missing
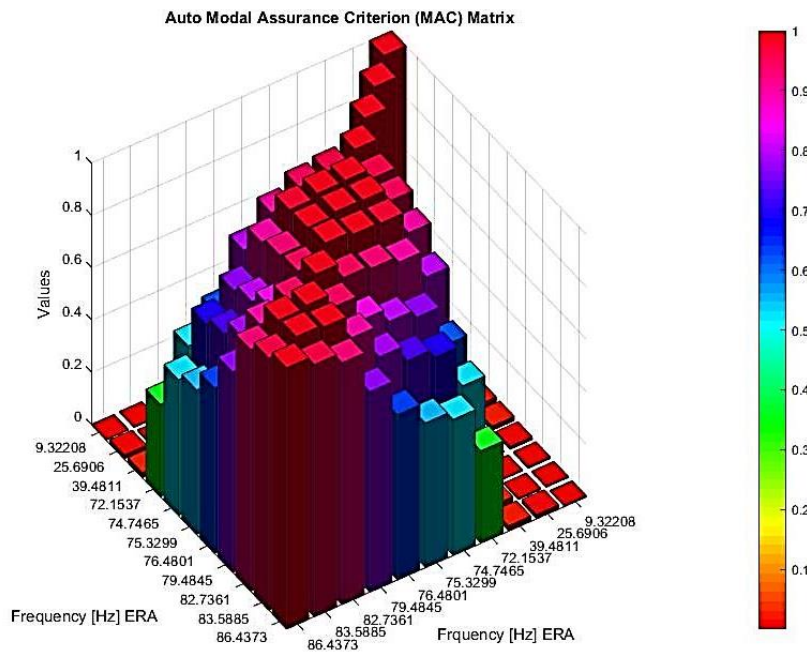
Fig 4.5.15: Auto-Modal Assurance Criterion of modes extracted by ERA.

Observing the Fig 4.5.15, an equal correlation between modes from different families can be detected. Then the unwanted modes should be eliminated and the AutoMAC should be entirely reconstructed as shown in the Fig 4.5.16, where it can be seen that the off-diagonal terms are not too high indicating. Only the modes that have frequency values in the Fig 4.5.16 are considered.

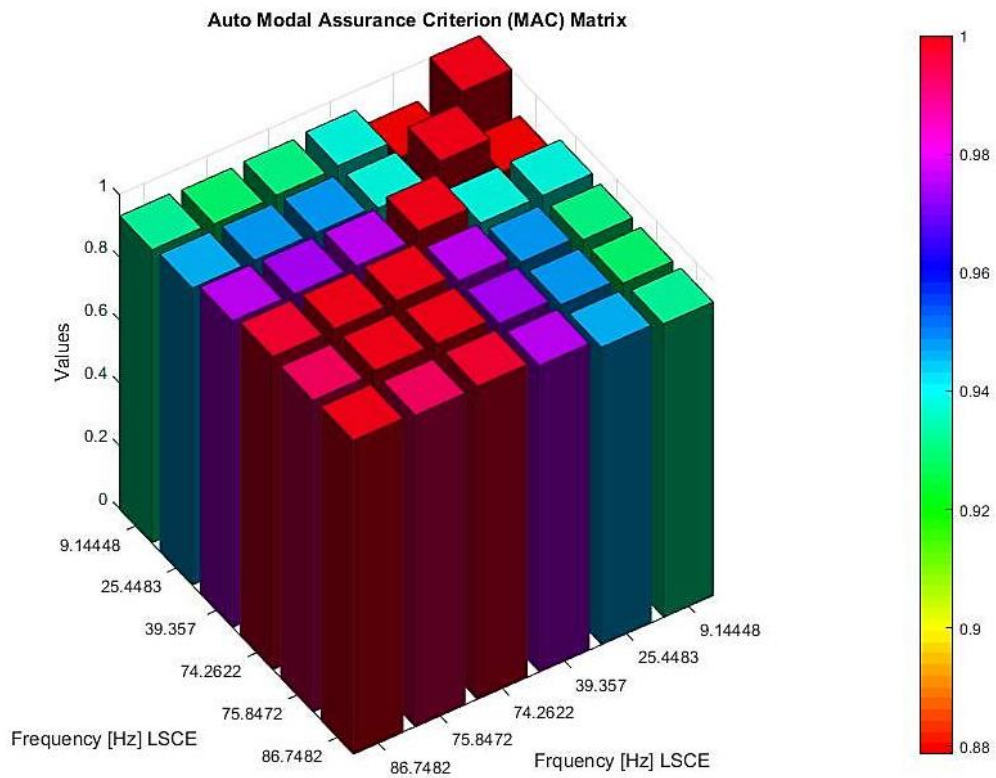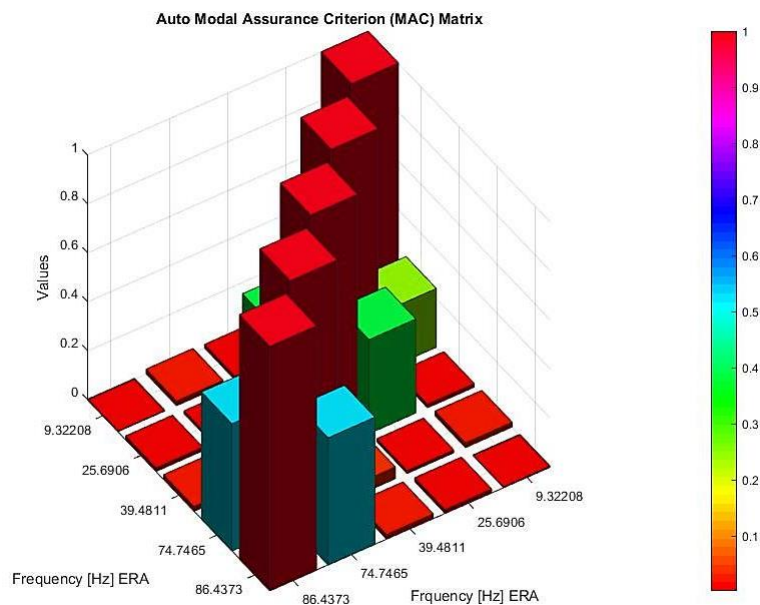*Fig 5.5.16: New Auto-Modal Assurance Criterion of modes extracted by ERA.*
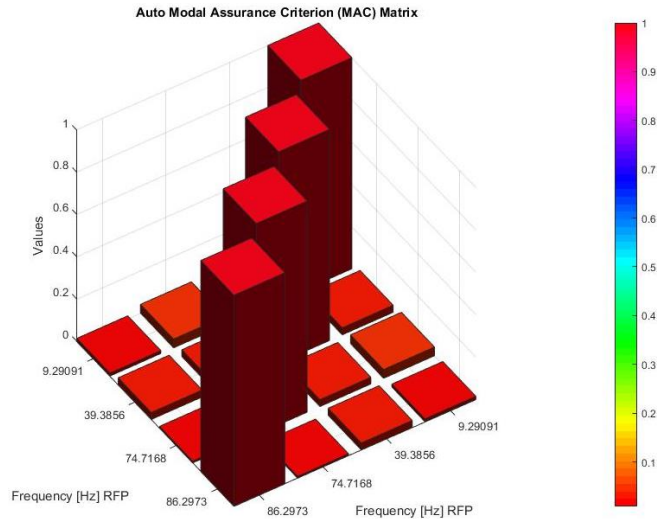
Fig 4.5.17: Auto-Modal Assurance Criterion by modes extracted by RFP.

From the Fig.4.4.17 illustrating the comparison between the mode shapes extracted by the RFP, it can be noted that the off-diagonal are very low. Using this Method make it seems that enough degrees of freedom was considered, this result was scene in all the examples when the mode shapes were compared between each other, it have been always noticed that the AutoMAC present always low off-diagonals, this do not lead to affirm that the sensors considered were sufficient because this method has a lot of problems in the ill-conditioning system.
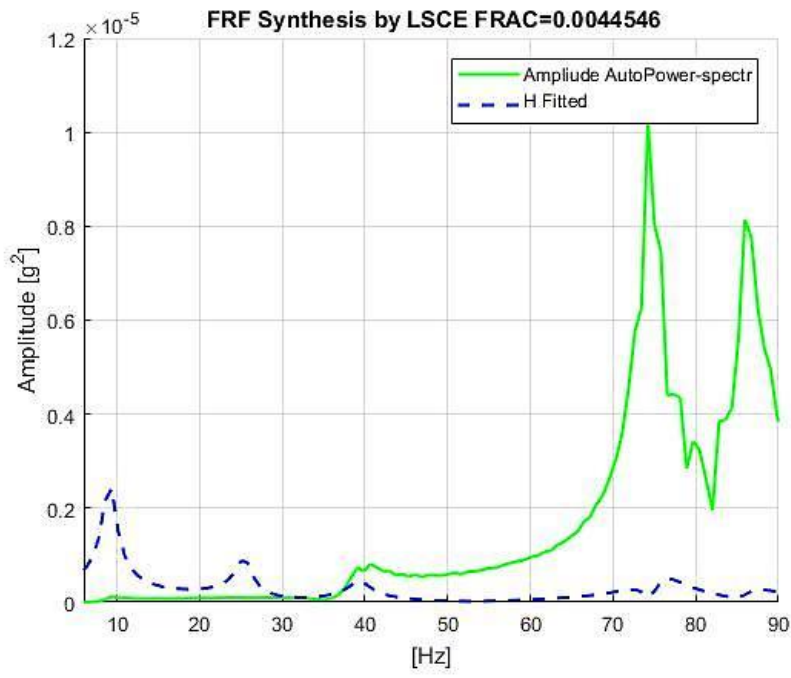
Fig 4.5.18: Fitting the FRF by LSCE of the airplane.
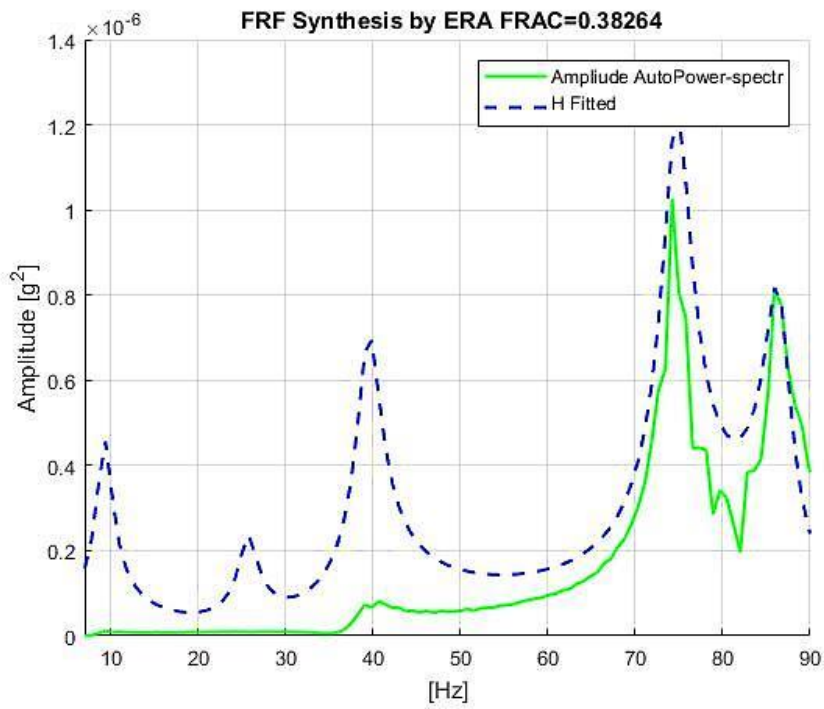
Fig 4.5.19: Fitting *the FRF by ERA of the airplane.*

171
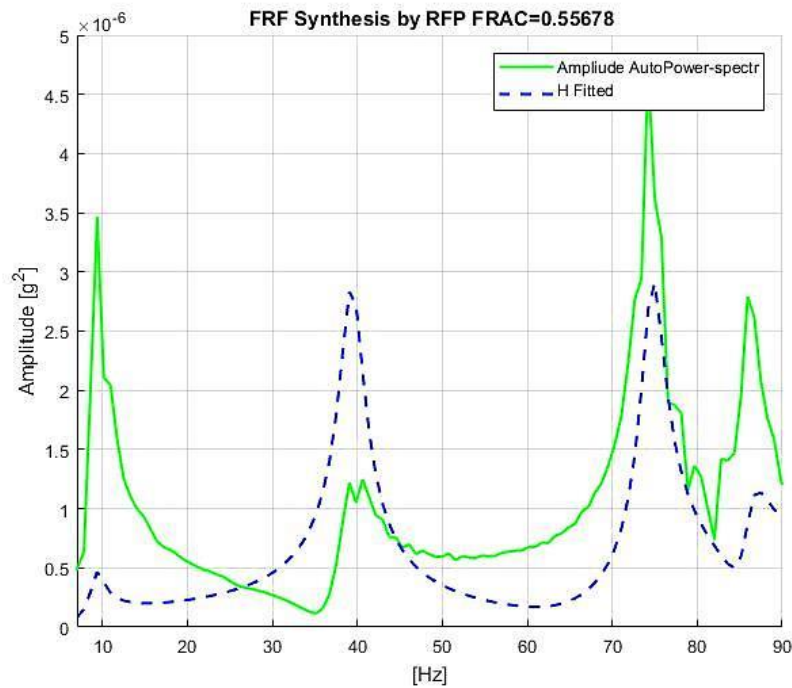
Fig 4.5.20: Fitting the FRF H11 by RFP of the airplane.

In this section, in the Fig.4.5.18, Fig.4.5.19 and Fig.4.5.20 a comparison within the range 0-90 Hz was made between Amplitute AutoPower Spectral measured and the one regenerated. It can be noted that the values for the FRAC were very low and the highest values of FRAC was obtained by the RFP Method, one of the reasons for this was the presence of a lot of noise in the function measured, and in this case the usage of FRAC to determine the validity of the modal parameters is not reliable.
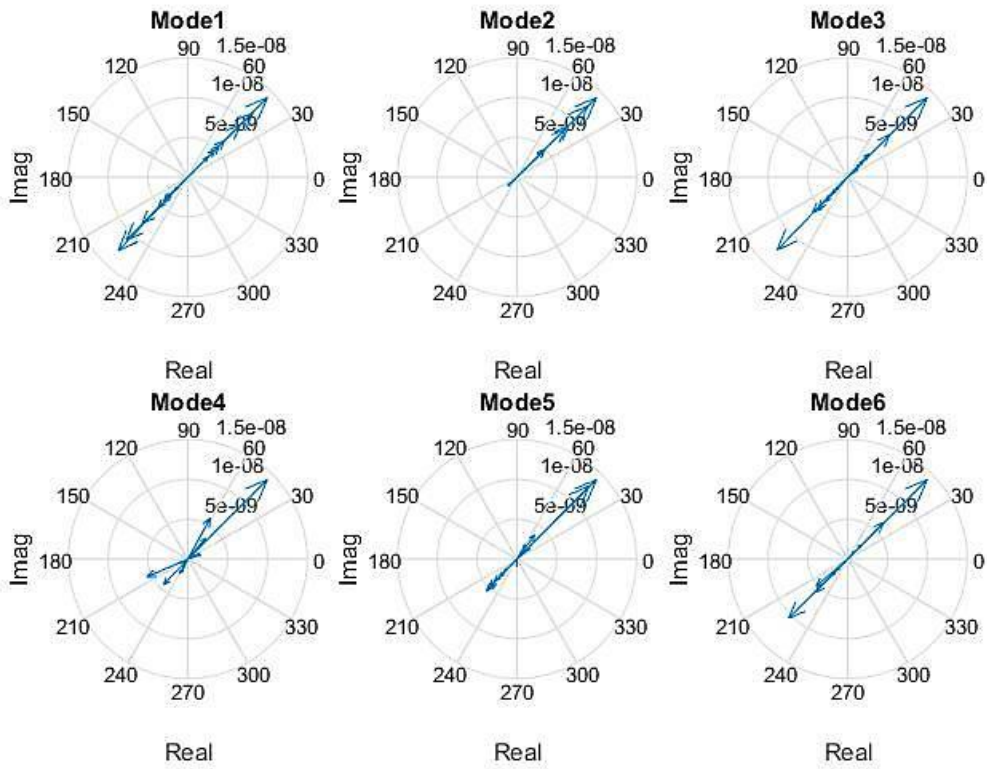
Fig 4.5.21: mode shapes extracted by Test-Lab Polymax method of the airplane.
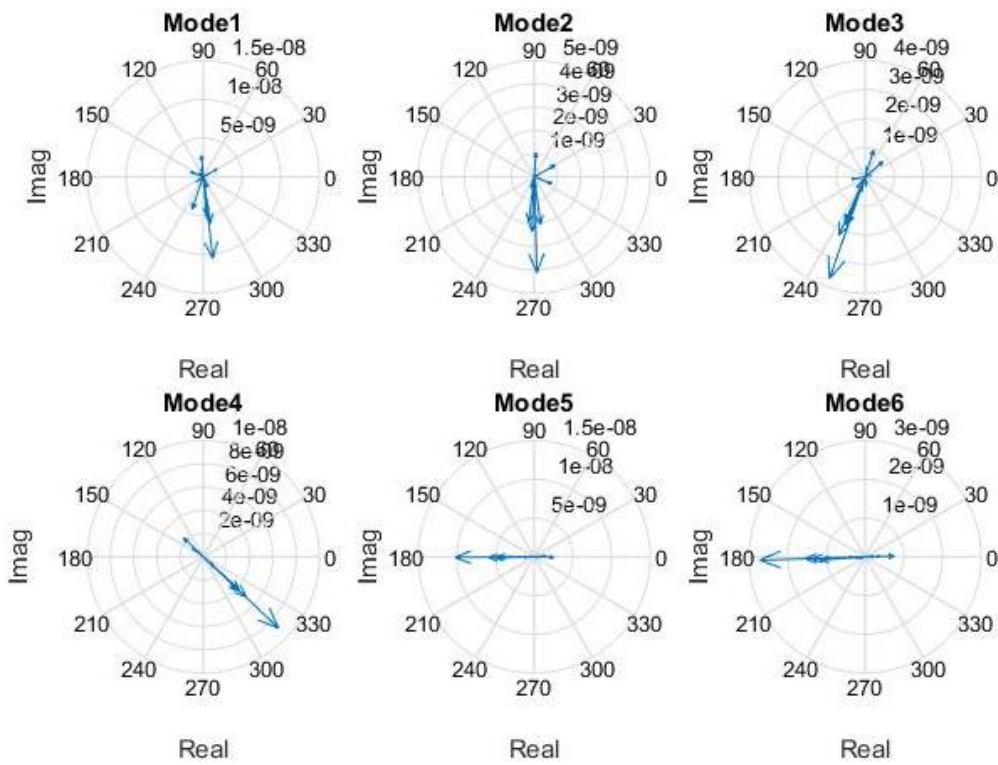
Fig 4.5.22: mode shapes extracted by LSCE of the airplane.
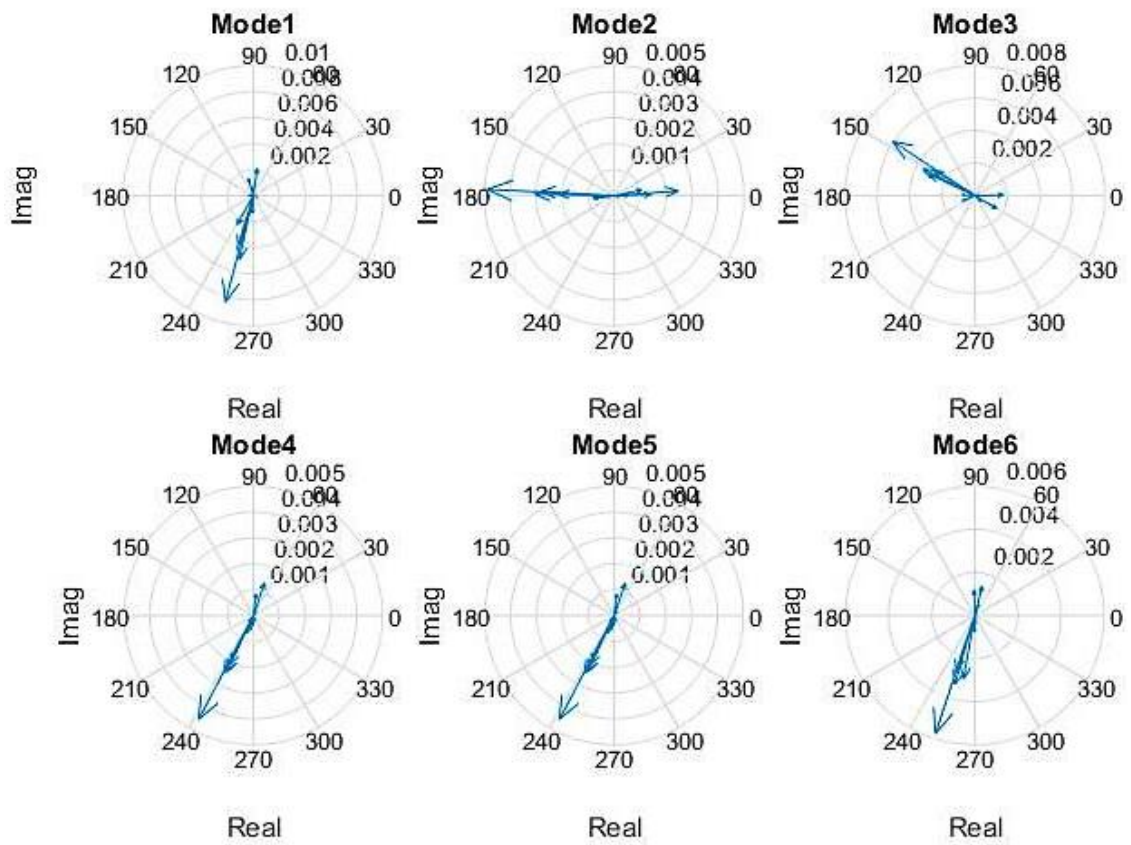
Fig 4.5.23: mode shapes extracted by LSCE Matlab toolbox of the airplane.
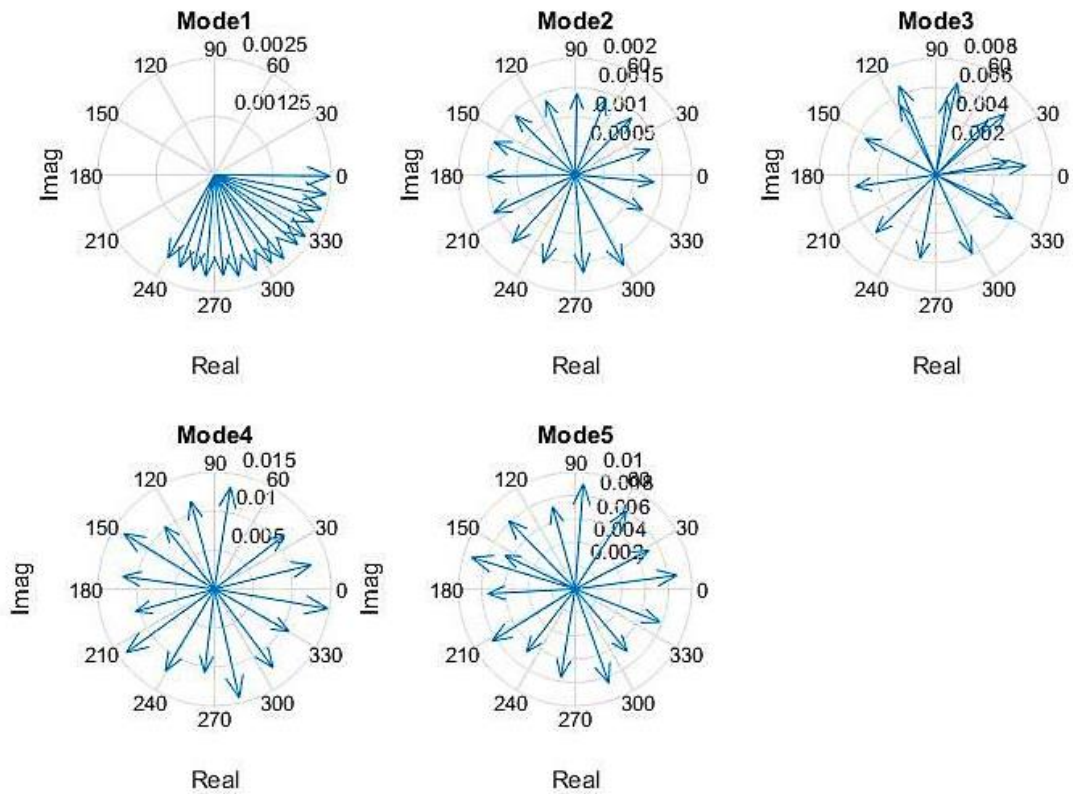
Fig 4.5.24: modes Shapes extracted by ERA of the airplane.
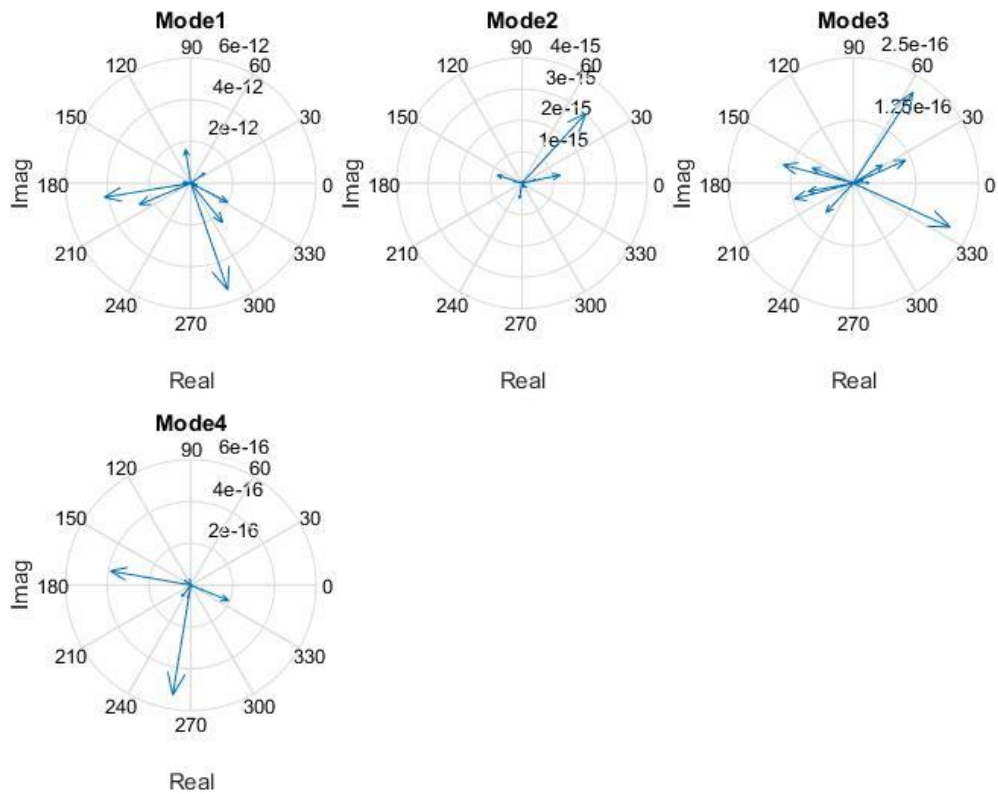
Fig 4.5.25: modes shapes extracted by RFP of the airplane.

The figures arranged from Fig.4.5.21 to Fig.4.5.25 represent the plot of the mode shapes in the complex plane extracted respectively by Polymax, LSCE, LSCE Matlab Toolbox, ERA and RFP Methods. In thee Fig.4.5.21 all the modes if rotated by an α angle, the mode shapes are entirely real except the fourth mode, this means that from the Polymax Method the damping is close to be proportional. When the other methods were applied the mode shapes appear to be chaotically dispersed, with a general look on these modes. It can be noted that every method gave distinct results for the mode shapes.
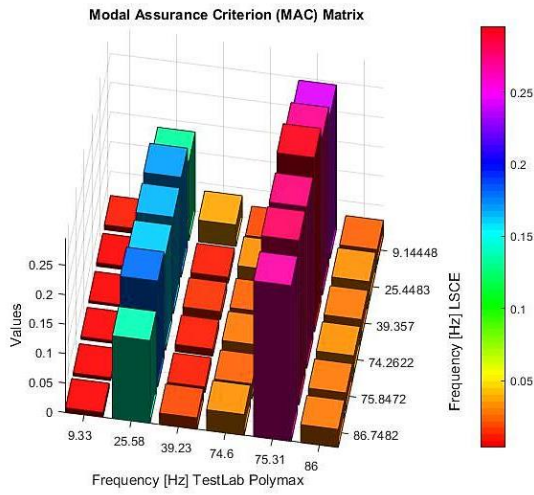
Fig 4.5.26: MAC of mode shapes extracted by LSCE and Test-Lab Polymax.
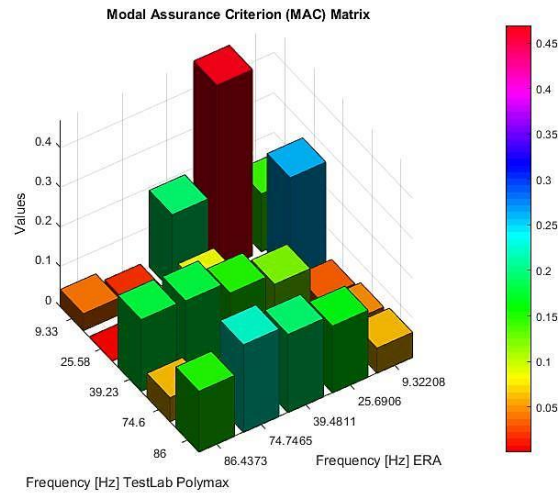
Fig 4.5.27: MAC of the mode shapes extracted by ERA and Test-Lab Polymax.
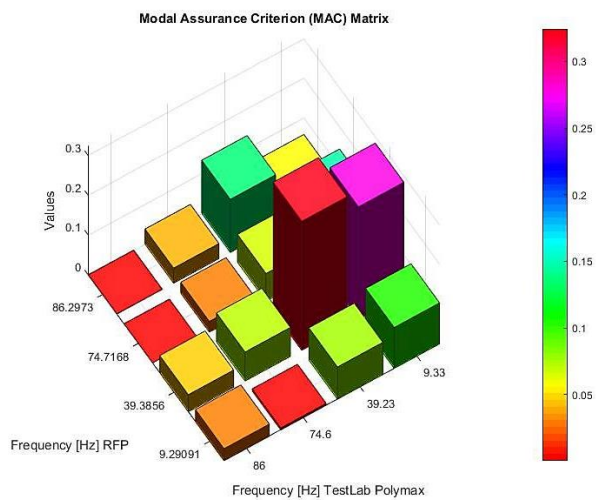
Fig 4.5.28: MAC of the mode shapes extracted by RFP and Test-Lab Polymax.

176

The Fig.4.5.26, Fig.4.5.27 and Fig.4.5.28 represent a comparison between the mode shapes extracted respectively by the LSCE, ERA and RFP with the mode shapes extracted by Polymax Method using MAC. The modes shaped were poorly estimated in all the cases because the values of MAC acquired were very low, and the correlation between the modes shapes was absent when they were compared to reach other.

Conclusions

In the airplane example the LSCE, ERA continue to give good estimation of the frequency and damping ratio, as can be seen in the tables 4.5.2, table 4.5.4.

The LSCE Matlab Toolbox gave the first and the last modes different damping ratios than other methods as the table 4.5.3 has showed.

In all the methods except for the RFP Method, clear stabilization diagrams were obtained as seen in the Fig 4.5.2, Fig 4.5.3, Fig 4.5.4 and Fig 4.5.6. Noted that when the ERA was applied, the major number of the poles presented in the stabilization diagram in the EMA and OMA examples were stable, while in the other methods a lot of poles presented in the stabilization diagram were unstable, then it can be said that the clearest stabilization diagram was the one obtained by the ERA.

In the RFP there was difficulty in finding the best frequency range, thus on the second mode 25 Hz and the third mode 75 Hz no cluster did appear to find the stable poles, this is due to the high level of noise. The other modes however gave good estimations for the frequency and damping.

Chapter 5

Conclusions & Remarks

Conclusions

The present study supply with essential results to understand the factors that affect the accuracy of the frequency, the damping ratio and mode shapes with respect to the method in use. Found on the results and their discussion in chapter 4, the following conclusions can be drawn:

- It is convenient to use as first estimation the Peak Amplitude and the Circle fit method that gave us a good estimation of the natural frequency and the damping ratio, they are simple to use and require a little time.

- The LSCE Matlab toolbox had some problems estimating the damping ratio. Then it is not practical to use only on this method to extract the modal parameters. The advantage of this LSCE Matlab toolbox is that it is simple and time conceiving. It has the disadvantage of not allowing the possibility to show the Least Square Error of the Hankel matrix. Then the max number of order is 50.

- Referring to the LSCE implemented, the number of row of the Hankel Matrix can be changed until a clear stabilization of matrix is obtained. In this case a good estimation of the frequency and the damping ratio can be achieved, and the error Least Square can be displayed. The disadvantage is that it requires more time than LSCE Matlab toolbox.

- Between the results collected for the values of frequency and damping from the analytical cases, the best results are of course the RFP. This is the most reliable method because it works in the frequency domain. The truncation of the FRF does not affect the frequency and damping ratio, but in the experimental case the true result are unknown. Basing on the results of the tables in the experimental case the LSCE implemented considered to be the best, the RFP and the ERA gives reliable results for damping. The damping results from the LSCE Toolbox are consistently lower than the others.

- The RFP is very sensitive to the noise and it is difficult to find the best bandwidth to be selected in order to achieve a good estimation of the damping ratio.

- It is not convenient to work in time domain to isolate the mode because the FRF loses a lot of information, and calculating the IRF will give another error.

- Regarding the stabilization diagrams resulting of each method, it can be noticed that the best stabilization diagram is achieved using ERA method because it is very clear even if in the case of modes close to each other. It is followed then by LSCE method stabilization diagram, and at the last place comes the one resulted by the RFP method.
- The ERA and the LSCE do not give good estimation of the modes shapes
- The best method to fit the FRF is the RFP that works in the frequency domain.
- In OMA the ERA and the LSCE reveal all the modes shapes especially when the modes are close to each other and when the level of noise is quite high. By using the RFP some modes do not appear but all other modes continue to give a good estimation of the frequency and damping. Finally, the quality of experimental modal parameter estimates depends so heavily on the quality of the FRFs measurements.

Remarks

In order to improve the accuracy of the modal parameters, the following recommendations were made:

- Ameliorate a solution that reduces the error generated from the truncation of the FRFs. Then each mode can be isolated when the LSCE and ERA are used.
- Use another type of excitation in order to verify if the methods depend of the excitation considering a frequency range.
- Ulterior study can be done related to result dispersion; the dispersion of MAC values can be calculated to better examine the mode shapes relation to the incoherence of modal parameters results.
- Construct the *Hankel* Matrix in an advanced way that permits to obtain the best number of rows when the number of order is increased

References

[1] *LMS Test.Lab Theory and Background Book*, LMS International-2004.

[2] Matlab R2017 Signal Processing Toolbox*. Modal Parameters of MIMO System.*

[3] Allyn W. Phillips and Randall J. Allemang*. Data presentation schemes for selection and identification of modal parameters. In 23th International Modal Analysis* Conference, Orlando, 2005.

[4] Anderas Brandt. *Noise and Vibration Analysis Signal Analysis and Experimental Prcedures*, Department of industrial and Civil engineering, University of Southern Denmark.

[5] A. Fasana – S. Marchesiello. Meccanica Delle Vibrazioni. Edizioni C. L. U. T – Torino.

[6] D. J. Ewins, *Modal Testing: Theory, Practice and Application*. Second Edition. RESEARCH STUDIES PRESS LTD .

[7] W.Helyen, S.Lammens, P.Sas, *Modal Analysis theory and testing.* Katholieke University Leuven.

[8] Randall.J Allemang and D. Brown 1982. *Proceedings of the 1st International Modal Analysis Conference, Orlando,* A correlation coefficient for modal vector analysis

[9] Michael R. Hatch. Vibration Simulating Using Matlab and Ansys. Boca Raton London New York Washington, D.C.

[10] Dr.Randall J.Allemang, Professore*. Vibration Experimental Modal Analysis.* University of cincinnati ohio 45221-0072.

[11] Kihong shin. Joseph K. Hammond. *Fundamentals of signal Processing for sound and vibration Engineers.* Andong National University Republic Korea, University of Southampton UK.

[12] P. Vacher, B. Jacquier, A. Bucharles*. Extensions of the MAC criterion to complex modes.* ONERA, Department of Systems Control and Flight Dynamics, 2, av. Edouard Belin, B.P. 4025, 31500 TOULOUSE, FRANCE.

[13] H.Ahmandian,G.M.L Gladwell, F. Ismail. *Extracting Real Modes from Complex Measured Modes.* Faculty of Engineering, University of Waterloo, Ontario, Canada N2L 3G1.

[14] Nuno Manuel Mendes Maia. *EXTRACTION OF VALID MODAL PROPERTIES FROM MEASURED DATA IN STRUCTURAL VIBRATIONS.* Department of mechanical Engineering Imperial college, London SW, U. K.

[15] Brian J. Schwarz & Mark H. Richardson. *EXPERIMENTAL MODAL ANALYSIS. Vibrant Technology*, Inc. Jamestown, California 95327.

[16] Peter Avitabile *Experimental Modal Analysis A Simple Non-Mathematical Presentation,* University of Massachusetts Lowell, Lowell, Massachusetts.

[17] Andre Lundkvist. Modal Analysis Project L7005A- Senior Sound Design Project. Lulea University of Technology

[18] Filipe Manuel Rodrigues Leite de Magalhães *Operation Modal Analysis For Testing And Monitoring of Bridges And Special Structures*, Universidade do Porto Faculdade de Engenharia.

[19] Rune Brincker, Carlos Ventura. Operation Modal Analysis. Technical University of Denmark, Denmark. University of British Columbia, Canada.

[20] Fimin He, Zhi-Fang Fu *Modal Analysis.* Butterworth–Heinemann.

[21] J. He and Z.-F. *Fu, Modal Analysis,* Butterworth-Heinemann, 2001.

[22] Nuno Manuel Mendes Maia and JúlioMontalvão e Silva, Eds., *Theoretical and Experimental Modal Analysis*, John Wiley & Sons Inc., New York,

[23] R. B. Randall, G. Zurita * and T. Wardrop. *EXTRACTION OF MODAL PARAMETERS FROM RESPONSE MEASURMENTS.* SCHOOL OF Mechanical and Manufacturing Engineering The University of New South Wales, Sydney 2052, Australia.

[24] Richardson, M. H., Formenti, D. L., Parameter estimation from frequency response measurements using rational fraction polynomials, IMAC I, Orlando, Florida, Nov .1982.

[25] Dave Formenti, *Mark Richardson , Parameter Estimation From Frequency Response Measurements Using Ration Fraction Polynomials (Twenty Years of Progress)*, Sage Technologies Morgan Hill, California, Vibrant Technology, Inc Jamestown, California

[26] Angel Moises Iglesias. Investigating Various Modal Analysis Extraction Techinques to Estimate Damping Ratio. Faculty of Virginia Polytechnic Institute and State University

[27] Dr.Randall J.Allemang, Professore. *Vibrations:Analytical and experimental modal analysis*. University of Cincinnati Ohio 45221-0072 . UC-SDRL-CN20-263-662.

[28] Richard S. Pappa, Kenny B. Elliott, and Axel Schenk. Consistent-mode indicator for the eigensystem realization algorithm Journal of Guidance, Control, and Dynamics, Spetember–October 1993.

[29] Randall J. Allemang.*The modal assurance criterion:* Twenty years of use and abuse.Sound and vibration Magazine, 2003.

[30] R.J.Allemang, A.W. Philips. *The Unified Matrix Polynomial Approach to Understanding Modal Parameter Estimation: An Update*. Structural Dynamic Research Laboratory, Univesity of Cincinnati.

[31] Code of the MatLab Software's "invfreqs" function, The MathWorks.
[32] Patrick Guillaume. Department of Mechanical Engineering,Vrije Universiteit Brussel, Pleinlaan 2, B-1050 Brussel, Belgium.

[33] Rabdall L. Allemang, *The Modal Assurance criterion twenty years of use,* university of Cincinnati,Cincinnati, Ohio.

[34] N D Newman ,M I Friswell and J E T Penn. THE PARALLEL IMPLEMENTATION OF THE RATIONAL FRACTION POLYNOMIAL METHOD. Department of Mechanical and Electrical Engineering, Aston University, Birmingham B4 7et, U. K.

[35] Jeroen Lanslots, Bert Rodiers, Bart Peeters *Automated Pole-Selection:Prof-of-Concept & Validation* LMS International, TST Technology Deployment & Research.

Appendix A

Fit a Circle Using Least Square method.

Considering a set of points $\mathbb{R}^2$ and we will find the best circle using Least Square method. Thus;

$$\{(x_i, y_i) \text{ with } 0 \leq i < N\} \tag{A,1}$$

Define the means of x_i and y_i as follow:

$$\bar{x} = \frac{1}{N} \sum_i x_i \text{ and } \bar{y} = \frac{1}{N} \sum_i y_i \tag{A,2}$$

Having an equation of Circle with center (u_c, v_c) and radius R.

$$g(u, v) = (u - u_c)^2 + (v - v_c)^2 - R^2 \tag{A,3}$$

Considering $u_i = x_i - \bar{x}$ and $v_i = y_i - \bar{y}$; define the S function that we will minimize as follow:

$$S = \sum_i \left(g(u_i, v_i) \right)^2 \tag{A,4}$$

Suppose $\alpha = R^2$, then differentiate $S(\alpha, u_c, v_c)$; Hence.

$$\frac{\partial S}{\partial \alpha} = -2 \sum_i g(u_i, v_i) \tag{A,5}$$

If $\frac{\partial S}{\partial \alpha} = 0$, Thus

$$\sum_i g(u_i, v_i) = 0 \tag{A,6}$$

Deriving respect to u_c recalling equation (A, 5) we have the following expression:

$$\frac{\partial S}{\partial u_c} = -4 \sum_i u_i g(u_i, v_i) + 4u_c \underbrace{\sum_i g(u_i, v_i)}_{=0} \tag{A,7}$$

If $\frac{\partial S}{\partial u_c} = 0$, Thus

$$\sum_i u_i g(u_i, v_i) = 0 \qquad \text{(A,8)}$$

Using the same procedure of and considering $\frac{\partial S}{\partial v_c} = 0$ then we can write.

$$\sum_i v_i g(u_i, v_i) = 0 \qquad \text{(A,9)}$$

Developing equation (A,8) as follow:

$$\sum_i u_i [u_i^2 - 2u_i u_c + u_c^2 + v_i^2 - 2v_i v_c + v_c^2 - \alpha] = 0 \qquad \text{(A,10)}$$

Defining $S_u = \sum_i u_i$, $S_{uu} = \sum_i u_i^2$, *etc*, we can rewrite the equation (A,10) as :

$$S_{uuu} - u_c S_{uu} + u_c^2 S_u + S_{uvv} - 2v_c S_{uv} + v_c^2 S_u - \alpha S_u = 0 \qquad \text{(A,11)}$$

Since $S_u = 0$,we obtain.

$$u_c S_{uu} + v_c S_{uv} = \frac{1}{2}(S_{uuu} + S_{uvv}) \qquad \text{(A,12)}$$

In a similar way, developing Equation (A,9) and hypothesis $S_v = 0$,Thus :

$$u_c S_{uv} + v_c S_{vv} = \frac{1}{2}(S_{vvv} + S_{vuu}) \qquad \text{(A,13)}$$

From equation (A, 12) and (A, 13) we can determine the (u_c, v_c), then we can find immediately the center (x_c, y_c) of the circle fitted by Least square as :

$$x_c = u_c + \bar{x} \quad and \quad y_c = v_c + \bar{y} \qquad \text{(A,14)}$$

To find the Radius, develop equation (A,6) then :

$$\sum_i [u_i^2 - 2u_i u_c + u_c^2 + v_i^2 - 2v_i v_c + v_c^2 - \alpha] = 0 \qquad \text{(A,15)}$$

Considering $S_u = 0$ and $S_v = 0$ again, we get

187

$$N(u_c{}^2 + u_v{}^2 - \alpha) + S_{uu} + S_{vv} = 0 \qquad\qquad (A,16)$$

$$\alpha = u_c{}^2 + u_v{}^2 + \frac{S_{uu} + S_{vv}}{N} \qquad\qquad (A,17)$$

With $R = \sqrt{\alpha}$;

$$N(u_c{}^2 + u_v{}^2 - \alpha) + S_{uu} + S_{vv} = 0$$

Appendix B

Method implementation (Matlab code)

This appendix provides an explication for the Matlab implementation of the five methods described in the previous chapter which are PP, CF, LSCE, ERA and RFP. For a better understanding of this process, the steps required to extract the modal parameters will be explained in detail. In this section, the MAC and the FRF synthesis parts were not included.

B.1   Peak Amplitude:

First step: Load all the FRFs

Second step: isolate the modes

Third step: Determine the Natural Frequency

Fourth step: Determine the Damping and Modal Constant

Fig 4.1: Steps of Peak Amplitude Method

First step: load all the output (frequency response function g/N)

-        load (' Name-file.mat');

-        Order the FRF in column, and select one FRF(:,i);

Second step: select your bandwidth for isolating each modes presented in the FRF.

-        Freq= 0:delta_freq(N-1)*delta_freq ; % define the vector of the frequency in [Hz], N is the spectral lines.

189

-         F_{min} =input('select the minimum   frequency') .
-         F_{max} = input('select the maximum frequency').
-         FRF_selected=FRF(f_{min}:f_{max});
-         freq_selected=delta_freq*fmin:delta_freq:delta_freq*fmax;

Third step : find the Peak of the bandwidth selected.

-         [Hmax freq_r]=findpeaks(abs(FRF_selected));

-         freq_resonance=(freq_r+fmin)*delta_freq;

-         y1=Hmax./(sqrt(2));

Fourth step: Find the intersection between y1 and FRF_selected, then the Damping ratio and modal constant .

-         inter1 = abs(FRF_selected)-y1;

indice_puntizero1= [];
-   for n=1:length(freq_selected)-1;
-    if ((inter1(n)<0 && inter1(n+1)>0) || (inter1(n)>0 && inter1(n+1)<0));
-   indice_puntizero1(end+1)=n;
-   end
-   end
Find the natural damping ratio and the modal constant.
-         freq_halfpower1=(2*pi).*freq_selected(indice_puntizero1);
-         omega_1=freq_halfpower1(1); %[rad/s]
-         omega_2= freq_halfpower1(2);% [rad/s]
-         zita_modale1=(omega_2-omega_1)/(4*pi* freq_resonance);
-         Ar1=Hmax(1)*freq_risonanza*zita_modale1;% modal constant

if imag(H_selected)<0; % sign of the modal constant.

  Ar1=-Ar1;

End

B.2   Circle Fit:
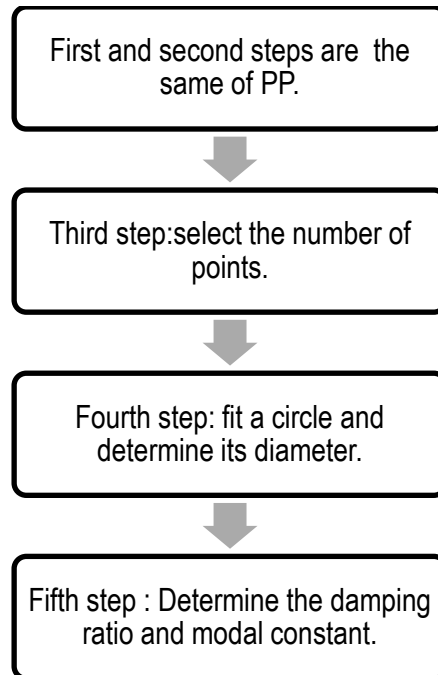
Fig 4.2: Steps of Circle Fit method.

The first and the second steps are the same of the Peak Amplitude method.

Third step: select the points near on the peak of the FRF_selected that are symmetric respect on the Peaks.

- nb = input(' input the number of points') ; % select the number of points.
- nb=nb+1;
- x=real(FRF_Selected)
- y=imag(FRF_Selected)

Fourth step: Fit a circle in this step we will determine the center C(xc,yc) and the diameter D:

- xm=mean(x);
- ym=mean(y);
- u=zeros(1, length(x));
- for i=1:length(x);
- u(i)=x(i)- xm;
- end
- v=zeros(1,length(y));
- for   j=1:length(y);

- v(j)= y(j)-ym;
- end
- suu= sum(u.^2);
- suv= sum(u.*v);
- svv= sum(v.^2);
- suuu= sum(u.^3);
- svvv= sum(v.^3);
- suvv=sum(u.*v.^2);
- svuu=sum(v.*u.^2);
- F=[suu suv ;suv svv];
- E=0.5.*[suuu+suvv; svvv+svuu];
- uvc = F\E ;
- xc = uvc(1,1)+xm;
- yc=uvc(2,1)+ym;
- R=sqrt((uvc(1,1).^2)+(uvc(2,1).^2)+ ((suu+svv)/length(x)));
- DIAM= 2*R;

Fifth step: Estimate the natural frequency and the damping factor.

- theata= atan(y./x)*180/pi;
- nn=floor(nb/2);
- theata_a= 2.*(pi/2 -(theata(:,nn:nb+1)*pi/180));
- theata_b=2.*(pi/2 +(theata(:,1:nn).*pi/180));
- omega_vectb=omega_vect(:,1:nn);
- omega_vecta=omega_vect(:,nn+2:nb+1);
- zita_est= -(omega_vecta. ^2-omega_vectb.^2)

./(2.*freqr*2*pi.*(omega_vecta.*tan(theata_a./2)+omega_vectb.*tan(theata_b./2)));

- zita=mean(zita_est); % determine the damping ratio

- sigma=std(zit_est); % estimate the standard deviation

- A_r= 2*D*zita;

- If imag(FRF_selected)<0;

- A_r = -A_r

- End

B.3   Least Square Complex Exponential Method:
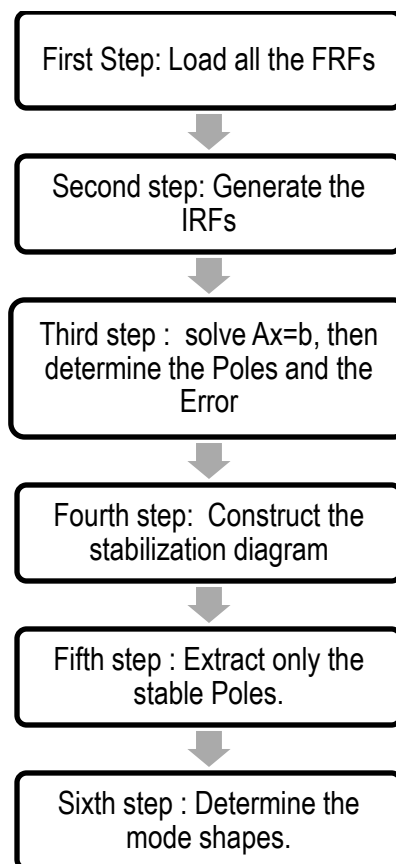
Fig 4.3: Steps of Least Square Complex Exponential Method.
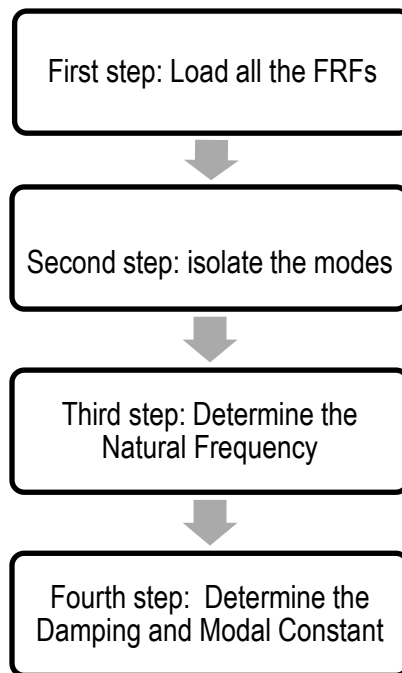
First step: load all the output (frequency response function g/N)

- load (' Name-file.mat');
- Order the FRF (H) in column ;

Second step: Transform the Inertance to Receptance.

- Freq ; % insert the vector of the frequency in Hz
- w=double(2*pi*freq); %
- FRF_R=zeros(size(H)); % determine the matrix of the Receptance
- for i=1:size(H,2);
- FRF_R(:,i)=double(H(:,i)./(w.^2)); % Transform the Inertance in
Receptance
- FRF_R(1,i)=0;
- end

193

-      fc=200;

-      delta_f=f(2)-f(1);

-      delta_t=1/(2*fc);

the Test Lab just gives the positive frequency components

-      n = length(FRF_R) ;

-      frf_conj=conj(FRF_R); % Adding the conjugate components to the FRF

-      FRFH=[FRF_R(1:end,:) ;frf_conj(n-1:-1:2,:)]; %create the double side of the FRF.

-      N = length(FRFH) ;

-       time = double([0:(N-1)]*delta_t) ;

-      for i=1:size(FRFH,1);

-      x(i,:) = real(ifft(double(FRFH(i,:)))) ; % determine the Impulse Response Function

-      end

Third step: solve Ax=b, by least square method .

-      Construct the Hankel matrix (Hank) from considering y=x.

-      band=input('select your bandwidth');

-      y=y(:,band);

-      [l,m]=size(y);

-      clear righ

-      righ =number of rows for each FRF ; j1=number of column

-      ll=l-rig-1;

-      Hank=zeros(m*righ,ll);

-      for k=1:righ;

-        Hank((k-1)*m+1:k*m,:)=y(:,k:k+ll-1);

-      end

-      Hank=Hank(1:end,1:j1); % Hank =A;

-      h0=Hank(2:size(Hank,1),j1); % Hank=h0;

-      for ww=1:size(Hank,2)-1;

-        Hankel=Hank(1:size(Hank,1)-1,1:ww+1);

-        h00=-h0(1:size(Hank,1)-1,1);

-        beta=pinv(Hankel)*h00;

-        Vp=roots(flipud([beta;1]));

```
-         t=find(Vp-conj(Vp)); % find only the complex pairs poles
-         pp(ww).poles=log(Vp(t))./delta_t;  % matrix of poles
-      %%%%% determine the error of the least square %%%%%
-         err = norm(h00-(Hankel*beta));
-         er(ww).error=err;
-      End
```

Fourth step: Construct the stabilization diagram.

```
-      n=length(pp(end).poles);
-      totale=zeros(length(pp),n);
-      for j=1:length(pp);
-       if length(pp(j).poles)==0;
-      totale(j,:)=zeros(1,n);
-      else
-       for  i=1:length(pp(j).poles);
-      totale(j,i)=pp(j).poles(i);
-      end
-      end
-      end
-      totale_nconj=totale(:,1:2:size(totale,2)); % select one  part of pole
-      [nn mm]=size(totale_nconj);
-      %%%%%%% find the stable frequencies with tolerance 0.01 %%%%%%
-      freq=zeros(nn,mm);
-      freq =abs(totale_nconj)./(2*pi);
-      freqr=sort(freq(:),'ascend');
-      t=find(freqr==0);
-      freqr(t)=[];
-      a=zeros(length(freqr),1);
-      clear i j
-      for i=1:length(freqr)-1;
-          a(i,:)=abs(freqr(i)-freqr(i+1))./freqr(i);
-           if a(length(freqr)-1)<=0.01;
-              a(length(freqr))=0.01;
-           elseif a(length(freqr)-1)>0.01;
-              a(length(freqr))=0;
-               end
```
195

```matlab
end
 [tr tc]=find(a<=0.01 & a>0);
t_f=find(a<=0.01 & a>0);
poli_filt_freq=freqr(t_f);
clear i j
for i=1:length(t_f);
 [ X_freq(i) Y_freq(i)]=find(freq==poli_filt_freq(i));
End
%%%Now we can plot the poli_filt_freq  vs  X_freq


%%%%%%% find the stable damping  with tolerance 0.05 %%%%%%%

clear i j
zita_matrix=zeros(nn,mm);
for i=1:nn;
  for  j=1:mm;
    zita_matrix(i,j)=-real(totale_nconj(i,j))/abs(totale_nconj(i,j));
    if zita_matrix(i,j)<0 ;
        zita_matrix(i,j)=0;
        end
   end
end
clear i j
for i=1:length(freqr);
  t1(i)=find(freq==freqr(i));
end
clear i j
zita_r=zita_matrix(t1).';
Z=zeros(length(zita_r),1);
 for i=1:length(zita_r)-1;
        Z(i,:)=abs((zita_r(i)-zita_r(i+1)))./(zita_r(i));
        if Z(length(zita_r)-1)<=0.05;
           Z(length(zita_r))=0.05;
        elseif Z(length(zita_r)-1)>0.05;
           Z(length(zita_r))=0;
```

196

-         end
-       end
-       zisnan=find(isnan(Z));
-     for zis=1:length(zisnan);
-        Z(zisnan(zis))=0;
-     end
-     % now we will extract the stable damping
-     [trz,tcz]=find(Z>0 & Z<=0.05);
-     t_z=find(Z>0 & Z<=0.05);
-     poli_filt_zita=zita_r(t_z);
-     zita=freqr(t_z);
-     clear i j

for i=1:length(t_z);
-     [X_zita(i) Y_zita(i)]=find(freq==zita(i));
-     End
-     %%%%% plot the zita vs X_zita.

%%%%%%%% in this section will identify the stables poles that have%%%%%%

$$\partial f < 0.01 \ \& \ \partial \zeta < 0.05$$

-     [loc_r,loc_c]=ismember(t_z,t_f);
-     t10=find(loc_c==0);
-     loc_c(t10)=[];
-     t_f_z=t_f(loc_c); % this is the index of the stable poles in the matrix freqr
-     t_freq_smor=freqr(t_f_z);
-     clear i j
-     for i=1:length(t_f_z);
-     [X_freq_smor(i) Y_freq_smor(i)]=find(freq==t_freq_smor(i));
-     End

%%%%% plot t_freq_smor vs X_freq_smor.

Fifth step: Extract the stable poles from the stabilization diagram.
-     Poli_ext = []; % stable pole
-     freq_LSCE=abs(poli_ext)./(2*pi);
-     zita_LSCE=-real(poli_ext)./abs(poli_ext);

Sixth step: determine the Mode shapes.

- VV=exp(poli_ext.*delta_t);
- poli_extconj=conj(poli_ext);
- poli_tot=[poli_ext poli_extconj];
- poli_tot=exp(poli_tot.*delta_t);
- L=input('choose your order');
- lp=input('insert the number of point');
- clear i j
- Vandr_final=zeros(2*L,length(poli_tot));
-     for j=0:2*L-1;
-         Vandr_final(j+1,:)=(poli_tot.^j).';
-       End
- clear i j
- j=0;
- for i=1:lp;
-     j=j+1;
-     mode_final(j,:)=pinv(double(Vandr_final))*y(1:2*L,j);
- end
- mode_final=mode_final(:,1:length(poli_ext));

B.4 Eigen Realization Algorithm

```
┌─────────────────────────────────────┐
│     First Step: Load all the FRFs.   │
└─────────────────────────────────────┘
                  ▼
┌─────────────────────────────────────┐
│   Second step: Generate the IRFs.    │
└─────────────────────────────────────┘
                  ▼
┌─────────────────────────────────────┐
│   Third step :  Generate the Hankel  │
│       Matrices, H0 and H1.           │
└─────────────────────────────────────┘
                  ▼
┌─────────────────────────────────────┐
│  Fourth step:  Eigen values problem  │
│  solving, poles,  mode shapes and    │
│        Singular Values.              │
└─────────────────────────────────────┘
                  ▼
┌─────────────────────────────────────┐
│  Fifth step : Contract the Stabilization │
│             Diagram                  │
└─────────────────────────────────────┘
                  ▼
┌─────────────────────────────────────┐
│  Sixth step : Extract the stable poles │
│        and the mode Shapes.          │
└─────────────────────────────────────┘
```

Fig 4.4: Steps of Eigen system Realization Algorithm.
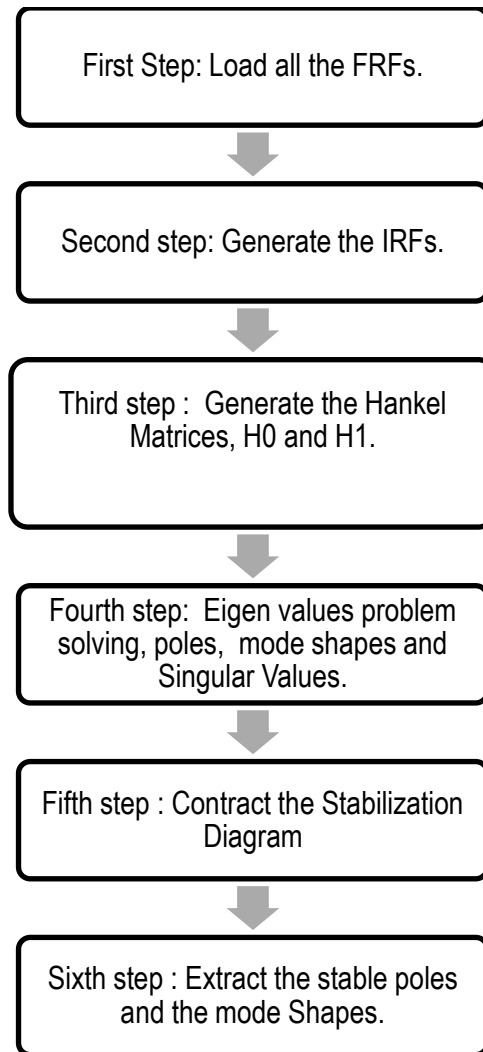
The First and the second step are the same of the LSCE Method

Third step: Generate the Hankel Matrix and the *H0, H1*

- band=input('select your bandwidth');

- Construct the Hankel matrix (Hank) from considering y=x.

- band=input('select your bandwidth');

- y=y(:,band);

- [l,m]=size(y);

- clear righ

- righ =number of rows for each FRF ; j1=number of column

```
-       ll=l-rig-1;
-       Hank0=zeros(m*righ,ll);
-       for k=1:righ;
-           Hank0((k-1)*m+1:k*m,:)=y(:,k:k+ll-1);
-       end

-       Hank1=zeros(m*righ,j);

-        for k=1:righ;

-       Hank1((k-1)*m+1:k*m,:)=y(:,k+1:k+j-1);

-       end

-       H0=Hank0.';

-       H1=Hank1.';
```

Fourth step: Generate the matrices [A], [B] and [C]. Then solving the Eigen-problem, and extract the poles and modes shapes of the system .

```
-       [U,sigma,V]=svd(H0);
-       s=diag(sigma);
-       s1=s/max(s);

-       jj=input('number of the order')

-       for n=1:jj;

-       A=sign^-0.5*U(:,1:n).'*H1*V(:,1:n)*sign^-0.5;

-       sign=sig(1:n,1:n);

-       C=U(:,1:n)*sign^0.5;

-       B=sign^0.5*V(:,1:n).';

-       C=C(1:m,:);

-       [vv,pol]=eig(A);

-       lambda=diag(pol);

-       kw=find(lambda-conj(lambda));
```

```
-      lamda=log(lambda(kw))./(delta_t);

-      pp(n).poles=lamda;% find our poles of all iterations

-      ms=C(:,kw)*vv(kw,kw);

-      mode_shape(n).resid=ms;

-      end
```

In this paragraph we will ordinate the mode shapes in a normal matrix

```
-      clear i

-      for i=1:n(end);

-      mode_shape_nonconj(i).res=mode_shape(i).resid(:,2:2:end);

-      end

-      clear i j n1

-      n1=length(pp(end).poles);

-      totale=zeros(length(pp),n1);

-      for j=1:length(pp);

-      if length(pp(j).poles)==0;

-      totale(j,:)=zeros(1,n1);

-      else

-      for  i=1:length(pp(j).poles);

-      totale(j,i)=pp(j).poles(i);

-      end

-      end

-      end

-      totale_nconj=totale(:,1:2:size(totale,2));

-      [nn mm]=size(totale_nconj);
```

- clear i j n1

- n1=length(mode_shape_nonconj(end).res(:));

- mode=zeros(length(pp),n1);

- for j=1:length(pp);

- if length(mode_shape_nonconj(j).res)==0;

- mode(j,:)=zeros(1,n1);

- else

- for i=1:length(mode_shape_nonconj(j).res(:));

- mode(j,i)=mode_shape_nonconj(j).res(i);

- end

- end

- end

- clear i j

- mod=zeros(mm*nn,m);

- for i=0:mm-1;

- mod((1:nn)+i*nn,:)=mode(:,(1:m)+i*m);

- end

Fifth step: This step is very similar to fourth steps of LSCE in this step we will only add the stabilization of vector, then we will Construct the stabilization diagram.in this section the tolerance between the iterations is 0.9.

- clear i j

- [or oo]=size(mod);

- for j=1:or-1;

- mac(j,:)=
(abs(conj(mod(j,:))*mod(j+1,:).'))^2./((conj(mod(j,:))*mod(j,:).')*(conj(mod(j+1,:))*mod(j+1,:).'));

- End

- if mac((nn*mm)-1)>=0.9;

- mac(nn*m)=1;

- Else

- mac(nn*mm)=0;

- end

- t_vett=find(mac>=0.9);

- freq_vett=freq(t_vett);

- clear i j

- for i=1:length(t_vett);

- [X_vett(i) Y_vett(i)]=find(freq==freq_vett(i));

- end
 %%%% plot freq_vett vs X_vett

 % now we will find the stable poles and vector

- clear i j

- [loc_rs,loc_cs]=ismember(t_f_z,t_vett);

- t11=find(loc_cs==0);

- loc_cs(t11)=[];

- t_stable=t_vett(loc_cs); % find the index that correspond to the stable poles
    and vector.
- freq_poli_stabili=freq(t_stable);

- clear i j

- for i=1:length(t_stable);

- [X_stable(i) Y_stable(i)]=find(freq==freq_poli_stabili(i));

- end

Sixth step: after we have plot the stabilization diagram we will from our stable poles.

Disp('select you stable pole and give it pole name').
- mod_estratti=mod(t_stable,:);
- poli_interi_stabili=totale_nconj(t_stable);
- freq_estratti=abs(poli_interi_stabili)./(2*pi).
- fattori_smorzameti_estratti=-real(poli_interi_stabili)./(2*pi.*freq_estratti);
- Index=find(freq_estratti==pole(1).Position(1));
- frequency=freq_estratti(Index(1)); disp(frequency)
- modal_costant=mod_estratti(Index(1),:).'; disp(modal_costant)
- damping_ratio= fattori_smorzameti_estratti(Index(1)); disp(damping_ratio)
- polo=poli_interi_stabili(Index(1),:);% stable pole
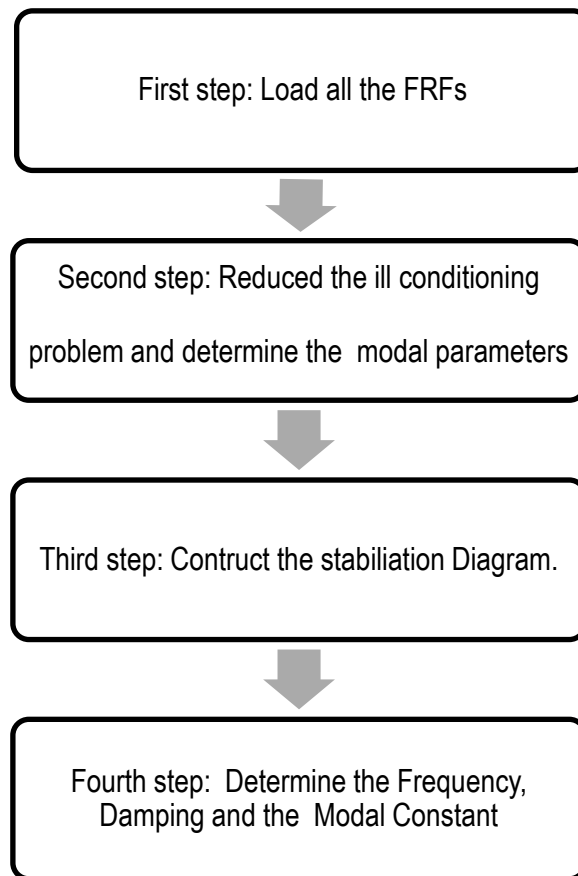
B.5   Rational Fraction Polynomial.

First step: Load all the FRFs

↓

Second step: Reduced the ill conditioning problem and determine the modal parameters

↓

Third step: Contruct the stabiliation Diagram.

↓

Fourth step: Determine the Frequency, Damping and the Modal Constant

Fig 4.5: Steps of Rational Fraction Polynomial Method

First step: load all the FRFs

- load('Receptance_GearBox_34points.mat');
- H_inc=FRF.y_values.values.'. ;
- H=H_inc.';
- f= ;%Hz
- w=2*pi.*(f);%Rad/s

Second step: in order to obtain a better estimation of the modal parameters, the ill conditioned characteristic of matrices that are described in the chapter 2 can be reduced, but not eliminated, as follow.

- ➢ Minimizing the frequency range, as first estimation we can consider only 16 points [3] [4].
- ➢ Minimizing the order of the modal.

- ➤ Normalizing the frequency range of the data dividing by the maximum number of the frequency.

- band=input('select your bandwidth');
- omega=w(band);
- H_sel=H_inc(1:34,band);
- omega_scal=omega./(max(omega));
- N=input('input the order')
- GRD=ones(1,length(omega));
- iter=;% number of iteration
- tol= % chose your tolerance
- clear i j

- for j=1:size(H_sel,1);

- for i=1:N;

- m=2*i;

- mm=2*i-1;

- [PP QQ]=invfreqs(H_sel(j,:),omega_scal,mm,m,GRD,iter,tol); [31]

- numerator(i).num=PP; % determine the numerator values of (a_0*s^0+a_1*s^1+a_2*s^2+.....+a_2N-1*s^2N-1) with s=j*omega

- denominator(i).denom=QQ; % determine the denominator values of (b_0*s^0+b_1*s^1+b_2*s^2+.....+b_2N*s^2N)con s=j*omega

- [R P]=residue(numerator(i).num,denominator(i).denom); % Residui e poli

- pp(i).poles=P; % determine the Poles for one FRF

- Ar(i).(['Resid' num2str(j)]) = R; % determine the Modal constant using all FRF
- End
- End

Now we will pass to extract only the complex conjugate poles.

- clear i
- for i=1:N,
- tt=find(pp(i).poles-conj(pp(i).poles));
- ttt(i).indice=tt;% find only the conjugate part
- end

in this section we used the same procedure in LSCE for transform the structure matrix to a normal matrix, then we multiplied by max(omega). Thus

- totale_nconj=max(omega).*totale(:,1:2:size(totale,2);

Third step are the same fourth LSCE step.

Fourth step are the same last step ERA.

Sezioni

UNIVERSITÀ
DEGLI STUDI
DI FERRARA

Dottorati di ricerca

Il tuo indirizzo e-mail

zryblk@unife.it

Oggetto:

Dichiarazione di conformità della tesi di Dottorato

Io sottoscritto Dott. (Cognome e Nome)

Zrayka Abdel Kader

Nato a:

El Minie

Provincia:

Libano

Il giorno:

14/03/1989

Avendo frequentato il Dottorato di Ricerca in:

Scienze dell'Ingegneria

Ciclo di Dottorato

30

Titolo della tesi:

On the modal parameter estimation methods: critical review, implementation in Matlab environment and effectiveness

Titolo della tesi (traduzione):

Revisione critica, implementazione in ambiente Matlab ed efficacia di metodi di stima dei parametri modali

Tutore: Prof. (Cognome e Nome)

Mucchi Emiliano

Settore Scientifico Disciplinare (S.S.D.)

ING/IND 13

Parole chiave della tesi (max 10):

Parametri modali

Consapevole, dichiara

CONSAPEVOLE: (1) del fatto che in caso di dichiarazioni mendaci, oltre alle sanzioni previste dal codice penale e dalle Leggi speciali per l'ipotesi di falsità in atti ed uso di atti falsi, decade fin dall'inizio e senza necessità di alcuna formalità dai benefici conseguenti al provvedimento emanato sulla base di tali dichiarazioni; (2) dell'obbligo per l'Università di provvedere al deposito di legge delle tesi di dottorato al fine di assicurarne la conservazione e la consultabilità da parte di terzi; (3) della procedura adottata dall'Università di Ferrara ove si richiede che la tesi sia consegnata dal dottorando in 2 copie di cui una in formato cartaceo e una in formato pdf non modificabile su idonei supporti (CD-ROM, DVD) secondo le istruzioni pubblicate sul sito: http://www.unife.it/studenti/dottorato alla voce ESAME FINALE – disposizioni e modulistica; (4) del fatto che l'Università, sulla base dei dati forniti, archivierà e renderà consultabile in rete il testo completo della tesi di dottorato di cui alla presente dichiarazione attraverso l'Archivio istituzionale ad accesso aperto "EPRINTS.unife.it" oltre che attraverso i Cataloghi delle Biblioteche Nazionali Centrali di Roma e Firenze; DICHIARO SOTTO LA MIA RESPONSABILITA': (1) che la copia della tesi depositata presso l'Università di Ferrara in formato cartaceo è del tutto identica a quella presentata in formato elettronico (CD-ROM, DVD), a quelle da inviare ai Commissari di esame finale e

alla copia che produrrò in seduta d'esame finale. Di conseguenza va esclusa qualsiasi responsabilità dell'Ateneo stesso per quanto riguarda eventuali errori, imprecisioni o omissioni nei contenuti della tesi; (2) di prendere atto che la tesi in formato cartaceo è l'unica alla quale farà riferimento l'Università per rilasciare, a mia richiesta, la dichiarazione di conformità di eventuali copie; (3) che il contenuto e l'organizzazione della tesi è opera originale da me realizzata e non compromette in alcun modo i diritti di terzi, ivi compresi quelli relativi alla sicurezza dei dati personali; che pertanto l'Università è in ogni caso esente da responsabilità di qualsivoglia natura civile, amministrativa o penale e sarà da me tenuta indenne da qualsiasi richiesta o rivendicazione da parte di terzi; (4) che la tesi di dottorato non è il risultato di attività rientranti nella normativa sulla proprietà industriale, non è stata prodotta nell'ambito di progetti finanziati da soggetti pubblici o privati con vincoli alla divulgazione dei risultati, non è oggetto di eventuali registrazioni di tipo brevettale o di tutela. PER ACCETTAZIONE DI QUANTO SOPRA RIPORTATO

Firma del dottorando

Ferrara, lì 02/02/2018 (data) Firma del Dottorando _____

Firma del Tutore

Visto: Il Tutore Si approva Firma del Tutore _____